THE UNIVERSITY
of EDINBURGH

Dual role of Lin28a in the regulation of miRNA biogenesis during neuronal differentiation

Jakub S. Nowak

THE UNIVERSITY *of* EDINBURGH

Thesis presented for the degree of Doctor of Philosophy

October 2015

Declaration

I declare that this thesis was compose by myself, that the work contained herein is my own except where explicitly stated otherwise in the text, and that this work has not been submitted for any other degree or processional qualification except as specified.

The work presented in chapter 1.3 has been published in Biochemical Society Transactions 08/2013; 41(4):815-20 as review - "miRNA in development and pathogenesis of nervous system" by Jakub Nowak and Gracjan Michlewski. I composed the manuscript that was further edited with the help of my supervisor Gracjan Michlewski.

Parts of the work presented in chapter 3 and 4 has been published in Nature Communications 04/2014; 5: 3687 as article – "Lin28a regulates neuronal differentiation and controls miR-9 production" by Jakub S. Nowak, Nila Roy Choudhury, Flavia de Lima Alves, Juri Rappsilber & Gracjan Michlewski. I contributed to vast majority of experimental work presented in the article as well as being involved in process of drafting end editing the manuscript together with my supervisor Gracjan Michlewski.

Jakub S. Nowak

Ediburgh,

October, 2015

Acknowledgments

I would like to dedicate this work to my family especially my wife Agata and son Henryk. It would not be possible to reach to the very end of this journey without their constant support, understanding and patience. I also thank my parents for their role in keeping me motivated.

I would also like to thank my supervisor Dr. Gracjan Michlewski for his exceptional supervision and mentoring over the period of my study. His support was invaluable in overcoming *"the dark corners"* of the project and having some of the findings gratefully communicated outside.
I also express my gratitude to all of my colleagues especially Dr. Nila Roy Choudhury for their support and enthusiasm.

I would like to acknowledge the Wellcome Trust for financial contribution to the work carried out in my PhD project.

I will finish my acknowledgments with two quotes that best express my state of mind after finishing drafting this thesis:

"Choose a job you love, and you will never have to work a day in your life"
by Confucius

"Veni, Vidi, Vici"
by Julius Cesar

Table of Content

Table of Figures

Abstract

Many cellular functions depend on the tightly regulated expression of various proteins. Canonical control of the protein expression is associated with transcriptional regulation. However, the small non-coding RNAs called microRNAs (miRNAs) were identified as post-transcriptional regulators of gene expression. In a typical manner, miRNAs originate similarly to the coding RNAs and are processed in a multi-step maturation process. It has been shown that miRNAs are very important for the proper functioning of tissues. Interestingly, the human nervous system contains over 70% of all miRNAs; thus, the maturation process has to be tightly regulated. However, despite the important role of miRNAs, little is known about the mechanisms regulating their biogenesis. In my PhD project, I showed that during early stages of neuronal differentiation, Lin28a controls levels of neuro-specific miRNA-9. I demonstrated that Lin28a binds to the conserved terminal loop (CTL) of pre-miRNA-9 and decreases the cellular levels of miRNA-9 during retinoic acid-mediated neuronal differentiation of mouse teratocarcinoma P19 cells. I revealed that the Lin28a-mediated inhibition of miRNA-9 production was uridylation-independent. Furthermore, constitutive expression of GFP-tagged Lin28a reduced the levels of let-7a but not miRNA-9, whereas untagged Lin28a inhibited both miR-9 and let-7a during the course of neuronal differentiation. Using small RNAseq analysis of P19 cells with constitutive expression of Lin28a I showed that it controls many more miRNAs than previously recognised. Intriguingly, many miRNAs were upregulated by Lin28a overexpression. I demonstrated with high-throughput, the limited function of GFP-tagged Lin28a results, and I also showed that untagged Lin28a inhibits the production of a number of brain-specific miRNAs including miRNA-9. Finally, I revealed that 3'-5'exoribonuclease Dis3l2 was responsible for uridylation-independent degradation of pre-miRNA-9. Altogether, my results provided evidence that Lin28a has both positive and negative roles in the regulation of miRNA production and has a dual role in triggering pre-miRNA degradation.

Lay abstract

The human brain consists of millions of cells that have clearly stipulated roles in the proper functioning of the nervous system. A single cell can customise its own functions through proper regulation of the molecules that execute these functions. These molecules are called proteins and are encoded by genes during the process known as gene expression. In a canonical manner, this process can be controlled by factors that associate with the region of DNA containing the expressed gene. However, a new class of regulators called microRNAs (miRNAs) was recently identified to play an essential independent role in the regulation of gene expression. The importance of miRNAs has been shown in many studies displaying their defective function during disease development, including the progression of cancer. Interestingly, the nervous system, compared to all human tissues, harbours a major fraction of all miRNAs. These molecules are produced in cells during the biogenesis pathways that involve several steps in which a miRNA precursor is converted into mature miRNA. Despite the importance of miRNAs, little is known about the cellular mechanisms regulating their production. In my PhD project, I employed cutting-edge techniques to identify Lin28a (protein factor) as the regulator of miR-9 biogenesis (miRNA involved in the neuronal differentiation). Furthermore, I used genome-wide approaches to investigate the broad role of this regulator in miRNAs biogenesis during the neuronal development and identified large group of miRNA that levels are positively and negatively regulated by Lin28a. I also investigated the molecular mechanism of this regulation and identified Dis3l2 as an enzyme involved in degradation of the miR-9 precursor during the early stages of neuronal development. In the future, the results obtained in this study can be used in biomedical applications where the induced development of neurons (cells of the nervous system) would display therapeutic benefits.

Abbreviations

3'-, 5'-UTR	3'-, 5'-Untranslated Region
ADAR	Adenosine Deaminase acting on RNA
AGO	Argonaute family proteins
AMP	Adenine Mono-Phosphate
AMPAR	α-amino-3-hydroxy 5-methylisoxazole 4-propionic acid receptor
APT1	Acyl protein thioesterase 1
ASEL	Amphid Neuron Single Left
ASER	Amphid Neuron Single Right
ATP	Adenine Tri-phosphate
AVS	Avian Sarcoma Virus
BAF	Brahma-associated factor
BCDIN3D	BCDIN3 Domain Containing
BDNF	Brain-derived neurotrophic factor
BMP	Bone Morphogenic Protein
BrdU	Bromodeoxyuridine
C3PO	Component 3 promoter of RISC
CAF1-CCR-NOT	Carbon Catabolite Repressor 4 and Negative On TATA proteins
CCHC	Cys-Cys-His-Cys
ChIP	Chromatin Immunoprecipitation
CLIP-RNAseq	cross-linking immunoprecipitation RNA-sequencing
CMV	Cytomegalovirus
CNS	Central Nervous System
COG-1	Connection Of Gonad defective
CREB	cAMP response element binding protein
CSD	Cold Shock Domain
CTL	Conserved terminal loop
DCP2	Decapping Enzyme 2
Dcr2	Dicer 2

DGCR8	DiGeorge Syndrome Critical Region 8
DGS	DiGeorge Syndrome
DHX9	DEAH (Asp-Glu-Ala-His) box helicase 9
DIE-1	Dorsal Intercalation and Elongation defect 1
Dis3l2	DIS3 Like 3'-5' Exoribonuclease 2
DMEM	Dulbecco's Modified Eagle Medium
DN	Dopamine Neurons
Dox	Doxocycline
dsRBD	double-stranded RNA binding domain
EB	Embryonic bodies
EDTA	Ethylenediaminetetraacetic acid
EF	Elongation Factor
eIF4G	eukaryotic translation-initiation factor 4G
EMSA	Electromobility Shift Assay
ER	Endoplasmic Reticulum
ERK	Extracellular-signal Regulated Kinase
EXOSC3	Exosome Component 3
FMR1	Fragile X Mental Retardation 1
FXS	Fragile X Syndrome
GB	Glioblastomas
GFAP	Glial fibrillary acidic protein
GFP	Green Fluorescent Protein
Gld2	Germ line development 2
GluRs	Glutamate receptors
gRNA	guide RNA
GSK3β	Glycogen Synthase Kinase 3β
GST	Glutathione S-Transferase
H2a, b, -3, - 4	Histone 2a, 2b, -3, - 4
HBD	Haem binding domain
HDAC	Histone Deacetylase
HEK293	Human Embryonic Kidney 293 cells
HeLa	Henrietta Lacks cells

hnRNP-A1	Heterogeneous nuclear Ribonucleoprotein A1
HRP-ab	HRP-anti-mouse antibody
IAA	Iodoacetamide
iDo-PAR-CLIP	individual domain PAR-CLIP
IGF2	Insuling Growth Factor 2
IgG ab	anti-IgG antibody
IL-6	Interleukin 6
IMPs	IGF2 mRNA-binding Proteins
IP	Immunoprecipitaiton
IRES	Internal Ribosome Entry Site
JNK	c-JUN N-terminal Kinase
KSRP	Far upstream element-binding protein 2
Limk1	LIM domain kinase 1
Lin28	Cell Lineage Abnormal 28
lncRNAs	long non-coding RNAs
LTD	Long-term depression
LTP	Long-term potentiation
MAPK	Mitogen-Activated Protein Kinase
MB	Meduloblastomas
MCPIP1	MCP-induced protein 1
MCPIP1	Monocyte chemotactic protein-induced protein 1
Me-CP2	Methyl-CpG binding protein 2
MHB	Midbrain-hindbrain boundary
miRISC	miRNA-mediated silencing complex
miRNAs	micro RNAs
mRNA	messenger RNA
MS	Mass spectrometry
MWKO	Molecular Weight Cut Off
NaAc	Sodium Acetate
ncRNAs	non-coding RNAs
NLoS	Nucleolar Localisation Signal
NLS	Nuclear Localisation Signal

NMDAR	N-methy-D-aspartate receptor
NMR	Nuclear Magnetic Resonance
NSRF	Neuron-restrictive silencer factor
Oct4	Octamer-binding Transcription factor 4
PABP	poly-A binding protein
PAZ-domain	Piwi Argonaut and Zwille domain
PDGF	Platelet-derived Growth Factor
PI3K-mTOR	Phosphoinositide 3-kinase - mammalian Target of Rapamycin
piRNAs	piwi-interacting RNAs
PNK	T4 polynucleotide kinase
PNPT1	PNPase-old-35
PolII	Polymerase II
PTEN	Phosphatase and tensin homologue deleted on chromosome 10
PTM	Post-translational modification
QC	Quality Control
qRT-PCR	qunatitative Reverse Transcription - Polymerase Chain Reaction
RA	Retinoic Acid
RBD	RNA Binding Domain
REST	RE1-silencing transcription factor
RIIIDs	RNAse III domains
RNAi	RNA inhibition
RT	Room Tempreature
SDS-PAGE	Sodium dodecyl sulfate polyacrylamide gel electrophoresis
SILAC	Stable isotope labelling by amino acids
siRNAs	small interfering RNAs
SIRT1	Sirtuin1
SMAD	Sma and Mad Related Family
snoRNAs	small nucleolar RNAs

SOD-1	Superoxide Dismutase 1
SOP	Sensory precursors
TBS-T	Tris-Buffered Saline and Tween 20
Tet	Tetracycline
TFIIB	Transcription Factor II B
TGF-β	Transforming Growth Factor β
TH	Tyrosine Hydroxylase
TRBP	TAR RNA-binding protein
TRIM32	Tripartite motif-containing protein 32
TSS	Transcription Start Site
Tuj1	β-tubulin class III
TUT4	Terminal Uridylyltransferase 4
UTP	Uridine Tri-Phosphate
VSNL1	Visinin like 1
XRN1	5'-3' exoribonuclease 1
Zcchc11	Zinc Finger CCHC Domain Containing Protein 11
ZnF	Zinc-finger domain

Chapter 1

1 Introduction

Animal development requires the existence of molecular and cellular mechanisms that organise cells within tissues and tissues within bodies. The essential objective of these mechanisms is to achieve the correct spatial-temporal expression of genes into proteins, which execute a variety of developmental programs. A key component of these mechanisms is RNA – a molecule involved in the transcription of genetic information. Importantly, RNA also plays an active role in the regulation of processes converting the genetic information into functional signals. Moreover, less than 2% of the transcribed genetic information is considered protein-coding transcripts with the remainder classified as non-coding (Dunham et al., 2012). For many years, the majority of this non-coding information was considered as genetic "junk". However, with time, there was more evidence suggesting its regulatory role in the flow of genetic information. Furthermore, protein-coding sequences in the genome have encountered very modest changes during evolution, whereas the non-coding part has been considerably scaled-up and diversified across various organism within prokaryotic and eukaryotic kingdoms (Liu et al., 2013). Therefore, it is tempting to hypothesise that the development of more complex cellular arrangements can be, at least partially, explained by evolution of the systems that increased the genetic complexity allowing better spatial and temporal control of existing cellular processes. Consequently, non-coding RNAs (ncRNAs), which are transcribed from the non-coding part of the genome, could facilitate that role, as they include classes of genetically conserved regulatory elements. One possible classification of non-coding RNAs is based on their size. Small non-coding RNAs (sncRNAs) are evolutionary well-conserved short RNAs that include small nucleolar RNAs (snoRNAs), small interfering RNAs (siRNAs), micro RNAs (miRNAs), and piwi-interacting RNAs (piRNAs). They are usually

less than 200bp long and have evolved at different points during evolution, but their functions are well conserved. Both siRNAs and miRNAs play an inhibitory role in gene expression by directing repression of target mRNA (Bartel, 2009; Shabalina and Koonin, 2008). snoRNAs are the oldest form of ncRNA species and are present in Archaea, bacteria and eukaryotes. They are involved in chemical modifications, such as methylation and pseudouridylation, of other RNA molecules, including transfer and ribosomal RNAs (Matera et al., 2007).

The other class of ncRNAs, containing transcripts larger then 200bp, is called long non-coding RNAs (lncRNAs). This group evolved much later and is present in invertebrates, vertebrates and plants (Pauli et al., 2012; Young et al., 2012; Zhang and Chen, 2013). Interestingly, approximately one-third of lncRNAs are primate-specific (Derrien et al., 2012). LncRNAs are currently extensively studied and, similarly to sncRNAs, have been shown to have important regulatory functions in the cell. The brain is one of the organs where their function is particularly visible. For example, Malat1 is an lncRNA that acts as a decoy for splicing factors in neuronal cells and has also been shown to be involved in synaptogenesis (Anko and Neugebauer, 2010; Bernard et al., 2010).

1.1 miRNA biogenesis and function in vertebrate systems

Among the sncRNA families, miRNAs are considered to dominate in somatic tissues. The first miRNA was discovered in 1993 by Lee and colleagues. Using technique called chromosomal walking followed by transformation rescue they identified a genomic sequence called *lin-4*, which encoded trans-acting element responsible for regulation of protein Lin-14 – important for temporal control of postembryonic developmental events in *C. elegans*. Interestingly *lin-4* genomic region were not considered protein coding but instead two small transcripts, originating from this locus, were found to complement with regions within the 3'-UTR of Lin-14. Therefore, they suggested a mechanism of post-transcriptional control of Lin-14 driven by RNA-RNA interaction (Lee et al, 1993). Field of miRNA rapidly grow and their mechanisms were extensively studied. In 2000 Pasquinelli and colleagues identified other miRNA called *let-7* to be, together with *lin-4*, important for postembryonic developmental events in *C. elegans* – former governing transition from larvae to adult stage whereas later controlling transition events between larvae first and second stages. Importantly *let-7* and its mechanism of action turned out to be highly conserved across animal kingdom including vertebrate, ascidian, hemichordate, mollusc, annelid and arthropod (Pasquinelli et al, 2000).

In general miRNAs are ~22nt long RNA molecules that are produced in a multi-step fashion by the RNAse III class enzymes Drosha and Dicer, as shown in extensive biochemical studies using *in vitro* processing assays (Bartel, 2004; Carthew and Sontheimer, 2009; Hutvagner et al., 2001; Lee et al., 2003). Following Dicer cleavage, one strand of mature miRNA duplex, selected based on thermodynamic properties and called the guide strand, is loaded into the miRNA-mediated silencing complex (miRISC complex). This complex is responsible for recognition of a target mRNA that is achieved by seed sequence, a 6-8nt sequence within the first nucleotides counting from the 5'-end of mature miRNA (Bartel, 2009) (Figure 1-1).

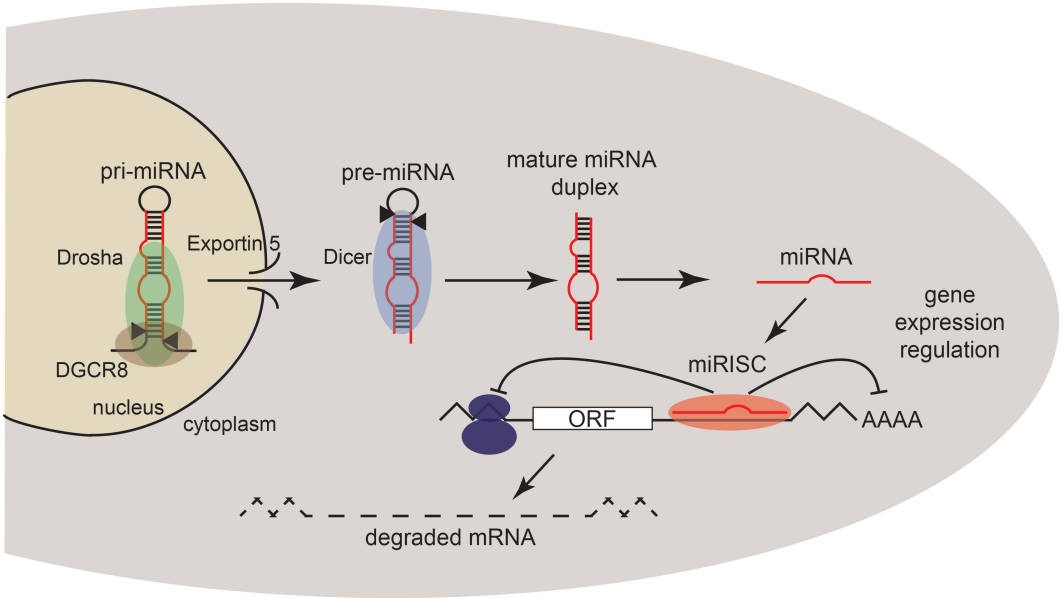

Figure 1-1 Summary of miRNA biogenesis
miRNAs are produced in the cell in a multi-step process. In the first step, pri-miRNA is transcribed from the genome and subsequently processed by the Drosha/DGCR-8 complex – also known as the microprocessor complex. Following the microprocessor trimming, pre-miRNA is exported to the cytoplasm where it is cleaved by the Dicer complex into a mature miRNA duplex. Following unwinding, one strand is incorporated into the miRISC complex which executes miRNA function in mRNA destabilisation or the repression of protein translation.

In principle, miRNAs are considered to serve as guides recognising target mRNAs and recruiting a complex of Argonaute family proteins (AGO) together with effectors that induce mRNA degradation or translational repression (Huntzinger and Izaurralde, 2011). Several studies have suggested that translational repression could occur at either the initiation or post-initiation steps of the translation (Humphreys et al., 2005; Mathonnet et al., 2007; Olsen and Ambros, 1999; Pillai et al., 2005; Seggerson et al., 2002; Thermann and Hentze, 2007). For instance, one of the first studies in *C. elegans* showed that lin-4 miRNA represses the translation of Lin-14 and Lin-28 mRNAs (Olsen and Ambros, 1999; Seggerson et al., 2002). Moreover, sucrose gradient revealed that both of the mRNAs associate with active polysomes (Maroney et al., 2006; Nottrott et al., 2006; Petersen et al., 2006). Treatment of these polysomes with various translational inhibitors results in their dissociation into monosomes (Maroney et al., 2006). Therefore, it has been concluded that molecular mechanisms of translational repression are caused by miRNA-

driven dissociation of polysomes (Petersen et al., 2006). Furthermore, in another study, Petersen and colleagues showed that translational repression also occurs in cases where translation is initiated from an internal ribosome entry site (IRES), which is a 5′-cap-independent mechanism, providing additional proof for miRNA affecting the post-initiation stages of translation (Petersen et al., 2006).

Nevertheless, several studies have displayed conflicting results suggesting that translational repression occurs at the translational initiation stage (Humphreys et al., 2005; Mathonnet et al., 2007; Pillai et al., 2005; Thermann and Hentze, 2007). Pillali and colleagues showed that using sucrose gradient that the expression of certain miRNAs does not lead to accumulation of their targets in polysomes but instead results in the formation of lower molecular weight free messenger ribonucleoproteins (Pillai et al., 2005). Moreover, at least two studies reported in cells that IRES driven translation was resistant to the presence of miRNA (Humphreys et al., 2005; Pillai et al., 2005). This finding was confirmed *in vitro* using cell-free extracts where IRES-initiated translation was not inhibited in the presence of miRNAs (Mathonnet et al., 2007; Wakiyama et al., 2007). At the initiation stages, poly-A binding protein (PABP), which is associated with 3′-poly-A tail of mRNA, interacts with eukaryotic translation-initiation factor 4G (eIF4G) that is associated with 5′-cap structure of mRNA (Derry et al., 2006). Molecularly, it has been suggested that miRNAs act at the initiation stages by targeting the 5′-cap structure and subsequently interfering with eIF4G function (Ding and Grosshans, 2009; Zdanowicz et al., 2009).

Nevertheless, dozens of studies using specific miRNAs or transcriptome-wide profiling showed that the expression of cognate miRNAs led to a reduction in their target mRNA levels (Bagga et al., 2005; Eulalio et al., 2009; Guo et al., 2010; Hendrickson et al., 2009; Lim et al., 2005; Rehwinkel et al., 2006; Schmitter et al., 2006). In particular, ectopic expression of miRNAs in cells leads to decrease of the transcript levels containing their binding sites (Guo et al., 2010; Lim et al., 2005; Selbach et al., 2008). In contrast, depletion of miRNAs resulted in an increase of their mRNA targets (Baek et al., 2008; Krutzfeldt et al., 2005; Selbach et al., 2008). Also,

depletion of the components of miRNA biogenesis factors (Dicer, Ago, GW182) subsequently resulted in an overall increase of mRNA levels (Rehwinkel et al., 2005; Rehwinkel et al., 2006; Schmitter et al., 2006). Molecularly, it has been shown that miRNAs direct their targets to the 5′-to-3′ mRNA decay pathway (Behm-Ansmant et al., 2006; Giraldez et al., 2006; Piao et al., 2010; Rehwinkel et al., 2005; Wu and Belasco, 2005). In the first step of this pathway, targeted mRNA is deadenylated by the deadenylase complex composed of chromatin assembly factor 1, carbon catabolite repressor 4 and negative on TATA proteins (CAF1-CCR-NOT complex) (Behm-Ansmant et al., 2006; Piao et al., 2010). Subsequently, mRNA decapping enzyme 2 (DCP2) leads to the removal of a 5′-cap, which triggers major cytoplasmic 5′-3′ exoribonuclease 1 (XRN1) to degrade the miRNA target (Giraldez et al., 2006; Rehwinkel et al., 2005). Several studies have provided evidence that a depletion of either deadenylation or decapping pathway components led to an increase in the abundance of miRNA targets – providing evidence for miRNA-driven destabilisation of their mRNA targets (Behm-Ansmant et al., 2006; Eulalio et al., 2009; Eulalio et al., 2007).

Moreover, studies measuring both mRNA and protein levels displayed that mRNA destabilisation is a major pathway of miRNA action and translation is only modestly inhibited, rarely exceeding four-fold reduction in protein synthesis (Baek et al., 2008; Selbach et al., 2008). In particular, measuring mRNA and protein levels in HEK-293 cells transfected with miR-124 showed that among 600 identified mRNA targets, a reduction in their protein levels is seen in 75% of cases for mRNA degradation (Hendrickson et al., 2009). Moreover, Bartel and colleagues also showed using high-resolution ribosome mapping that a decrease of steady-state mRNA levels could explain an 84% reduction in protein synthesis mediated my miRNAs (Guo et al., 2010).

miRNAs are widely distributed across species and account for one of the largest gene families in their genomes (Griffiths-Jones et al., 2008). Interestingly, through extensive research and abundant access to next-generation genome wide sequencing data, new miRNAs are still being

discovered. For example, in humans alone, over 2000 new miRNAs have been described since 2010 (Ha and Kim, 2014; Krol et al., 2010b). Currently, 434 miRNAs in *Caenorhabditis elegans*, 466 miRNAs in *Drosophila melanogaster* and 2588 miRNAs in *Homo sapiens* have been deposited in miRBASe – a commonly used miRNA repository (Kozomara and Griffiths-Jones, 2014). Comprehensive genomic research and sequencing proved that in many species, miRNAs of related sequences exist at multiple loci. This is most likely the result of gene duplication events (Berezikov, 2011; Hertel et al., 2006). If multiple genomic loci encode the same miRNAs, a numeric suffix is added at the end of the name; for instance, miR-124-1, miR-124-2, and miR-124-3 are the same miRNAs but located at different genomic locations. The most important domain responsible for its functional outcome is located at the 5′ end of the miRNA, between nucleotides 2-8, and is called the seed sequence. This sequence is essential for base pairing with the target mRNA. Moreover, miRNAs with the same seed sequence are classified as the same family (Bartel, 2009). For instance, using next-generation sequencing and bioinformatics, it has been shown that the let-7 family contains 14 paralogous miRNAs. Moreover, 34 miRNA families are conserved from *C. elegans* to *H. Sapiens* and 196 miRNA families are conserved among mammals only (Wheeler et al., 2009).

In addition, each miRNA locus can produce two mature miRNAs. For example, miR-29a-5p and miR-29a-3p are produced from the 5′ and 3′ ends, respectively, of precursor miR-29a. However, in many cases, only one miRNA (from the guide strand) is chosen for an executive AGO-complex whereas the other (from the passenger strand) often undergoes degradation after the strands separate (Krol et al., 2010b).

The abundance and spatiotemporal expression of miRNAs and their targets requires the existence of precise controlling events that can regulate the biogenesis of miRNAs. These events can be divided into transcriptional and post-transcriptional (Fig 1-2).

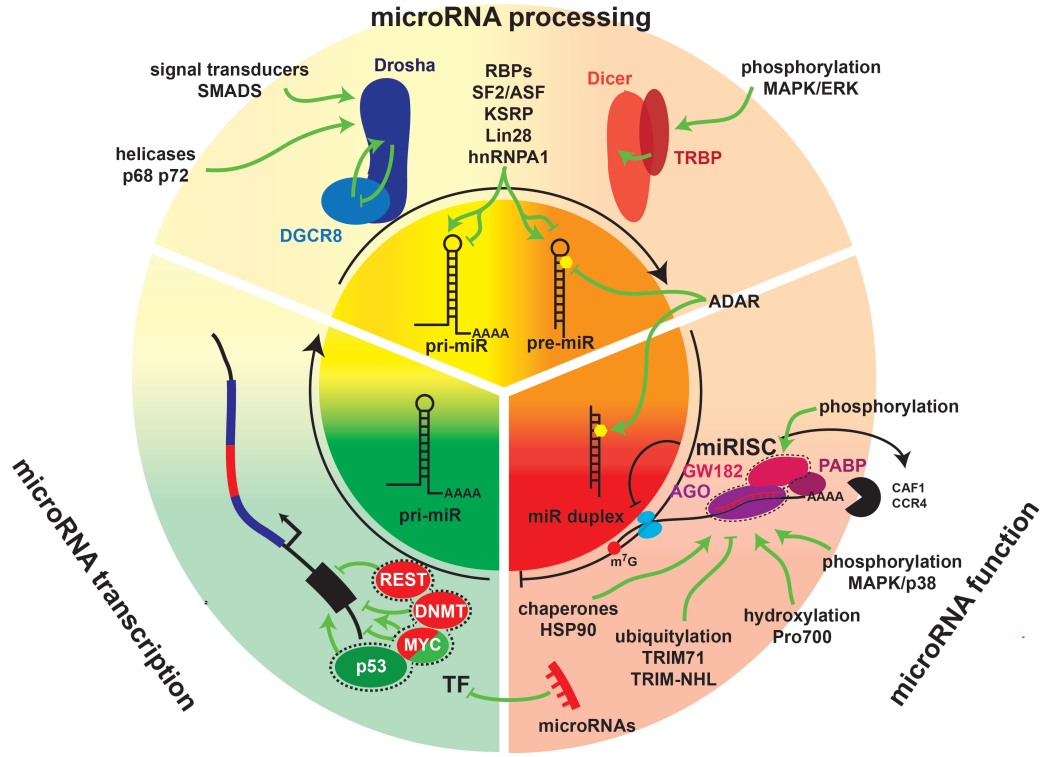

Figure 1-2 Summary of miRNA biogenesis regulation in the cell
Production of miRNAs in the cell is regulated at the transcriptional and post-transcriptional stages and involves a variety of auxiliary factors.
The transcriptional stage of regulation involves mechanisms also regulating the transcription of protein coding genes. In particular, transcription and chromatin remodelling factors are the major contributors to this regulatory step.
At the post-transcriptional stage, regulatory factors could directly associate with precursor miRNA molecules or interact with miRNA processing machinery. Major contributions in this step are associated with the editing of either the RNA molecule or the protein factor, which leads to stability alterations and consequently changes miRNA biogenesis.
The functional miRISC complex with loaded miRNA strand could also be modified with various post-translational modifications affecting its regulatory efficiency.

1.1.1 Transcriptional control of miRNA synthesis

In the canonical, DGCR8/Drosha dependent, model miRNAs are transcribed from intronic regions of coding and non-coding transcripts as pri-miRNAs (Ha and Kim, 2014). It was shown that the majority of pri-miRNAs are transcribed in the cell using Pol II (Ha and Kim, 2014). However, some pri-miRNAs that originate from t-RNAs or are related to viral RNAs utilise Pol III in their synthesis of primary transcripts (Babiarz et al., 2008; Pfeffer et al., 2005). The primary transcripts of miRNAs are very similar to those of coding mRNAs and have both a 5′-7-methyl-

guanylate cap and 3'-poly A tail signalling sequences (Cai et al., 2004). Moreover, Chromatin Immunoprecipitation (ChIP), nucleosome-mapping and genetic analysis indicated the presence of DNA sequences associated with protein coding mRNAs, like frequencies of CpG islands, TATA-box TFIIB recognition and initiation sequences, as well as methylation sites. This would mean that the regulatory network associated with the expression of protein coding genes also influences the association of transcription factors and enhancers associated with the promoters of pri-miRNA transcripts (Corcoran et al., 2009; Ozsolak et al., 2008).

Bisulphite sequencing analysis showed that, in the case of bladder cancer, the expression of miR-127 is decreased due to hypermethylation of its promoter (Saito et al., 2006). Also, alterations of histones by Histone Deacetylase (HDAC) enzymes have been shown to affect the transcription of pri-miRNAs. For example, LAQ284 HDAC inhibitor treatment followed by microarray analysis showed that 27 miRNAs are affected by HDAC activity. This included miR-27a, which was strongly repressed by the inhibition of HDAC. Also, its target genes were shown to be affected by HDAC treatment (Scott et al., 2006). Furthermore, growth factors like platelet-derived growth factor (PDGF) and transforming growth factor-β (TGF-β) indirectly influence the levels of miRNAs (Chan et al., 2010; Davis et al., 2009).

Feedback loops in gene regulation have previously been suggested to play an essential role in gene expression and the specification of terminal differentiated states (Jacob and Monod, 1961; Monod and Jacob, 1961). Due to the intrinsic nature of miRNA function, these molecules are particularly well-suited to playing a central role in regulatory feedback mechanisms. In fact, within the midbrain area, a simple negative circuit between miR-133b and the Pitx3 transcription factor controls the development of dopamine neurons (DNs). The Aphakia mouse strain (a Parkinson disease model which lacks the expression of Pitx3) was shown to have significantly lower levels of mir-133b (Kim et al., 2007). Using the luciferase reporter system, it was shown that the proximal promoter region of miR-133b is sufficient to convey Pitx3 binding. Concurrently, the

Pitx3 3'-untranslated region contains a motif that is recognised by miR-133b. This reciprocal binding of the transcription factor and miRNA is sufficient to produce a physiological response as demonstrated *in vivo* using an oligonucleotide inhibiting miR-133b and by FACS sorting Tyrosine Hydroxylase (TH) positive DNs. In this setting, overexpression or reduction of miR-133b leads to a decrease or increase of Pitx3, respectively. Also, Pitx3 levels were upregulated in DNs from TH+FACS sorted Dicer mutant neurons, which is consistent with an overall role of miRNAs, specifically miR-133b, in the regulation of the expression of this transcription factor (Kim et al., 2007).

In addition, even more complex regulatory circuits with miRNAs playing a central role have evolved. In *C. elegans*, neurons involved in the development of two distinctive taste receptors (ASEL and ASER) are initially interlocked in a quasi-stable hybrid state with the expression of genes specific for both types. In the course of cell fate specification, two miRNAs, lys-6 and miR-273, are required to determine the terminally stable states. Mutation analysis and gene reporter assays in ASER neurons helped to determine that the expression of ASEL-specific genes is blocked by expression of the transcription factors COG-1 and miR-273, which targets the transcription factor DIE-1. Conversely, the ASEL state is established when neurons retain expression of DIE-1 and the lys-6 miRNA, which blocks the expression of COG-1 and fundamentally inhibits the expression of ASER-specific genes in this sensory organ (Johnston et al., 2005).

Notably, the precise locations of the promoters of most miRNAs have not yet been experimentally determined, but can be inferred based on the positions of other transcriptional regulatory elements (Ozsolak et al., 2008). Also, the transcription start sites (TSS) for some intronic miRNAs have been shown to be different from the TSS of their host genes (Monteys et al., 2010).

1.1.2 Post-transcriptional mechanisms regulating miRNA production

Since miRNAs have a substantial capacity to manage cellular and developmental programs, their expression has to be tightly regulated.

Transcriptional regulation is the first line in the control of miRNA expression. However, this regulation requires the means of controlling transcription factor levels, which by its own nature is an indirect effect and demands an additional amount of time. Therefore, more direct means could be more beneficial as they would require less time and would potentially benefit from being more precise, allowing the regulation of only specific subsets of miRNAs. Importantly, *in vitro* processing assays of radiolabelled precursor miRNAs revealed that their biogenesis pathway requires multi-step maturation events occurring post-transcriptionally (Lee et al., 2002). Hence, this provides several opportunities for the direct regulation of each processing step, allowing for greater fine-tuning of miRNA levels.

1.1.2.1 Drosha mediated pri-miRNA processing in the cell nucleus

Pri-miRNAs are on average 1kb long and consist of multiple intrinsic features including a stem (32-35bp) and a single-stranded terminal loop and are flanked by single-stranded regions at both sides of the base of the stem. (Davis-Dusenbery and Hata, 2010). In the first step of maturation, the Microprocessor complex, consisting of Drosha and its partner DGCR8, crop at the base of the pri-miRNA stem releasing a 60-70bp long hairpin-like structure called the pre-miRNA. Drosha-DGCR8 cleavage determines the terminus of the miRNA, which will ultimately affect the miRNA functional output (Han et al., 2004). Therefore, the microprocessor trimming point has to be precisely guided. It has been shown that the microprocessor cleaves approximately 11nt from the basal junction between ssRNA and dsRNA and 22nt away from the apical junction converging with the terminal loop (Han et al., 2006; Zeng et al., 2005), leaving an overhang that is characteristic of RNAse-III-mediated cleavage reactions (Zamore, 2001). Deletion mutagenesis and *in vitro* processing assay showed that cis-acting regulatory elements reside in close proximity, covering a ~50bp region across the cleavage site (Lee et al., 2003). Furthermore, site-directed mutagenesis revealed that internal loops are not essential for Microprocessor processivity; however, disruption of dsRNA significantly reduced the efficiency of the reaction, proving again

the RNAse-III class characteristics of the Drosha/DGCR8 complex (Blaszczyk et al., 2001; Lee et al., 2003).

Drosha is a 160kDa nuclear protein that belongs to a family of RNAse III-type endonucleases (Denli et al., 2004). The N-terminal part of Drosha is responsible for its cellular localisation, whereas the C-terminal region contains tandem RNAse III domains (RIIIDs) and a dsRNA-binding domain (dsRBD) (Han et al., 2004; Tang et al., 2010). The RIIIDs dimerise intramolecularly forming a processing centre at their interface (Han et al., 2004). The first RIIID (RIIIDa) cuts at the 3′ end whereas the second RIIID (RIIIDb) cuts at the 5′ end of the pri-miRNA, leaving a 2-nt long 3′ overhang (Blaszczyk et al., 2001; Han et al., 2004). *In-vitro* processing assays showed that Drosha dsRBD interaction with the pri-miRNA is not sufficient for efficient cleavage (Han et al., 2004). However, the reaction normally occurs upon the association of DGCR8 with the middle part of Drosha, which contain an Arginine, Serine-rich region (Han et al., 2004).
DGCR8 is also a nucleolar protein with a molecular weight of around 90kDa. The N-terminal part of DGCR8, similarly to Drosha, is involved in localisation events (Shiohama et al., 2007; Yeom et al., 2006). The central part of the protein contains a haem-binding domain (HBD) involved in ferric-ion binding (ferric-ions have a positive effect on processing efficiency) and two dsRBDs involved in the interaction with pri-miRNA molecules (Cochran and Michael, 2008; Han et al., 2006; Yeom et al., 2006). The remaining C-terminal part of DGCR8 is involved in the interaction with Drosha and formation of the microprocessor complex (Yeom et al., 2006).

In most cases, microprocessor activity shapes the levels of mature miRNAs; consequently, its expression and activity is controlled at three distinct levels. In the first instance, the auto-regulatory mechanism between Drosha and DGCR8 has a strong effect on the overall activity of the microprocessor complex (Gregory et al., 2004). DGCR8 has a positive effect on the stability of the complex via its interaction with the middle region of Drosha. On the other hand, Drosha destabilises the DGCR8

mRNA leading to its degradation. This cross-regulatory loop is very important for the processing efficiency of the microprocessor, as it has previously been shown using *in vitro* processing that even a three-fold increase in DGCR8 significantly reduces the activity of the microprocessor complex.

In addition to the auto-regulatory mechanism, several posttranslational modifications (PTM) of microprocessor components have been shown to affect its stability, localisation and reactivity. Fluorescent microscopy studies and *in vitro* kinase assay suggested that Drosha is a target for glycogen synthase kinase 3β (GSK3β), with residues S300 and S302 being phosphorylated, allowing the protein to localise to the nucleus (Tang et al., 2011).

Mass spectrometry analysis of phosphorylation sited showed that DGCR8 is phosphorylated at 23 sites (Herbert et al., 2013). In this study, co-immunoprecipitation assays were used to identify JNK and ERK kinases as the enzymes phosphorylating DGCR8. Additionally, an *in vitro* kinase assay coupled with phosphatase inhibitors showed that the role of DGCR8 phosphorylation is to increase the stability of DGCR8 (Herbert et al., 2013).

Acetylation was also shown to play a role in activity of the microprocessor. It has been shown with *in vitro* acetylation assays that acetylation and de-acetylation of Drosha and DGCR8, respectively, positively regulates the reactivity of the microprocessor (Tang et al., 2013; Wada et al., 2012). Mass spectrometry analysis showed that K382 was one of the acetylated Drosha residues (Tang et al., 2013). In this study, it was shown that acetylation competes with ubiquitination of Drosha and ultimately leads to stabilisation of the protein. Consequently, gene reporter assays and qRT-PCR analysis demonstrated that acetylation leads to increased levels of certain miRNAs, including miR-143 (Tang et al., 2013). Recently, another study illustrated that phosphorylation of MeCP-2, a protein involved in binding to methylated CpG islands, leads to its association with DGCR8 (Cheng et al., 2014). MeCP-2 competes for Drosha binding and decreases miRNA production. Deep sequencing analysis showed that MeCP-2 knockout mice have an overall increased production of miRNAs. Moreover, co-immunoprecipitation analysis showed that

interaction between phosphorylated MeCP-2 and DGCR8 is direct and depends on the phosphorylation of Ser80 in MeCP-2.

The last vital regulatory category involves auxiliary proteins that interact either with the microprocessor complex or the pri-miRNA and influence activity of the complex. It has been reported that TGF-β and bone morphogenetic protein (BMP) leads to activation of SMAD signalling molecules. They were shown to interact with p68 and the stem of certain pri-miRNAs and consequently increase the activity of the microprocessor (Davis et al., 2008; Davis et al., 2010).

Several proteins have been shown to interact with the terminal loop or stem of pri-miRNAs. For instance, *in vitro* footprinting analysis demonstrated that hnRNP-A1 interacts directly across various positions with pri-miR-18a. Structural analysis suggested that this interaction leads to some essential re-arrangements within pri-miR-18a that consequently trigger increased activity of the microprocessor (Guil and Caceres, 2007; Michlewski et al., 2008). Interestingly, hnRNP-A1 was also suggested to inhibit processing of pri-let-7a-1. Footprinting analysis and *in vitro* processing assays showed that hnRNP-A1 binds to the terminal loop of pri-let-7 and its depletion from extracts leads to an increase in the *in vitro* processing of pri- to pre-let-7 (Michlewski and Caceres, 2010). Even more importantly, hnRNP-A1 was shown to compete with KSRP for binding with the pri-let-7 terminal loop. KSRP is an alternative splicing factor that was shown, with UV-crosslinking, to associate directly with the pri-let-7 terminal loop and positively regulate the *in vitro* processing of pri-let-7 and, if supplemented with Dicer, also of pre-let-7 (Trabucchi et al., 2009).

There have been several other studies describing the role of auxiliary proteins binding directly to pri-miRNAs and regulating their processing. For example, pluripotency-promoting factor Lin28a has been shown to interact with the pri-let-7 precursor and inhibit its maturation (Viswanathan and Daley, 2010). Similarly, other studies linked the role of the HuR and Msi2 proteins in the processing of the miR-7 precursor (Choudhury et al., 2013).

1.1.2.2 Dicer-mediated pre-miRNA processing in the cell cytoplasm

Following microprocessor-mediated processing of the pri-miRNA to pre-miRNA, the pre-miRNA is exported by Exportin-5 to the cytoplasm (Gwizdek et al., 2003; Okada et al., 2009; Yi et al., 2003). Upon being released from the exporting complex, the pre-miRNA undergoes the final step of maturation directed by Dicer, as shown by a series of *in vitro* processing assays and Dicer silencing assays (Hutvagner et al., 2001; Ketting et al., 2001). Dicer, similarly to Drosha, belongs to RNAse III type endonucleases and has a molecular weight of approximately 200kDa (Zhang et al., 2004). The C-terminal part of Dicer contains two tandem RIIIDs. Crystallographic studies and *in vitro* processing of various Dicer point mutants showed that these RIIIDs form an intramolecular dimer and the processing centre of the protein (Figure 1-3) (Zhang et al., 2004). The N-terminal part of the protein contains a helicase that is involved in the recognition of the single-stranded terminal loop of pre-miRNA, as shown by EMSA analysis (Tsutsumi et al., 2011). Moreover, *in vitro* dicing reactions indicated that the interaction between the N-terminus of Dicer and the terminal loop of the pre-miRNA is essential for efficient activity of the reaction (Gu et al., 2012). The heart of the substrate recognition and specificity is within the PAZ domain of Dicer, which occupies the centre of the protein and is involved in the interaction with the terminus of the pre-miRNA (Macrae et al., 2006; Park et al., 2011; Tian et al., 2014). The PAZ domain binds the 3′ end with the characteristic 2nt overhang of substrate pre-miRNA. It has been proposed that cleavage sites for Dicer are also determined based on the interaction of the PAZ-domain with the 3′ terminus (Zhang and Chen, 2013). The usual distance of 21-25nt between the RNA terminus and the cleavage sites is a consequence of the presence of the helix linking PAZ-domain and RIIIDs (Park et al., 2011). Interestingly, in flies and mammals, Dicer developed a more stringent method of controlling the position of cleavage sites (Park et al., 2011). In this case, the PAZ-domain contains an additional pocket for binding the phosphorylated 5′-terminus of the pre-miRNA. Moreover, the relative positions of both pockets require a 2nt overhang at the 3′ end. *In vitro* and *in vivo* analysis showed that binding to both pockets accurately determines

the product size of 22nt. Site directed mutagenesis and *in vitro* processing assay determined that residues Y926 and R927 are essential for 3′ terminus binding and their mutation results in an almost complete loss of the counting mechanism. However, mutations of residues R778, R780, R811, R986 and R993, which are important for 5′ terminus binding, resulted in loss of the cleavage precision and effectively the heterogeneous population of products characteristic of lower evolutionary organisms (Park et al., 2011). Moreover, crystal studies also suggested that the 5′ and 3′ binding pockets within PAZ determine two different stages of Dicer, cleavage competence and substrate release (Tian et al., 2014).

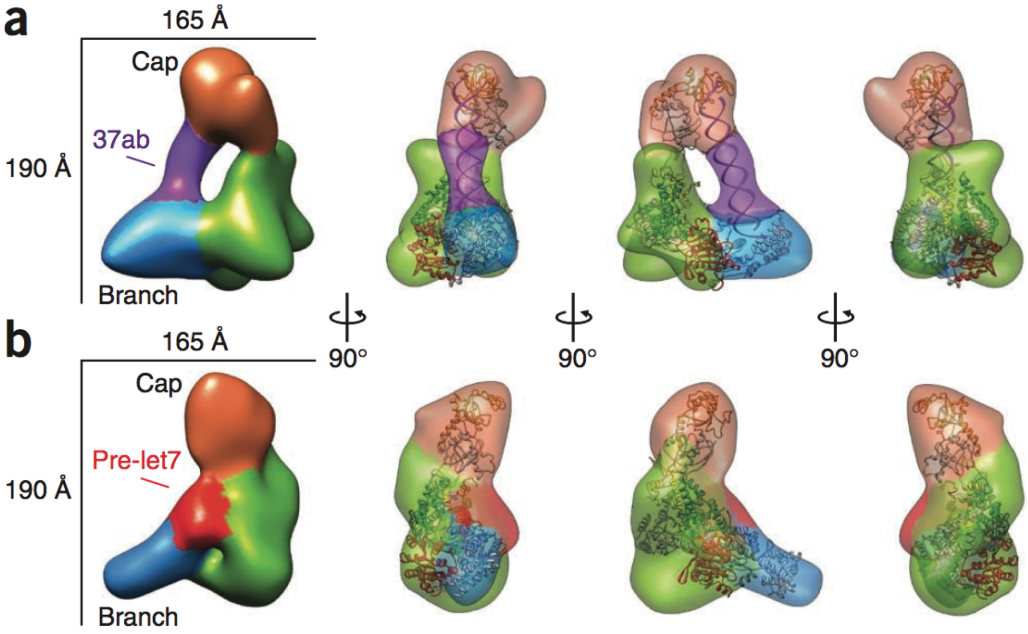

Figure 1-3 A pre-siRNA spans human Dicer between the cap and branch while a pre-miRNA binds the platform of the enzyme.
(**a**,**b**) Cryo-EM reconstructions of human Dicer–37ab (**a**) and human Dicer–pre-let7 (**b**) at ~29-Å and ~31-Å resolution, respectively. Regions labeled by the antibodies and the DExH/D are segmented and colored on the EM density. Orange, mAb 83-labeled region; green, mAb 77-labeled region; light blue, DExH/D domain. Ab Crystal structures of homologous domains have been docked into the map on the basis of c antibody localization and segmentation and are color coded and labeled. Yellow, RNase IIIa; green, RNase IIIb; orange, PAZ domain from Giardia intestinalis Dicer (PDB 2QVW28), Red, ATP-binding domain; light blue, helicase domains from a homology model of Dicer's helicase based on human RIG-I (PDB 2YKG30). The pre-siRNA, 37ab, is modeled as a 35-bp A-form RNA duplex within its segmented density, colored purple in **a**. The pre-miRNA, pre-let7, is not modeled, and the segmented density is colored red in **b**.
Reprinted from the article of Taylor and colleagues "Substrate-specific structural rearrangements of human Dicer". Permission obtained from NSMB journal - licence number 3772151319850.

RNAse III class proteins have a tendency to interact with dsRBD proteins. Dicer, similarly to Drosha, interacts with the TAR RNA-binding protein (TRBP), which is a homologue of Drosophila's Loqs-PB (Chendrimada et al., 2005; Haase et al., 2005). TRBP contains three dsRBD and the interaction with Dicer supports stabilisation of the former (Chendrimada et al., 2005; Melo et al., 2009). Northern blot and gene reporter assays showed that knockdown of TRBP leads to an overall decrease in mature miRNA levels but does not completely block their pre-miRNA processing

(Chendrimada et al., 2005). Interestingly, certain cancers have been described to have lower levels of TRBP (Melo et al., 2009). Additionally, phosphorylation assays showed that TRBP is under regulation of MAPK/ERK. Consequently, this regulation contributes to increased levels of miRNAs associated with growth stimulation. In contrast, TRBP phosphorylation leads to a decrease in mature levels of let-7 – a known suppressor of cell proliferation (Paroo et al., 2009).

It has been demonstrated that auxiliary RNA binding proteins can affect the activity of the Dicer complex. For example, KSRP protein binds to a series of pre-miRNAs and induces their processing by Dicer (Trabucchi et al., 2009). On the other hand, Lin28a recognises the terminal loop of pre-let-7 and inhibits Dicer cleavage. Lin28a-mediated inhibition relies on pre-let-7 poly-uridylation, which ultimately leads to a decrease in mature let-7 levels (Heo et al., 2009; Viswanathan and Daley, 2010; Viswanathan et al., 2008).

1.1.3 miRISC complex – executioner of miRNA function

Following the final cropping step, the mature double-stranded miRNA duplex is loaded into the microRNA-induced silencing complex (miRISC) complex (Kawamata and Tomari, 2010). Fractionation studies indicated that this is a multiprotein complex with nuclease activity of around 500kDa. Additional sub-fractionations followed by mass spectrometry analysis identified the Argonaute (Ago) protein as the main component of the complex (Hammond et al., 2001).

Crystal structure studies showed that Ago arranges itself in bilobal fold (Figure 1-4). The overall structure is very well conserved across , bacteria, yeasts and humans, with the human one adopting the most open conformation (Elkayam et al., 2012; Nakanishi et al., 2012). The C-terminal lobe of Ago is shaped by the PIWI and MID domains that are in close proximity of the N-terminal lobe containing the N-domain. These two lobes form a cradle that is closed from the top by the PAZ-domain (Elkayam et al., 2012). The PIWI-MID interface contains a 5’-phosphate binding pocket that recognises the 5’-end of the guide RNA (gRNA). Additionally, human Ago2 contains a loop that favours either A or U at

the gRNA 5′-end (Frank et al., 2010). The remaining body of gRNA threads across a basic channel built by the PIWI-MID domain and its 3′-end reaches to the PAZ domain (Wang et al., 2008a; Wang et al., 2008b). This arrangement allows the gRNA to take on an A-form conformation helix that allows efficient scanning of the target mRNA (Elkayam et al., 2012; Song et al., 2004; Wang et al., 2008a; Wang et al., 2008b). Moreover, the crystal structure of the PIWI domain indicated that it arranges itself into a catalytic domain resembling the RNase H active site and avian sarcoma virus (AVS) integrase (Figure 1-4) (Liu et al., 2004). Upon mRNA recognition, the Ago active site was shown to slice the target between position 10 and 11 relative to the 5′ end of the gRNA (Song et al., 2004). Interestingly, all human AGO1-4 isoforms are capable of interacting with specific machinery that can induce translational repression or mRNA decay. However, only AGO-2 has the potential to slice perfectly matched target mRNA (Huntzinger and Izaurralde, 2011).

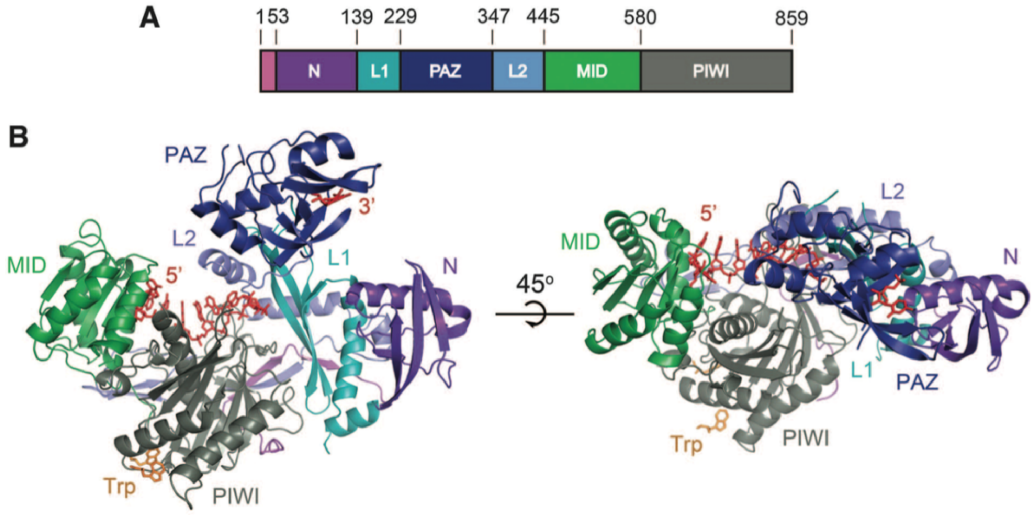

Figure 1-4 Structure of human Ago2
(A) Schematic of the Ago2 primary sequence. (B) Front and top views of Ago2 with the N (purple), PAZ (navy), MID (green), and PIWI (gray) domains and linkers L1 (teal) and L2 (blue). A generic guide RNA (red) can be traced for nucleotides 1 to 8 and 21. Tryptophan molecules (orange) bind to tandem hydrophobic pockets in the PIWI domain.
Reprinted from the article of Shirle and colleagues "The Crystal Structure of Human Argonaute2". Permission obtained from Science – licence number 3772150814815.

Furthermore, flies have an additional mechanism allowing for segregating perfectly matching (siRNA) from not perfectly matching (miRNA) small

RNA guides into specific Ago isoforms. Immunoprecipitation assays and Northern blots showed that central mismatches at gRNA positions 9 and 10 are essential structure characteristics responsible for ultimately guiding the duplex into Ago1 (Ghildiyal et al., 2010), whereas *in vitro* sorting assays, northern blots and site directed mutagenesis showed that Fly-Dcr2 binds perfectly complementary duplex gRNAs, acting to a certain degree as a gate-keeper assuring loading of the gRNA into Ago2 (Okamura et al., 2009). Also, *Drosophila* Ago have certain preferences towards the identity of the 5′ nucleotide of the gRNA. miRNA duplexes with a 5′ U is preferably bound to Ago1, whereas a 5′ C favours siRNAs to bind Ago2 (Czech et al., 2009).

In the final step of loading, the double stranded miRNA associated with the pre-miRISC complex undergoes unwinding, generating guide and passenger strands (Krol et al., 2010b). Two mechanisms directing this process were previously described and their selection depends on presence of a mismatch at the centre of the mature miRNA (Diederichs and Haber, 2007; Forstemann et al., 2007; Leuschner et al., 2006; Liu et al., 2004; Matranga et al., 2005; Meister et al., 2004; Rand et al., 2005). The first and most common mechanism involves unwinding without cleavage (Diederichs and Haber, 2007; Kawamata et al., 2009; Yoda et al., 2010). A series of EMSA analyses using synthetic wild-type duplexes and their mutants suggested that unwinding was based on a mismatch present in the majority of miRNAs at positions 2-8 and 12-15 and did not require the slicing activity of Ago in most cases (Kawamata et al., 2009).

However, in rare cases with perfect matching in the central position of the duplex miRNA, an alternative mechanism involving slicing of the passenger strand by Ago2 occurs (Miyoshi et al., 2005; Rand et al., 2005).

In vitro reconstitution assays with Dcr2 and Ago2 indicated that additional protein co-factors could be involved to enhance unwinding of the dsRNA (Liu et al., 2009). Through immunoprecipitation followed by liquid chromatography, the component 3 promoter of RISC (C3PO) endonuclease complex was isolated, with a depletion of C3PO leading to decreased levels of mature miRNA *in vivo*. Step-wise *in vitro* reconstitution of the RISC complex showed that C3PO is an essential component

involved in the conversion of pre-RISC containing double-stranded miRNA into mature RISC with single-stranded guide miRNA (Liu et al., 2009). Further crystallographic, mass spectrometry and processing assays showed that C3PO is an asymmetric octamer with six Translin and two Trax subunits, with the last component containing Mg-dependent endonuclease activity. These studies suggested that C3PO allows for efficient removal of the passenger strand from the pre-RISC, incorporating the guide miRNA in a complex with Ago2 (Liu et al., 2009; Ye et al., 2011).

A key step of the unwinding process is the selection of the guide RNA that remains incorporated in the RISC. *In vitro* RNAi reactions using siRNAs targeting Superoxide dismutase 1 (SOD-1) sense and anti-sense and their modified synthetic versions showed that even a single hydrogen bond energy difference at the 5'-end is sufficient to determine the entry point for helicases (Schwarz et al., 2003). Furthermore, potential mismatches at positions 2-4 co-ordinated from the less stable 5'-end of the duplex (corresponding to the helicase binding sites) were shown to act in favour of strand selection (Hu et al., 2009; Khvorova et al., 2003; Schwarz et al., 2003). Additional nucleotide specificity was observed, as strands with U at the 5'-end were frequently selected as guides (Hu et al., 2009; Kawamata et al., 2009).

Various *in vivo* studies analysing post-translational modifications suggested that Ago could be efficiently hydroxylated, phosphorylated, ribosylated, as well as ubiquitinated. These modifications resulted dominantly in reduced overall activity of miRISC and in some instances were triggered by environmental factors like viral infection or hypoxic stress (Qi et al., 2008; Rudel and Meister, 2008; Rudel et al., 2011; Shen et al., 2013; Wu et al., 2011; Zeng et al., 2008). Interestingly, immunoprecipitation and kinase activity assays followed by *in vitro* cleavage assays indicated that Akt3-mediated phosphorylation of Ago2 at position S387 acts as a molecular switch (Horman et al., 2013). It was suggested that upon phosphorylation, the overall miRISC activity is redirected from target cleavage to translational repression.

1.1.4 Modifications of miRNAs and its role in biogenesis regulation

In addition to the processes regulating miRNA biogenesis through interference with the processing machinery, the sequence of the precursor or mature miRNA can be chemically altered with considerable effects on its cellular fate (Ameres and Zamore, 2013).

The pre-let-7 family of miRNAs have been found to interact with the pluripotency-promoting Lin28a protein, which inhibits let-7 biogenesis (Newman et al., 2008; Rybak et al., 2008; Wulczyn et al., 2007). The Lin28-pre-let-7 complex was found to interact with Zcchc11, a member of the Tutase family (TUT) (Hagan et al., 2009) and *in vitro* processing assays found that reconstituted Lin28-TuT complex in the presence of UTP catalyse the reaction of adding a poly-U tail to pre-let-7. This ultimately results in pre-let-7 destabilisation and lack of mature let-7 (Hagan et al., 2009; Heo et al., 2009). Global profiling of mature miRNAs revealed that the depletion of Zcchc11 leads to downregulation of mature let-7 levels across the whole family (Piskounova et al., 2011). This finding was in accordance with the gene reporter analysis that showed repression of known let-7 targets upon Zcchc11 RNAi (Piskounova et al., 2011).

Interestingly, another study suggested that Lin28 functions as a molecular master switch that promotes the processing of pre-let-7 if a single uracil is added to its end or causes its degradation following the addition of a poly-U tail (Heo et al., 2012).

Another modification of the 3′ pre-miRNA that has been described is adenylation. Katoh and colleagues discovered a single A at the 3′-end of miR-122 (Katoh et al., 2009). Further immunoprecipitation analysis followed by an *in vitro* processing assay showed that this modification is added by poly-A RNA-polymerase, Gld2, that can add AMP monomers to the 3′-end of RNA. Finally, results obtained from Gld-2 knockout mice confirmed the functional relevance of miR-122 adenylation as a reduction in the miR-122 level was observed in the absence of the polymerase (Katoh et al., 2009). Interestingly, another study suggested that upon viral infection the viral poly-A, RNA-polymerase can adenylate the host miRNAs and subsequently trigger their degradation (Backes et al., 2012; Katoh et al., 2009). The exact molecular mechanism that could differentiate

between these two very different outcomes of miRNA adenylation remains unknown.

Apart from tailing, three other mechanisms acting on the precursor miRNA were identified (Krol et al., 2010b). One of the mechanisms involves the editing of adenosine to inosine within the stem of precursor miRNA, as previously shown with thin-layer chromatography *in vitro* and primer extension analysis *in vivo* for precursors of miR-142 (Yang et al., 2006). *In vitro* processing assays indicated that Adenosine Deaminases acting on RNA 1 and 2 (ADAR1, ADAR2) are the enzymes responsible for the reaction, which was further supported by the fact that ADAR-1 null or ADAR2 null mice have increased levels of miR-142.

The other mechanism involves recruiting the BCDIN3D enzyme, which is a methyltransferase that belongs to the Bin3 family (Xhemalce et al., 2012). It was shown *in vitro* that BCDIN3D is able to monomethylate the 5'-end of pre-miR-145, rendering it a poor substrate for Dicer processing. Moreover, qRT-PCR and northern blots confirmed that RNAi of BCDIN3D leads to increased levels of miR-145 but not pre-miR-145, suggesting that this modification is acting post-transcriptionally. Interestingly, a genome-wide study of MCF-7 cells showed that knockdown of BCDIN3D affected a wide pool of pre-miRNAs and caused both an increase and decrease of certain miRNAs.

Finally, endoribonucleases like MCP-induced protein 1 (MCPIP1) and Ser/Thr protein kinase/endoribonuclease Ire1α were shown to cleave within the terminal loops of several pre-miRNAs, for example pre-miR-146a and pre-miR-17, resulting in lowered mature miRNA levels *in vivo* (Suzuki et al., 2011; Upton et al., 2012). Other studies showed that the stability of mature miRNAs could be regulated through various exonucleases. This in turn can modulate the functionality of the miRISC complex. However, the mechanisms regulating the specificity of degradation mediated by XRN-1, XRN-2 PNPT1 or ERI1 for instance, as well as the mechanisms of unloading mature miRNA from the miRISC complex remain unknown (Chatterjee and Grosshans, 2009; Das et al., 2010; Krol et al., 2010a; Ramachandran and Chen, 2008; Thomas et al., 2012).

1.2 The role of Lin28 in miRNA biogenesis

Cell Lineage Abnormal 28 (Lin28) is one of the best-studied proteins in respect to its role in regulating miRNA biogenesis. It is very well conserved across many species and was first described in *C. elegans* where mutations of the protein caused defects in developmental timing and accelerated the differentiation of several types of cells (Moss et al., 1997). Expression profiling in *C. elegans*, *D. melanogaster, X. laevis* and *H. sapiens* showed that Lin28 is abundantly expressed during the embryonic stage and its expression is gradually restricted with lineage progression (Darr and Benvenisty, 2009; Moss and Tang, 2003; Seggerson et al., 2002).

Lin28 has two paralogues, Lin28a and Lin28b, which in humans share around 50% sequence identity (EMBOSS, (Rice et al., 2000)). Many studies have associated both Lin28a and Lin28b proteins with the regulation of miRNAs, post-transcriptional RNA processing and the translational repression of mRNA (Mayr and Heinemann, 2013). Both of the paralogues share very similar protein domain arrangements. Two RNA binding domains essential for the protein activity are N-terminal Cold Shock Domain (CSD) and C-terminal Zinc-finger domain (ZnF), which contain two consecutive retroviral CCHC zinc knuckles (Nam et al., 2011) (Figure 1-5). Additionally, Lin28b contains an N-terminal putative bipartite Nucleolar Localisation Signal (NLoS) and C-terminal Nuclear Localisation Signal (NLS) (Piskounova et al., 2011). Therefore, Lin28 proteins can access their targets in both the cytoplasm and nucleus to execute their functions.

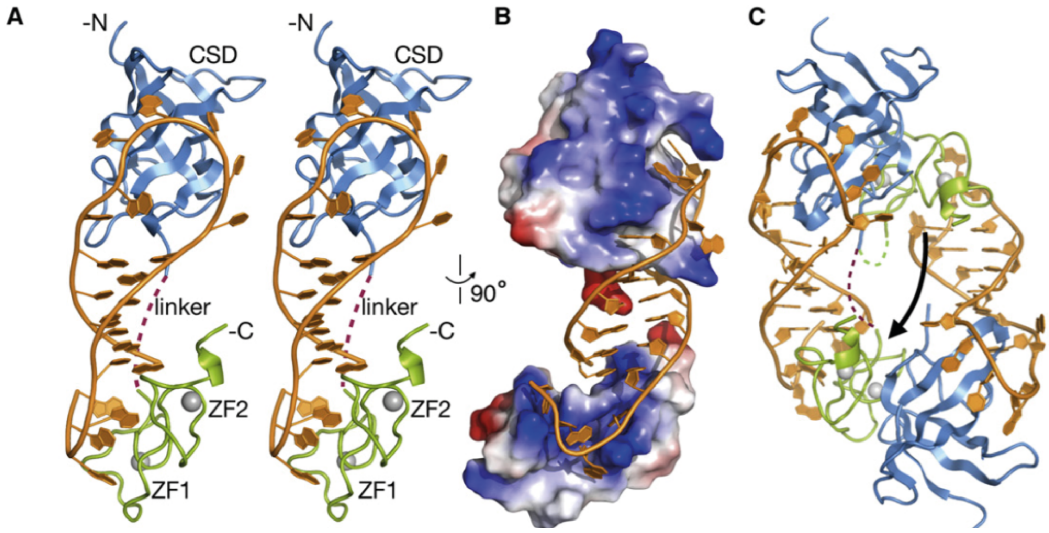

Figure 1-5 Structure of the Lin28:PreEm-*let7d* complex
Cartoon representations were colored by domain: blue, CSD; green, CCHCx2; gray, zinc; orange, RNA.

(A) Stereo representation of the monomeric complex. Interdomain linker is represented by a purple dotted line.
(B) Same complex in (A) represented with surface colored by electrostatic potential and rotated.
(C) Domain-swapped dimer. Arrow points from the domain-swapped to the biologically relevant CCHCx2 domain. Linker connecting swapped domains is marked in green, dotted line. Linker connecting unswapped domains is marked in purple, dotted line.

Reprinted from the article of Nam and colleagues "Molecular basis for interaction of let-7 microRNAs with Lin28." Permission obtained from Cell – licence number 3774090155352.

1.2.1 Implications to let-7 levels

The implications of Lin28 on the regulation of let-7 have been very well studied. Expression levels of both molecules display mutually exclusive patterns during cellular differentiation and development (Moss and Tang, 2003). In *C. elegans*, it was shown that Lin28 is expressed in the embryo and through the larval stages until day 20. In contrast, probing for let-7 and its precursors with northern blot showed that pri-let-7 is expressed from early developmental stages, peaking at day 8-10. Interestingly, levels of mature let-7 and pre-let-7 are not observed prior to day 20 (Van Wynsberghe et al., 2011). Immunoprecipitation assays showed that Lin28 associated co-transcriptionally with pri-let-7. Moreover, *C. elegans Lin28-null* mutants expressed mature let-7 ten days earlier, proving the role of Lin28 in repressing let-7 (Van Wynsberghe et al., 2011). In a similar

fashion, using a neuronal differentiation model of human embryonic stem cells, it was shown that miR-125 and let-7 are highly expressed in differentiated neuronal stem cells, but the expression of let-7 during the embryonic state is inhibited. This was mechanistically explained by the autoregulatory circuit activated during the differentiation steps and involving miR-125 and let-7 driven inhibition of Lin28 expression. Thus, Lin28 knockdown in undifferentiated cells release the blockage of pre-let-7 processing (Rybak et al., 2008). Furthermore, mass spectrometry analysis of the proteins associated with the let-7 precursor identified Lin28 as a putative member of the complex, providing additional evidence for its direct involvement (Newman et al., 2008; Viswanathan et al., 2008).

Two possible scenarios were proposed to regulate let-7 levels. The first relies on competition between Lin28 and the miRNA processing machinery. In his work, Newman and colleagues used cell extracts from teratocarcinoma P19 cells, a model cell for neuronal differentiation, to show that processing of pri-let-7 to pre-let-7 is significantly inhibited. Further, mutagenesis of several regions within the pri-let-7 terminal loop increased let-7 processing. UV-crosslinking of undifferentiated P19 cells, followed by immunoprecipitation, showed that Lin28 was bound to pri-let-7. Furthermore, using specific terminal loop competitors, they showed that this interaction occurred in the evolutionarily conserved regions of the loop (Newman et al., 2008). RNAi knockdown and overexpression of Lin28 were shown to release the processing blockage and decrease levels of pre-let-7, respectively. This study speculated that the potential mechanism of this inhibitory action could be direct competition with the microprocessor machinery or a sequestration mechanism.

Subsequently, other groups independently reported Zinc Finger CCHC Domain-Containing Protein 11 (Zcchc11), also known as Terminal Uridylyltransferase 4 TUT4, to be a factor that mediates cytoplasmic poly-uridylation of pre-let-7 leading to its degradation (Hagan et al., 2009; Heo et al., 2009). Moreover, they used global miRNA profiling to show that the depletion of TUT4 almost exclusively affected the let-7 family of miRNAs. Heo and colleagues showed that a mutation in the Lin28a ZnF abolished uridylation of pre-let-7 but did not affect binding of the mutant to the

RNA (Heo et al., 2008). Previously, it was shown that the "GGAG" motif is a target for CCHC-Zinc finger domains and it was confirmed to be the key sequence within the pre-let-7 terminal loop. In his work, Heo and colleagues generated several mutants of pre-miR-16 with an artificial "GGAG" sequence. Interestingly, only one mutant was uridylated, which raised the possibility that additional molecular mechanisms restrict uridylation to a selected subset of pre-miRNAs, including pre-let-7. Indeed, in work from our group, Roy Choudhury and colleagues used pull-downs and mass spectrometry to identify the E3 ligase Trim25 to associate with pre-let-7 and act as a Lin28/TUT4 co-factor during the uridylation reaction (Choudhury et al., 2014).

Poly-uridylation of pre-let-7 was shown to be an essential mechanism that mediates degradation of the precursor in undifferentiated ES cells (Chang et al., 2013). Pull-downs of protein complexes and subsequent mass spectrometry of peptides allowed two groups to determine that mammalian 3′-5′ Dis3l2 Pearlman syndrome exonuclease is involved in the degradation of poly(U)-pre-let-7 (Chang et al., 2013; Ustianenko et al., 2013). Additionally, *in vitro* reconstitution cleavage assays as well as siRNA knockdown of Dis3l2 further verified the role of the RNA exonuclease in the degradation of pre-let-7 and the poly(U)-tail as its decay signal in embryonic cells.

Additionally, Lin28a was shown to inhibit pre-let-7 processing in the cytoplasm not only through its degradation via the Trim25/TUT4/Dis3l2 pathway but also by direct competition with Dicer to the pre-let-7 terminal loop (Lightfoot et al., 2011). In their work Lightfoot and colleagues showed that Lin28a binding to pre-let-7g induced relaxations of the double-stranded RNA region adjacent to the terminal loop (Lightfoot et al., 2011). In particular, the base-paired nucleotides U21 and U22 in the stem together with the stacked U23 base from the adjacent terminal loop displayed around a 3-fold increase in RNAse I enzymatic cleavage sensitivity. Furthermore, Dicer cleavage assays confirmed that this melting interfered with the binding of Dicer and the subsequent processing of pre-let-7g, which was verified using an open-conformation mutant of pre-let-7g (Lightfoot et al., 2011).

In other work, Piskounova and colleagues suggested that Lin28a and Lin28b act through independent molecular mechanisms. In a series of immunoprecipitation assays, they found that Lin28a but not Lin28b associates with Zcchc11 (TUT4) (Piskounova et al., 2011). Moreover, RNAi knockdown of Zcchc11 in a panel of cells suggested differential outcome on let-7 levels depending on the type of Lin28 expressed in these cells. Cells expressing Lin28a but not Lin28b had elevated levels of let-7 upon knockdown of both Zcchc11 and Lin28a, resulting in increased levels of let-7. In contrast, cells expressing Lin28b but not Lin28a had increased levels of mature let-7 upon knockdown of Lin28b but not Zcchc11 (Piskounova et al., 2011). The authors suggest that these different observations could be accounted for by the distinctive subcellular localisation of Lin28a and Lin28b. In fact, as mentioned above, Lin28b contains two domains that are absent in Lin28a that could be responsible for its localisation. Using microscopy and various mutants of Lin28b, they showed that this protein paralogue localises to the nucleolus of the cell. Furthermore, this Lin28b localisation allowed for its compartmentalisation away from the microprocessor machinery (Piskounova et al., 2011). This study, together with the findings of Newman and colleagues, suggests that Lin28b inhibits pri-let-7 processing in the nucleus by sequestering it from Drosha and the processing machinery.

1.2.2 Effect of Lin28-mRNA interaction on protein translation

As mentioned above, Lin28 contains two very potent RNA binding domains. Therefore it is very likely that it also will interact with other RNA molecules. Bearing that in mind, Cho and colleagues carried out cross-linking immunoprecipitation RNA-sequencing (CLIP RNA-seq) and ribosomal footprinting and found that the majority of Lin28a targets are mRNA molecules (Cho et al., 2012). They were also able to show that in most cases the interaction of Lin28a with the mRNA lead to translational suppression. Building a similarity network, they identified purine-rich hexamers “AAGNNG”, “AAGNG(N)”, and “(N)UGUG(N)” as the most common Lin28a binding sites. Gene Ontology analysis showed strong

clustering of several groups related to integral membrane proteins, secretory proteins and Endoplasmic Reticulum (ER) or Golgi apparatus proteins. These proteins are known to be translated by ER-bound ribosomes and undergo co-translational ER translocation. For instance, mRNAs of integral membrane proteins were found to interact 4- to 6-fold stronger with Lin28a than other mRNAs. However, they have not found significant enrichment of Lin28a binding motifs in ER-associated mRNAs compared to non-ER-associated mRNAs. They resolved this confusing finding by performing microscopy studies of sub-cellular Lin28a localisation. From this experiment, it was concluded that Lin28a localises in close vicinity to the ER and therefore interacts more strongly with mRNAs that are destined to the ER for completion of their translation (Cho et al., 2012).

Interestingly, another group found that Lin28a associates with the translational initiation complex (Polesskaya et al., 2007). They found that associated in the complex with Lin28a were the poly(A)-binding protein, 5′ cap-binding protein, nucleolin, hnRNP-F, H1, and IGF-2 mRNA-binding proteins (IMPs) 1, 2, and 3, as well as structural ribosomal proteins, eIF3β translation initiation factor, and elongation factors (EF1-α and EF1-α2) (Polesskaya et al., 2007). Moreover, using the sucrose gradient, they were able to show that Lin28a sedimented together with other components of active polysomes. In addition, immunoprecipitation following RNAse treatment validated that the interaction between EF1-α and Lin28a is direct and microscopy studies confirmed that these two proteins co-localise in differentiated myoblasts and P19 cells. It was also shown that one of Lin28a's targets is the Igf22 mRNA. Its levels are post-transcriptionally regulated via a Lin28a-mediated increase in the number of translational initiation events reflected by an increase in the number of ribosomes per Igf2 mRNA molecule (Polesskaya et al., 2007).

In a similar fashion, using Flag-tagged Lin28a, Xu and colleagues showed that Cdk4 and cyclin B mRNAs exhibited the most dramatic enrichment in the immunoprecipitated complexes, followed by cyclin A mRNA, Oct4, cdk6, and cyclin D mRNAs (Xu et al., 2009). Moreover, transient transfection of Lin28a or its RNAi-mediated knockdown confirmed that

the levels of these proteins were either upregulated or downregulated, respectively. These changes at the protein levels did not correspond to the changes of individual mRNAs as they were shown by qRT-PCR to remain stable. Furthermore, using gene reporter assays with 3'-UTRs of the regulated mRNAs they were able to conclude that the observed mechanism was similar to the stimulation of translation initiation of Igf2 (Xu et al., 2009).

Further evidence for a positive role of Lin28a in initiation of translation came from the work by Xu and colleagues. They were interested specifically in the possibility of Lin28a binding to replication-dependent histone mRNAs. Using radiolabelled mRNA of core histones (H2a, H2b, H3 and H4) and UV-crosslinking combined with competition assays, they showed that Lin28a interacts specifically with H2a. Additional gene reporter assays with a synthetic construct containing H2a 3'UTR and several mutants allowed the conclusion that two or more Lin28a binding motifs are required for enhanced regulation (Xu and Huang, 2009).

1.2.3 Functional importance of the regulatory role of Lin28

Lin28 was previously shown to be associated with several processes important for tissue homeostasis, including cell growth, differentiation and proliferation, as well as glucose metabolism (Polesskaya et al., 2007; Qiu et al., 2010; Xu and Huang, 2009; Xu et al., 2009; Zhu et al., 2011). Given the high abundance of Lin28 binding motifs across mRNA and miRNAs, it is very likely that more functions still remain unknown. Expression of Lin28a was shown to be particularly high in embryonic stem cells where it is required for maintenance of the pluripotent state and cell proliferation (Darr and Benvenisty, 2009; Moss and Tang, 2003; Qiu et al., 2010; Yu et al., 2007; Zhu et al., 2011). One of the possible mechanisms involves the regulation of Oct-4, a very well conserved POU-transcription factor and regulator of cell fate (Pei, 2009). A two-fold increase in Oct-4 directs cells towards the mesoderm and endoderm whereas its reduction points differentiation towards the trophectoderm, suggesting the existence of very precise regulatory mechanisms (Niwa et al., 2000). Moreover, Oct-4 was shown to be a key pluripotency factor and was demonstrated to be

necessary and sufficient to reprogram mouse adult neuronal stem cells to pluripotency (Kim et al., 2009). Qiu and colleagues used Lin28a immunoprecipitation (IP) of protein-RNA complexes followed by qRT-PCR as well as UV-crosslinking experiments to show that Lin28a binds directly to the Oct-4 mRNA *in vivo*. Loss-of-function experiments showed that a reduction in Lin28a leads to lower Oct-4 levels. IP of polysomes verified that the regulation of Oct-4 is achieved through translational activation. In fact, Lin28a was shown to act via RHA (also called DHX9) a conserved DEAD-box protein that functions in multiple cellular processes, including transcription, splicing, nuclear export, translation, and RNAi, by catalysing RNA–RNA and RNA–protein rearrangements in RNP complexes (Bleichert and Baserga, 2007). Furthermore, Lin28 was also shown to regulate other factors required for cell growth and proliferation. It has been demonstrated that higher Lin28a levels result in a 30% increase in ES cell numbers, while siRNA-mediated reduction of its levels corresponds to around 25% decrease in ES cell numbers. Moreover, BrdU incorporation and FACS sorting showed that endogenous Lin28a facilitates the progression of cells from S to M/G_2 phase, which could accelerate proliferation (Xu et al., 2009). Similar findings were obtained from muscle myoblasts where increased levels of Lin28 resulted in increased muscle differentiation, contrary to a reduction of the protein which resulted in the decreased efficiency of differentiation (Polesskaya et al., 2007).

Lin28/let-7 axis was also suggested to play a role in glucose metabolism via mechanism that targets several components of the PI3K-mTOR pathway (Zhu et al., 2011). Two inducible Lin28a and Lin28b mouse models individually demonstrated that ectopic expression of Lin28a/b allowed for more efficient metabolism of glucose. Induction of either protein in transgenic mice resulted in glucose metabolism that was four times faster, measured as a concentration decrease in blood during the twelve days after the diet commenced. Moreover, Lin28a knockout in mice caused growth defects and glucose metabolism intolerance. This study showed that these observations could be accounted for by Lin28a/b

regulation of let-7 and subsequent de-repression of let-7 targets, including members of the PI3K-mTOR pathway. Interestingly, similar effects to loss of Lin28a or overexpression of let-7 were observed using rapamycin - an mTOR pathway inhibitor (Zhu et al., 2011). In another study, Zhu and colleagues showed that Lin28a transgenic mice manifested increased body-size and crown-rump length, as well as delayed onset of puberty, findings that also relied on the Lin28-let-7 regulatory pathway (Zhu et al., 2010).

Involvement of Lin28 in cell cycle regulation and proliferation made this protein an interesting candidate to study in cancer biology. Importantly, Lin28a/b reactivation was observed in various malignancies, which suggested its role as an oncogene (Viswanathan et al., 2009). As a result, depletion of let-7 in nude mice resulted in tumour formation (Chang et al., 2009b; Viswanathan et al., 2009). This is most likely a result of de-repression of let-7 targets like c-myc, N-RAS, NF-κB and Il-6 that are well-known oncogenes (Iliopoulos et al., 2009). Finally, it was suggested that re-activation of Lin28a/b is correlated with tumour aggressiveness and its advanced stages (Viswanathan et al., 2009; Yang et al., 2010).

1.2.4 Structural determinants for Lin28 action

Both Lin28 paralogues contains two RNA-binding domains essential for protein function (Piskounova et al., 2008). Using EMSA of pre-let-7 with the wild-type and point-mutants of Lin28a, it was shown that both domains support pre-let-7 binding. Specifically, substitutions of F47A and F73A within the Cold-Shock Domain (CSD) and C161A in Cys-Cys-His-Cys (CCHC) within the Zn-Finger Domain (ZnFD) abolished this interaction (Piskounova et al., 2008). However, Graf and colleagues applied individual domain PAR-CLIP (iDo-PAR-CLIP) to characterise the sequence-specificity of the individual domains in their binding to mRNA (Graf et al., 2013). They determined that GGGAG is the lead sequence that is recognised by the CCHC ZnFD where the CSD is bound to less specific U-rich stretches within the pre-let-7 hairpin.

1.2.4.1 Role of the zinc-knuckle domain in substrate recognition and uridylation

Upon interaction with pre-let-7, the second CCHC ZnFD undergoes a large conformational twist with 25Å transition of chelated Zn^{2+}(Loughlin et al., 2012; Nam et al., 2011). Characteristic within the CCHC domain is a Pro-rich linker and its Pro158 undergoes a 130° rotation that greatly contributes to the overall transition of the ZnFD. Structural studies also showed that each CCHC domain interacts specifically with the first (G1) and fourth (G4) guanosine of the GGAG motif by sequence-specific hydrogen bonds to the nucleobases (Mayr et al., 2012). Moreover, apart from the formation of hydrogen bonds, G1 and G4 were also shown to be placed in a hydrophobic pocket formed by the conserved Tyr and His residues of the first CCHC and His and Met residues of the second CCHC (Nam et al., 2011).

Interestingly, mLin28a and hLin28a displayed certain differences in the mode of binding to the terminal loop. In the mLin28a:GGAG complex, it was shown that the G2 residue also interacts with the A3 residue which contributes to the formation of a strong kink within the RNA-backbone and allowing an additional interaction between A3 and G1 (Nam et al., 2011). This could explain the potential molecular mechanism by which Lin28 interferes with Dicer processing. However, such strong bending of the terminal loop was not observed in the case of the hLin28a:GGAG complex, which stayed in a more open conformation (Mayr et al., 2012; Nam et al., 2011).

1.2.4.2 Implications of the Cold Shock Domain's role in structural rearrangement of RNA

The second RNA-binding domain (RBD) that is important for the interaction between Lin28 and the pre-let-7 terminal loop is the Cold Shock Domain (CSD). CSDs are very broadly distributed RBDs, across several kingdoms, and contribute to many processes related to RNA-metabolism (Mihailovich et al., 2010).

Mayer and colleagues performed systematic analysis of *Xenopus* Lin28b CSD-binding specificity and they showed that this CSD has highest

affinity towards pyrimidine-rich RNA octamers that has at least one guanosine at the 5′ flank (Mayr et al., 2012). Other groups who used PAR-CLIP and genome-wide approach to analyse Lin28 binding motifs validated these findings. In general, CSD-specific motifs were located upstream of ZnFD "GGAG" motifs, suggesting a fixed arrangement of Lin28's domains on its targets (Graf et al., 2013).

Co-crystal studies of Lin28 with the pre-let-7 terminal loop showed substantial differences between ZnFD and CSD modes of binding. The CSD proved to be more rigid and only subtle changes were allowed during the formation of the complex (Mayr et al., 2012). The association of Lin28a with ssRNA was dominated by π-stacking interactions between the RNA molecule and the aromatic residues of the CSD-binding platform. In particular, the Lin28 CSD binding platform was determined to bind up to 8-nucleotides organised in a curved single-stranded stretch with a defined orientation (Nam et al., 2011). Moreover, Mayer and colleagues showed that the specificity of interaction is mainly achieved via interaction with the sixth nucleotide of the octamer. A Lys-Asp salt bridge present in the vicinity was shown to limit the flexibility and size of a binding pocket at that position, contributing to the formation of a hydrogen bond with Uracil (Mayr et al., 2012; Nam et al., 2011). However, the nature of the π-stack interactions was suggested to play an essential role in the recognition of a broader group of targets compared to ZnFD (Mayr et al., 2012).

Importantly, aside from its binding affinity, the Lin28 CSD domain was suggested to play an important role in remodelling of the secondary structure of target RNAs. Nam and colleagues showed that the CSD was able to partially melt dsRNA to achieve proper binding properties (Nam et al., 2011). Previous enzymatic footprinting studies also showed that upon Lin28a binding pre-let-7g was more susceptible to RNAse I cleavage, a pattern which is characteristic for ssRNA (Lightfoot et al., 2011). Furthermore, using point-mutants of Lin28a, it was shown that the CSD binds the terminal loop introducing secondary structure rearrangements that facilitates the subsequent binding of the ZnFD to the "GGAG" motif.

(Mayr et al., 2012). This co-operative binding hypothesis is strongly supported by genome-wide studies showing that the majority of Lin28 motifs are buried in stable secondary structures (Cho et al., 2012; Hafner et al., 2013).

1.3 The role of miRNAs in the development and pathogenesis of the nervous system

miRNA-mediated repression of gene expression plays an essential role during early animal development and adulthood. The brain is one of the tissues that display an extraordinary level of complexity, achieved by a multitude of orchestrated cellular programmes. Approximately 70% of experimentally detectable miRNAs are expressed in the human nervous system and, by regulating the production of thousands of genes, they ensure the complex development and function of this elusive organ (Cao et al., 2006).

Surprisingly, only a handful of miRNAs are expressed in a brain-enriched or brain-specific manner (Landgraf et al., 2007). Despite this, the time-dependent accumulation of some ubiquitously expressed miRNAs is essential for proper neurogenesis. Several well-studied examples have been reported on how miRNAs can regulate the function of the nervous system at various stages of development, starting from embryonic neurogenesis to synaptogenesis and synaptic plasticity in adults.

Moreover, it has also been shown how disruptions of global or discrete profiles in miRNA networks may lead to aberrant development and various neurological disorders.

1.3.1 The role of miRNAs in neuronal differentiation

1.3.1.1 let-7

At the early stages of neuronal differentiation, Lin28a and Lin28b inhibit the maturation of miRNAs from the let-7 family (Wulczyn et al., 2007). Subsequently, low levels of Lin28 allow let-7 miRNAs to be expressed in embryonic and adult brains (Piskounova et al., 2011). The role of let-7 in inducing the maturation of neuronal progenitor cells into early neurons can be explained by several mechanisms (Nishino et al., 2008). One mechanism involves the interaction of Ago1/let-7 with the NHL domain of TRIM32 (tripartite motif-containing protein 32) (Schwamborn et al., 2009). This complex facilitates the asymmetric division of neural progenitor cells by activation of let-7 and ubiquitin-mediated degradation

of the transcription factor c-Myc (Schwamborn et al., 2009). An alternative mechanism suggests that let-7 acts as a suppressor of Tlx and cyclin D1 expression (Zhao et al., 2009). These proteins are important in regulation of neuronal stem cell proliferation and differentiation, by the recruitment of histone deacetylases to genes encoding cyclin-dependent kinase inhibitor (p21) and PTEN (phosphatase and tensin homologue deleted on chromosome 10) (Shi et al., 2004). Both of the above examples highlight the importance of co-ordinated expression and maturation of let-7.

1.3.1.2 miR-9 and miR-124

miR-9 and miR-124 display a brain-specific expression pattern and have a crucial role in neuronal development (Krichevsky et al., 2006). mir-9 is expressed from three different loci, pri-miR-9- 1, pri-miR-9-2 and pri-mR-9-3, which are highly conserved at the nucleotide level. Interestingly, miR-9 displays a diverse expression profile within the nervous system across different species (Leucht et al., 2008; Li et al., 2006; Shibata et al., 2008). In *Drosophila,* miR-9 has been suggested to repress the transcriptional activator senseless in selected maturating neurons and developing sensory organ precursors (Li et al., 2006). In the zebrafish nervous system, *miR-9* is linked with the development and maintenance of the MHB (midbrain–hindbrain boundary), one of the central organisers of the vertebrate CNS (central nervous system) (Wurst and Bally-Cuif, 2001). The suggested mechanism of miR-9's role in the formation of the MHB involves the repression of neuron production via inhibition of the mammalian transcription factor Hes orthologues Her-5 and Her-9 (Leucht et al., 2008). Furthermore, miR-9 was shown to interfere with the signalling cascade of the Fgf8 (fibroblast growth factor 8) molecule (Leucht et al., 2008). This signalling pathway was previously shown to be important during neural plate patterning and the development of the MHB (Wurst and Bally-Cuif, 2001). Interestingly, it has been proposed that miR-9 regulates the neurogenesis of the mouse telencephalon by orchestrating the adjustments of a network of transcription factors rather than by the strong inhibition of individual elements (Shibata et al., 2011). In human neuronal progenitor cells, miR-9 regulates proliferation and migration by targeting *Stathmin*, a

gene implicated in the regulation of microtubule assembly (Delaloy and Gao, 2010). Similarly to let-7, miR-9 was also suggested to suppress the function of Tlx and leads to the inhibition of neuronal stem cell proliferation, resulting in enhanced neuronal differentiation (Zhao et al., 2009).

Like miR-9, miR-124 is expressed from three different loci (pri-miR-124-1, pri-miR-124-2 and pri-miR-124-3) and is limited to the nervous system and is implicated in neurogenesis. One suggested mechanism indicates a link between miR-124 and PTBP (polypyrimidine-tract binding protein) (Cao et al., 2006; Makeyev et al., 2007). PTBP is a RNA-binding protein that exerts a variety of functions that are important in RNA metabolism (Dreyfuss et al., 2002). Previous studies have shown that the PTBP function differs among various cell types depending on which isoform and splice variant is expressed (Romanelli et al., 2000). It has been shown that miR-124 regulates neurogenesis by reducing levels of non-neuronal PTBP-1, a global repressor of alternative splicing in non-neuronal cells. One of the targets of PTBP-1 is an exon of neural-specific PTBP-2. Therefore, miR-124 mediated downregulation of PTBP-1 leads to the direct activation of a neural-specific PTBP-2 variant (Makeyev et al., 2007). Similarly to miR-9, proper co-ordination of Lin28a's neurogenesis driven by the miR-124 is complex and many targets for miR-124 have been identified (Fowler et al., 2011; Visvanathan et al., 2007).

Co-ordination of neuronal development is mainly driven by chromatin-mediated regulation of multiple genes. The REST [RE1 (repressor element 1)-silencing transcription factor]/NSRF (neuron-restrictive silencer factor) complex is a suppressor of neurogenesis in non-neuronal cells and its major function is to bind RE1 at neuronal gene loci and further recruit the co-repressor complex containing histone deacetylases and MeCP2 (methyl CpG-binding protein 2) (Huang et al., 1999). It has been shown that *miR-124* contributes to the down-regulation of several components of the REST/NSRF complex by targeting the expression of SCP1 (small C-terminal domain phosphatase 1), MeCP2 and CoREST (co-RE1-silencing transcription factor) (Visvanathan et al., 2007). Interestingly, REST also regulates the expression of miR-124 via RE1 in all three genomic pri-miR-

124 loci, suggesting that a feedback loop generated between miR-124 and the REST function is important for proper neuronal development (Conaco et al., 2006).

miR-9 and miR-124 have been shown to co-operate during neurogenesis by regulating the stage-specific activity of the chromatin-remodelling enzyme BAF (Brahma-associated factor) complex (Ho and Crabtree, 2010). The BAF complex displays its function during neuronal specification depending on its subunit composition, which is remodelled during the course of maturation. The BAF53a subunit is associated with the complex during the neuronal progenitor phase and becomes replaced by BAF53b at the post-mitotic neuronal stage. It has been shown that BAF53a represses expression of BAF53b during neurogenesis (Ho and Crabtree, 2010). However, during progression through neuronal maturation, REST-mediated repression of miR-9 and miR-124 is disrupted. It has been suggested that up-regulation of these miRNAs inhibits BAF53a translation, allowing the BAF53b subunit to enter the BAF complex (Ho and Crabtree, 2010). Finally, miR-9 and miR-124 alone displayed the capacity to transform adult fibroblasts into neurons (Yoo et al., 2011), proving their role as master regulators of neuronal development.

1.3.2 Role of miRNAs in synaptic plasticity and adult neurogenesis

The regulation of adult neurogenesis and synaptic plasticity has also been linked with various miRNAs (Shi et al., 2010). The architecture of fully matured neurons, with protrusions leading from cell bodies to synapses, suggests that local regulation of miRNA levels could play an important role during adaptation to environmental stimuli. In line with this hypothesis, miR-134, miR-132, miR-212 and miR-485 were reported to have a function in the regulation of local translation, which shapes long-term synaptic plasticity (Shi et al., 2010).

1.3.2.1 miR-132 and miR-212

LTP (long-term potentiation) or LTD (long-term depression) have been linked with instant changes in miRNA levels in the adult mouse hippocampus (Park and Tang, 2009). These changes triggered temporal mRNA expression profiles that differed between these two forms of

activities (Park and Tang, 2009). LTD activity mediated via GluRs (glutamate receptors) in the adult hippocampus was shown to cause spikes of miR-132 and miR-212 expression (Wibrand et al., 2010). Knockout of miR-132/miR-212 resulted in deleterious alterations of dendrites (Magill et al., 2010). Moreover, miR-132 has also been shown to regulate synaptic plasticity through NMDAR (*N*-methyl-D-aspartate receptor)-mediated LTP via a mechanism that involves the regulation of various downstream signalling events, remodelling of the actin cytoskeleton and voltage-dependent Ca^{2+} influx (Cull-Candy et al., 2001). Furthermore, it has been demonstrated that miR-132 interacts with FMRP (fragile X mental retardation protein), which can potentiate its role during development and neuronal function (Edbauer et al., 2010).

1.3.2.2 miR-134 and miR-138

Other miRNAs that play important roles in synaptic plasticity include miR-134 and miR-138. The former was shown to be involved in the processes of cytoskeletal rearrangements and transcriptional regulation of genes involved in neurogenesis (Sakamoto et al., 2011). miR-134 is suggested to target Limk1 (LIM domain kinase 1), a known regulator of actin filament growth, thus displaying potential to control the dynamics of spine development. Inhibition of this miRNA resulted in an increase in dendritic spine growth in rats (Schratt et al., 2006). The inhibitory effect of miR-134 on Limk1 expression is abolished by BDNF (brain-derived neurotrophic factor) which helps to maintain correct levels of Limk1 during neuronal development. Furthermore, miR-134 was shown to inhibit BDNF both *in vivo* and *in vitro* concomitantly with CREB (cAMP-response-element-binding protein), a transcription factor involved in both neurogenesis and synaptic plasticity (Sakamoto et al., 2011; Schratt et al., 2006). Moreover, plasticity defects were observed upon knockdown of NAD-dependent histone deacetylase SIRT1 (sirtuin 1) in the mouse brain. SIRT1 binds to DNA-regulatory elements upstream of the miR-134 locus inhibiting its expression and therefore allowing the expression of CREB, BDNF and Limk1, as well as other targets of miR-134 involved in synaptogenesis and plasticity formation (Schratt et al., 2006).

miR-138 has been found in the dendrites of rat hippocampal neurons where it regulates dendrite spine morphogenesis (He et al., 2007). The suggested mechanism involves *miR-138*-mediated local inhibition of APT1 (acyl protein thioesterase 1) (Siegel et al., 2009). Post-translational modifications of APT1 regulate association of small G-protein subunits within the cell membrane, a process that could significantly alter the activity of various cellular receptors. It has been shown that expression of miR-138 results in shrinkage of GluR-containing AMPAR (α-amino-3-hydroxy-5-methylisoxazole-4-propionic acid receptor) clusters and subsequently alters the amplitude of postsynaptic currents at excitatory synapses (Siegel et al., 2009).

All of the above examples demonstrate the importance of miRNAs at various stages of neuronal development. Their involvement in the processes related to the early stages of neurogenesis, as well as the regulation of the synapse morphogenesis, underline the detrimental consequences that could result from the disruption of miRNA levels during development and maintenance of the nervous system.

1.3.3 A link between miRNAs and selected neurological disorders

Perturbations of neurogenesis and adult neural function are primary triggers of neurological disorders. Therefore, disruption of the neuronal miRNA network has the potential to lead to various pathologies of the nervous system. Although some genetic studies have shown the involvement of miRNAs in Alzheimer's disease, Parkinson's disease, schizophrenia and other diseases, the detailed molecular basis of their action remain largely unknown (Beveridge et al., 2008; Maes et al., 2009).

1.3.3.1 Global disruption of miRNA function

DGS (DiGeorge syndrome) and FXS (fragile X syndrome) exemplify neurological disorders that are associated with a general role for miRNAs. The clinical manifestations of DGS are linked to cognitive and behavioural deficits leading to various disorders such as obsessive-compulsive disorder or autism spectrum disorder (Chang et al., 2009a). The pathogenesis of DGS is the result of a common 3 Mb chromosomal deletion of a region on chromosome 22 (Chang et al., 2009a). Detailed analysis has revealed that the *DGCR8* (DiGeorge syndrome critical region gene 8) gene lies within the deleted region (Chang et al., 2009a). The product of this gene is a component of the Microprocessor complex, which, together with the ribonuclease Drosha, mediates nuclear miRNA maturation. A mouse model of the 22q11 deletion showed the abnormal levels of the mature miRNA fraction in the brain of the animals with this chromosomal aberration (Stark et al., 2008).

FXS was the first disorder to be linked with miRNA functions. Individuals suffering from FXS present with learning disabilities as well as cognitive and intellectual impairments (Chang et al., 2009a). Genetic analysis revealed the molecular basis of the FXS syndrome as expanded CGG trinucleotide repeats in the 5′-UTR (untranslated region) of the FMR1 (fragile X mental retardation 1) gene, which cause instability of the gene locus as well as the inhibition of FMR1 expression. The product of the gene is FMRP, a small conserved RNA-binding protein implicated in translational repression (Chang et al., 2009a). FMRP has been suggested to

bridge miRNAs and their target mRNA to guide the miRNA–miRISC (miRNA-induced silencing complex) complex to facilitate its function (Jin et al., 2004). One model of FXS suggests that loss of FMRP results in the disruption of miRISC-mediated repression of translation and subsequent deleterious alteration of miRNA target levels.

1.3.3.2 Individual miRNA-mediated disruption of neurogenesis

Although there have been many studies linking the role of individual miRNAs to the molecular basis of neurological disorders, it is very difficult to dissect their molecular role in the pathogenesis of these disorders, mainly due to the daunting complexity of the miRNA/mRNA network in the brain. However, there is some evidence that individual miRNAs can contribute to the pathogenesis of certain neurological disorders. For instance, down-regulation of miR-9-5p/miR-9-3p has been linked to Huntington's disease. In healthy neurons, the repressive function of the REST–CoREST repressor complex is abolished by its binding to huntingtin and its subsequent transfer to the cytoplasm. In Huntington's disease patients, polyglutamine expansion of huntingtin abrogates its binding to the co-repressor complex, which remains active and represses many genes involved in the early stages of neurogenesis, including miR-9-5p/miR-9-3p (Packer et al., 2008). In another example, miR-124 was linked with disrupted dendrite branching in the pathogenesis of FXS. Interestingly, it was suggested that dFMR1 (*Drosophila* FMR1) assists in the biogenesis of miR-124 (Chang et al., 2009a). Indeed, it has been shown that ectopic expression of miR-124 results in modulation of dendrite branching and this effect was disrupted by the loss of dFMR1 (Chang et al., 2009a). Further evidence, based on individual miRNA gene knockouts and transgenic animals, is still needed to prove a direct role for these miRNAs in neuronal disorders.

1.3.3.3 miRNA-mediated disruption of neuron maturation and synaptogenesis

Some studies suggest that the disruption of certain miRNAs involved in synaptic plasticity could play a role in disorders such as Rett syndrome or schizophrenia. Rett syndrome represents a severe autism spectrum

disorder in which inefficient silencing of certain regions of the genome facilitated by MeCP2 leads to progression of the disease (Amir et al., 1999; Wan et al., 1999). Interestingly, it has been suggested that miR-132 can modulate the expression of MeCP2 via the BDNF–CREB feedback loop (Klein et al., 2007). This could represent a potential mechanism for maintaining certain levels of MeCP2 during development of the nervous system (Klein et al., 2007).

In patients with schizophrenia, levels of certain miRNAs involved in the development of synaptic plasticity, including miR-132, miR-181b or miR-219, are elevated in the prefrontal cortex (Maes et al., 2009; Olde Loohuis et al., 2012). It has been suggested that miR-181b can regulate the levels of the AMPAR subunit GluR2, and RNA-binding protein VSNL1 (visinin-like 1). GluR2 is involved in synaptic plasticity and regulation of excitatory potentials of neurons, whereas VSNL1 modulates neuronal maturation via targeting the BDNF signalling pathway (Olde Loohuis et al., 2012). These mechanistic insights could potentially explain how the up-regulation of miR-181b observed in schizophrenia patients can contribute to the pathogenesis of the disease (Beveridge et al., 2008).

Chapter 2

2 Materials and Methods

2.1 Cell culture and differentiation

Mouse teratocarcinoma P19 and HeLa cells were maintained in standard DMEM medium (Life Technologies), supplemented with 10% foetal bovine serum (Life Technologies). Retinoic acid-induced neuronal differentiation of P19 cells was performed as described before (McBurney, 1993). Briefly, ~12x10^6 cells were plated in a non-adhesive 100mm dish (Scientific laboratory supplies SLS2002) in DMEM supplemented with 5% serum and induced with 1μM of retinoic acid (RA). This induced the formation of embryonic bodies. After 4 days, the embryonic bodies were re-suspended in DMEM supplemented with 10% serum and re-plated in an adhesive dish. Differentiation was followed up to day 9 when cells in culture displayed neuronal-like morphology.

For SILAC Mass Spectrometry, undifferentiated cells were cultured in DMEM supplemented with [13C]Arg/[13C]Lys isotopes and differentiation was performed using DMEM supplemented with [12C]Arg/[12Lys] isotopes (Pierce SILAC Proteins Quantitation Kit – ThermoScientific).

2.1.1 Stable cell line generation

The P19 cell lines with stable Lin28a-GFP or GFP only expression were gifts from Dr Eric Moss, The University of Medicine and Dentistry New Jersey, USA (Balzer et al., 2010). Both lines were maintained in standard culture conditions. A P19 cell line expressing untagged Lin28a was developed using the Flp-in system (Life Technologies), according to the manufacturer's instructions. Briefly, the FRT site was randomly integrated in the genome and its integration was verified using Zeocin and lacZ selection markers. The Lin28a cDNA was integrated into the FRT site

using Flp-mediated recombination and the event was confirmed using hygromycin selection.

P19 stable cell line with inducible expression of Lin28a was generated using the Tet-on-3G system from Clontech. In the first step, the Tet-on-3G transactivator was integrated in P19 genome. Briefly, 2μg of CMV-Tet3G plasmid was nucleofected in P19 cells. Following the first 48hr cells were split and after additional 48hr 500μg of G418 was added. Within the first two weeks, G418-resistant colonies appeared and 24 individual clones were harvested and transferred to the individual wells of 6-well plates. In the second step, 2μg of pCMV-3G-Lin28a vector was co-nucleofected with 100ng of linearised puromycin selection marker. Following the first 48hr, cells were split and after an additional 48hr period, 500μg of puromycin was added. Within the first two weeks, G418- and puromycin-resistant P19 colonies appeared and 24 individual clones were harvested and transferred to the wells of 6-well plate. Doxocyclin (Dox) at a concentration of 1000ng/mL was then added to activate the expression of Lin28a. The induction of Lin28a was confirmed by western blot and clones expressing the protein were stored.

2.2 Transient transfection of miRNA and protein coding plasmids

The pCGT7 plasmids carrying sequences coding for the miRNAs or specified proteins were transfected into P19 or HeLa cells using Lipofectamine 2000 transfection reagent according to instructions provided by the supplier (Life Technologies). One day before transfection, cells were seeded in a 6-well plate in an amount of $2x10^5$ cells per well. This allowed over 90% confluence to be obtained on the transfection day. For single over-expression experiments, 400ng of plasmid DNA was transfected into the cells, whereas for co-expression experiments, 200ng of plasmid-expressing recombinant protein was mixed with 400ng of plasmid expressing miRNA and transfected into the cells. The cells were incubated overnight at 37°C and RNA and protein samples were collected one day following the transfection.

2.3 RNAi in P19 cells

Pools of siRNAs were obtained from Dharmacon in the format of three independent siRNAs targeting different regions of mRNA coding for the protein of interest. Then, 4μg of siRNAs was delivered into two transfection events separated by 48h using nucleofection technology from Lonza. Just prior, the reaction 2mL of media was added to each well of a 6-well plate. Also, 500μL of media per reaction was transferred to a 15mL tube. The plate and tube were placed in the cell culture incubator for equilibration. P19 cells were trypsinised and counted. Approximately $2x10^6$ of cells were distributed accordingly to a number of reactions in 15mL centrifuge tubes and spun. Cells were re-suspended in 100μL of nucleofector solution (82μL of nucleofector solution V plus 18μL of supplement – both provided by Lonza Amaxa). Cells were transferred to a nucleofector cuvette containing 4μg of siRNA. Each cuvette was gently flicked to mix the solutions and placed into the nucleofector device. C-020 program was run and briefly 500μL of previously equilibrated complete media was added to the cuvette. Content of the cuvette was transferred to the previously equilibrated 6-well plate. Cells were collected for analysis 48h after the nucleofection procedure. If a second round of siRNA treatment was required, cell media was aspirated and 200μL of trypsine was added to each well. Briefly, after cells detached, 800μL of media was used to neutralise the reaction. Cells were subsequently collected by centrifugation. At that point, the process was repeated according to the description above. After an additional 48h (total of 96h), cells were collected for analysis.

2.4 DNA sequence modification and standard cloning

2.4.1 Mutagenesis of DNA sequences

Mutations in DNA sequences were introduced using a PCR approach with primers bearing modified single nucleotide changes or designed to introduce deletion or insertion via non-complementary flanking sites. In the PCR reaction, high-fidelity KOD polymerase was used.

KOD polymerase reaction settings		
Component	Volume	Final Concentration
10x KOD buffer	5µl	1x
25mM Mg_2SO_4	3µl	1.5mM
10mM Primer Forward	1.5µl	0.3µM
10mM Primer Reverse	1.5µl	0.3µM
2mM dNTPs	5µl	0.2mM
Template DNA	1-5µl	1µg
KOD polymerase	1µl	0.02U/µl
water	Up to 50µl	
KOD polymerase amplification settings		
Step	Temperature	Time/cycles
Polymerase activation	95°C	2min/1
Denaturation	95°C	20sec/40
Annealing	Lowest primer Tm°C	10sec/40
Extension	75°C	25sec per kb/40

2.4.2 Restriction Nuclease cleavage and gel extraction

DNA inserts prepared via mutagenesis or PCR steps were digested accordingly to the requirements with specific complementary restriction enzymes. The reaction was performed in water in a total volume of 60µL containing up to 4µL of each restriction enzyme, and 6µL 10x Cutsmart buffer (or other NEB recommended buffer). Subsequently, the reaction was incubated at 37°C for a time in the range of 15-60min. Then, 10µL of 6x loading buffer was added and products were resolved on 0.8–1.2% agarose gel with added ethidium bromide under 120V for 30min. The DNA bands were visualised under UV light, and then excised and weighed.

Three volumes of buffer QG (Qiagen Gel Extraction Kit, 28704) were added to 1 volume of the gel (100mg ~ 100µL) in a 1.5mL microcentrifuge

tube. The gel slice was incubated at 50°C for 10min, periodically mixing vigorously. After the gel slice was completely dissolved, 10μL of 3M sodium acetate and 1 volume of isopropanol were added and mixed. The solution was transferred into the spin column provided with the collection tube and centrifuged 10000 rpm for 60sec. The column was washed with 750μL of buffer PE (Qiagen Gel Extraction Kit) and centrifuged at 13000rpm for 60sec. Subsequently, this was dried by an additional centrifugation step as above. Then, 25μL of water was added and incubated at RT for 1min. DNA was collected in the new collection tube by centrifugation 13000rpm for 60sec.

If DNA was used as a template for the T7 *in vitro* transcription reaction, an additional step of wash with 500μL QG buffer was added preceding the wash with PE buffer.

2.4.3 Ligation with T4 DNA ligase

The cleaved and gel-purified insert fragment was merged with a vector cleaved with reciprocal restriction enzymes using either T4 DNA ligase or Quick Ligation systems (NEB, M0202, M2200). For standard T4 ligation, 50ng of vector was mixed with a suitable amount of insert to match the 3:1 molarity ratio of insert to vector. The reaction was performed in water in a total volume of 20μL containing 2μL 10x T4 DNA ligase buffer and 1.5μL of T4 DNA ligase. The ligation was incubated at either 4°C overnight (for inserts <2kb) or 16°C overnight (for inserts >2kb).

For the Quick Ligation system, 50ng of vector was mixed with a suitable amount of insert to match the 3:1 molarity ratio of insert to vector. The mix was made up to 10μL with water and 10μL of 2x Quick Ligation Buffer was added. Then, 1μL of Quick T4 DNA ligase was mixed thoroughly and the reaction was collected by a short spin. Subsequently, the mix was incubated at 25°C for 5min and chilled on ice.

In the next step, ligated DNA was propagated in the bacteria.

2.4.4 Bacterial transformation

In the current work, the following *E. coli* strains were used in transformation procedures – DH5α, TOP10, Stbl3, and Mach1 (Life

Technologies). DH5α strain was used as first choice method for standard cloning procedures. TOP10 strain has 1000x higher transformation efficiency then DH5α cells and was used for cloning of difficult targets. Stbl3 cells reduce the frequency of homologous recombination of long terminal repeats and result in 10x higher yield than TOP10 cells – these cells were used for transformation of large plasmids. Mach1 strain was engineered to reduce time required to produce plasmids and were used in instances were results had to be quickly obtained.

Here, 50μL of cells was gently thawed on ice in a 1.5mL microcentrifuge. Up to 5μL of ligation reaction or DNA plasmid was added to the cells and gently mixed. Cells were incubated for 30min on ice. Subsequently, tubes were transferred to a thermo bloc and incubated for 45sec at 42°C. Following that, the cells were placed for 2min on ice and subsequently 450μL of S.O.C. media was added. The reaction was incubated at 37°C for 1hr with vigorous shaking. Subsequently, 200-500μL of the reaction was plated on the agar plate with a selective antibiotic.

2.4.5 DNA extraction from bacterial cells

A single colony from the transformant plate was used to inoculate 5mL LB liquid culture with an appropriate selection antibiotic. After 24h of vigorous shaking at 37°C, cells were spun down at 3000 x g for 15min at 4°C. The supernatant was discarded and cells were re-suspended in 250μL of buffer P1 (QIAgen Spin miniprep kit) and transferred to a microcentrifuge tube. Here, 250μL Buffer P2 (QIAgen Spin miniprep kit) was added to initiate cell lysis, mixed by inversion and incubated for no longer then 5min at RT. Lysis was stopped by adding and inverting 350μL of Buffer N3 (QIAgen Spin miniprep kit). Lysed cells were centrifuged at 12000 x g for 10min at RT. Supernatants were transferred to the QIAgen Spin column by decanting and were centrifuged at 12000 x g for 60sec at RT. Subsequently, the flow-through was discarded and the column was washed with 750μL of Buffer PE. Following that step, flow-through was discarded and the columns were dried by an additional centrifugation step at 12000 x g for 60sec at RT. Subsequently, DNA was eluted using 20-

200μL of water, incubated for 1min at RT and centrifuged at 12000 x g for 60sec at RT. The concentration of DNA was measured by the Nanodrop and transferred to other protocols or sent for sequencing.

2.5 RNA pull down

In vitro transcribed precursor miRNA or commercially synthesised RNA purchased from Sigma-Aldrich (table S1) was coupled to adipic acid dihydrazide-agarose beads (Sigma-Aldrich) in a two-step reaction. The activation step included mixing 1000pmol of RNA with 100mM sodium acetate and 5mM m-sodium periodate, away from light for 1h at room temperature. Following the 1h incubation step, the RNA was precipitated on dry ice for 30min by the addition of 800μL of 100% ethanol. The precipitated RNA was centrifuged at top-speed at 4°C for 20min. The pellet was washed with 1mL 70% ethanol and re-suspended in 500μL of 100mM sodium acetate pH5.

Then, 200 μL of beads washed and equilibrated with 100mM sodium acetate was mixed with 500μL periodate-treated RNA and left mixing overnight at 4°C away from the light. The non-bound fraction of RNA was washed away by incubation with 700μL 4M KCl for 30min at RT. The resin was collected by 2min centrifugation at 8000rpm. Beads were washed twice with 1mL of 2mM KCl and equilibrated with Roeder D buffer (100mM KCl, 20% (v/v) glycerol, 0.2mM EDTA, 100mM Tris pH8.0). Total protein extracts were prepared by sonication (two times for 5 minutes each in ice-chilled water bath) of p19 cells suspended in 600μL of RoederD buffer. Resin coupled with RNA was incubated with protein extract in the following reaction. Then, 1000μg of the total protein extract was mixed with 1.5mM $MgCl_2$, 25mM Ceratin-phosphate, 0.5mM ATP, 5μL RNAse out (Roche) and water in a total volume of 650μL. The reaction was incubated shaking at 400RPM for 30min at 37°C. The RNA-protein complexes were collected by centrifugation for 3min at 1000RPM at 4°C. The reaction was washed four times with 1mL Roeder D buffer containing 1.5mM $MgCl_2$ and twice with Milli-Q-water. Beads were collected by 3min centrifugation at 1000rpm between each step.

Following the final wash step, the beads were mixed with 6μL of structure buffer (10mM Tris-HCl pH7.2, 1mM $MgCl_2$, 40mM NaCl), 5μL A/T1 RNAse, 5μL RNAse I, 44μL of water and incubated for 30min at 37°C shaking at 1400rpm for 10 seconds in one minute intervals. After incubation, the beads were collected by a short 1000rpm centrifugation and analysed by SDS-PAGE.

2.6 SILAC assisted quantitative mass spectrometry

2.6.1 In-gel digestion

SDS-PAGE with protein samples was resolved briefly until two first size marker bands were clearly separated.

Prior to the procedure, 50mM ABC solution was prepared by dissolving 0.16g of ABC in 40mL of water in a well-rinsed bottle. The well-rinsed bottle was filled with 40mL of acetonitrile and the bench was washed with 70% ethanol. Work was always performed in nitrile gloves to avoid contaminants common for mass spectrometry. The microcentrifuge tubes were prepared according to the number of reactions and 200μL of ABC solution was transferred into each tube.

Subsequently, the gel was placed on glass slide and protein bands were cut out, sliced into small pieces and transferred into corresponding microcentrifuge tubes containing ABC solution. The gel slices were left for 5min at RT in ABC solution, after which ABC solution was replaced with 200μL of acetonitrile. These steps were repeated until the gel was de-stained or the solution stopped turning blue. Subsequently, 50mM ABC was supplied with 10mM DTT (10μL 1M DTT added to 990μL 50mM ABC) and added to the gel slices until covered completely. The solution was left at 37°C for 30min.

During that step, trypsin buffer was prepared. On ice, 20μL of 0.1% TFA was added to 20μg of trypsin in the vial provided. Trypsin buffer base containing 10% acetonitrile and 10mM ABC was prepared (100μL 100%

acetonitrile, 200µL 50mM ABC, 700µL water). Trypsin buffer was prepared by transferring 3µL of trypsin into 227µL of trypsin buffer base.
After 30min of incubation, liquid was removed from the gel slice and 200µL of acetonitrile was added for 5min. Subsequently, 50µL (or more until gel slice covered) 55mM Iodoacetamide (IAA, Sigma I1149) in ABC buffer was added and the gel slice was incubated for 20min at RT in the dark. IAA was removed and 50mM ABC solution was transferred to the gel slice followed by washing with acetonitrile for 5min. Subsequently, the wash solution was replaced with trypsin buffer in the amount sufficient to cover gel slices and incubated on ice for 15min. An additional amount of trypsin buffer was added to gel slices and incubated at 37°C overnight.
On the following day, 1:1 volume of 0.1% TFA was added and left to incubate at RT for 20min (usually around 100µL). The pH was checked and brought to pH=1-3 if necessary by the step-wise addition of 0.5µL 10% TFA.
C18 stage tip was made with two column pieces and labelled. The tip was activated with 20µL of methanol followed by 40µL of 0.1% TFA. The sample was loaded and washed with 60µL of 0.1% TFA until all of the liquid was removed.

2.7 MS analysis and peptide identification

MS-analysis were performed in a Velos LTQ-Orbitrap mass spectrometer (ThermoFisher Scientific, UK) coupled on-line to an Ultimate 3000 RSLCnano System (Dionex, ThermoFisher Scientific, UK). Injections were performed in an analytical column with a self-assembled particle frit (*34*) and C18 material (ReproSil-Pur C18-AQ 3 µm; Dr. Maisch, GmbH) was packed into a spray emitter (75-µm ID, 8-µm opening, 300-mm length; New Objective) using an air-pressure pump (Proxeon Biosystems). Mobile phase A consisted of water and 0.1% formic acid; mobile phase B consisted of 80% acetonitrile and 0.1% formic acid. The gradient was used over 160 min. The peptides were loaded onto the column at a flow rate of 0.5 µL min-1 and eluted at a flow rate of 0.2 µL min-1 according to the following

gradient: 2% to 40% buffer B for 120 min, then to 95% B for 16 min. FTMS spectra were recorded at 60,000 resolution and the twenty most intense peaks of the MS scan were selected in the ion trap for MS2 (normal scan, wideband activation, filling 5.0E5 ions for MS scan, 1.0E4 ions for MS2, maximum fill time 100 ms, dynamic exclusion for 60 s). The scan range was set between 300 and 1700 m/z. Data analysis was performed using the MaxQuant software (ver. 1.0) (Cox and Mann, 2008). Searches were conducted against Uniprot database containing *Mus musculus* sequences. Regarding the search parameters, the first search peptide tolerance was set to 20 ppm while the main search peptide tolerance was set to 4.5 pm. Isotope mass tolerance was 2 ppm and maximum charge 7. Digestion mode was set to "specific" with trypsin allowing two missed cleavages. Fixed modifications were set to carbamidomethylation of cysteine and acetylation of the N-terminal while variable modifications were set to oxidation of methionine. Multiplicity was 2 with Lys6 and Arg10 to be the heavy labels.

2.8 Western blot protein level analysis

The total protein samples (100μg per lane), isolated by sonication, were resolved by standard SDS-PAGE electrophoresis and transferred onto nitrocellulose membrane. The membrane was blocked overnight at 4°C with blocking solution (1:10 Western Blocking Reagent (Roche) in TBS buffer with 0.1% of Tween-20 (TBS-T)). On the following day, the membrane was blotted for 1h at RT with antibody solution (1:20 Western Blocking Reagent in TBS-T, 1:1000 of primary antibody and 1:1000 of appropriate secondary antibody) (table S4). After incubation for 1h, the membrane was washed three times with TBS-T and the blot was developed with ECL Western Blotting Substrate (Pierce), according to the instructions provided by the supplier.

2.9 Detection of miRNAs levels

2.9.1 RNA extraction

Total RNA was isolated from cells using TRIzol reagent (Life Technologies), which is a monophasic solution of phenol, guanidine

isothiocyanate, and other components that facilitate the extraction of various size RNA species. TRIzol reagent is an improvement to the single-step RNA extraction method developed by Chomczynski and Sacchi (Chomczynski and Sacchi, 1987).

TRIzol or TRIzol LS was used depending on whether the starting material was cells, tissues or liquid solution, for instance cell extract.

Cells were washed with 1x PBS and re-suspended in 1mL of TRIzol (note: 1mL per a 35mm, 3mL per a 60mm, 8mL per a 100mm dish). If the cell extract was used, 1mL of TRIzol LS was added to a total volume 1mL of cell extracts (note: cell extract can be diluted with lysis buffer to final volume 1mL). The solution was pipetted up and down and left at RT for 5min to complete the TRIzol lysis. 0.2mL of chloroform was added per 1mL of TRIzol reagent. The tube was shaken vigorously for 15sec at RT (not vortexed) and left to equilibrate for 3 min at RT. The solution was subsequently centrifuged at 12000 x g for 15min at 4°C, after which the mixture separated into three phases; the upper aqueous phase contains exclusively RNA. The tube containing the reaction was slightly tilted and the aqueous phase was transferred to the new tube. Here, 0.5mL of 100% isopropanol was added to the aqueous phase per 1mL of TRIzol reagent. The reaction was incubated for 10min at RT. Subsequently, the mix was centrifuged at 12000 x g for 10min at 4°C. The pellet was washed with 1mL of 70% ethanol. The reaction was centrifuged at 7500 x g for 5min at 4°C. The supernatant was discarded and the pellet was dried for 5-10min, after which the pellet was resuspended in 20-50μL of water and incubated at 55°C. The quantity and quality of the RNA was assayed using the Nanodrop and agarose gel electrophoresis. Purified total RNA was subsequently used in the methods described below or stored at -80°C.

2.9.2 Northern blots RNA absolute levels analysis

Here, 20μg of total RNA was mixed with an equal volume of loading buffer (95% Formamide, 18mM EDTA, 0.025% SDS, Xylene Cyanol, Bromophenol blue) and resolved on a 10% PAGE-Urea gel. The ribosomal RNA was visualised with ethidium bromide to confirm equal loading. The RNA was transferred from the gel onto nitrocellulose membrane (Hybond

N). The membrane was cross-linked twice with UV and pre-hybridised overnight at 40°C with 10mL of hybridisation buffer (1xSSC, 1%SDS, 200μg/mL ssDNA).

A Northern probe was prepared using the *mir*Vana™ miR Probe Construction Kit (Life Technologies). In the first step, a dsDNA template for T7 transcription was generated according to the manufacturer's instructions. The probe was denatured at 95°C for 1min, placed on ice and hybridised against the membrane for 2h at 40°C in 10mL of hybridisation buffer. Subsequently, the membrane was washed 2-3 times for 30min each with 50mL of wash buffer (0.2%SSC, 0.2%SDS). The signal was registered with a radiographic film.

2.9.3 qRT-PCR relative RNA fold change analysis

In this step, 20μg of total RNA was mixed with an equal amount of 2x sample buffer and run on a 10% PAGE-Urea gel. The small RNA fraction was cut out of the gel and incubated with 300μL of elution buffer overnight at room temperature. The following day, the liquid phase was transferred to a new tube and the small RNAs precipitated with three volumes of 100% ethanol at -20°C. The samples were then centrifuged and washed with 70% ethanol. The RNA was re-suspended in 20μL of water. The levels of miRs were assayed using the miRscript kit (Qiagen) and Roche Lightcycler, as described by the manufacturer.

2.10 *In vitro* transcription of precursor miRNA templates

2.10.1 T7 templates synthesis

Pri-miRNA templates for *in vitro* transcription were generated by linearisation of pGEM vector with cloned pri-miRNA sequence. Linearisation was performed using SpeI restriction enzyme. For this, 1μg of the vector containing pri-miRNA sequence was incubated with 1μL of SpeI (10,000 units/ml, NEB - R0133S), 2μL of 10x NEBcutter buffer and water in total volume of 20μL. The reaction was performed at 37°C for 1h.

Pre-miRNA templates for *in vitro* transcription were generated from pGEM vector containing pri-miRNA sequence by standard PCR

conditions using Taq polymerase (Life Technologies 10342-020) and forward primers containing T7 transcription starting site.

PCR reaction setting:	
Reaction component	Volume required
10x PCR buffer –Mg^{2+}	5µL
10mM dNTPs	1µL
50mM $MgCl_2$	1.5µL
10mM Forward primer	2.5µL
10mM Reverse primer	2.5µL
100ng pGEM template	1µL
5U/µL Taq polymerase	0.25µL
H_2O	36.75µL

Taq Polymerase T7 template PCR program setting:		
Step	Temperature	Time/Cycles
Initiation	94°C	3min/1
Denaturation	94°C	30sec/35
Annealing	55°C	30sec/35
Extension	72°C	30sec/35
Final extension	72°C	10min/1

2.10.2 *In vitro* transcription of unlabelled probes using T7 polymerase.

Approximately 1µg of template was added to the *in vitro* transcription reaction mix containing T7 polymerase (Lucigen, NxGen T7, 30223-1). The mix contained 1-2µL of T7 polymerase (50u/µL), 2.5µL of 10x transcription buffer (Lucigen, NxGen, 30223-1), 1.25µL of 10mM rNTPs (Roche, 11969064001), and, if used for 5′ γ-ATP labelling, 7µL of Guanosine, 0.5µL RNAse out (Life Technologies, 10777-019) and water up to a total volume

25μL. Each reaction was incubated for 1.5h at 37°C. Following the incubation step, the reaction was stopped by the addition of 25μL of 2x UED (7.5M Urea, 10mM Tris pH8.0, xylene cyanol, bromophenol) and boiled at 94°C for 2.5min. Subsequently, the reaction was cooled on ice for 2min and resolved using PAGE-Urea gel electrophoresis. For pri-miRNA and pre-miRNA templates, 6% and 10% gels were used, respectively. RNA bands were visualised by staining with RNA stain solution (0.005% "stain-all" SERVA, 5% formamide, 25% isopropanol, 15μM TrisHCl pH 8.0). The bands were excised and eluted from the gel. Subsequently, RNA was precipitated and re-suspended in water.

2.10.3 *In vitro* transcription of internal labelled probes using T7 polymerase.

Approximately 1μg of template was added to the *in vitro* transcription mix containing T7 polymerase (Lucigen, NxGen T7, 30223-1). The mix contained 1-2μL of T7 polymerase (50u/μL), 2.5μL of 10x transcription buffer (Lucigen, NxGen, 30223-1), 1.25μL of 10mM rCGA nucleotides (Roche, 11969064001), 1.25μL of 1mM rUTP, 0.5μL RNAse out (Life Technologies, 10777-019), 1μL of stock ^{32}P-αUTP and water up to total volume 25μL. The reaction was incubated for 1.5h at 37°C. Following the incubation step, the reaction was stopped by the addition of 25μL of 2x UED and boiled at 94°C for 2.5min. Subsequently, the reaction was cooled on ice for 2min and resolved using PAGE-Urea gel electrophoresis. For pri-miRNA and pre-miRNA templates, 6% and 10% gels were used, respectively. RNA bands were visualised by exposure to radiography film for a brief moment. The bands were excised and eluted from the gel. Subsequently, RNA was precipitated and re-suspended in water.

2.10.4 5′ labelling of *in vitro* transcribed probes.

Unlabelled, *in vitro*-synthesised probe was 5′ labelled with ^{32}P-γATP using T4 polynucleotide kinase (PNK) (NEB, M0201S) in PNK reaction mix. The solution consisted of 10μL unlabelled template, 1.5μL of 10x T4 PNK

buffer (NEB, M0201S), 1μL T4 PNK (10u/μL), and 2μL of stock ^{32}P-γATP. The reaction was performed at 37°C for 10 min. Subsequently, 15μL of 2x UED was added to quench the reaction. The solution was heated up to 94°C for 2min and placed on ice for an additional 2min. For pri-miRNA and pre-miRNA templates, 6% and 10% gels were used, respectively. RNA bands were visualised by exposure to radiography film for a brief moment. The bands were excised and eluted from the gel. Subsequently, RNA was precipitated and re-suspended in water.

2.10.5 RNA probe gel extraction and precipitation

Following visualisation the band of corresponding precursor probe was cut out of the gel and incubated with 300μL of elution buffer (0.3M NaAc pH5.2, 0.5M EDTA, 0.1%SDS) overnight at RT. Subsequently, the RNA was precipitated by the addition of 900μL of 100% ethanol and left on dry ice for approximately 30min or placed at -20°C overnight. Samples were centrifuged at top speed for 15min at 4°C and washed with 1mL of 70% ethanol. RNA probe was re-suspended with 10-15μL of MilliQ-water.

2.11 *In vitro* processing and uridylation assays of precursors miRNAs

Probes consisting of the pri-miRNA or pre-miRNA were incubated for 30min at 30°C with total protein extracts derived from P19 cells at a specific developmental stage or condition. Following the incubation, proteinase-K mix (2μL SDS-20%, 2μL proteinase-K, 66μL MilliQ-water) was added to the reaction and incubated for 10min at 37°C. Subsequently, RNA was extracted with 100μL of phenol-chloroform solution and precipitated with solution-P (10μL 3M NaAc pH5, 1μL carrier-tRNA, 300μL 100% ethanol, approximately 90μL of the aqueous phase from the phenol-chloroform extraction). Solution-P was placed on dry ice for 30min. After precipitation, the RNA was centrifuged at 12000 x g for 15min at 4°C and subsequently washed with 1mL of 70% ethanol. The RNA was re-suspended in 20μL of sample buffer. The samples were resolved on a 10% PAGE-Urea gel and visualised by radiography.

2.12 EMSA analysis of RNA binding

Pre-miR-9 and pre-let-7a probes were *in vitro*-transcribed and internally labelled with ^{32}P-αUTP as described before. Then, 1μL of probe (100k cpm/μL) was mixed with 100 and 200 ng/μL of recombinant proteins in the reaction buffer, which consisted of 1μL of solA (32mM $MgCl_2$, 5μM ATP, 0.4M CIP), 5μL of RoederD (100mM KCl, 20%(v/v) glycerol, 0.2mM EDTA, 100mM Tris pH=8.0, 0.5mM DTT, 0.2mM PMSF), 0.5μL RNAse-out (LifeTechnologies) and water to a final volume of 10μL. Reactions were performed on ice for 30 min. Following the incubation 10μL of 2x native loading buffer was added (0.02% Xylene Cyanol, 0.02% Bromophenol Blue). Then, 20μL of samples were loaded on 6% non-denaturing poly-acrylamide gel. To prevent excessive heating, the gel was resolved in 0.5x TBE at 8W with 5min pre-run at 3W. Following the electrophoresis, the gel was dried and exposed to a phosphoimager cassette overnight.

2.13 RNA-protein binding analysis with structural probing

Pre-miR-9 and pre-let-7a substrates were synthesised by T7 *in vitro* transcription and 5' labelled with T4 PNK, as described elsewhere in this chapter.

Formamide ladder was generated by incubating 2μL of substrate (100k cpm/μL) with 9μL of F buffer (0.5mM $MgCl_2$ in 99.5% Formamide (Molekula Deutshland Limited) at 100°C for 10min. The reaction was stopped by adding 9μL of 2xUED and placed on ice.

T1 ladder was generated by incubating 2μL of substrate (100k cpm/μL) with 2μL of T1 2x buffer (20mM Sodium Citrate, 7M Urea), which had to be prepared shortly before. Then, 1μL of T1 (1u/μL) was added and incubated at 55°C for 15min. The reaction was stopped by adding 15μL of 2xUED and placed on ice.

Probes for cleaving substrate RNA were prepared from stock solutions in three trial concentrations as follows:

- Pb(II) – 0.2, 0.3, and 0.4mM prepared in water from 20mM Pb(II) stock water solution.
- T1 – 0.5u/μL, 0.25u/μL, and 0.125u/μL prepared in water from T1 stock solution 1000u/μL.
- V1 – 0.00075u/μL, 0.000375u/μL, and 0.00019u/μL prepared in water from V1 stock solution 0.1u/μL.

Subsequently, the best cleavage conditions were selected per probe.
Reactions were run in the presence and absence of the recombinant Lin28a protein. For the cleavage optimisation, 200ng/μL of protein was used. In the final experiments with fixed probe concentrations, Lin28a was used at a gradient of 50, 100 and 200ng/μL.
Each reaction was prepared as follows: 1μL of substrate (100k cpm/μL) was added to 7μL of 1x Structure Buffer (12mM Tris-HCl pH=7.5, 48mM NaCl, 1.2mM $MgCl_2$). Samples were incubated at 90°C for 1min and left at RT for 5min. Then, 2μL of probes was aliquoted into 8μL of substrate solution and incubated at RT or 37°C for 10min. Reactions were stopped by adding 10μL of 2xUED and placed on ice.
Samples were resolved on an ultra-thin large polyacrylamide gel that was pre-heated before. Then, 2-5μL of samples were loaded per well.

2.14 Immunofluorescence analysis of samples

2.14.1 Cell culture staining

Here, 24h prior to cell staining, coverslips were coated with poly D-Lysine (PDL) by adding 2mL of 10μg/mL solution per well and incubated for 20min at RT. Coverslips were washed with 1x PBS and cells were plated on top of them according to standard tissue culture conditions.
On the day of staining, culture medium was disposed and 1mL per well of 4% formaldehyde was added. Cells were incubated in this solution for 10min at RT. Then, 2mL of 1x PBS was added to dilute 4% formaldehyde and fixing solution was aspirated. Cells were washed 3 times for 5min each with 1x PBS.

Cells were permeabilised by adding 1mL of 0.2% Triton-X per well and incubating at RT for 10min. Subsequently, wells were washed three times 5min each with 1x PBS.

Following washing, cells were blocked with goat serum at RT for 15min by adding 1 drop on parafilm and placing a coverslip inverted on top of it. Subsequently 25μL of primary antibody diluted accordingly (Appendix A) was placed on parafilm. Coverslip was placed inverted on top at RT for 1h.

Following the primary antibody, the secondary fluorescent labelled antibody was incubated in the similar manner. Coverslips at that point were protected from light by foil. Between blocking, primary and secondary steps, cells were washed three times for 5min each. Finally, cells were counterstained with 20μL of Hoechst (1/2000 in water) at RT for 5min and washed once with 1x PBS for 5min. Excess liquid was evacuated gently and 15μL of mounting media was placed on the slide; the coverslip was inverted on top of it with the specimen facing toward the slide. Samples were left to dry in the dark for 1h and analysed by fluorescent microscope (Zeiss Axio Imager). If required, samples were stored in the dark at -20°C.

2.15 Protein purification

Full-length Lin28a coding sequence was cloned into modified pGEX-6p3 vector where linker containing TEV-cleavage site between GST-tag and ORF was deleted. This approach allowed for the effective expression of soluble N-terminally tagged Lin28a. This protein interacts very strongly with RNA present in bacterial cells. GST-tag stabilised Lin28a, allowing for efficient purification in an RNA-free manner using PEI-precipitation technique.

2.15.1 Protein expression in bacterial cell system

pGEX-6p3-Lin28a constructs were transformed into chemically competent *E. coli* BL21 X-gold strain. Briefly, around 100ng of the plasmid was incubated with 50μl of bacteria for 30 minutes on ice. In the subsequent step, bacterial cells were exposed to heat shock by incubating at 42°C for

45 sec followed by 2 minutes on ice. Then, 450µl of SOC media was added to the bacteria and cells were incubated for 1h at 37°C. After the incubation period, cells were plated on agar plates with kanamycin resistance.

The following day, a single bacterial colony was inoculated in 5mL LB with kanamycin. Liquid cultures were incubated overnight at 37°C. In the next step, liquid cultures were scale up by inoculating 2L of LB medium with kanamycin at 37°C until OD ~0.6 were reached. At that point, liquid cultures were placed at 4°C for 20 min to equilibrate growth rate. In the final step of expression, large-scale cultures were induced with 1mM IPTG and incubated overnight at 16°C.

2.15.2 Bacterial cell lysis and lysate preparation

Large-scale bacterial cultures were centrifuged at 5000 x g for 15 min at 4°C. Pellets were weight and re-suspended 5ml/g of pellet in lysis buffer (50mM Tris pH=7.5, 2M NaCl, 0.5% polyethyleneimine (PEI), 2mM DTT, 10% sucrose) supplemented with pepstatin, leupeptin and AEBSF protease inhibitors. Cells were incubated on ice for 20min and sonicated at full power with 8-10 pulses with 2-minute gapes between the pulses.

Cells were spun down 15000g for ~45min at 4°C. Supernatant was collected and diluted 4x slowly using dilution buffer (50mM Tris pH=7.5, No salt, 0.5%PEI, 2mM DTT, 10%sucrose). Dilution buffer was added in steps by adding 5ml at a time. After white precipitate appeared, cells were centrifuged at 15000 x g for 50min at 4°C and supernatant was collected. Subsequently, ammonium sulphate was added to 60% saturation and lysate was spun down 15000 x g for 50min at 4°C. Supernatant was discarded and the pellet was resuspended in 5mL of buffer A (50mM Tris pH=7.5, 150mM NaCl, 2mM DTT, 10%sucrose). Resuspended fractions were pulled and analysed for UV absorbance below 0.7.

2.15.3 Liquid chromatography approach to purify expressed protein

A combination of GST-trap affinity column and size exclusion chromatography was used to purify expressed protein. Columns were

installed and equilibrated on AKTÅ FPLC instruments. Briefly, 5mL HP GST-trap column (GE Healthcare) was equilibrated with 5CV water, 2CV buffer B (50mM Tris pH=8.5, 150mM NaCl, 2mM DTT, 25mM Glutathione, 10% sucrose) and 5CV of buffer A. Samples were run at a 1mL/min flow rate at 4°C. After the sample load was complete, the column was washed with 10CV of buffer A and the bound protein was eluted with 10CV of buffer B. During the whole process, fractions of 1mL were collected and analysed on SDS-PAGE for protein composition.

Lin28a containing fractions were pooled and buffer exchanged to buffer GF (10mM Tris pH=7.5, 500mM NaCl, 2mM DTT, 5% sucrose) using Sephadex G-25 HiPrep 26/10 Desalting column. Samples were concentrated up to a final volume of 500μL using 10 kDa MWKO Pierce Protein concentrators. Concentrated samples were loaded on S75 16/60 gel filtration column (GE Healthcare). The size exclusion step was run at a flow rate of 0.5 mL/min and fractions of 1mL were collected. Fractions containing Lin28a were pooled and buffer exchanged to storage buffer (10mM Tris pH=7.5, 150mM NaCl, 2mM DTT, 5%sucrose). Then, 20μL aliquots were flash-frozen in liquid nitrogen and stored at -80°C.

2.16 Next generation sequencing analysis of global small RNA fraction

2.16.1 RNA library preparation

Total cell RNA was extracted with TRIzol solution and submitted for quality control (QC) for SOLEXA sequencing. After a positive QC-result, RNA was run on PAGE gel and species below 30nt were extracted and ligated to SOLEXA adaptors at 5′ and 3′ ends. Small RNA molecules were amplified for 17-cycles using PCR primers against SOLEXA adaptors and fragments of around 90bp (small RNA + adaptor) were gel purified and used directly for cluster generation and sequencing analysis using the Illumina Genome Analyser. The images files generated by the sequencer were then processed to produce digital-quality data. Subsequently, raw data were processed to generate clean reads by masking adaptor sequences and removing contaminant reads (rRNA, tRNA, mRNA).

2.16.2 Small RNA sequencing data analysis

Clean reads were mapped with a zero-match allowance onto a reference mouse genome using BGI-designed SOAPaligner software to locate each read on the genome sequence (Li et al., 2008). Subsequently, annotation was performed against information in miRBase. Next, newly sequenced miRNAs were compared to the reference miRNAs from the database to identify potential mutations. Remaining reads that were not included in any category were classified as potential novel miRNAs and analysed with Mireap (Gu et al., 2013).

2.16.3 Lin28a binding motif mapping and RNA secondary structure analysis

The locations of pre- and pri-microRNAs were extracted from miRBase v21 [doi: 10.1093/nar/gkt1181]. The genomic DNA of these sequences and their flanking region was extracted using Ensembl [doi: 10.1093/nar/gkt1196] and Biomart [doi: 10.1093/nar/gkv350] on mouse assembly GRCm38. A customised perl script was engineered to map the location of the Lin28a identified binding motifs. The total number of Lin28a binding motifs was displayed in the context of P19 stable cell line context.

The RNA mfold algorithm was used to determine a secondary structure of the miRNAs. In order to determine the number of base-paired nucleotides, an algorithm was developed in python. Briefly, the centre of the terminal loop was referenced as position 0 and paired nucleotides were counted upstream and downstream of the pre-miRNA sequences.

Detail of the algorithms used to generate plots and map the binding motifs could be found in repository:
https://github.com/AlastairKerr/Nowak2015.

Chapter 3

3 Post-transcriptional regulation of miRNAs biogenesis during neuronal differentiation of P19 cells

3.1 General consideration regarding P19 differentiation system

In order to study the biogenesis of neuronal miRNAs, I decided to use P19 teratocarcionoma cells. They have the potential to differentiate into neurons very easily using retinoic acid (RA). Therefore, they make a convenient mouse model with which to induce early neuron development. The differentiation process was described before and is summarised in Figure 3-1 (McBurney, 1993). Briefly it involves plating cells on non-adhesive plates in presence of RA for four days, which is the stage referred to as early neuronal differentiation, followed by withdrawal of RA and re-plating on adhesive plates for an additional five days when they reach the stage which is referred to as late neuronal differentiation.

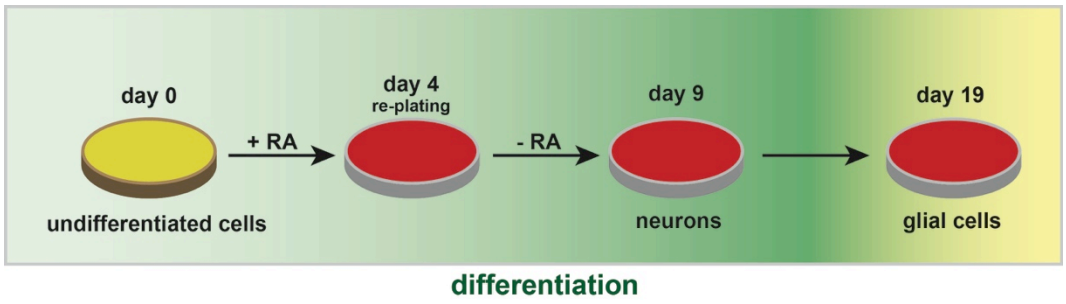

Figure 3-1 P19 cells – neuronal differentiation model
Undifferentiated P19 cells were placed in culture on non-adhesive plates in media containing 5% serum. To induce differentiation, cells were treated with Retinoic Acid (RA) and left to form embryonic bodies. On day 4, embryonic bodies were transferred to an adhesive dish and cultured in media with 10% serum in absence of retinoic acid until day 9 or day 19 to obtain neurons or glia cells respectively.

To confirm the successful differentiation, I collected cells at different time points of the differentiation and analysed expression markers. I compared changes in Lin28a and Lin28b that were shown in the past to be expressed in cells in the undifferentiated state (Balzer et al., 2010) (Figure 3-2). To determine the generation of early neurons, I analysed the expression of Tuj-1 (β-tubulin class III) that is specifically expressed in early neurons (Aggarwal et al., 2015). I also verified equal loading when checking the expression of α-tubulin, which is a commonly expressed protein in cells regardless of their differentiation state.

With these in mind, I was able to confirm that Lin28a and Lin28b expression is gradually decreased during the differentiation of P19 cells. Although their expression was still detectable in the early stages of neuronal differentiation, it was not detected beyond day 6. On the other hand, the expression of neural markers Tuj-1 and GFAP was not detected in undifferentiated cells. Tuj-1 protein gradually started to appear at day 2 of differentiation reaching maximum expression at days 8-10. Interestingly, its expression started to decrease beyond that point. However GFAP expression was detected only at the very late stages of neuronal differentiation. As expected, the expression of α-tubulin remained stable across differentiation (Figure 3-2).

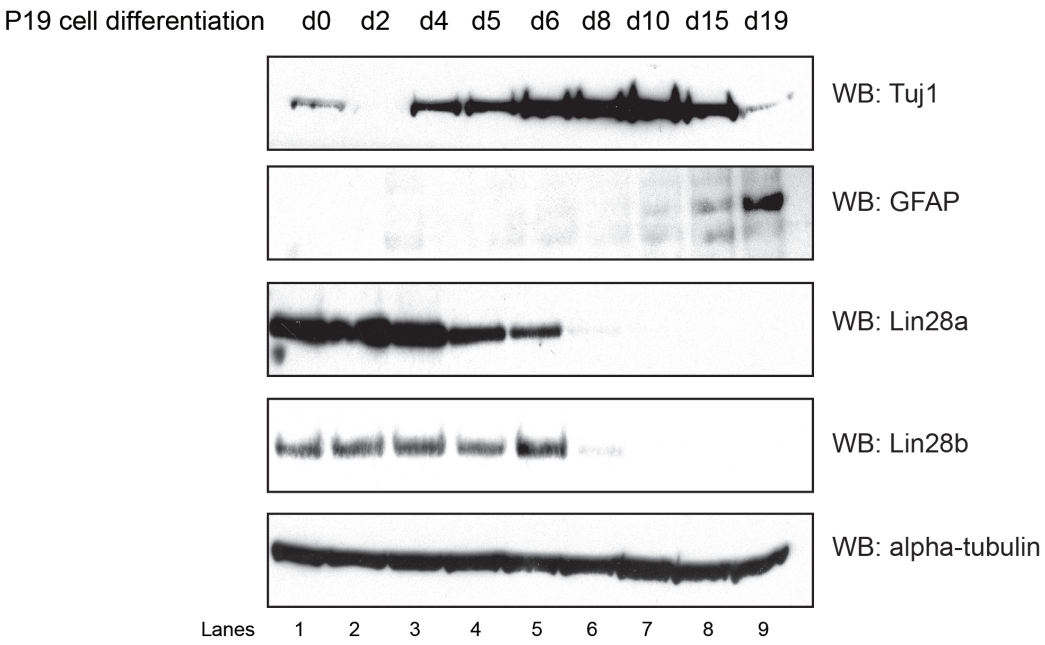

Figure 3-2 P19 neuronal differentiation markers

P19 cells at various stages of neuronal differentiation were harvested and analysed with western blot for the expression of stage-specific protein markers. Starting from day 0 (d0), cells were collected on every other day until day 10 (d10) and then on day 15 (d15) and day 19 (d19). β-tubulin class III (Tuj1) and Glial fibrillary acidic protein (GFAP) antibodies were used to validate neuro- and glio-genesis respectively. Lin28a and Lin28b antibodies were used to confirm differentiation of the cells. Alpha-tubulin antibody was used to ensure equal loading.

3.2 miRNA levels are dynamically regulated throughout neuronal differentiation

3.2.1 Dynamic regulation of miRNA levels during neuronal differentiation of P19 cells.

To characterise the dynamics of changes in the miRNA levels during the neuronal differentiation, I applied qRT-PCR analysis. I then correlated these levels with corresponding levels of their pri-miRNAs. miR-9 and miR-124 were analysed from a subset of neuro-enriched miRNA. Additionally, let-7 and miR-302a levels were used to determine differentiation efficacy, as let-7 is expressed in differentiating cells, whereas miR-302a is responsible for maintenance of the undifferentiated state. Throughout the genome, pri-miR-9 and pri-miR-124 have each three copies of their pri-miRNAs. Therefore, I analysed pri-miR-9-1, pri-miR-9-2, pri-miR-9-3 as well as pri-miR-124-1, pri-miR-124-2 and pri-miR-124-3. Let-7 and miR-302 are both large families of miRNAs with eleven loci of let-7 genes and four isoforms of miR-302. I selected let-7a and miR-302a for further analysis. This analysis allowed me to determine whether the observed changes in mature miRNA levels could directly account for the alterations in their steady-state transcript levels.

For pri-let-7a, I observed a very modest ~2-fold increase in the primary levels at early stages of neuronal differentiation that slightly increased to ~5-fold at the late stages. Pri-miR-302a displayed less defined pri-miRNA expression pattern with its levels being at the early differentiation stages downregulated ~2-fold. However, in later stages of differentiation, its pri-miRNA levels oscillate around those observed at the starting point of the differentiation (Figure 3-3).

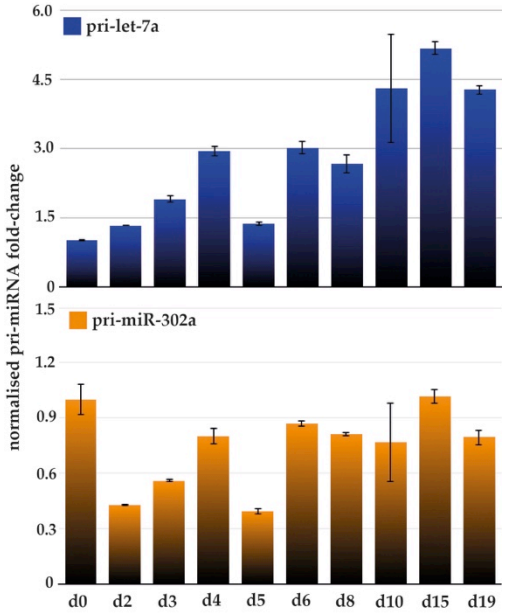

Figure 3-3 P19 differentiation time points - pri-miRNAs levels
qRT-PCR analysis of pri-miR-let-7a and pri-miR-302a levels during neuronal differentiation of P19 cells. Expression of pri-miR-302a and pri-let-7a were normalised using Cyclophilin A (CypA) expression. Levels were analysed on every second day starting from day 0 (d0) until day 10 (d10) and then on day 15 (d15) and day 19 (d19).

In the case of the pri-miR-124 family, only pri-miR-124-2 displayed a 40-fold increase in transcription at the early stages of neuronal differentiation and its expression also remained at a similar level during later stages of P19 differentiation (Figure 3-4). However, the expression level of pri-miR-124-1, which remained silenced during early stages reported an abrupt ~100-fold increase, exceeding the expression of pri-miR-124-2. Contrary to pri-miR-124-1 and pri-miR-124-2, the last member of the family, pri-miR-124-3, did not display any major increase in levels during the neuronal differentiation of P19 cells. Similarly to pri-miR-124, the pri-miR-9 family transcription level is also relatively low during the early stages of neuronal differentiation when compared to the late stages. In particular, on day 4 I detected an ~520-fold increase in pri-miR-9-2 levels with no comparable changes in pri-miR-9-2, or -3. However, on day 8, which corresponds to the late stage of P19 differentiation, pri-miR-9-1, -2, -3 expression levels increased by ~400-, ~1300- and ~260-fold, respectively (Figure 3-4).

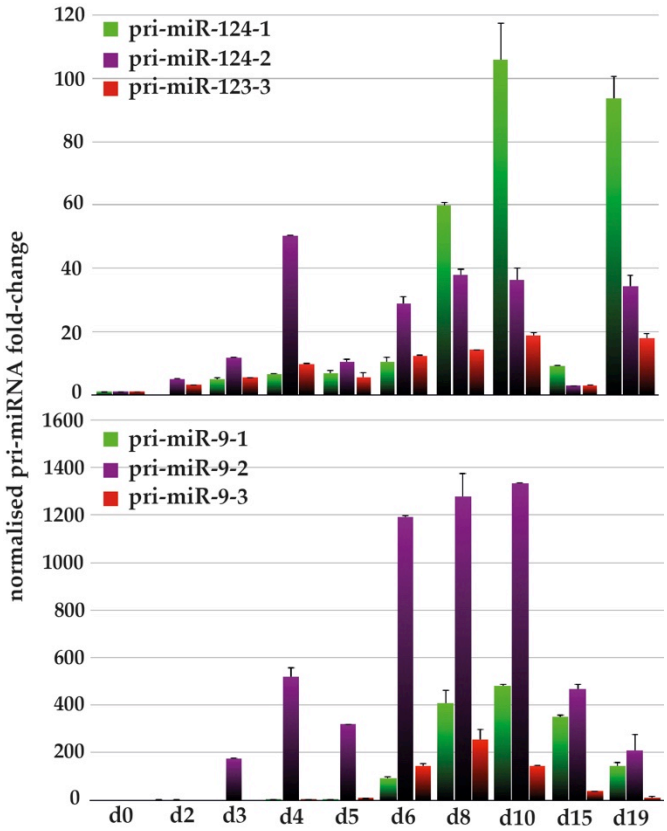

Figure 3-4 P19 differentiation time points - pri-miRNAs levels
qRT-PCR analysis of expression levels of pri-miR-124 and pri-miR-9 families during neuronal differentiation of P19 cells. Expression of pri-miR-124 and pri-miR-9 were normalised using Cyclophilin A (CypA) expression. Levels were analysed on every second day starting from day 0 (d0) until day 10 (d10) and then on day 15 (d15) and day 19 (d19).

The analysis of mature miRNAs indicated very dynamic regulation of their production. In particular, I observed a gradual increase of let-7 levels, which corresponded to the decrease of Lin28a and Lin28b. This change at day 8 reached a ~260-fold upregulation. In contrast, levels of mature miR-302a very rapidly dropped at the early stages of neuronal differentiation and by day 2 they were detected below ~20% of their initial expression. These patterns of let-7 and miR-302a expression are in agreement with those previously observed during cell differentiation (Balzer et al., 2010; Lipchina et al., 2011; Parchem et al., 2015; Wang et al., 2014). Also, let-7 levels correlated with expression pattern of its known regulator – Lin28. Additionally to suggesting post-transcriptional mechanisms regulating miR-302a and let-7 production, these two observations validate our neuronal differentiation system.

Following the initial validation of the assay, I decided to determine changes to the mature neuro-enriched miR-9 and miR-124. Interestingly, throughout the differentiation, mature levels of miR-124 remained undetected. However, levels of miR-9 were changed dramatically but did not correlate linearly when compared to pri-miR-9 expression pattern. Specifically at the early stages of neuronal differentiation, miR-9 levels were induced by ~50-60-fold which suggests that only approximately 10% of pri-miR-9 expressed at this stage is processed. Importantly, at the late stages of neuronal differentiation I observed a 500-550-fold increase in miR-9 expression levels, indicating ~40% processing of its primary transcript (Figure 3-5).

Data presented here was normalised to miR-16 and CypA levels in the case of mature and primary miRNA levels analysis respectively.

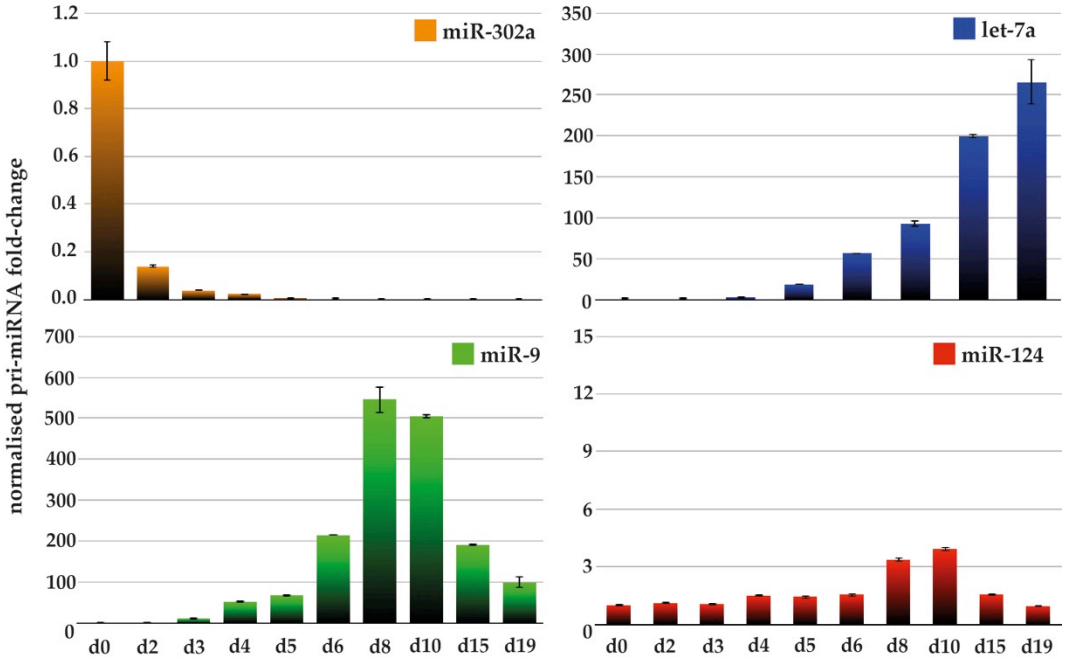

Figure 3-5 P19 differentiation time points - miRNA levels
qRT-PCR analysis of mature miR-302a, let-7a, miR-124 and miR-9 levels throughout neuronal differentiation of P19 cells. Expression levels were normalised using miR-16 expression. Levels were analysed on every second day starting from day 0 (d0) until day 10 (d10) and then on day 15 (d15) and day 19 (d19).

qRT-PCR is a very good method allowing for the accurate and fast quantification of expression changes. However, it relies strongly on the specificity of primers and does not allow for the direct measurement of this specificity during the quantification process. However, I determined the specificity of primers used in qRT-PCR assays after the amplification process with analysis of their melting curve (data not shown). I decided to confirm my qRT-PCR results in a more direct way. Therefore, I performed northern blot analysis with probes specific for mature miR-9, miR-302a and let-7. As the probing sequence is also present in their precursor miRNAs, this approach should allow the detection of both mature and pri-miRNA levels. Furthermore, northern blot analysis allows for the absolute detection of RNA levels. Therefore, the observed changes did not require any normalisation step.

I confirmed with northern blot the abundance of miR-9, miR-302a and let-7a at differentiation stages characteristic for a given miRNA (Figure 3-6). Importantly, for pri-let-7, northern blot did not show any changes of levels at three different time-points of differentiation, but clearly indicated a strong induction of mature let-7 levels on day 9. Similarly to pri-let-7, pri-miR-302a levels detected by northern blot were also not changed throughout the differentiation. However, probe against mature miR-302a showed its strong downregulation following the initiation of differentiation. In the case of miR-9, using northern blot showed a gradual increase throughout P19 cell differentiation. Unfortunately, the detection of pri-miR-9 was not strong enough to state with high confidence its increase throughout the differentiation process. Interestingly, I also did not observed any changes of mature miR-124 throughout the differentiation process (Figure 3-6).
Equal loading of RNA was ensured comparing levels of U1, S5 and tRNA at three different time points of the neuronal differentiation analysed.

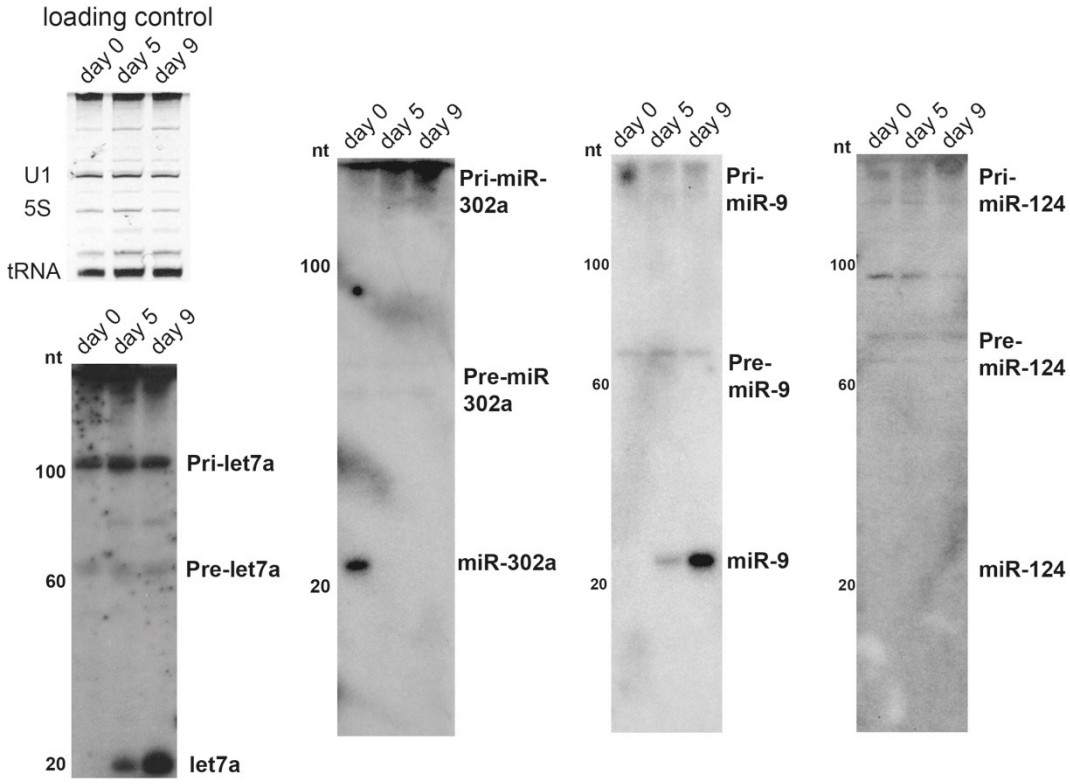

Figure 3-6 P19 differentiation time point - northern blot analysis
Northern Blot analysis of let-7a, miR-302a, miR-9, miR-124 and their precursors at day 0, day 5, day 9 of neuronal differentiation of P19 cells. Equal loading was ensured by staining total RNA with ethidium bromide to visualise U1, 5S and tRNA fractions prior to probe hybridisation.

Finally, to reach a complete level of confidence, I measured in an unbiased way levels or pri-miR-9 and mature miR-9 as counts detected in RNA-sequencing and small RNA-sequencing, respectively. This analysis was performed for undifferentiated (day 0) and early-differentiated (day 4) cells (**Error! Reference source not found.**). I confirmed previous observations and showed that pri-miR-9-2 normalised counts increased from undetectable on day 0 to ~400 on day 4. Importantly, this change very poorly corresponded to the change of mature miR-9, which accumulated very modestly to ~4 normalised reads on day 4. This was in contrast to another miRNA, which is strongly induced upon retinoic acid treatment – miR-10a. In this case, pri-miR-10a levels increased from undetectable on day 0 to ~170 normalised reads on day 4. Unlike miR-9, mature levels of miR-10a followed this change and increased from ~4 normalised counts on day 0 to ~460 normalised counts on day 4.

Importantly, the levels of pri-miR-16 and mature miR-16 remained relatively stable during the differentiation. This further supported the use of miR-16 as a normalisation factor for qRT-PCR.

Figure 3-7 P19 day4 neuronal differentiation - RNA sequencing.
Small RNA sequencing and regular RNA sequencing were performed on day 0 (orange bars) and day 4 (red bars) of retinoic acid-induced P19 neuronal differentiation. Primary and mature miRNA levels were analysed for miR-9, miR-10a and miR-16.

3.2.2 Post-transcriptional regulation of pri-miR-9 and pri-miR-124 processing

It has been previously reported that let-7 biogenesis is controlled post-transcriptionally and my current findings corroborate with these observations (Chang et al., 2013; Desjardins et al., 2014; Heo et al., 2009; Lightfoot et al., 2011; Loughlin et al., 2012; Piskounova et al., 2011; Piskounova et al., 2008). Moreover, they also suggest that miR-9 and miR-302a biogenesis could be regulated post-transcriptionally as their mature miRNA levels did not directly follow the pattern of pri-miRNA transcription.

To determine whether biogenesis of brain enriched miR-9 and stem cell specific miR-302a is post-transcriptionally controlled, I employed an *in vitro* processing assay. Briefly, radiolabelled *in vitro* transcribed primary miRNA probe was incubated with either extracts derived from undifferentiated (day 0 – lane 1) or differentiated (day 9 – lane 2) P19 cells (Figure 3-8). This approach allowed post-transcriptional and transcriptional events to be uncoupled by eliminating the later. Therefore, all of the observed changes could be related to the post-transcriptional mechanism.

As before, I used the performance of pri-let-7a as a benchmark, as its *in vitro* processing and post-transcriptional mechanisms have been previously extensively studied (Chang et al., 2013; Desjardins et al., 2014; Faehnle et al., 2014; Hagan et al., 2009; Piskounova et al., 2008). Importantly, I was able to recapitulate previous observations, as I did not observe efficient processing of pri-let-7a in extracts derived from early stages of neuronal differentiation. However, late-differentiation extracts provided favourable conditions for the processing of pri-let-7a, likely due to the absence of a known pri-let-7a processing inhibitor on day 9 – Lin28a.

In the case of pri-miR-302a, I observed the opposite situation as its primary miRNA was efficiently processed in undifferentiated extracts when compared to the day 9 reaction.

Interestingly, I observed a processing pattern for pri-miR-9 similar to that of pri-let-7a. Specifically, *in vitro* processing of pri-miR-9 was almost undetectable in day 0 extracts and became more efficient on day 9. These results suggested that processing of both miR-9 and miR-302a could be regulated by the presence of negative or positive factors in undifferentiated and differentiated cells, for both miRNAs acting in opposing manner. Moreover, in the case of pri-miR-9 processing in day 0 P19 extracts, I observed a non-specific product that did not correspond to pre-miR-9, as it was not detected in processing reaction in day 9 P19 and HeLa cell extracts. This observation could potentially suggest the destabilisation of pre-miR-9 in day 0 P19 extracts. Processing of pri-miR-101 was relatively equal between day 0 and day 9 extracts.

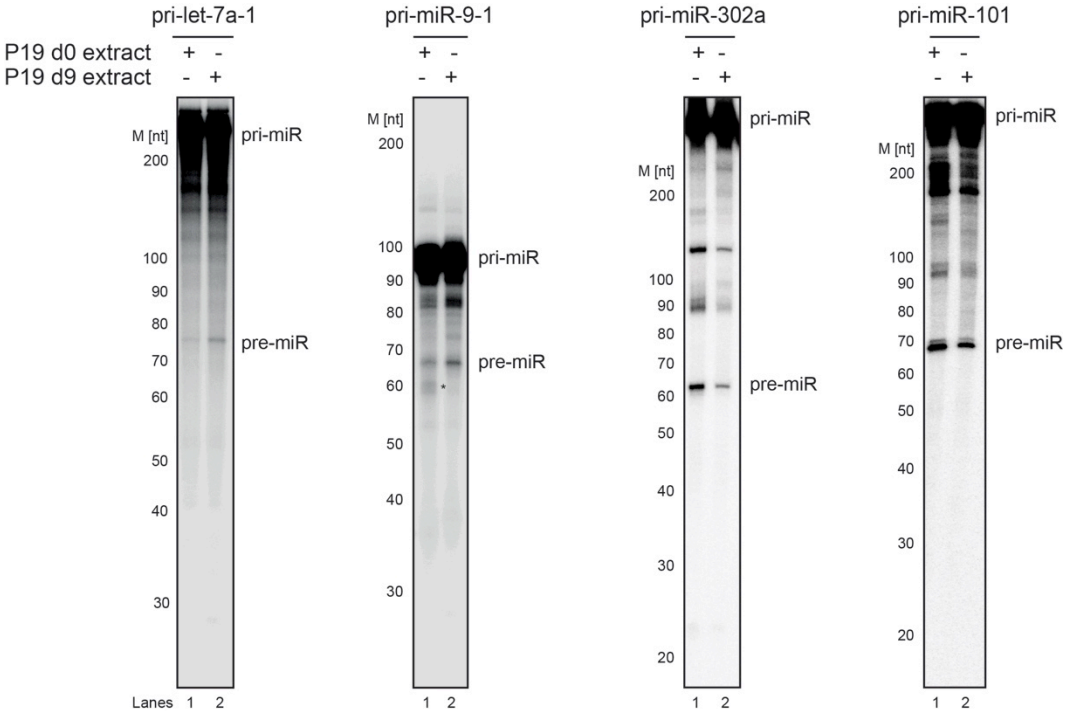

Figure 3-8 P19 neuronal differentiation *in vitro* processing - pri-miRNAs
Extracts from day 0 and day 9 (lanes 1 and 2, respectively) of P19 cell extracts were incubated with *in vitro*-transcribed pri-miR-9-1 to determine levels of post-transcriptional processing at different stages of neuronal differentiation. Pri-let-7a-1a, pri-miR-302a and pri-miR-101 were used to validate distinct differentiation stages of P19 cell extracts.

To confirm the specificity of the processing reaction and molecular weights of the precursor miRNAs, I compared processing of the pri-let-7a and pri-miR-9 in HeLa extracts before and after the depletion of Drosha or DGCR8. Importantly, *in vitro* processing in extracts derived from RNAi treated Drosha or DGCR8 cells displayed complete inhibition of the primary miRNA processing in the absence of the microprocessor components (Figure 3-9).

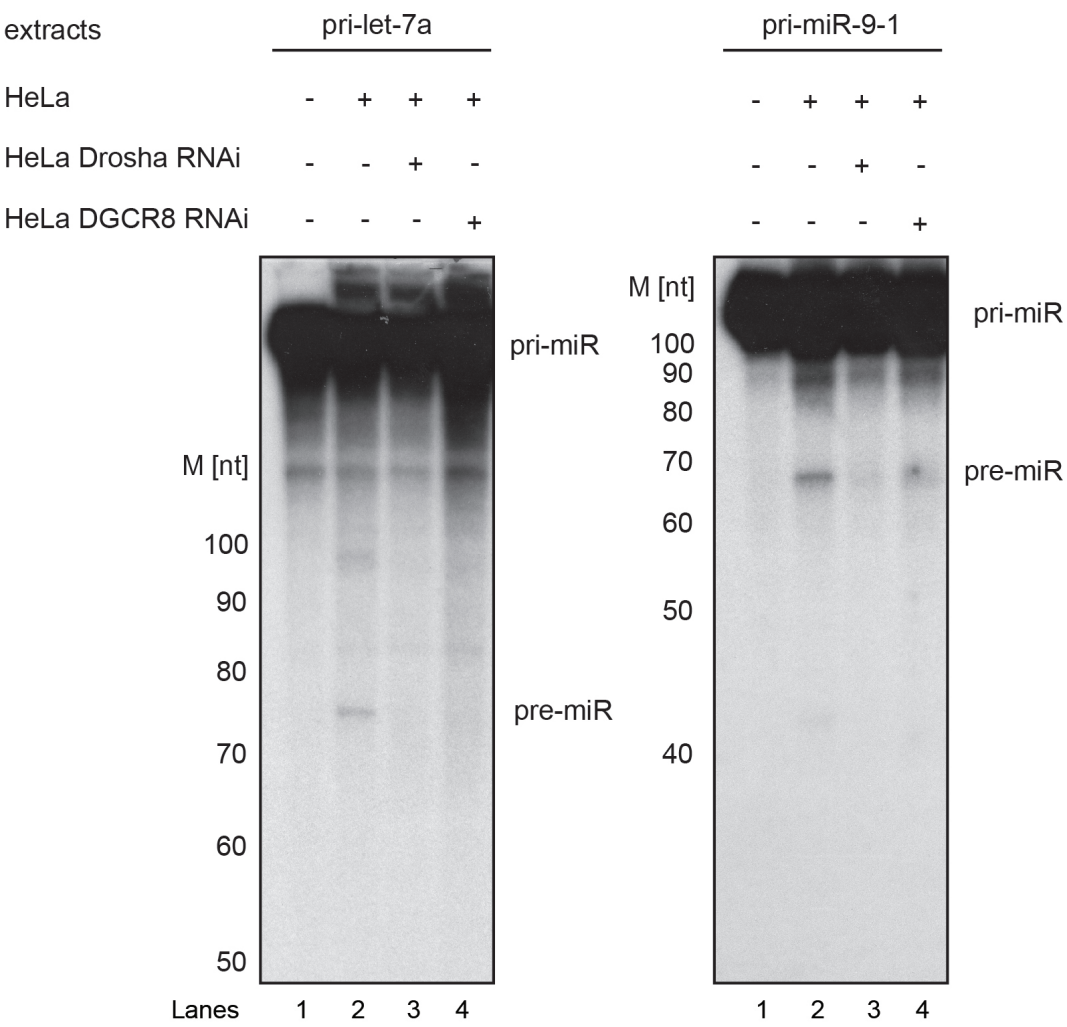

Figure 3-9 *In-vitro* processing in Drosha/DGCR8 null extracts - pri-miRNAs

Pri-let-7a and pri-miR-9-1 probes were incubated with HeLa wild type extracts (lane 2) and extracts derived from Drosha/DGCR8 siRNA treated cells to estimate specificity of the processing products (lanes 3 and 4).

These findings reinforced my previous *in vivo* observations of the dynamic character of miRNA production. Furthermore, they suggest the existence of auxiliary factors post-transcriptionally regulating pri-miR-9 and pri-miR-302a processing.

3.2.3 Terminal loop of pri-miR-9 and pri-miR-124 is involved in the post-transcriptional regulation of their processing

Previous work supported role of pri-let-7a conserved terminal loop (CTL) as a platform to mediate post-transcriptional events (Desjardins et al.,

2014; Lightfoot et al., 2011; Loughlin et al., 2012). Therefore, I decided to compare pri-miR-9 and pri-let-7a terminal loops. As the pri-let-7a terminal loop manifested strong evolutional conservancy across vertebrates, I determined the level of preservation of the pri-miR-9 terminal loop using the muscle DNA/RNA alignment algorithm (Edgar, 2004). As shown in Figure 3-10, pri-miR-9-TL is well conserved across mammals, which could potentially underline its biological importance.

Moreover, I used the mfold programme to predict secondary structures for both pri-miRNAs. Interestingly, both terminal loops vary in size and predicted secondary structures. The pri-let-7a terminal loop is larger, with 33nt, and is formed of two hairpins (Figure 3-11a). In contrast, the pri-miR-9 loop is much smaller and with only 14nt was predicted to form a classic single hairpin (Figure 3-11a). Interestingly, both loops contained the "GGAG" motif that was shown to play an important role in binding Lin28a ZnFD and the subsequent uridylation and degradation of pre-let-7a (Mayr and Heinemann, 2013; Nam et al., 2011). What is even more striking is that upstream of the "GGAG" motif, both pri-let-7a and pri-miR-9 terminal loops contain a stretch of sequence rich in "G" and "U" nucleotides that was shown to be important for binding Lin28a CSD (Mayr et al., 2012; Nam et al., 2011).

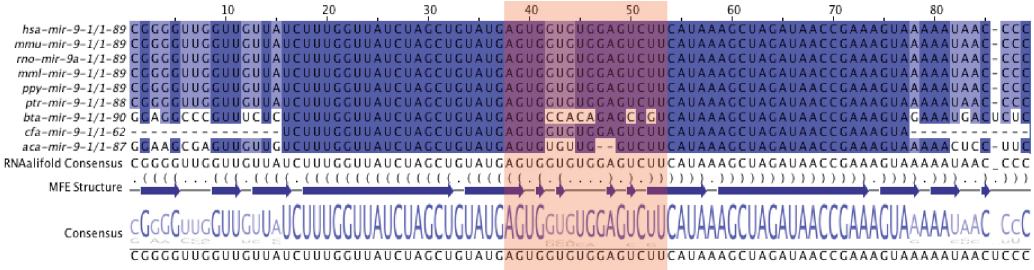

Figure 3-10 pre-miR-9 conservation.
Pre-miR-9 sequences of several species were aligned using multiple alignment muscle algorithm. RNAfold was used to predict secondary and free energy values (MFE) structure on the calculated consensus sequence. Red box represents the region corresponding to the conserved terminal loop.
hsa –Homo sapiens, mmu – Mus musulus, rno – Rattus norvegicus, ppy – Pongo pygmaeus, ptr – Pan troglodytes, bta – Bos Taurus, cfa - Canis familiaris, aca - Anolis carolinensis.

In order to determine the functional relevance of miR-9-CTL, I performed an *in vitro* processing assay in the presence of unlabelled pri-miR-9-CTL

and pri-miR-124-CTL, which served as competitors for potential processing factors. I used unlabelled pri-miR-124-CTL to control for the specificity of the competition assay. As expected, pri-miR-9 was not efficiently processed in day 0 P19 cell extracts. However, this processing was greatly increased upon addition of the unlabelled pri-miR-9-CTL. This effect was specific as I did not observe an increase in pri-miR-9 processing efficiency upon the addition of pri-miR-124-CTL (Figure 3-11).

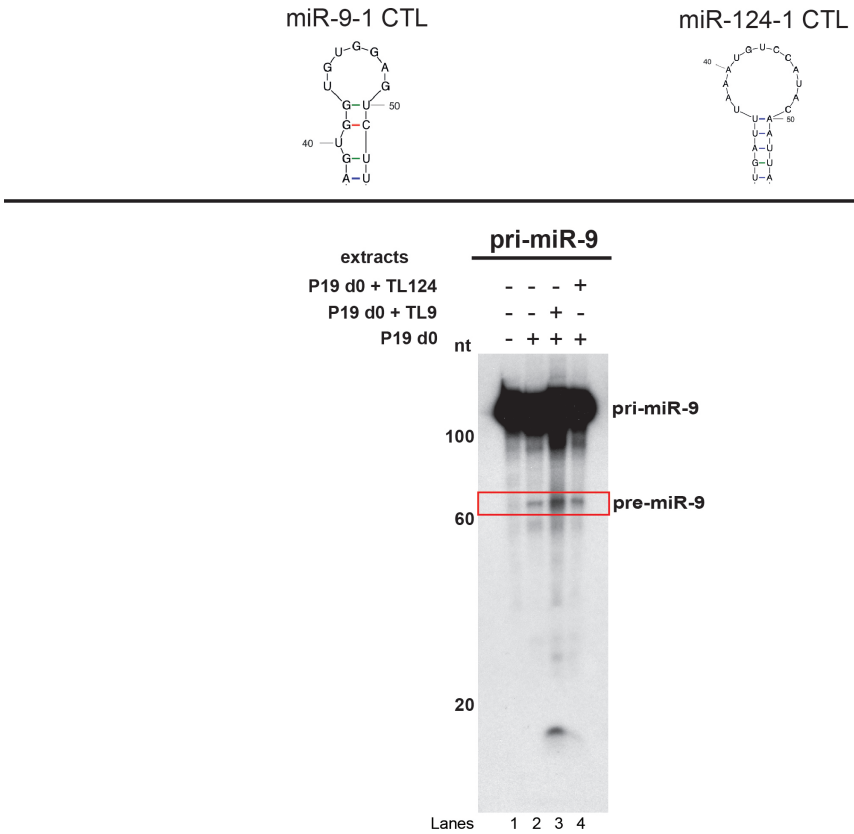

Figure 3-11 P19 day 9 - *in vitro* processing - CTL competition assay
In vitro processing was performed in presence of the terminal loops that served as competing factors.
Top panel) mfold representation of miR-9-1 and miR-124-CTL used in the assay
Bottom panel) Processing reaction of pri-miR-9-1 in undifferentiated cells. No competing terminal loop added – lane 2. Terminal loop of pri-miR-9-1 and pri-miR-124-1 added – lane 3 and 4 respectively.

3.3 Identification of putative factors mediating the post-transcriptional regulation

3.3.1 General consideration regarding protein identification strategy

Thus far, all of my findings suggested the presence of protein factors that could interact with the terminal loop of pri-miR-9 and inhibit the processing of the precursor miRNA or initiate its destabilisation.

I decided to use RNA-pull-down and mass spectrometry to identify these proteins. In order to obtain differentiation stage-specific RNA-pull-down, I performed stable isotope labelling of amino-acids (SILAC) in cultured P19 cells. Heavy [13C]Arg/[13C]Lys or light [12C]Arg/[12Lys] isotopes were incorporated in cultured P19 cells and confirmed using mass-spectrometry for proper peptide weight detection (data not shown). Subsequently, P19Light cells were differentiated as described above to obtain day 9 extracts, whereas P19Heavy were maintained undifferentiated to prepare day 0 extracts. I then mixed day 0 and day 9 extracts together before performing pull down to minimise an experimental error and obtain unbiased information about stage-specific protein composition.

As represented in Figure 3-12, precursor RNA molecules coupled to beads were used to precipitate protein complexes from extracts derived from undifferentiated (day 0) and differentiated (day 9) P19-labelled cells. The results for identified proteins were annotated as heavy to light peptide ratios. Therefore, protein complexes that were characteristic for undifferentiated P19 cells were represented as an increasing ratio above 1. Respectively, protein complexes that were characteristic for differentiated P19 cells were represented as a decreasing ratio between 0 and 1.

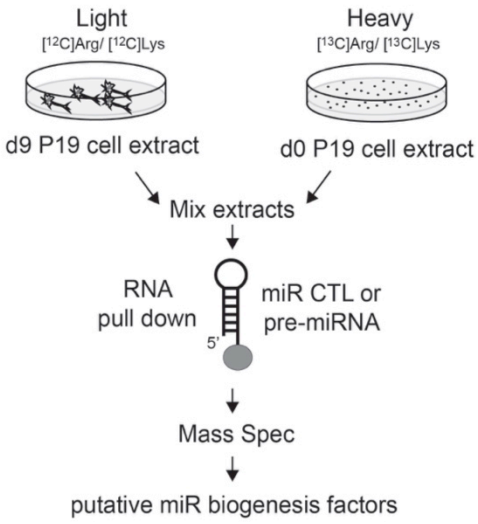

Figure 3-12 Schematic representation of SILAC-MS identification approach

In order to determine putative processing factors interacting with pre-miR-9-CTL. Full-length pre-miR-9 or its CTL were coupled with the beads and incubated with differentially labelled extracts derived from undifferentiated and differentiated cells. Extracts were mixed and incubated with bead conjugated RNA. Following series of stringent washed ribonucleoprotein complexes were analysed by mass spectrometry.

3.3.2 Protein identified to interact with pre-miR-9 and pre-miR-124

Using SILAC-assisted RNA-pull-down, I managed to identify several proteins that interacted with pri-miR-9-CTL in a stage-specific manner. Those who interacted, especially on day 0 P19, were RAP1-interacting factor homolog (Rif1), Lin28A, and Line1-type transposase domain-containing protein Sal-like protein 4 (Sall4). On the other hand, RNA-binding proteins Musashi-1 (Msi1) and Neuro-Oncological Ventral Antigen-2 (Nova2) were shown to interact in day 9 P19 extracts (Figure 3-13).

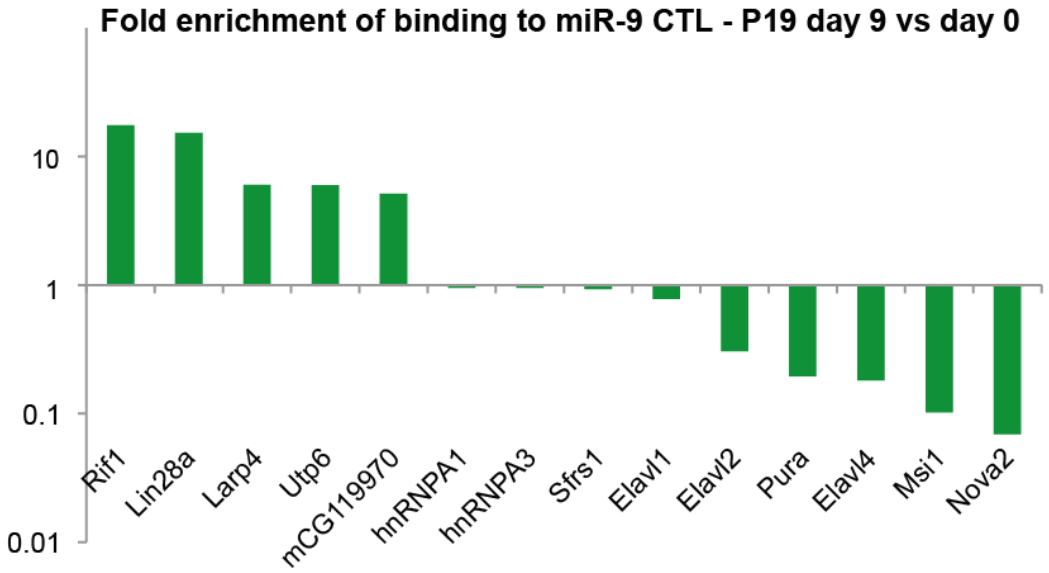

Figure 3-13 SILAC-MS analysis - pri-miR-9-1-CTL
Results of ribonucleoprotein complexes associated with pri-miR-9-1-CTL represented as day 0 / day 9 ratio.

To further confirm the interactions, I performed SILAC combined with full-length pre-miRNA pull-down and mass spectrometry using extracts from undifferentiated P19 cells. I was able to show that pre-let-7a interacted with Lin28a as well as Khsrp and hnRNPA1, all of which were implicated in the regulation of let-7 biogenesis. For some reason, I did not identify CCHC11 (Tut4) in my pull-down, potentially suggesting that Lin28a/Tut4 interaction might be transient under these experimental conditions.

The pre-miR-9 pull-down revealed a number of other specific factors that may contribute to the regulation of miR-9 processing. However, when full length pre-miRNA and terminal loop pull-downs were compared, only Lin28a was found to associate with pre-miR-9-1. Importantly, I could show that Lin28a fold-enrichment with these molecules were similar to that observed with pre-let-7a (Figure 3-14).

These data provide strong evidence that Lin28a can be involved in the post-transcriptional regulation of miR-9 biogenesis. Therefore, I decided to validate this finding and characterise its functional relevance.

Protein	Fold Enrichment (pre-miR/beads p19 d0)	
	pre-let-7a-1	pre-miR-9-1
Hnrnpa0	67.4	13.4
Hnrnpab	58.8	28.1
Hnrnpa1	57.1	65.3
Hnrnpd	52.7	17.4
Srsf3	50	30.3
Hnrnpa2b1	45.4	33.6
Hnrpdl	42.1	33.5
Rbmxl1	28.9	10
Ncl	26.9	13.3
Hnrnpa3	25.4	23.3
Hnrnpf	25.1	6.3
Hnrnph1	23.2	12.3
Srsf5	20.5	13.8
Rps20	18.1	NaN
Dhx9	15.5	9
Ssb	15	21.4
Dazap1	14.8	6.3
Elavl1	14.6	9.4
Syncrip	14.2	10.2
Fus	14.2	11.3
Lin28a	12.7	9.5
Dhx36	12.1	6.7
UPF0568	10.7	4
Srsf1	9.8	33
Igf2bp1	9.5	7.8
Ubap2l	8.7	4.3
Khsrp	8.4	21.4

Protein	Fold Enrichment (pre-miR/beads p19 d0)	
	pre-miR-9-1	pre-let-7a-1
Hnrnpa1	65.3	57.1
Cnbp	34.9	NaN
Hnrnpa2b1	33.6	45.4
Hnrpdl	33.5	42.1
Srsf1	33	9.8
Srsf7	30.5	NaN
Srsf3	30.3	50
Hnrnpab	28.1	58.8
MAST1	25.4	NaN
Srsf2	25.4	3
Hnrnpa3	23.3	25.4
Khsrp	21.4	8.4
Ssb	21.4	15
Rpl22	17.9	NaN
Hnrnpd	17.4	52.7
Fubp3	17.4	6.2
Srsf5	13.8	20.5
Hnrnpa0	13.4	67.4
Ncl	13.3	26.9
Celf1	12.6	NaN
Hnrnph1	12.3	23.2
Hnrnpm	11.5	3.6
Fus	11.3	14.2
Rps9	10.4	NaN
U2af2	10.3	6.9
Syncrip	10.2	14.2
Rbmxl1	10	28.9
Lin28a	9.5	12.7
Elavl1	9.4	14.6
Sfpq	9	7.7
Rtcd1	9	7.9
Ilf3	9	7.7
Dhx9	9	15.5
Sart3	8.9	NaN
Rpl26-ps4	8.8	NaN
Csda	8.7	6.2
Cpsf6	8.6	NaN
Tial1	8.6	NaN

Figure 3-14 SILAC-MS analysis - pre-miRNA pulldown
Ribonucleoprotein complexes associated with full length pre-let-7a-1 and pre-miR-9-1. Results represented as the enrichment of protein factors on RNA conjugated beads versus unconjugated beads. Two tables represents two repeats of the SILAC MS analysis.

3.3.3 Validation of Lin28a interaction with the terminal loop of pri-miR-9

In order to validate quantitative mass spectrometry findings, I performed separate pull-down reactions in day 0 and day 9 extracts (Figure 3-15). Subsequently, I resolved associated protein complexes using SDS-PAGE electrophoresis and identified proteins using specific antibodies. I was able to demonstrate that proteins bind specifically to conjugated RNA molecules as no antibody binding was observed in pull-downs performed with unconjugated beads. In day 0 extracts, I confirmed that Lin28a interacted with pri-miR-9-1-CTL. On the other hand, Msi1 interacted with the terminal loop only in day 9 extracts. Importantly, hnRNPA1, an abundant RNA-binding protein, was shown to interact with pri-miR-9-1-CTL in both day 0 and day 9 extracts. These observations strongly support SILAC MS findings that Lin28a interacts with pri-miR-9-1-CTL in undifferentiated P19 cells.

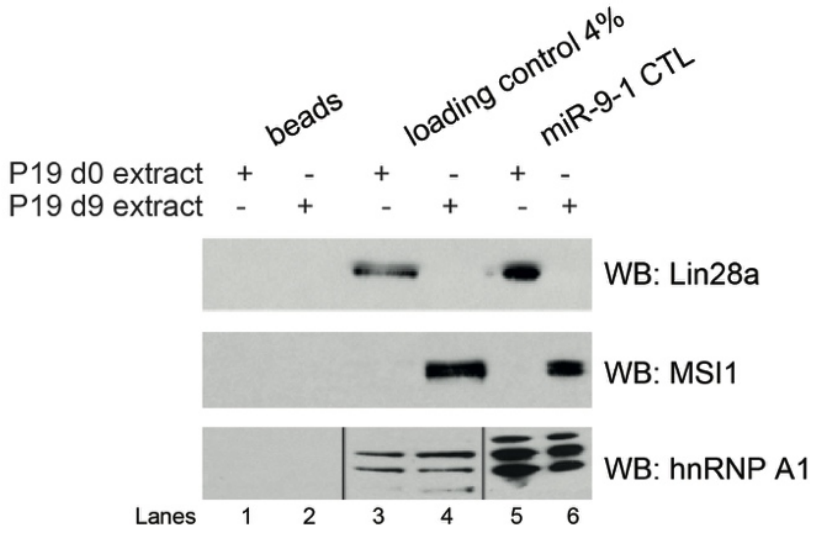

Figure 3-15 SILAC-MS - validation of assay specificity
Pull-downs with unconjugated beads and beads conjugated with pri-miR-9-CTL were performed on day 0 and day 9 separately to confirm the specificity of the assay and validate the MS results. Following the stringent washes, ribonucleoprotein complexes were resolved on PAGE and analysed with western blot for the expression of day 0 and day 9 specific Lin28a and MSI1, respectively. Equal loadings were ensured by incubation with hnRNP A1 that expression is constant between day 0 and day 9.

3.4 Functional relevance of Lin28a-pre-miR-9 interaction

The expression of Lin28a is dynamically regulated throughout neuronal differentiation. Its expression is elevated during the early stages of development and is switched off during differentiation (Vogt et al., 2012). The regulation of its levels is essential for the inhibition of let-7 production at the early stages of differentiation and development (Balzer et al., 2010). In order to determine whether Lin28a is also involved in the biogenesis of miR-9, I implemented two strategies. Firstly, I decided to deplete Lin28a in P19 cells and subsequently allow their differentiation, with lower than normal levels of Lin28a, until day 4. In the second approach, I generated P19 stable cell lines that maintain expression of Lin28a throughout the neuronal differentiation.

3.4.1 siRNA mediated knockdown of Lin28a leads to an increase of mature miR-9 levels

In order to knockdown Lin28a levels, I electroporated a pool of siRNAs against mouse Lin28a. Subsequently, 48h after electroporation, I induced differentiation with retinoic acid; on day 4, following the RA treatment, I collected the cells and analysed the material. Western blot analysis of Lin28a expression at day 4 of the differentiation demonstrated that the protein was depleted efficiently to around 20-30% of mock treatment (Figure 3-16).

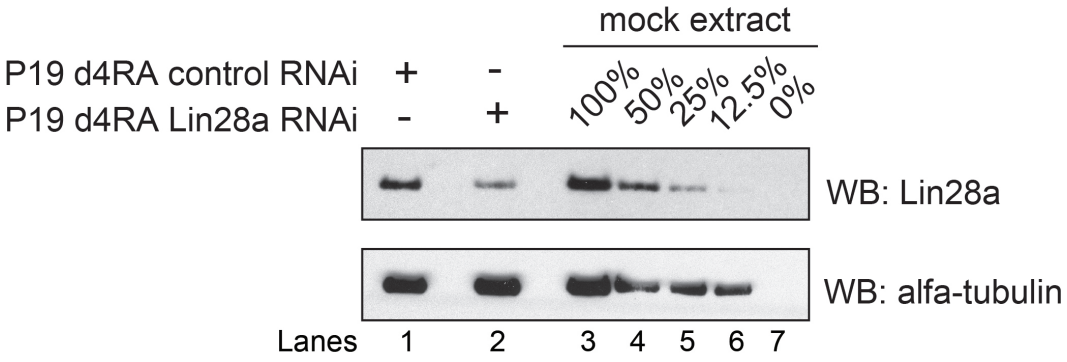

Figure 3-16 P19 d4RA - Li28a RNAi - western blot
P19 cells were treated with control and Lin28a siRNAs and differentiated until day 4 (lanes 1 and 2 respectively). Western blot shows levels of Lin28a depletion in relation to levels of α-tubulin. To estimate the efficiency of the knockdown, serial dilutions of mock extracts were analysed along the depleted samples (lanes 3 to 7).

Next, I analysed mature levels for panel of miRNAs at day 4 of P19 cells differentiation. The results were normalised to miR-16 levels and represented as fold-change in respect of mock RNAi treatment that was fixed to 1 (Figure 3-17). As expected, depletion of Lin28a resulted in a ~4-fold increase of let-7a levels at day 4 of differentiation. The levels of miRNAs unrelated to neuronal development, miR-101 and miR-122, remained unchanged. Crucially, Lin28a knockdown resulted in a modest but statistically significant 1.6-fold increase of miR-9 levels at day 4 of P19 neuronal differentiation.

This result suggested that miR-9 could indeed undergo Lin28a-mediated regulation. The discrepancy between the observed effect of Lin28 depletion on levels of miR-9 and let-7 could account for the different levels of the corresponding pri-miRNAs. As I showed previously expression of pri-let-7a is stable throughout the differentiation whereas pri-miR-9 is not present in undifferentiated P19 cells and its transcription is switched on early during neuronal differentiation (Laneve et al., 2010). This could suggest that the higher amounts of pri-let-7a would give rise to more mature let-7a in the absence of the inhibitor.

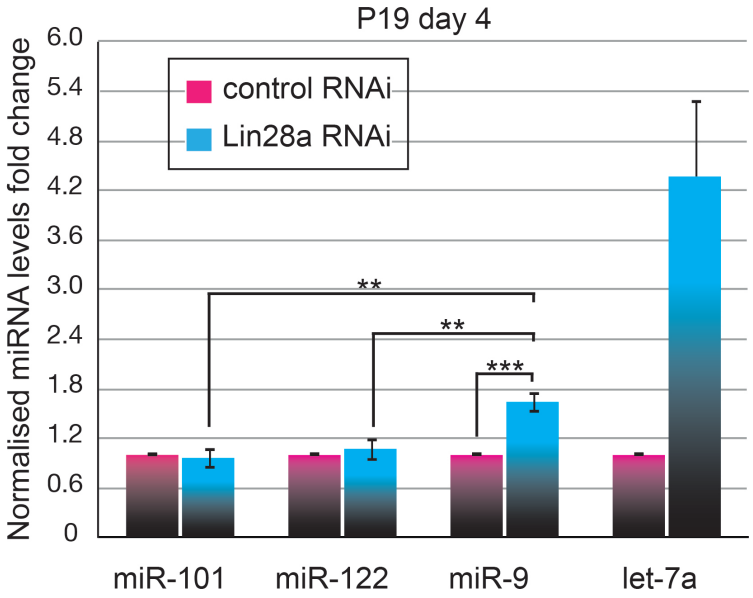

Figure 3-17 P19 d4RA - miRNA levels

Knockdown of Lin28a was followed with qRT-PCR analysis of mature miR-9 and let-7a levels at day 4 of analysis. miR-9 and let-7a levels were normalised to miR-16 and control RNAi-treated samples were fixed as a baseline. miR-101 and miR-122 were analysed as negative controls. Statistical analysis was performed using t-test on sample size n=3.

3.4.2 Constitutive expression of untagged but not GFP-tagged Lin28 is associated with downregulation of mature miR-9 levels

As RNAi mediated depletion of Lin28a resulted in modest upregulation of miR-9 levels likely due the low levels of pri-miR-9, I decided to check whether the maintenance of Lin28a in the later stages of P19 neuronal differentiation can complement the results of the RNAi experiment. At later differentiation stages, the expression of pri-miR-9 is high which should result in the stronger effects of Lin28a on its processing. To address this, I used two P19 stable cell lines.

In the first P19 cell line, human Lin28a was C-terminally tagged with GFP protein and randomly inserted into the genome. As a control for this line, P19 with the random integration of only GFP was used (the cells were gifts from Eric Moss). The second cell line was engineered using LifeTechnologies FLP-strategy. Briefly, this is a two-step process involving FRT recombinase. In the first step, I randomly integrated the FRT-site to the genome and confirmed the single integration site in open chromatin state using southern blot and lacZ assay (data not shown). In the second step, I targeted previously integrated site with a vector containing FRT complementary sequence and untagged-human Lin28a in the presence of FLP-recombinase. As a control for this a "mother" P19 cell line with integrated FRT only was used.

In order to determine whether prolonged expression of Lin28a affects let-7a and miR-9 levels, stable cell lines constitutively expressing Lin28a or Lin28aGFP were subjected to retinoic acid-mediated neuronal differentiation. Western blot analysis of both untagged and GFP-tagged Lin28a confirmed their constant expression throughout P19 differentiation (Figure 3-18).

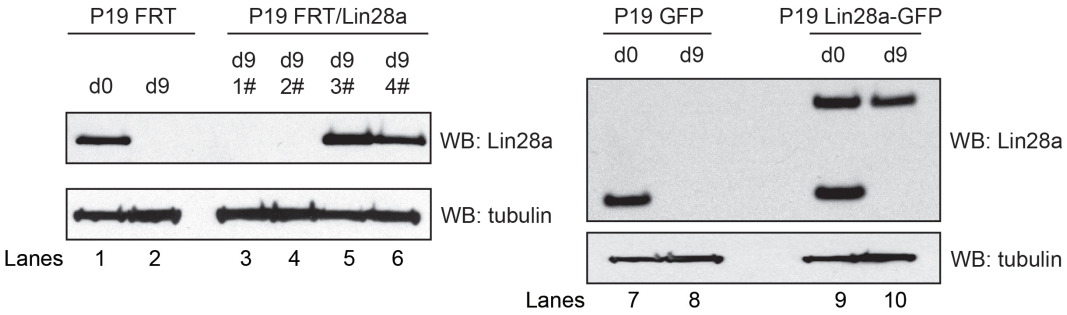

Figure 3-18 P19 Lin28a stable cell lines - western blots
Lin28a:untagged and Lin28a:GFP expression is sustained throughout differentiation and remains at similar levels at both undifferentiated and differentiated cells. Protein samples derived from day 0 (d0) and day 9 (d9) were resolved on 4-12% PAGE and analysed with western blot for the expression of Lin28a or Lin28aGFP. Endogenous Lin28a was expressed only in d0 protein extracts from control protein extracts – P19 FRT and P19 GFP cell extracts. Constitutive expression in d0 and d9 of untagged Lin28a was confirmed in P19 FRT:Lin28a cell extracts. Lin28a:GFP migrated as higher molecular weight band in respect to endogenous Lin28a and its constitutive expression was confirmed in d0 and d9 cell extracts. To validate equal loading western blot analysis of α-tubulin was performed.

The stable expression of untagged and GFP-tagged Lin28a resulted in a decrease of let-7 levels in the final stages of the neuronal differentiation of P19 cells (Figure 3-19). Surprisingly, constitutive expression of untagged Lin28a but not Lin28aGFP resulted in a significant reduction of miR-9 levels in the final stages of P19 cell neuronal differentiation (Figure 3-19). Similar results were obtained from two independent Lin28a integrations. This is a very important observation for a couple of reasons. Firstly, it validates Lin28a as a post-transcriptional regulator of miR-9 biogenesis. Secondly, it shows that GFP-tagged Lin28a could be functionally compromised. Finally, it provides evidence that the mechanisms of Lin28a-mediated inhibition of microRNA biogenesis might be different for let-7 and miR-9.

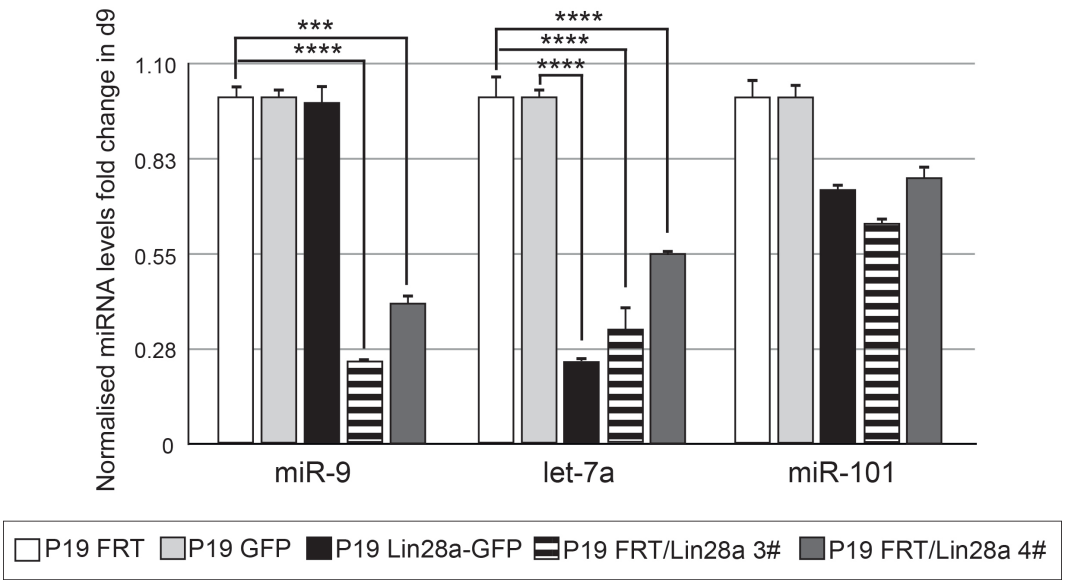

Figure 3-19 P19 Lin28a stable cell lines - miRNA levels
P19 stable cell lines were differentiated and mature miRNA levels of miR-9, let-7a and miR-101 were compared in day 0 and day 9 of individual P19 cell lines. Results were normalised to miR-16 expression and expression in the P19FRT cell line was set as the baseline. Statistical analysis was performed using t-test on representative sample size n=3.

In order to eliminate the possibility that observed down-regulation of miR-9 in day 9 is an indirect effect of Lin28a affecting the differentiation process in general, I used an inducible stable cell line. In this case, a P19 stable cell line was generated that expresses transactivator and untagged Lin28a upon treatment with doxycycline (Dox). Prior to Dox treatment, cells were differentiated with retinoic acid until day 9 at which point Dox was added to trigger the expression of Lin28a. The expression of Lin28a was confirmed with western blot (Figure 3-20a). Importantly, similarly to the untagged constitutive P19:Lin28a stable cell line, both let-7 and miR-9 levels were downregulated upon the induction of Lin28a (Figure 3-20b). Moreover, as the differentiation process occurred in this scenario as in the wild-type P19 cells, the observed decrease in let-7 and miR-9 levels could account for the induced ectopic expression of Lin28a.

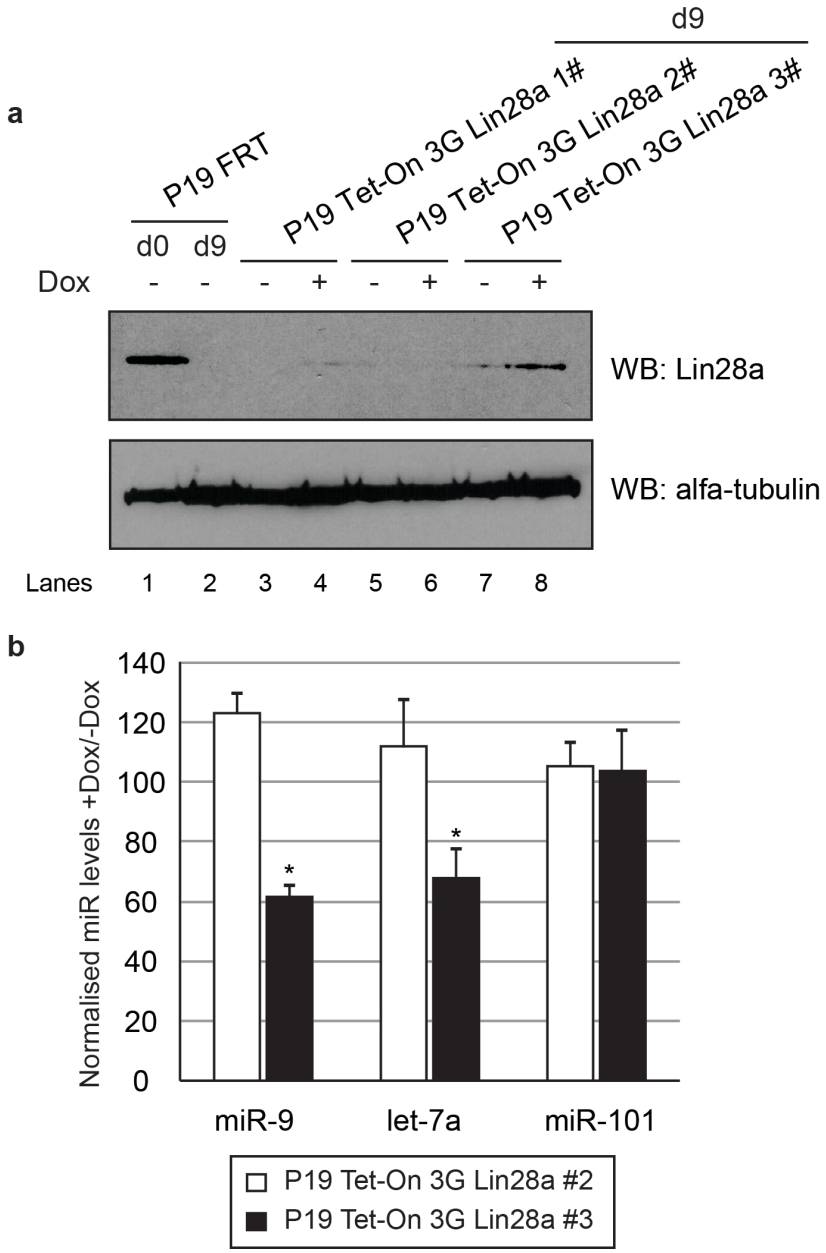

Figure 3-20 P19 Tet-On Lin28a - mature miRNA levels

P19 cells were differentiated as normal and Lin28a was induced with Doxycycline upon differentiation.

a) Western Blot – Comparison of Lin28a levels between day 0 (d0) and day 9 (d9) in P19FRT control cell line and Lin28a inducible P19 cells. Protein samples were resolved on 4-12% PAGE and analysed with western blot for the expression of Lin28a. Equal loading was ensured with western blot analysis of α-tubulin.

b) qRT-PCR – comparison of mature miR-9, let-7a and miR-101 levels in undifferentiated and differentiated cells. Results were normalised to miR-16 expression and expression of the miRNAs in day 9 of Dox(-) cells was set as a baseline. Dox(-) - doxycycline untreated; Dox(+) – doxycycline treated. Statistical analysis was performed using t-test on representative sample size n=3.

I also tested for a potential negative feedback loop on transcription by characterising the expression of pri-miR-9 and pri-let-7a in constitutive and inducible cell lines (Figure 3-21a and Figure 3-21b). Interestingly, the levels of pri-miR-9 transcripts were also decreased upon doxycycline treatment, suggesting that Lin28a can directly or indirectly influence the abundance of primary miR-9. However, pri-let-7a-1 levels were upregulated upon doxycycline treatment showing that Lin28a could play a dual role in feedback regulatory circuits. Nevertheless, these findings together confirm the role of Lin28a in the regulation of miR-9 production and also indicate its dual character by affecting both post-transcriptional and transcriptional events of miR-9 production.

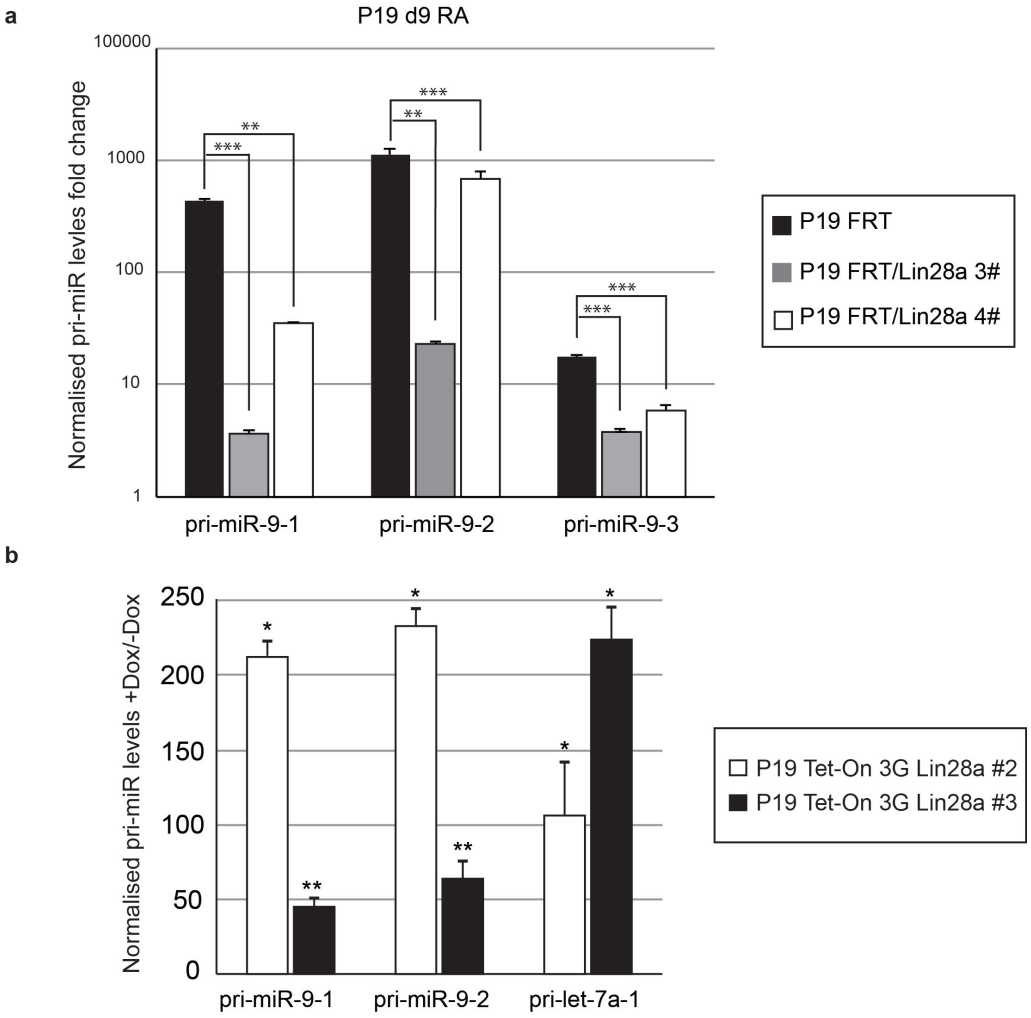

Figure 3-21 P19Lin28a stable lines - pri-miRNA levels

P19 Lin28a stable cell lines were differentiated and pri-miRNA levels were analysed.

a) pri-miR-9-1, -2, -3 levels upon differentiation of P19 cells with constitutive expression of Lin28a:untagged. Results were normalised to Cyclophilin A expression and the pri-miRNAs expression in day 9 P19 FRT control cell lines was set as a baseline.
b) Pri-miR-9-1, -2, -3 levels prior to the differentiation and induction with doxycycline in P19 inducible cell line. Results were normalised to Cyclophilin A expression and the pre-miRNAs expression in day 9 of Dox(-) P19 cells were set as a baseline. Dox(-) – doxycycline untreated; Dox(+) – doxycycline treated.

Statistical analysis was performed with t-test on representative sample size n=3.

3.4.3 Lin28a stable cell line displayed change in morphology of their embryonic bodies

Providing that the post-transcriptional regulation of miR-9 is important for proper neuronal differentiation, I decided to compare morphology of embryonic bodies obtained throughout the differentiation process of P19:Lin28a and P19:Lin28aGFP stable cell lines and their controls P19:FRT and P19:GFP, respectively. I used the size of embryonic bodies (EB) represented as an area, which was measured using image J software on a population of approximately 100 cells (Figure 3-22). I observed a striking difference between the size of embryonic bodies generated in the process of P19:Lin28a and P19:Lin28aGFP neuronal differentiation. Lin28aGFP line supported the normal formation of embryonic bodies with sizes in the range between 10^4 and 10^5 default area units, whereas the P19 line with constitutive expression of untagged Lin28a was able to generate embryonic bodies that were 10-times smaller with sizes in the range between 10^3 and 10^4. The average size of embryonic bodies in both P19:FRT and P19:GFP controls was similar to the size of P19:Lin28GFP embryonic bodies.

These observations prove two potential implications. First and most important is the consequence of Lin28a-mediated inhibition of miR-9 production, which leads to defects in differentiation and the formation of smaller embryonic bodies. Secondly, the phenotype associated with the constitutive expression of Lin28a and miR-9 on the EB formation is independent of let-7. The last observation is supported by the fact that the P19:Lin28aGFP stable cell line fails to produce mature let-7 but has no effect on mature miR-9 and subsequently on the observed size of the embryonic bodies formed (Figure 3-19).

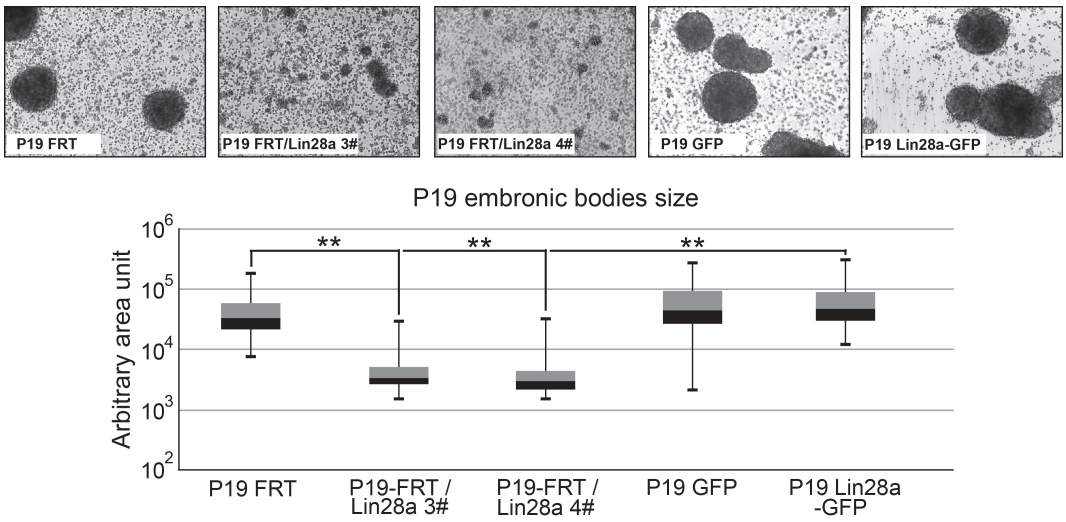

Figure 3-22 P19Lin28a stable lines - cell morphology
P19Lin28a:untagged and P19Lin28a:GFP lines were differentiated until day 4.
Top panel – Bright field images of representative groups of embryonic bodies formed during the differentiation of P19 FRT and P19 GFP control cell lines as well as untagged P19:Lin28a and P19:Lin28a:GFP stable cell lines.
Bottom panel – Area of the embryonic cell bodies was measured using imageJ analysis of microscopy pictures. Statistical analysis was performed using Mann-Whitney score test on a sample size of n=100 embryonic bodies.

3.4.4 GFP–tag does not affect expression levels or sub-cellular localisation of Lin28a

There are certain aspects of these two stable cell lines that require additional measurements to ensure that observed differences in EB size and the regulation of miR-9 levels are not artefacts of the experimental setting. First of all, the two stable cells used in the experiments were generated using different approaches. Therefore, I tested whether the expression of Lin28a and Lin28aGFP was at similar levels. Moreover, the GFP moiety has a size that is similar to Lin28a itself; therefore, it could affect not only expression of the protein, but also its localisation. First, I checked the expression levels of Lin28a and Lin28aGFP on day 9 using western blot. I compared their expression levels in three serial dilutions of the extracts and confirmed that the expression of untagged Lin28a and Lin28aGFP was at a similar level (Figure 3-23).

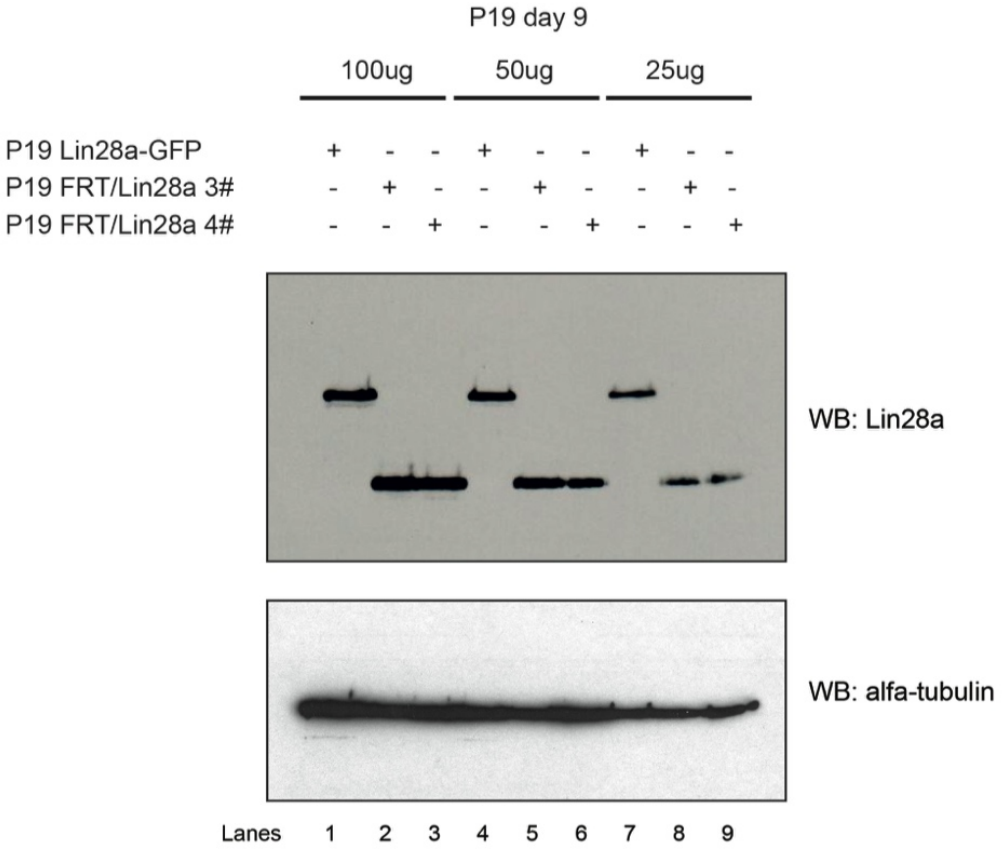

Figure 3-23 P19Lin28a - Western blot - Expression levels comparison
P19Lin28:untagged and P19Lin28a:GFP cells were differentiated and expression levels between Lin28a:untagged and Lin28a:GFP were compared on day 9 (d9) of differentiation. Protein samples were resolved on 4-12% PAGE and western blot analysis of Lin28a was performed on the group of serial dilutions of protein extract - 100μg, 50μg and 25μg. Equal loading within serial dilution groups was ensured with the western blot analysis of α-tubulin.

To determine whether the addition of C-terminal GFP affects the sub-cellular localisation of Lin28a, I performed immunofluorescence labelling of Lin28a and visualised the sub-cellular localisation with microscopy (Figure 3-24). Nuclei were stained with Hoechst as a reference. I was not able to observe differences in the sub-cellular localisation of Lin28a and Lin28aGFP in their stable cell lines. Therefore, both findings suggested that previous observations could account for the genuine effect of Lin28a and differences in the mechanisms post-transcriptionally regulating miR-9 and let-7 levels.

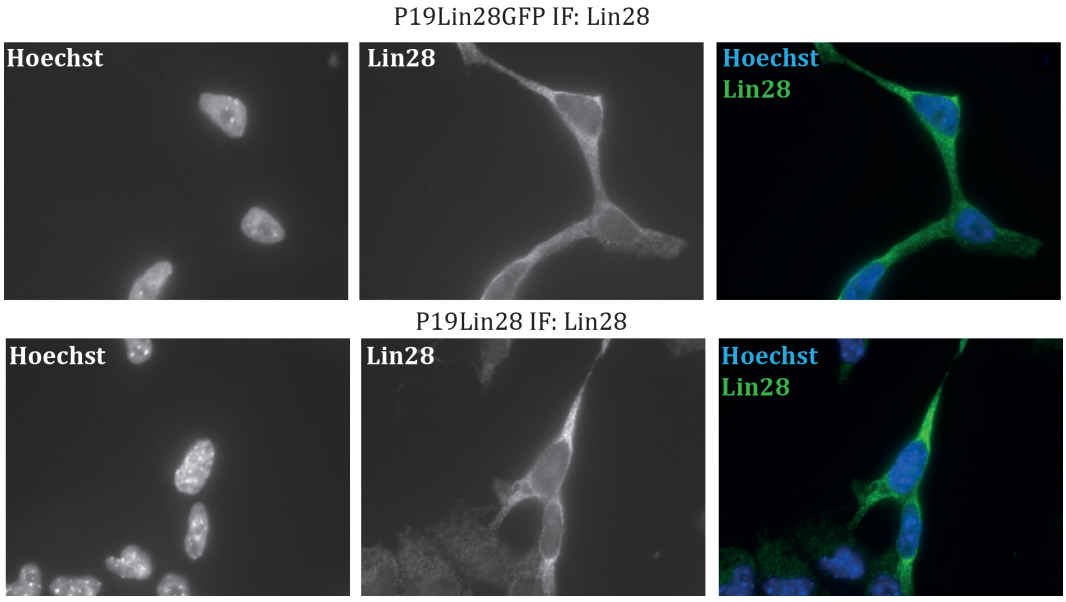

Figure 3-24 P19Lin28a - immunofluorescence
P19Lin28a:untagged and P19Lin28a:GFP cells were fixed on day 0 of differentiation and Lin28a subcellular localisation was visualised with a Lin28a-specific antibody. Nuclei were stained with Hoechst. Images to the left represent individual channels for Hoechst and Lin28a, respectively. Right image was composed by merging the individual channels. Top panel subcellular localisation in P19Lin28:GFP; bottom panel subcellular localisation in P19Lin28a:untagged.

3.4.5 Overexpression of pri-miR-9 and pri-let-7a in P19 day 0

To uncouple the effects of differentiation on miR-9 levels, I performed pri-miRNA transgene overexpression in undifferentiated P19 cells. Overexpression of pri-miR-9 and pri-let-7a driven by a cytomegalovirus (CMV) promoter resulted in the very low induction of mature miRNAs (Figure 3-25). Importantly, overexpression of pri-let-7a-1/miR-16 TL mutant, which escapes Lin28a-mediated regulation, produced more than ~20-fold mature let-7a. This suggests that the accumulation of miR-9 and let-7a levels in undifferentiated cells is post-transcriptionally suppressed. Interestingly, overexpression of cognate pri-miR-9-1/miR-16 TL mutant did not result in de-repression of miR-9 accumulation (Figure 3-25). This implies the existence of additional layers of post-transcriptional miR-9 regulation, most probably preventing an accumulation of mature miRNA in undifferentiated P19 cells.

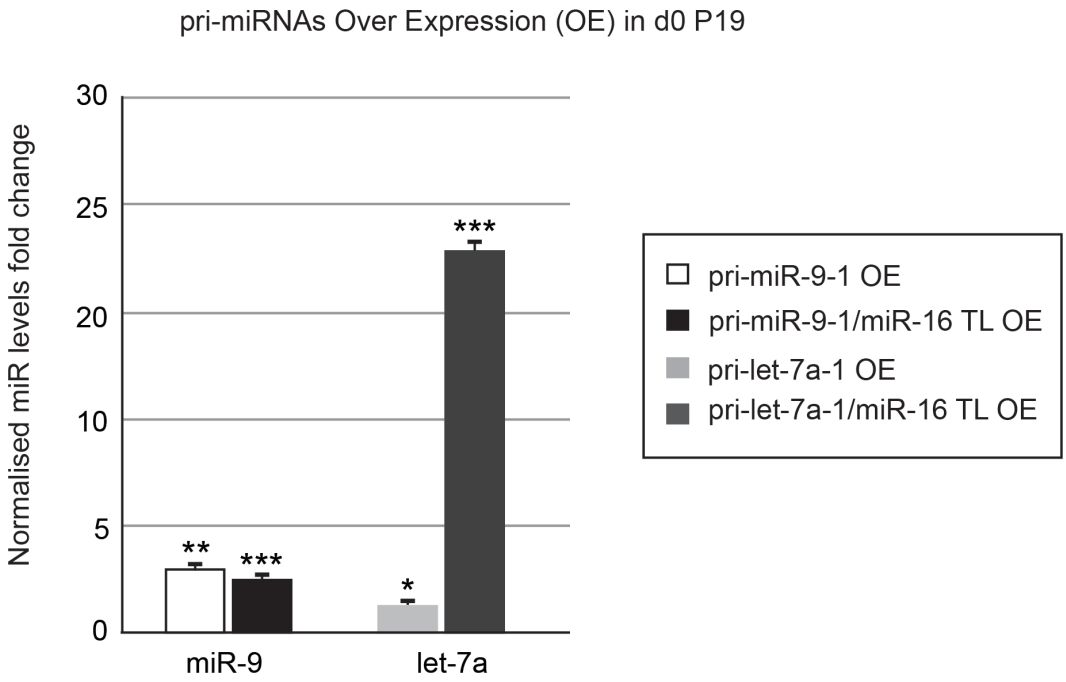

Figure 3-25 P19 - pri-miRNAs over expression
Mutants of pri-miR-9-1 and pri-let-7a conserved terminal loops were transfected into undifferentiated day 0 P19 cells. Subsequently levels of mature miR-9 and let-7a were analysed with qRT-PCR. Results were normalised to miR-16 expression levels and the miRNAs expression in day 0 cells transfected with wild-type pri-miRNAs were set as a baseline. Statistical analysis was performed using t-test on sample size n=3.

To test whether the observed blockage of miR-9 production by pri-miR-9-1/miR-16 TL mutant is characteristic for undifferentiated P19 cells, I performed co-transfection of wild-type pri-miR-9-1-TL or pri-miR-9-1/miR-16 TL and pri-miR-9-1/miR-30-TL mutants along with Lin28a expression vector in HeLa cells. Subsequently, I analysed mature levels of miR-9 and let-7a with qRT-PCR. Results were normalised to miR-16 levels and represented as fold-change in respect to the transfection of precursor miRNA only. According to mfold structural folding predictions, these mutants provide different sequence and structural characteristic of the pre-miR-9 terminal loop (Figure 3-26). As a benchmark, I also engineered similar mutations in pri-let-7a terminal loops.

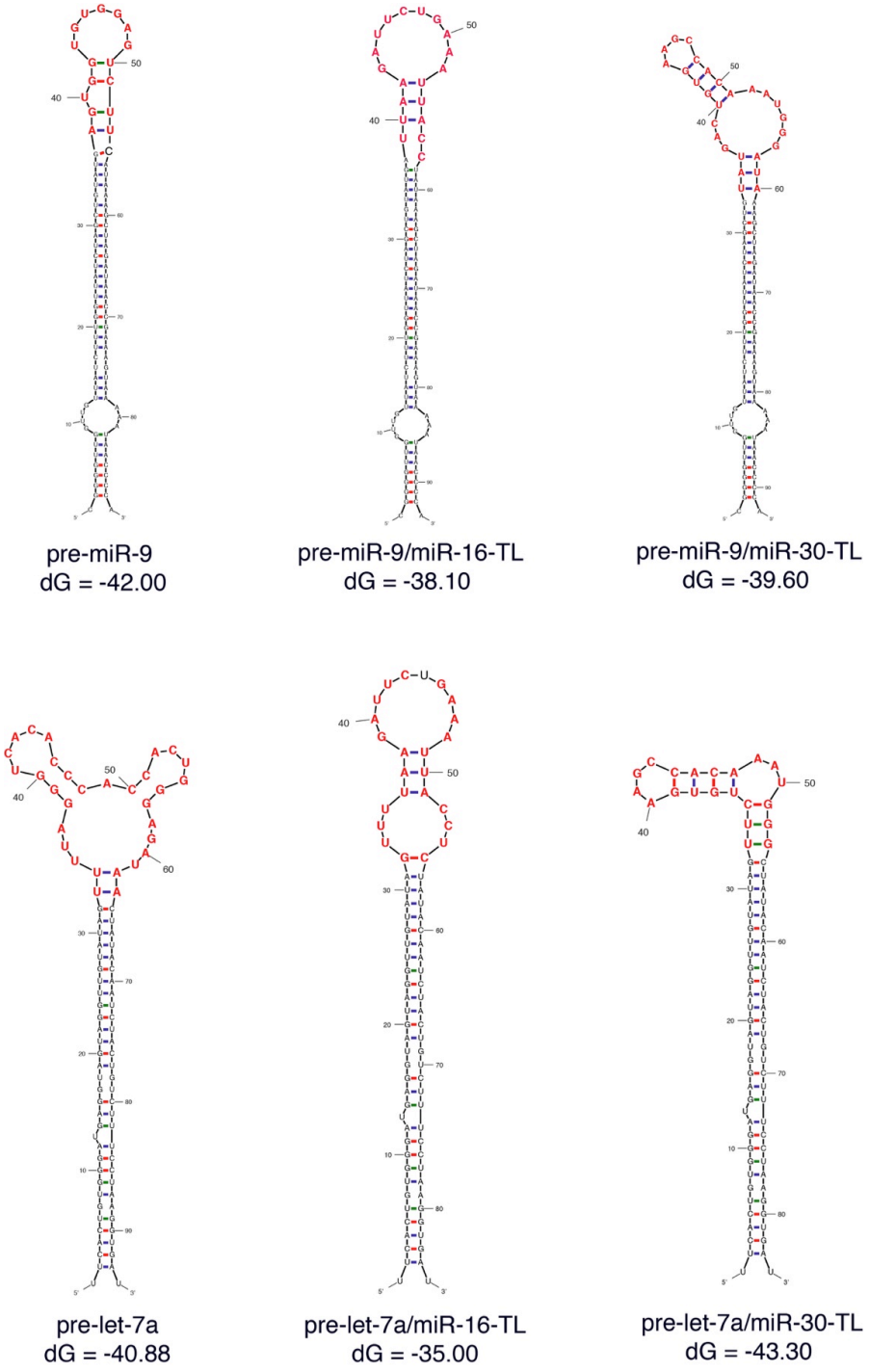

Figure 3-26 mfold prediction of pre-miRNAs mutants secondary structures

Top panel: graphical representation of pre-miR-9 secondary fold and its terminal loop mutants

Bottom panel: graphical representation of pre-let-7a secondary fold and its terminal loop mutants.

dG corresponds to free energy values calculated for the particular fold with mfold algorithm.

I observed that co-expression of Lin28a with wild-type pri-let-7a and pri-miR-9-1 resulted in strong inhibition of their mature miRNA levels, as shown in Figure 3-27a and Figure 3-27b. Importantly, mutants with miR-16-TL were able to generate more mature miR-9 and let-7a suggesting a decrease in Lin28a-associated post-transcriptional blockage. Interestingly, the terminal loop of miR-30 is bigger and contain sequence motifs that could be recognised by Lin28a and indeed pri-miR-9-1/miR-30-TL and pri-let-7a/miR-30-TL generated less mature miRNAs when compared to their miR-16-TL counterparts. These findings further strengthen the possibility that P19 undifferentiated cells could have additional layers of mature miR-9 regulation. However, most importantly, they demonstrated in a cellular context that Lin28a post-transcriptionally regulates miR-9 biogenesis in the differentiation-independent manner.

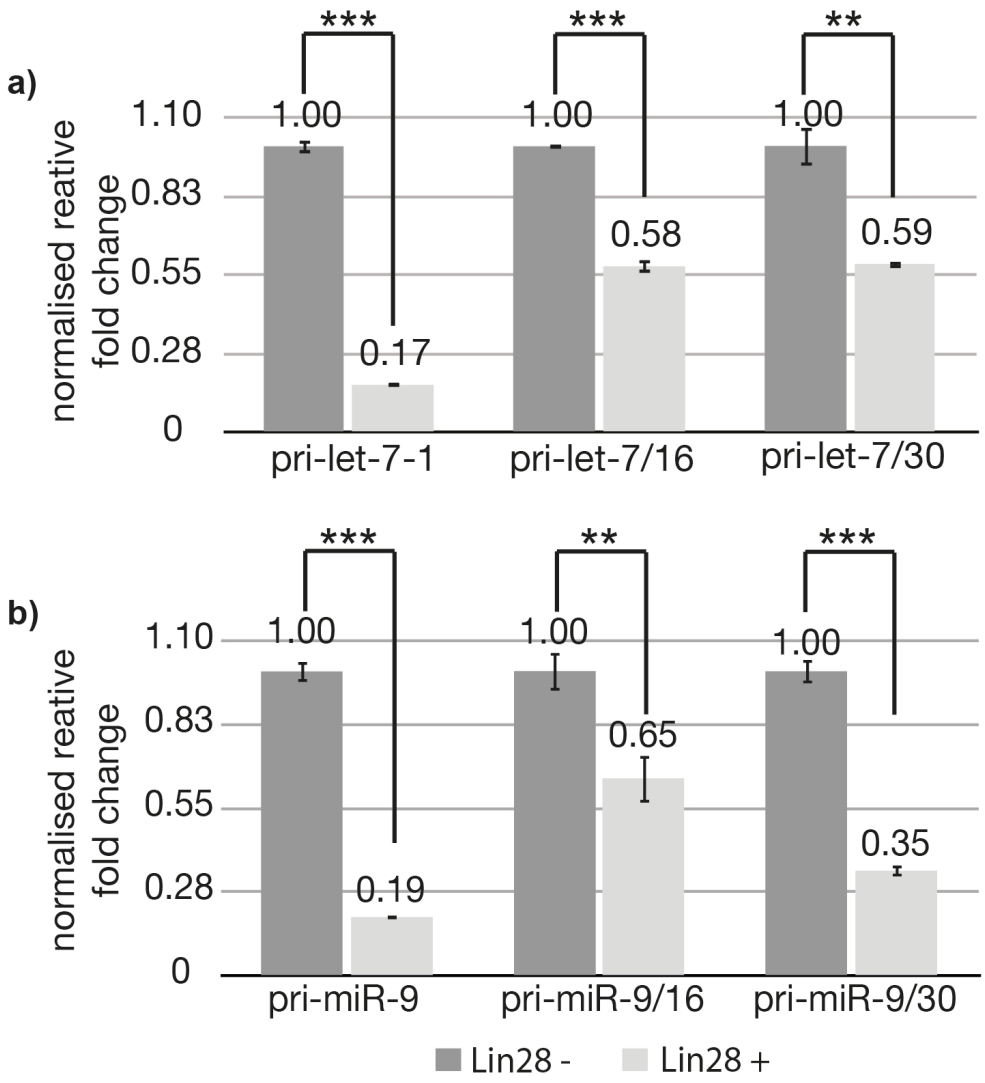

Figure 3-27 HeLa - pri-miRNA-TL mutants overexpression

a) pri-let-7a and its terminal loop mutant pri-let-7a/miR-16-TL and pri-let-7a/miR-30-TL were transfected together with Lin28a. Mature let-7a levels were detected with qRT-PCR.

b) pri-lmiR-9-1 and its terminal loop mutant pri-miR-9-1/miR-16-TL and pri-miR-9-1/miR-30-TL were transfected together with Lin28a. Mature miR-9 levels were detected with qRT-PCR.

Results were normalised to miR-16 expression levels and expression of the miR-9 and let-7a in HeLa cells not transfected with Lin28a were set as a baseline. Statistical analysis was performed using t-test on sample size n=3.

Chapter 4

4 Mechanism of Lin28a-driven post-transcriptional regulation of miR-9 levels

In the previous chapter, I showed that Lin28a interacts with pri-miR-9 and is involved in the regulation of miR-9, acting mainly at the post-transcriptional and transcriptional levels. Moreover, *in vivo* data suggest that Lin28a could inhibit miR-9 through a different mechanism because untagged Lin28a inhibited miR-9 and let-7 processing, whereas only let-7 was affected by expression of the Lin28aGFP fusion protein. Other groups have shown that Lin28a is also involved in post-transcriptional regulation of the let-7 family at the cytoplasmic step of pre-miRNA processing (Chang et al., 2013; Hagan et al., 2009; Heo et al., 2008; Nam et al., 2011). Therefore, I decided to understand in detail the mechanism of Lin28a post-transcriptional regulation of miR-9 production, focusing on its involvement in the metabolism of pre-miR-9.

4.1 Pre-miR-9 is destabilised in the early stages of neuronal differentiation.

To determine whether pre-miR-9 is regulated in a manner different from pre-let-7, I performed *in vitro* processing assays in P19 cell extracts from subsequent stages of neuronal differentiation (Figure 4-1). Incubation of pre-let-7a showed a slower migrating band, corresponding to the uridylated form of pre-let-7a, at day 0 of differentiation. The intensity of this band was reduced in reactions with extracts isolated from subsequent stages of neuronal differentiation. Importantly, quantification of bands corresponding to pre-let-7a at different stages of the differentiation enabled the verification that pre-let-7a is also moderately stabilised throughout P19 differentiation. In contrast, pre-miR-9 did not express signs of uridylation but was significantly destabilised in extracts from day 0 P19 cells, which was evident from the faster migrating degradation

products. Crucially, incubation of pre-miR-9 with extracts derived from day 4, 6, and 9 resulted in its gradual stabilisation – 2-, 4-, and 5-fold, respectively. Pre-miR-101 probes were more stable throughout the differentiation.

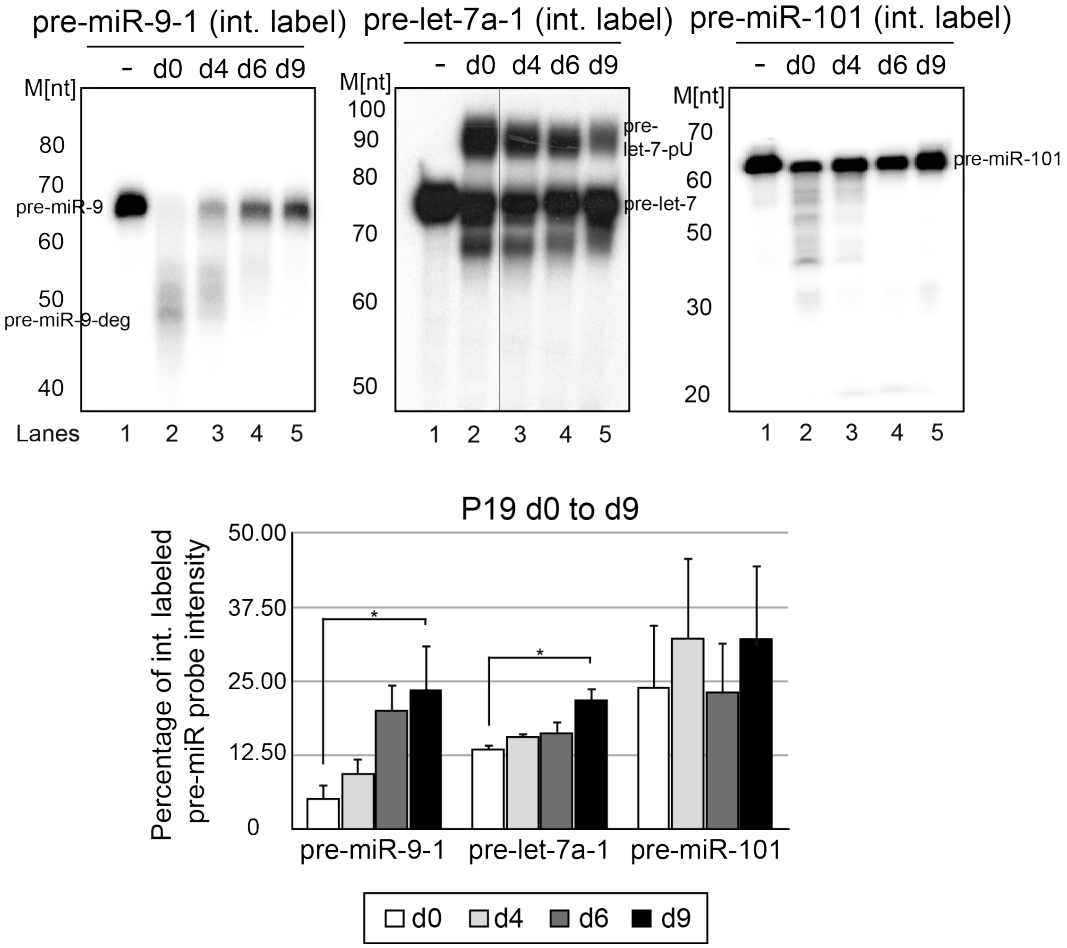

Figure 4-1 P19 neuronal differentiation - *in vitro* processing
Top panel - Radiolabelled pre-miRNAs probes were incubated with P19 cell extracts from progressive stages of neuronal differentiation – day 0 (d0), day 4 (d4), day 6 (d6), day 9 (d9). Bottom panel – quantification of the processing reactions. Results were normalised to processing of the control reaction (lane 1). Statistical analysis was performed using t-test on samples size of n=3.

miR-9 could be potentially produced in three different places in the genome. Although pri-miR-9-1, pri-miR-9-2 and pri-miR-9-3 are highly conserved, I decided to determine stability of their pre-miRNA probes at early stages of neuronal differentiation, especially as the terminal loop of pre-miR-9-2 bears single nucleotide mutation within "GGAG" motif, which is a well characterised Lin28a ZnFD binding site.

However, despite this small difference, both pre-miR-9-2 and pre-miR-9-3 were processed similarly to pri-miR-9-1 in extracts derived from day 0 and day 9. This suggested that all three isoforms of pre-miR-9 are destabilised in the early stages of P19 neuronal differentiation (Figure 4-2).

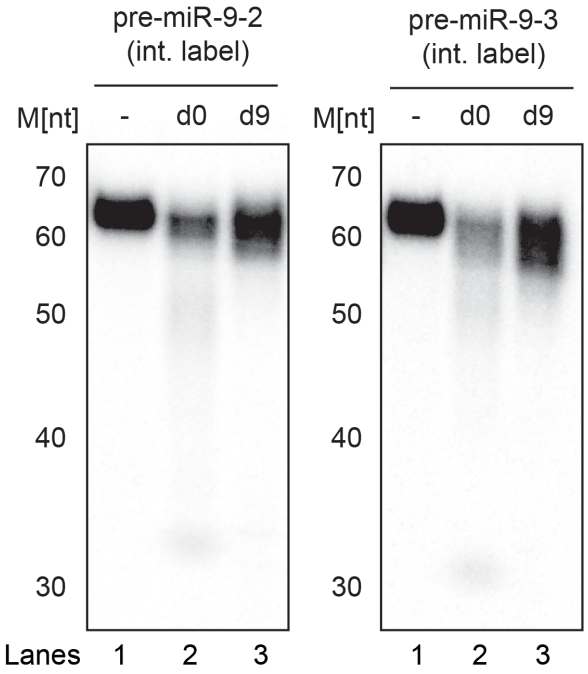

Figure 4-2 *In-vitro* processing of pri-miR-9-2, -3 in P19 day 0 and day 9 cells
Radiolabelled pre-miR-9-2 and -3 were incubated in P19 extracts derived from undifferentiated day 0 (d0) and differentiated day 9 (d9) cells.

To date, several RNA enzyme have been identified to degrade RNA using different mechanisms involving 5′- or 3′-end driven degradation, like Xrn1 or Dis3l2, respectively (Chang et al., 2013; Chatterjee et al., 2011; Chatterjee and Grosshans, 2009). To establish a pre-miR-9 degradation pattern, I incubated 5′-end-labelled miRNA precursors in day 0 extracts. Pre-miR-9-1 is more destabilised than pre-let-7a and pre-miR-101, showing signs of 3′–5′ and 5′–3′ degradation (Figure 4-3a-c). These results validate our *in vivo* data and point to different mechanisms by which pre-miR-9 and pre-let-7a are post-transcriptionally regulated during neuronal differentiation.

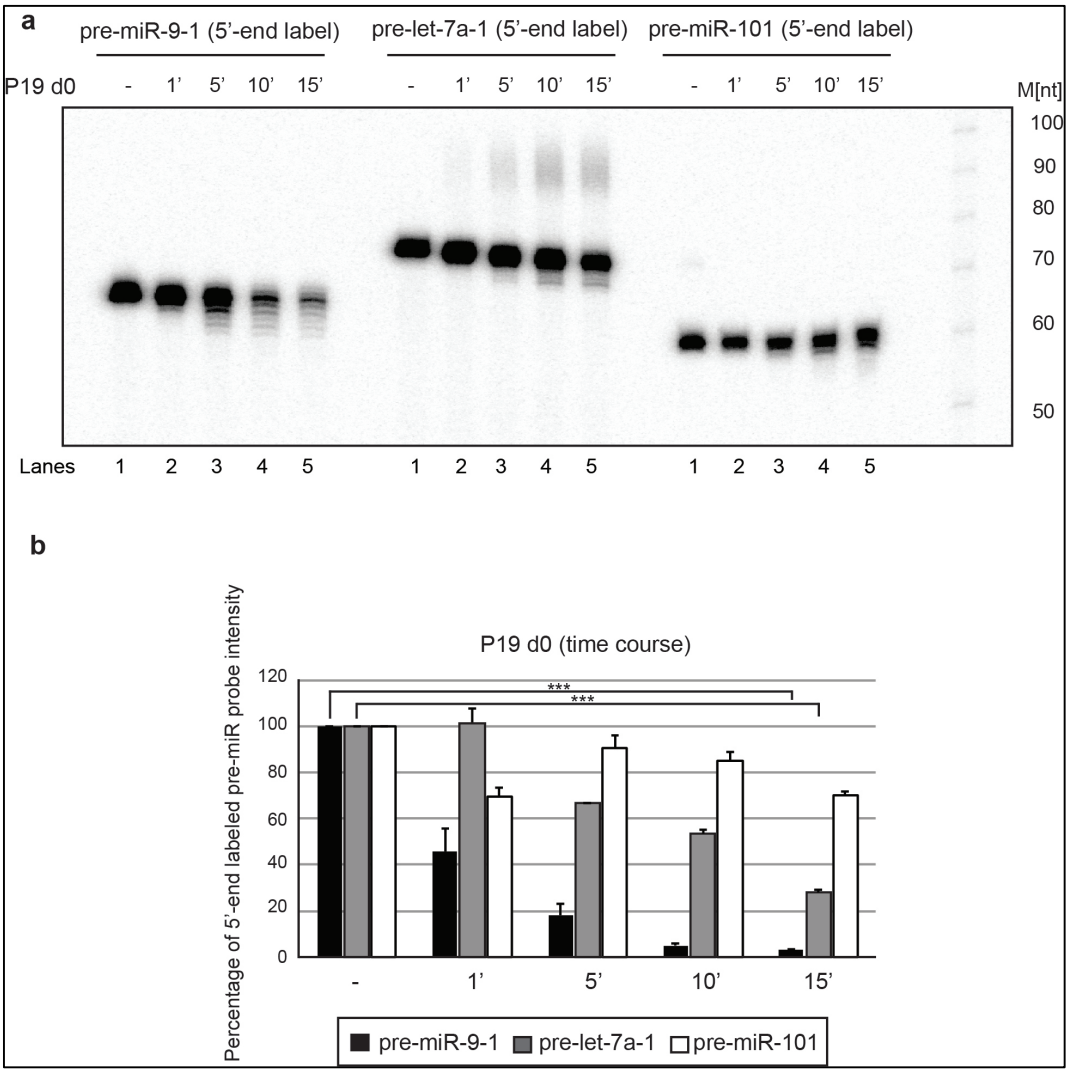

Figure 4-3 P19 d0 - *in vitro* processing - 5'end labelling

a) 5′end labelled pre-miR-9-1 and pre-let-7a were incubated in time-dependent manner with P19 d0 extracts. Reactions were performed in cell extracts derived from mock and Lin28a siRNA treated cells.

b) Quantification of the pre-miRNAs processing (5′ end labelled). Results were normalized to the processing of the control. Statistical analysis was performed using t-test on sample size n=3.

4.2 Character of Lin28a association with pre-miR-9

4.2.1 Lin28a interacts specifically with pre-miR-9

Lin28a has been previously shown to interact with a large variety of RNA targets (Cho et al., 2012; Wilbert et al., 2012). Therefore, it was particularly important to establish information about the specificity of its interaction. Previously, I showed that Lin28a interacted in stage specific manner and

did not interact with the matrix beads itself. However, to verify RNA target binding specificity, I used a panel of pre-miRNAs and performed pull-down in day 0 extracts (Figure 4-4). Pre-miR-9-1, pre-let-7a and pre-miR-101 displayed efficient Lin28a binding. Interestingly, I showed with *in vitro* processing that pre-miR-101 is relatively stable in extracts derived from various stages of P19 neuronal differentiation, which could suggest that the binding of Lin28a does not pre-empt all of the requirements necessary for its function. Most importantly, this experiment revealed that Lin28a did not bind to pre-miR-16, proving that sequence-specific features determined its association with pre-miR-9 and pre-let-7a. On the other hand, ATP-dependent RNA helicase A (DHX9) dsRNA, which binds in a non-specific manner, associated with all of the pre-miRNAs in the assay, including pre-miR-16.

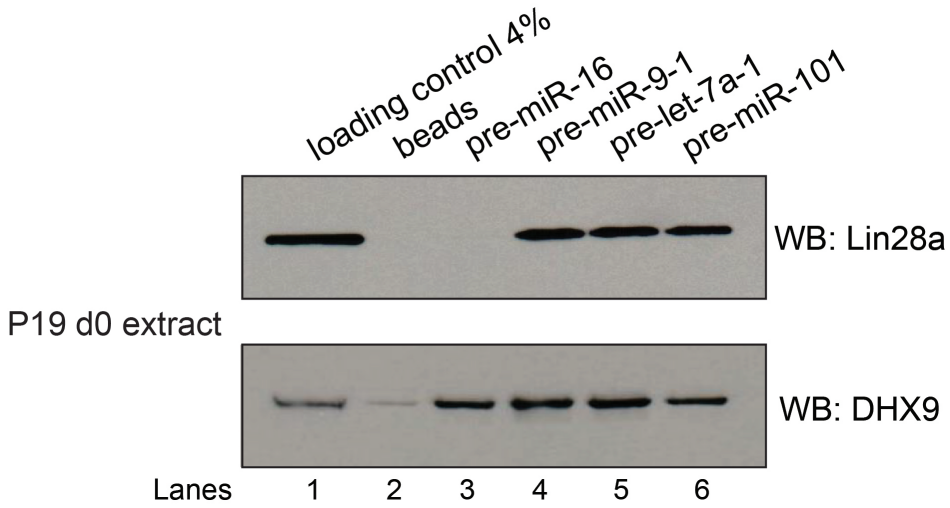

Figure 4-4 P19 day 0 - pre-miRNA pulldown
Panel of pre-miRNAs were conjugated to the beads and incubated with P19 day 0 (d0) extracts. Precipitated ribonucleoprotein complexes were resolved on 4-12% PAGE and results were analysed with western blot against Lin28a and non-specific RNA-binding helicase DHX9.

To further strengthen evidence for a specific interaction, I used a pre-miR-9/miR-16-TL mutant. Importantly, in the case of pull-down using pre-miR-9/miR-16-TL mutant, Lin28a failed to associate the RNA. This subsequently proved that sequence-specific features within pre-miR-9-CTL are required for the interaction with Lin28a (Figure 4-5).

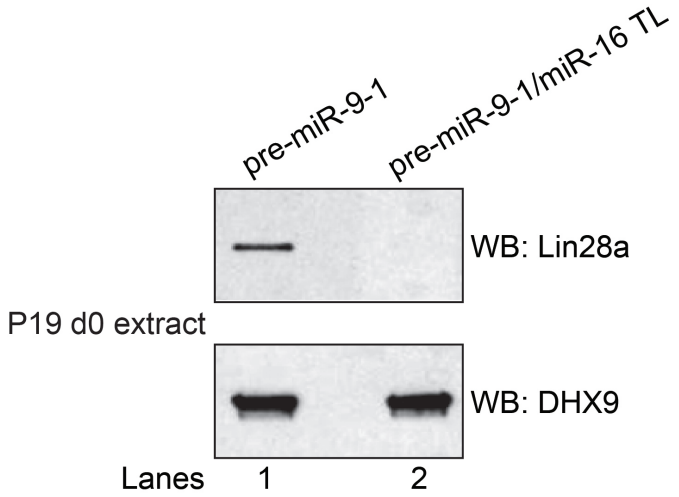

Figure 4-5 P19 day 0 - pre-miR-9-1/miR-16-CTL pulldown
Pre-miR-9-1/miR-16-CTL was conjugated to the beads and incubated with P19 day 0 extracts. Precipitated ribonucleoprotein complexes were resolved on 4-12% PAGE and results were analysed with western blot against Lin28a and DHX9.

4.2.2 Lin28a interacts directly with pre-miR-9

Many RNA-binding proteins associated with their targets and form multimeric complexes; therefore, Lin28a might either directly recognise and bind to the terminal loop of pre-miR-9, or this interaction might be mediated via other auxiliary factors. To establish whether Lin28a/pre-miR-9 interaction is direct, I deployed electromobility shift assay (EMSA) and used radiolabelled precursor miRNA molecules for visualisation purposes. In the results, any protein/RNA complexes were represented on the polyacrylamide gel as a band shift from the original position of the radiolabelled pre-miRNA alone. I performed the experiment using pre-let-7a as a positive control and pre-miR-16 as a negative control.

In the first assay, I incubated pre-miRNA probes with P19 day 0 cell extracts and competed for Lin28a binding with an antibody against Lin28a (Lin28a-ab). As a control for the specificity of competition assays, I used non-specific HRP-anti-mouse antibody (HRP-ab) (Figure 4-6). Incubation of pre-miR-16 with the extracts did not result in the formation of any RNP complexes, validating the specificity and stringency of the reaction. However, upon incubation of the pre-let-7a probe, I observed the formation of several RNP complexes represented as discrete bands above

the probe with one band of very high intensity. Importantly, the addition of Lin28a-ab but not HRP-ab resulted in the disappearance of this high intensity band, whereas other bands remained unchanged. This observation suggested that Lin28a directly interacts with pre-let-7a and the addition of Lin28a-ab interferes with the formation of the complex or binds to the pre-let-7a/Lin28a complex preventing it from entering the gel.

Similarly, in the case of pre-miR-9, I observed the formation of several complexes with two bands of strong intensity. However, the addition of Lin28a-ab but not HRP-ab resulted in the disappearance of one of the high intensity bands. Therefore, this finding suggested that Lin28a similarly to pre-let-7a associates directly with pre-miR-9 and that addition of the antibody interfered with the complex formation. Interestingly, a second high intensity band representing the complex of higher molecular weight did not disappear upon addition of the antibody. This could potentially suggest that pre-miR-9 is capable of forming multi-protein complexes or that an epitope for Lin28ab is buried inside the complex.

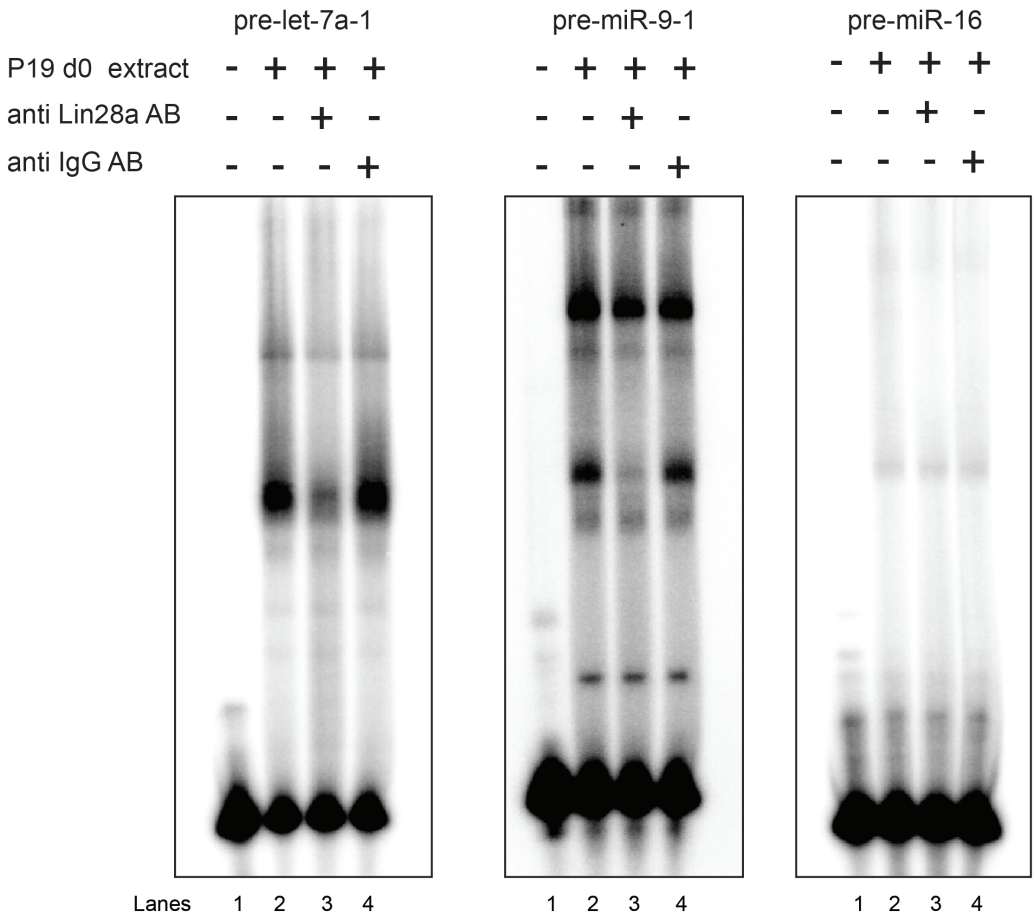

Figure 4-6 P19 day 0 - EMSA analysis
Radiolabelled pre-miR-9-1, pre-let-7a and pre-miR-16 were incubated under native conditions with P19 day 0 (d0) extracts (lane 2). Lin28a or mouse non-specific antibodies were added as competing factors (lane 3 and 4).

To further strengthen the evidence that Lin28a interacts directly with pre-miR-9, I performed EMSA analysis using recombinant Lin28a. In this scenario, any band shift observed corresponded to Lin28a/pre-miR-9 complex, as no other proteins were added to the assay. Similarly to previous experiments, binding to pre-miR-16 and pre-let-7a served as negative and positive control, respectively. I performed the experiment with a gradient of Lin28a concentrations. As expected, recombinant Lin28a did not form any complex with pre-miR-16. However, using both pre-miR-9 and pre-let-7a probes, I demonstrated that Lin28a binds directly to these molecules.

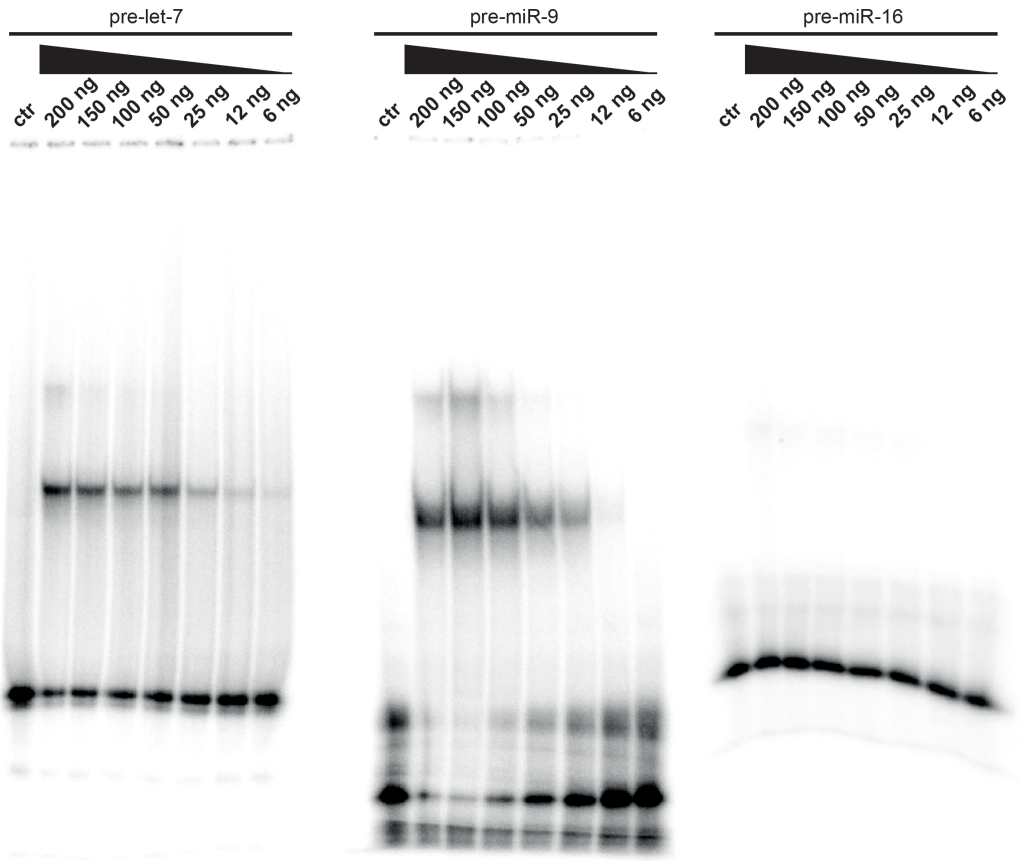

Figure 4-7 EMSA analysis of recombinant Lin28a binding to pre-miRNAs
Pre-let-7a, pre-miR-9 and pre-miR-16 were incubated with a gradient of recombinant Lin28a. Both pre-miR-9 and pre-let-7a efficiently formed protein complexes. Pre-miR-16 did not bind Lin28a. Series of standard dilutions of recombinant Lin28a in the range from 6–200 ng were used.

4.3 Involvement of Lin28a in the early stages destabilisation of pre-miR-9

In-vitro processing with extracts derived from different stages of neuronal differentiation clearly showed that pre-miR-9 is affected in a different way to pre-let-7a. My previous *in vivo* data suggested that Lin28a regulates miR-9 biogenesis. Therefore, it is essential to determine that the effects caused by Lin28a knockdown were related to the observed destabilisation of pre-miR-9 during the early stages of neuronal differentiation.

4.3.1 *In vitro* processing indicates that depletion of Lin28a leads to the stabilisation of pre-miR-9

In order to determine whether Lin28a interaction with pre-miR-9 is related to its destabilisation, I performed an *in vitro* processing assay using internally labelled pre-miR-9. Similarly to the previous experimental setting, I used pre-let-7a and pre-miR-101 as positive and negative controls, respectively (Figure 4-8).

Pre-miR-101 was previously shown to bind Lin28a, but in contrast to pre-let-7a and pre-miR-9, remained relatively stable throughout differentiation. Indeed, pre-miR-101 remained also stable during *in vitro* processing assays with P19 day 0 mock and RNAi-depleted Lin28a extracts. However, *in vitro* processing reactions in Lin28a RNAi-depleted extracts resulted in the decreased uridylation of pre-let-7a, which corroborates with a known molecular mechanism of Lin28a action on the let-7 family. Importantly, RNAi depletion of Lin28a leads to the stabilisation of pre-miR-9 in P19 day 0 extracts when compared to the processing in non-depleted extracts. Assays were performed in three independent reactions and the effects of Li28a RNAi depletion were also quantified to demonstrate the significance of the observation.

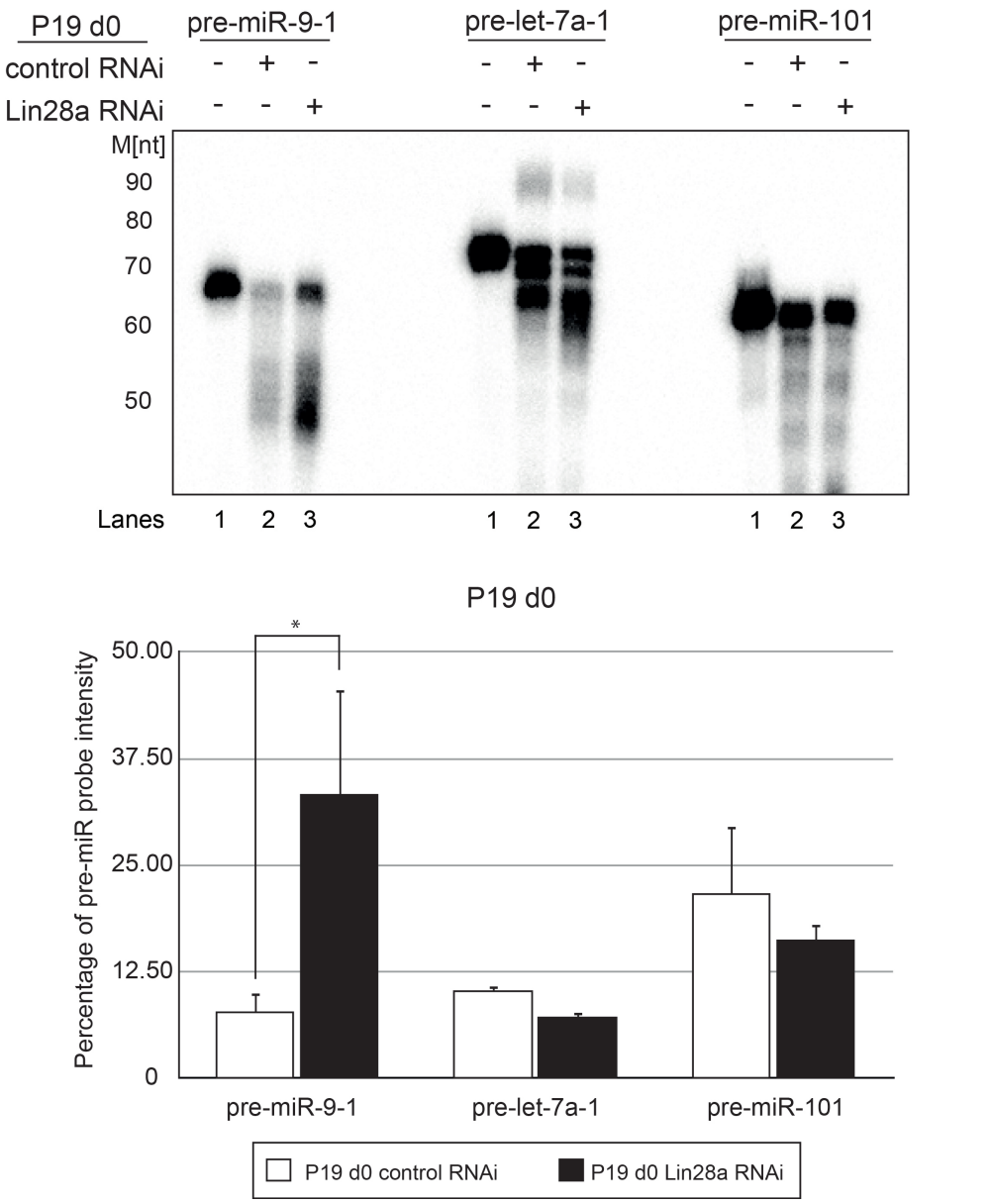

Figure 4-8 P19 day 0 Lin28a RNAi *in vitro* processing
Top panel - Radiolabelled pre-miR-9-1 was incubated in extracts derived from mock and Lin28a siRNA-treated P19 cells (lane 2 and 3 respectively). Pre-let-7a-1 and pre-miR-101 were used as positive and negative controls, respectively.
Bottom panel – quantification of the processing reactions. Results were normalised to the processing of the control reactions (lane 1). Statistical analysis was performed using t-test on sample size of n=3.

RNAi treatment of cells could potentially result in the silencing of additional off-targets parallel to Lin28a knockdown. To determine if the observed stabilisation is a direct effect of Lin28a depletion, I performed *in vitro* processing reaction in Lin28a-depleted cell extracts reconstituted with recombinant Lin28a (Figure 4-9). I clearly observed that the initial

stabilisation of pre-miR-9 in Lin28a-depleted extracts was terminated upon the addition of recombinant Lin28a to the reaction, which restored degradation of pre-miR-9.

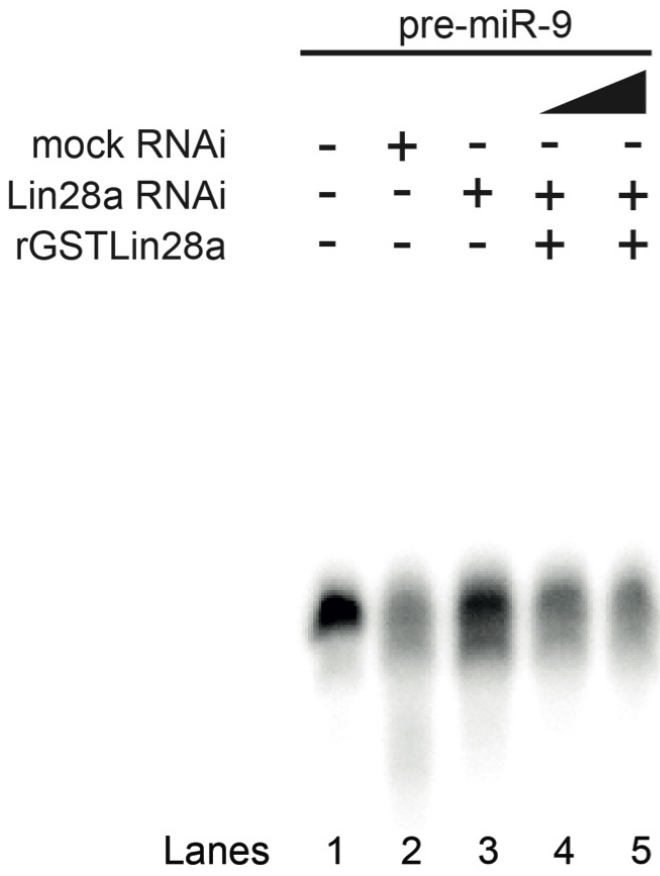

Figure 4-9 P19 day 0 Lin28a RNAi - reconstituted rec Lin28a
Radiolabelled pre-miR-9 was incubated in extracts derived from P19 day 0 mock and Lin28a siRNA treated cells (lane 2 and 3, respectively). Recombinant Lin28a was subsequently added to the Lin28a-depleted extracts at concentrations of 100 and 200 ng (lane 4 and 5, respectively).

Using a 5′-labelled probe, I demonstrated that pre-let-7a is stabilised in Lin28a RNAi-depleted extracts, as demonstrated by the *in vitro* processing reaction (Figure 4-10a-c). Moreover, I observed a sustained strong signal of radiolabelled pre-let-7a, which would suggest that the main mechanism of pre-let-7a degradation is via the 3′-end of the precursor. Interestingly, in the case of pre-miR-9, I observed strong destabilisation of both ends, which corresponded to previous analysis across differentiation stages. Moreover, processing using Lin28a RNAi-treated extracts clearly showed the stabilisation of pre-miR-9. However, it also might suggest that Lin28a could involve mechanisms mediating degradation via 3′- and 5′-ends,

especially as 5′ destabilisation was still present in Lin28a-depleted extracts. In order to validate destabilisation of the both ends of pre-miR-9 more detailed analysis should be performed to eliminate possibility of different turnover rates of pre-miR-9 and pre-let-7a.

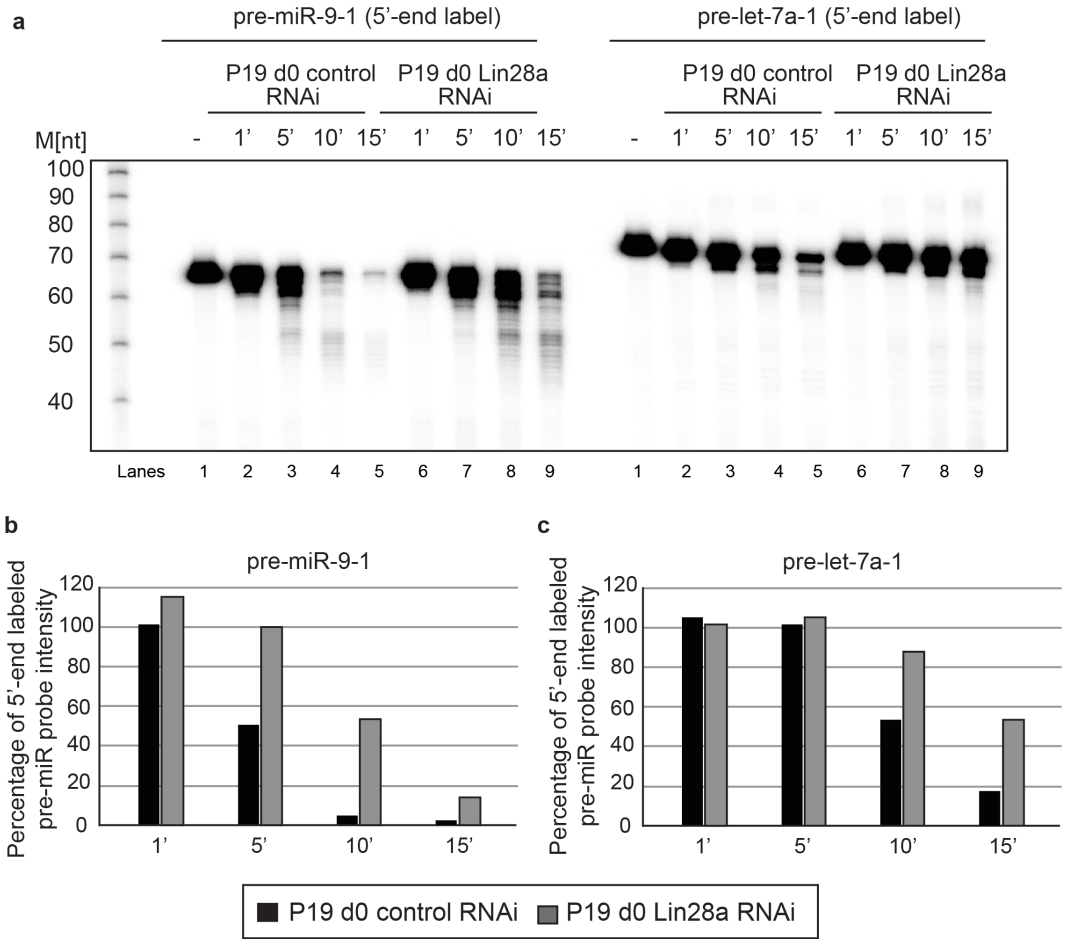

Figure 4-10 P19 day 0 Lin28a RNAi - *in vitro* processing 5'end labelled

a) *In vitro* processing reactions of pre-miR-9-1 and pre-let-7a (5′end labelled) incubated with extracts derived from control and Lin28a siRNA treated P19 day 0 (d0) cells. Reactions were performed with increased duration of time in range from 1′ to 15′ (lanes 2-5 and 6-9)

b-c) Quantification of pre-miR-9-1 and pre-let-7a-1 processing in extracts derived from mock and Lin28a siRNA treated samples. Results were normalised to the processing of the control (lane 1) which was set as a baseline.

4.3.2 Constitutive expression of Lin28a supports destabilisation in late stages of neuronal differentiation

Previously, I demonstrated that constitutive or induced expression of Lin28a leads to the downregulation of miR-9 levels *in vivo*. I also showed that reconstitution of depleted Lin28a with the recombinant protein reinstated the destabilisation of pre-miR-9 *in vitro*. Therefore, it would be beneficial to demonstrate that extracts derived from day 9 P19 cell lines with the stable expression of Lin28a also support the degradation of pre-miR-9. I decided to perform these experiments using day 9 extracts from both untagged Lin28a and Lin28aGFP stable cell lines. Moreover, I used internal-labelled pre-miR-9 and pre-let-7a as the analysis of their mature miRNA levels revealed significant differences in the activity of these two stable cell lines (Figure 4-11). In the case of pre-let-7a, I observed that initial uridylation of pre-let-7a in undifferentiated cells is abolished in day 9 extracts. As a result, the pre-let-7a molecule is stabilised, as demonstrated by the quantification of three independent experimental replicas. Importantly, day 9 extracts derived from both Lin28aGFP and untagged Lin28a P19 cells supported the uridylation and destabilisation of pre-let-7a (Figure 4-11).

In vitro processing of pre-miR-9 supported previous findings that on day 0 the precursor RNA is destabilised and becomes stabilised in the day 9 extract. Crucially, I observed a similar result in Lin28GFP day 9 extracts which supports previous *in vivo* findings that GFP-tagged protein does not influence miR-9 levels. Importantly, I demonstrated that day 9 extracts derived from the untagged Lin28a P19 line were supporting destabilisation of pre-miR-9 similarly to extracts derived from early stages of differentiation.

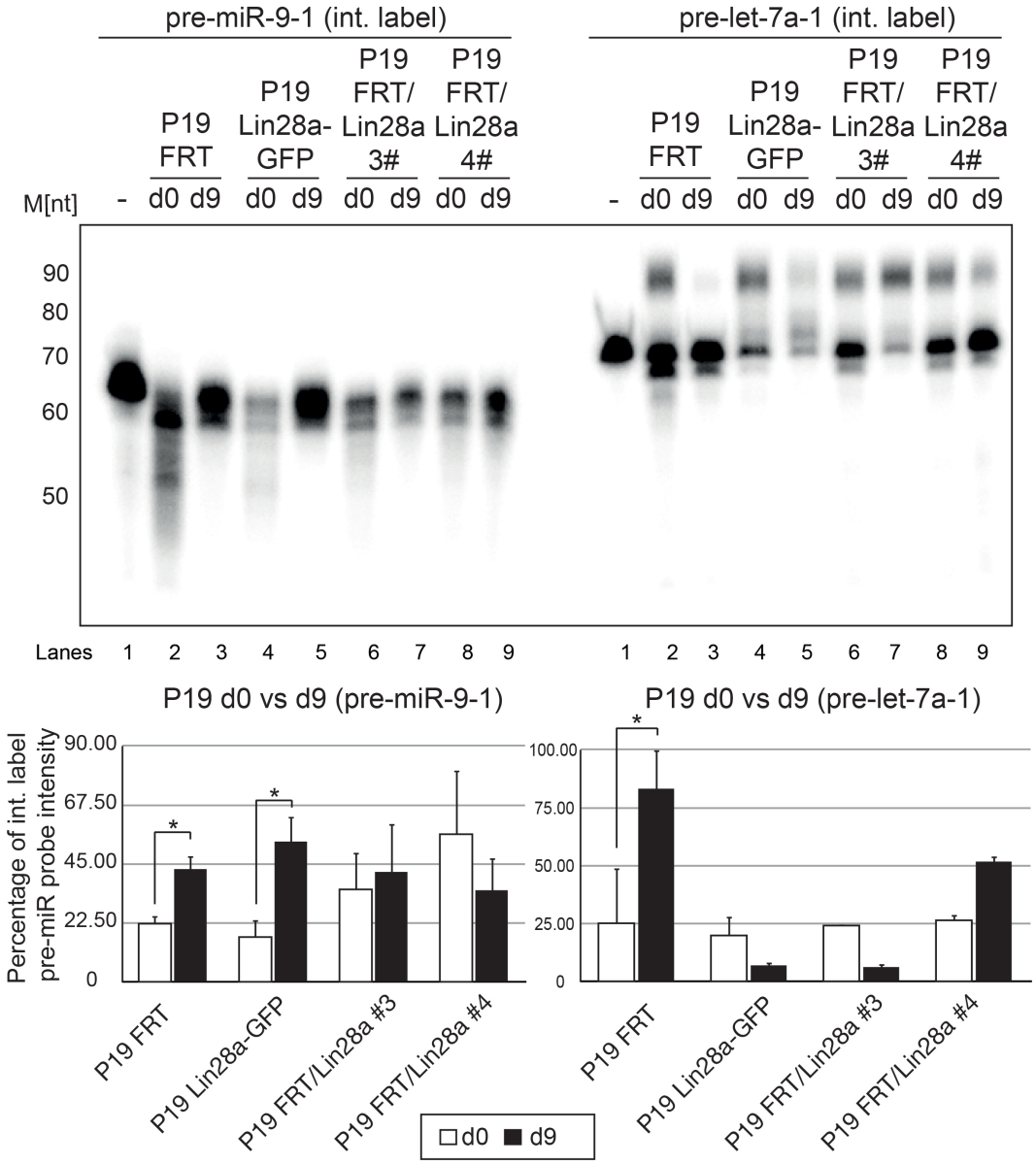

Figure 4-11 P19Lin28a stable cell lines - pre-miRNA *in vitro* processing
Top panel – *in vitro* processing of pre-miR-9-1 and pre-let-7a in day 0 and day 9 extracts of P19Lin28a stable cell lines: lane 2-3 – P19 FRT, lane 4-5 – P19:Lin28a:GFP, lane 6-7 and 8-9 P19:Lin28a clone 3 and 4, respectively.
Bottom panel – quantification of the processing reactions. Reactions were normalised to the processing of the controls – lane 1.

4.3.3 Effect of pre-miR-9 terminal loop mutagenesis on Lin28a mediated destabilisation of the pre-miRNA

My EMSA analysis of pre-miR-16 binding and pull-down with pre-miR-9/miR-16-TL suggested that Lin28a could not interact with the terminal loop of pre-miR-16. Therefore, I decided to test whether mutagenesis of

pre-miR-9-TL is sufficient to abolish destabilisation mediated by Lin28a. I performed the *in vitro* processing reaction in degradation permissive conditions of day 0 P19 cells (Figure 4-12). As expected, the pre-miR-9/16-TL mutant remained stable upon incubation with the extracts, further supporting the role of the terminal loop in Lin28a-mediated degradation of pre-miR-9.

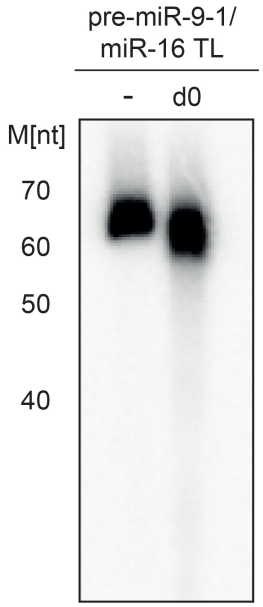

Figure 4-12 P19 day 0 - pre-miR-9-1/miR-16-CTL *in vitro* processing
Radiolabelled pre-miR-9-1/miR-16-CTL mutants were incubated in extracts derived from P19 day 0 (d0) cells.

4.4 Characterisation of motifs responsible for the interaction between Lin28a and pre-miR-9

4.4.1 Use of enzymatic cleavage assay and footprinting to characterise pre-miRNA secondary structure and Lin28a binding sites

RNA secondary structure analysis in the presence of proteins (footprinting) is a useful tool to obtain more information about the molecular mode of interaction between RNA and proteins. I showed that both pre-miR-9 and pre-let-7a interact with Lin28a, but the mechanisms of Lin28a action seem to be different. I decided to perform a footprinting analysis of 5'-labelled pre-miR-9 and pre-let-7a with RNAse V1, RNAse T and Pb^{++} and recombinant Lin28a. The properties of these cleavage enzymes would provide a wealth of information about the secondary pre-miRNAs structures. RNAse V1 is known to cleave double-stranded regions only, whereas RNA T1 specifically cuts single-stranded regions at G nucleotides. Pb^{++} ion is less specific but displays a preference for the open conformation for RNA. I used water as a mock treatment. To determine Lin28a binding sites, I performed cleavage reactions in the presence of a Lin28a gradient to visualise nucleotides that are associated and subsequently protected from cleavage.

In the case of pre-let-7, I determined that Lin28 interacts with AGGG and the well-known GGAG motif (Figure 4-13a). These regions have been previously shown by co-crystal and NMR structural studies to interact respectively with the cold-shock and zinc-finger domains of Lin28 (Loughlin et al., 2012). Interestingly, binding of Lin28 resulted in increased cleavage by V1 ribonuclease with the decreased activity of Pb(II) cleavage in the region within the terminal loop, which might suggest structural rearrangements of pre-let-7 resulting in higher stability of the terminal loop (Figure 4-13a,c).

Importantly, I identified the GU-rich region of pre-miR-9 terminal loop as an interaction site with Lin28 (Figure 4-13b). Due to the very short nature of pre-miR-9-CTL. this might suggest that Lin28 interacts with pre-miR-9

via only one of its possible RNA-binding domains. Similarly to pre-let-7a, association with Lin28 resulted in the increased activity of V1 ribonuclease, which might suggest some tertiary-related structural rearrangements that subsequently lead to structural stabilisation (Figure 4-13a,b).

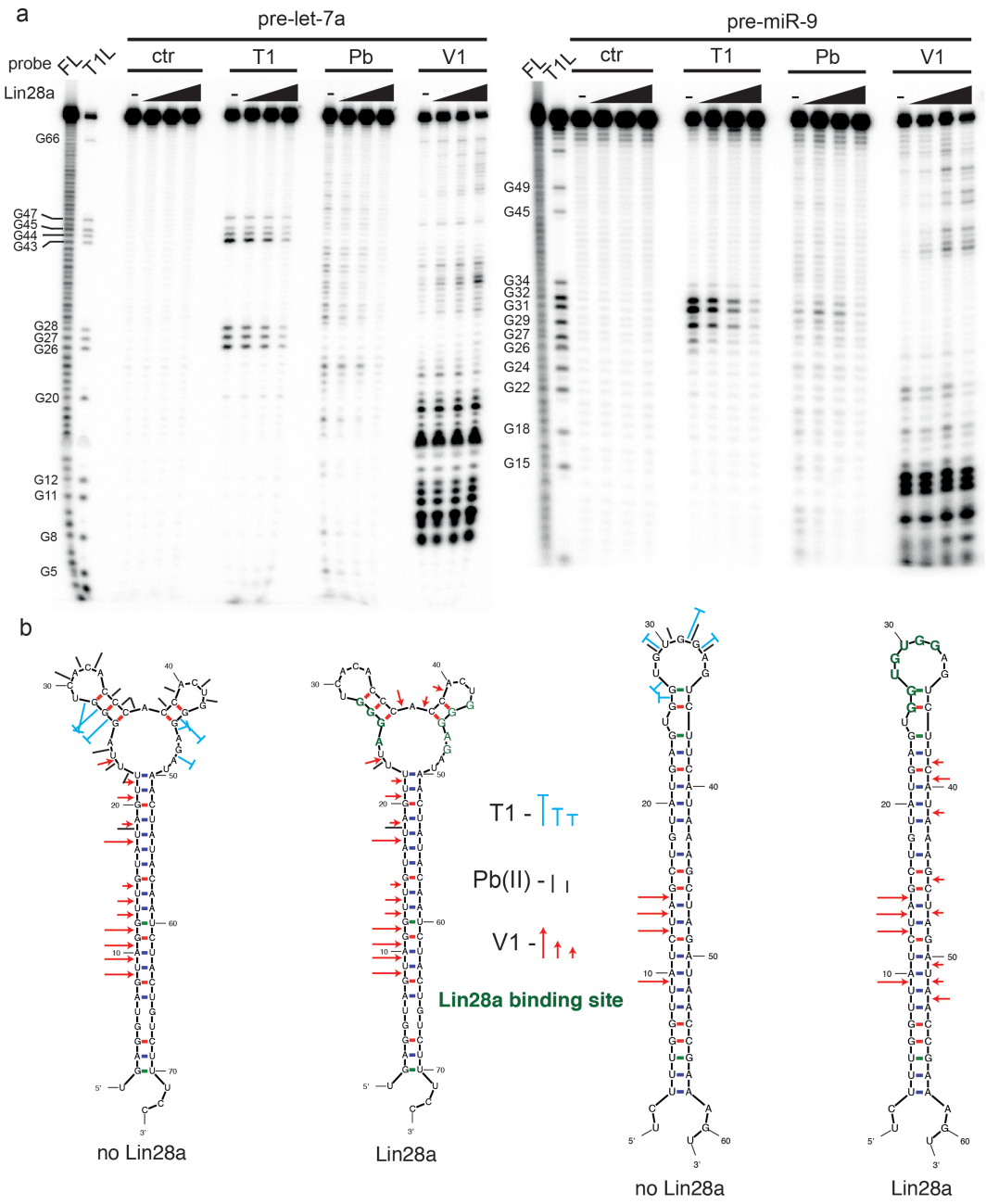

Figure 4-13 Structural probing and footprinting analysis of recLin28a interaction with pre-let-7a and pre-miR-9

a) Pre-let-7a and pre-miR-9 cleavage pattern on 8% PAGE. Reactions were processed in groups: ctr – no enzyme added, T1 – RNA T1, Pb – cleavage by lead ions, V1 – RNAse V1. Within each of the groups, increased concentrations of the recombinant Lin28a were used (50ng, 100ng, 200ng). FL and T1L are formamide and RNA T1 ladders, respectively.

b) Graphical representation of pre-let-7a and pre-miR-9 secondary structures generated with mfold with annotated cleavage sites and Lin28a binding site.

Interestingly, the pre-miR-9 terminal loop contains "GGAG" – a motif characterised to specifically associate with the zinc-finger domain of

Lin28a. However, my structural probing analysis suggested that Lin28a binds upstream of this motif. Therefore, I decided to test whether the "GGAG" motif within pre-miR-9 is functionally important. For that reason, I generated several mutants of pre-miR-9 TL with single and multiple nucleotide changes surrounding the motif. I transfected HeLa cells with these mutants along with Lin28a and compared their potential to generate mature miR-9. To my surprise, I observed no changes in the expression levels of miR-9 from pre-miR-9 containing either wild type or the mutant terminal loops.

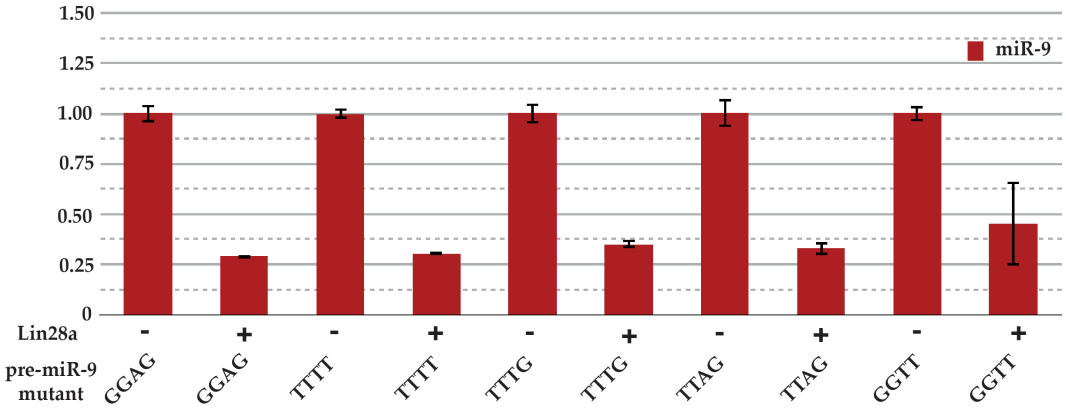

Figure 4-14 qRT-PCR - pre-miR-9 mutagenesis of the GGAG motif
Plasmids expressing pri-miR-9-1 containing wild type ZnF-binding motif (GGAG) and its various mutations were co-transfected into HeLa cells with Lin28a-expressing vectors. Results were analysed with qRT-PCR and mature miR-9 expression levels were normalised to miR-16 expression levels. Analysis was represented in pairs for each of the GGAG mutants and Lin28a untransfected cells were used as a baseline for each of the pairs.

4.4.2 Immunoprecipitation of Lin28a truncated mutants emphasise the role of Lin28a CSD in association with pre-miR-9

My data suggested that the association of Lin28a with pre-miR-9 occurred upstream of the "GGAG" motif, mutations of which did not cause any relevant effect in the expression of mature miR-9.
Therefore, I decided to compare the binding efficiency of CSD and ZnFD domains to pre-miR-9 and pre-let-7. To test this, I engineered a panel of T7-tagged Lin28a truncations and tested their binding abilities by

performing RNA pull-downs. As each truncation could affect the stability of the protein or its expression, I optimised transfection conditions to equilibrate protein levels between truncated mutants (Figure 4-15). This step should decrease the bias of RNA/protein interactions that depend on differences in protein levels.

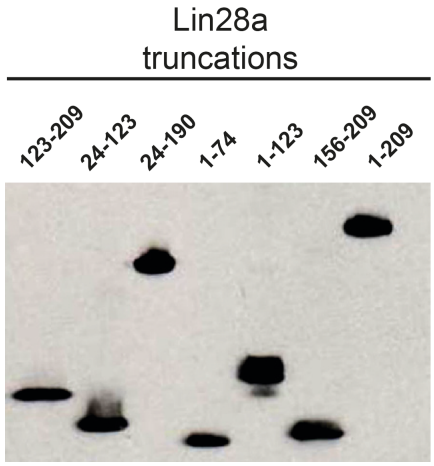

Figure 4-15 Optimisation of Lin28a truncations expression
Vectors expressing various Lin28a truncations were transfected to HeLa cells. Protein extracts were resolved on 12% PAGE and western blot analysis against Lin28a were used to confirm similar expression levels for each of the truncations.

Importantly I found that pre-miR-9 and pre-let-7a displayed strong differences in binding properties toward cold-shock and zinc-finger domains of Lin28a (Figure 4-16a,b). In particular, quantification of pull-down efficiency represented as a percentage of input binding revealed that pre-miR-9 interacted more strongly than pre-let-7a with mutants containing CSD only. Interestingly, I also observed that trimming of unstructured N- and C-terminal regions increased efficiency of pre-let-7a and pre-miR-9 binding. Also, to my surprise, pre-let-7a exhibits a strong binding increase to Lin28a mutants with removed CSD. Previous studies placed CSD binding to pre-let-7a prior to ZnFD association, which hypothetically should help to expose the "GGAG" motif. These factors suggest structural differences between terminal loops of let-7 families. However, Lin28a mutant 1-74 could potentially result in incorrectly folded CSD domain, therefore in the future it would be interesting to engineer more precise point-mutants of CSD to verify its involvement in binding to

pre-let-7a and pre-miR-9. Also analysis of Lin28a truncation mutants binding to the matrix itself should be performed to exclude possibility of non-specific interaction as an outcome of the misfolded mutants.

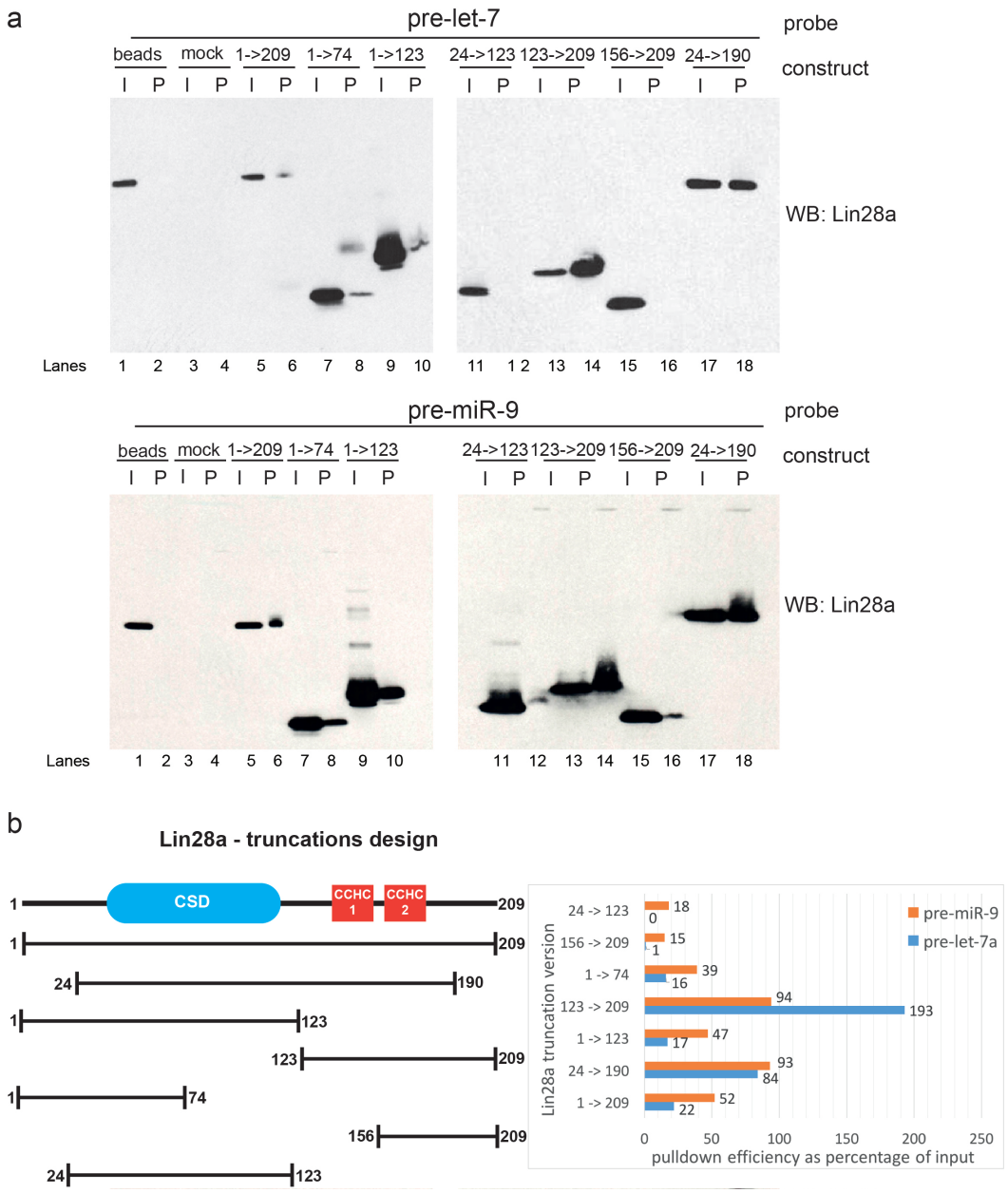

Figure 4-16 Lin28a truncations pull downs

a) Pre-let-7 (top) or Pre-miR-9 (bottom) were conjugated to the agarose beads and incubated with extracts derived from HeLa cells transfected with vector expression full length Lin28a (1->209) and various truncations of Lin28a. The first control contained beads without conjugated pre-miRNAs and were used in the pull-downs with extracts containing full length Lin28a (lane 1 and 2). The second control contained agarose beads with conjugated pre-miRNAs and was incubated with HeLa cells not-transfected with Lin28a (lane 3 and 4). Lanes 5 -18 represent pull-downs of pre-let-7a and pre-miR-9 with various mutants of Lin28a. Odd lanes visualise input of the reaction (I) and even numbers represent pull-down (P).

b) Analysis of mapping interactions between Lin28a and pre-miR-9.
Left side - map of the full length Lin28a and truncations used in the pulldown reactions.
Right side – quantification of the Lin28a mutant pull-downs normalised

to the amount of the input in each reaction.

4.5 Identification of the enzyme leading to the degradation of pre-miR-9 at early stages of neuronal differentiation

4.5.1 Depletion of several RNA nucleases indicates role of Dis3l2 in destabilisation of pre-miR-9

To find a factor that leads to the destabilisation of pre-miR-9 during neuronal differentiation, I performed knockdown of selected RNA nucleases using pool SMART Target-ON™ siRNAs. Here, 48h after siRNA transfection, neuronal differentiation of P19 cells was induced with retinoic acid and miRNAs levels were analysed after four days of differentiation and compared to reciprocal levels of miRNAs in mock siRNA-treated samples. I determined the depletion efficiency performing a western blot analysis of protein expression in mock and siRNA-treated cells (Figure 4-17b).
Interestingly, upon knockdown of Dis3l2 I observed an increase in miR-9 levels similar to that observed in Lin28 depletion (Figure 4-17a). However, the levels of let-7 remained unchanged (Figure 4-17a). This observation was in line with previously reported effect of Dis3l2 depletion on let-7 (Chang et al., 2013). I also determined that knockdown of EXOSC3, a structural component of an exosome, had no effect on levels of either miR-9 or let-7 Figure 4-17a.

It has been previously reported that Lin28 attracts Dis3l2 following poly-uridylation of pre-let-7 and subsequently leads to degradation of pre-let-7 (Chang et al., 2013). My results also suggest that Lin28 together with Dis3l2 play an important role in the downregulation of miR-9 levels during neuronal differentiation. However, I showed that the mechanism of pre-mir-9 destabilisation is uridylation-independent. Therefore, it might suggest that Lin28 directly interacted with Dis3l2, which subsequently resulted in pre-miR-9 destabilisation.

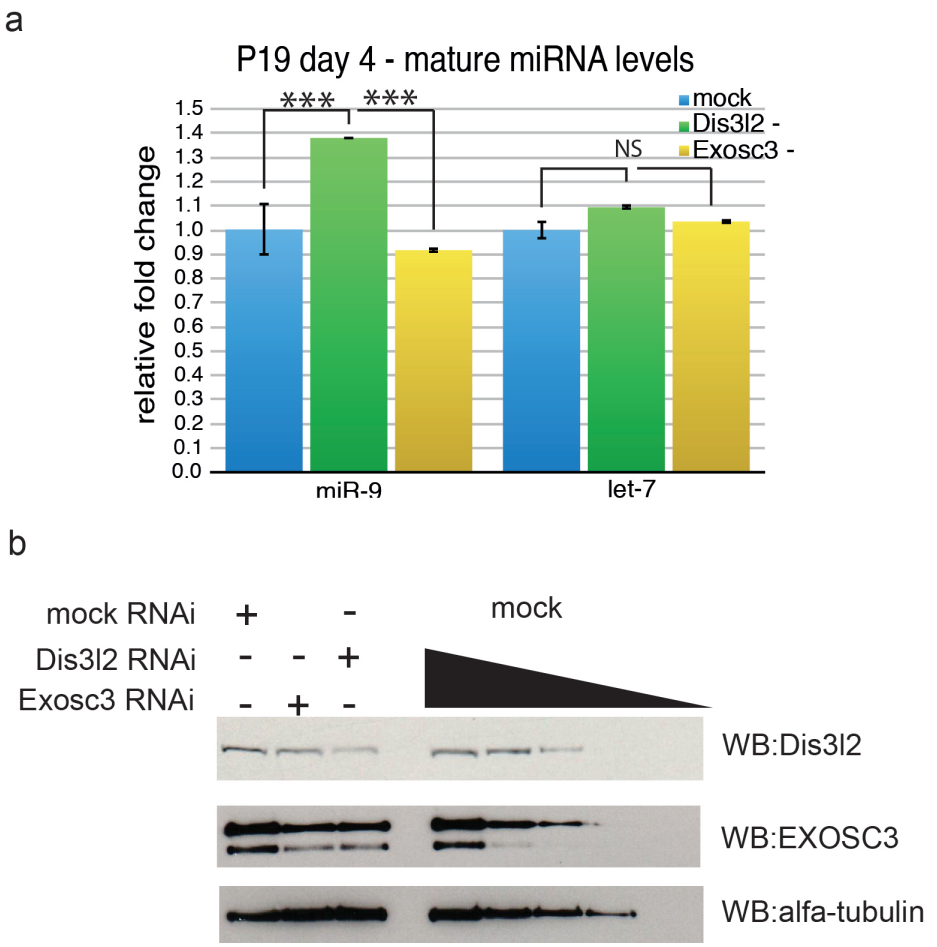

Figure 4-17 qRT-PCR analysis of microRNA upon depletion of effector candidates

a) P19 cells were treated with siRNA against Dis3l2 and Exosc3 and differentiated. Following four days of differentiation qRT-PCR analysis was performed to analyse mir-9 and let-7. Random siRNA with no predicted targets were used as a negative control Statistical analysis was performed with t-test on sample size n=3.

b) Protein samples derived from P19 day 4 cells treated with siRNA against Dis3l2 and Exosc3 were analysed with western blot to confirm then depletion of Dis3l2 and Exosc3. To estimate efficiency of the depletions, serial dilutions of mock siRNA-treated extracts were analysed in the range from 100% to 0% in two-fold reduction steps. Alpha-tubulin served as loading control.

4.5.2 Lin28a directly interacts with Dis3l2

To determine whether pre-miR-9 interacts with Dis3l2, I performed a pull-down assay with pre-miR-9 incubated with extracts derived from P19 day 0 and day 9 extracts (Fig.3A and Sup.Fig.1). As a control, I used pre-let-7a, which was conjugated via the 3′ end to beads. Coupling the pre-let-7a with beads via the 3′ end protects it from uridylation. In fact, I showed

that pre-let-7a was able to interact with Lin28 but not with Dis3l2, which requires pre-let-7a to be poly-uridylated at its 3' end (Figure 4-18a). However, despite the lack of uridylation, pre-miR-9 at day 0 interacted with both Lin28 and Dis3l2. Interestingly when we compared pull-down performed at day 0 and day 9 we observed much stronger binding of Dis3l2 to pre-miR-9 in differentiated cells than in undifferentiated cells Figure 4-18b.

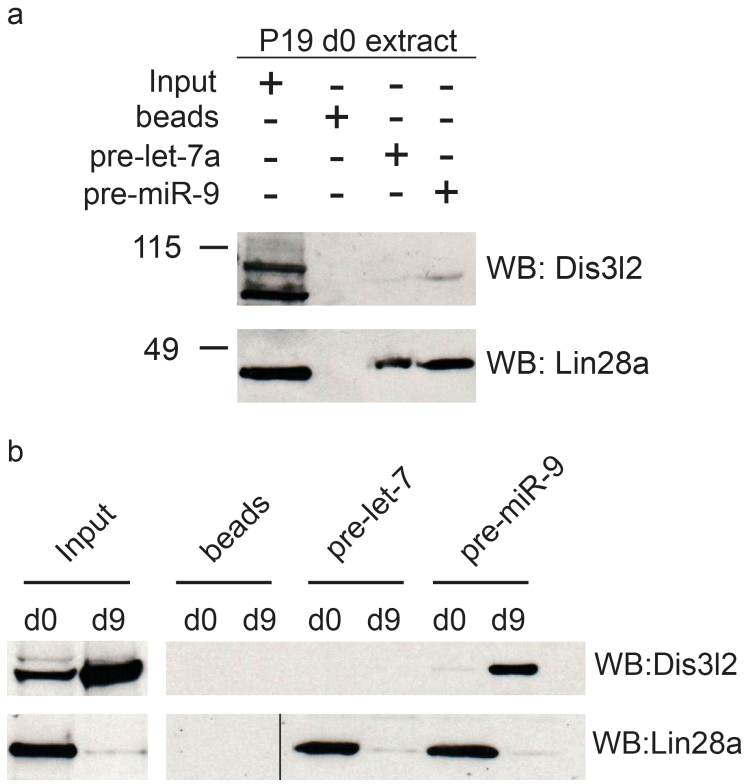

Figure 4-18 pre-miRNA Dis3l2 pulldowns in P19 cells
Pre-miRNAs were conjugated to the beads and incubated with P19 day 0 (d0) and day 9 (d9) cell extracts. Following the stringent washes, precipitated ribonucleoproteins were run on 4-12% PAGE and analysed with western blot against Dis3l2 and Lin28a.

a) Pre-let-7a and pre-miR-9 pulldown in P19 day 0 cells
b) Pre-let-7a and pre-miR-9 pulldown in P19 day 0 and day 9 cells

To establish whether Lin28 directly binds to Dis3l2, I performed Co-IP experiments using recombinant Dis3l2 and Lin28 (Figure 4-19). I showed that the addition of recombinant Lin28 and immunoprecipitation with anti-Lin28 antibody was able to pull-down slightly higher amounts of Dis3l2 when compared to pull-down without recombinant Lin28. These

results show that despite a lack of poly-uridylation in P19 cells, pre-miR-9 in contrast to pre-let-7a is interacting with Lin28a and Dis3l2.

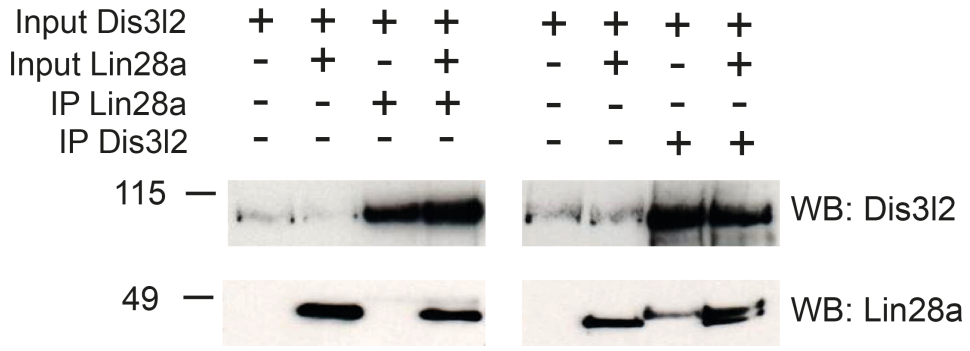

Figure 4-19 Recombinant Lin28a and Dis3l2 Co-IP
Recombinant Lin28a and Dis3l2 were mixed together and subsequently incubated with the beads conjugated with antibodies against Lin28a (left panel) or Dis3l2 (right panel). Following stringent washing, immunoprecipitated complexes were run on 4-12% PAGE and analysed with western blot against Lin28a or Dis3l2.

4.5.3 Formation of tertiary complex between Lin28a-Dis3l2-pre-miR-9 molecules

To establish whether the direct interaction between Lin28a and Dis3l2 is a result of tertiary complex formation upon binding to pre-miR-9, I performed EMSA analysis (Figure 4-20). As a reference, I used pre-let-7a, which is known not to interact with Dis3l2 when it is not poly-uridylated. I observed that recombinant Lin28a and Dis3l2 bind to pre-miR-9 independently, however when incubated together they form a tertiary complex on pre-miR-9. Moreover, in this, only residual amounts of monomeric complex remained present. However, for pre-let-7a, even though both recombinant Lin28a and Dis3l2 bound independently to the precursor RNA, the incubation of both proteins together showed that pre-let-7a dominantly associated as monomeric complexes, which is in contrast with pre-miR-9.

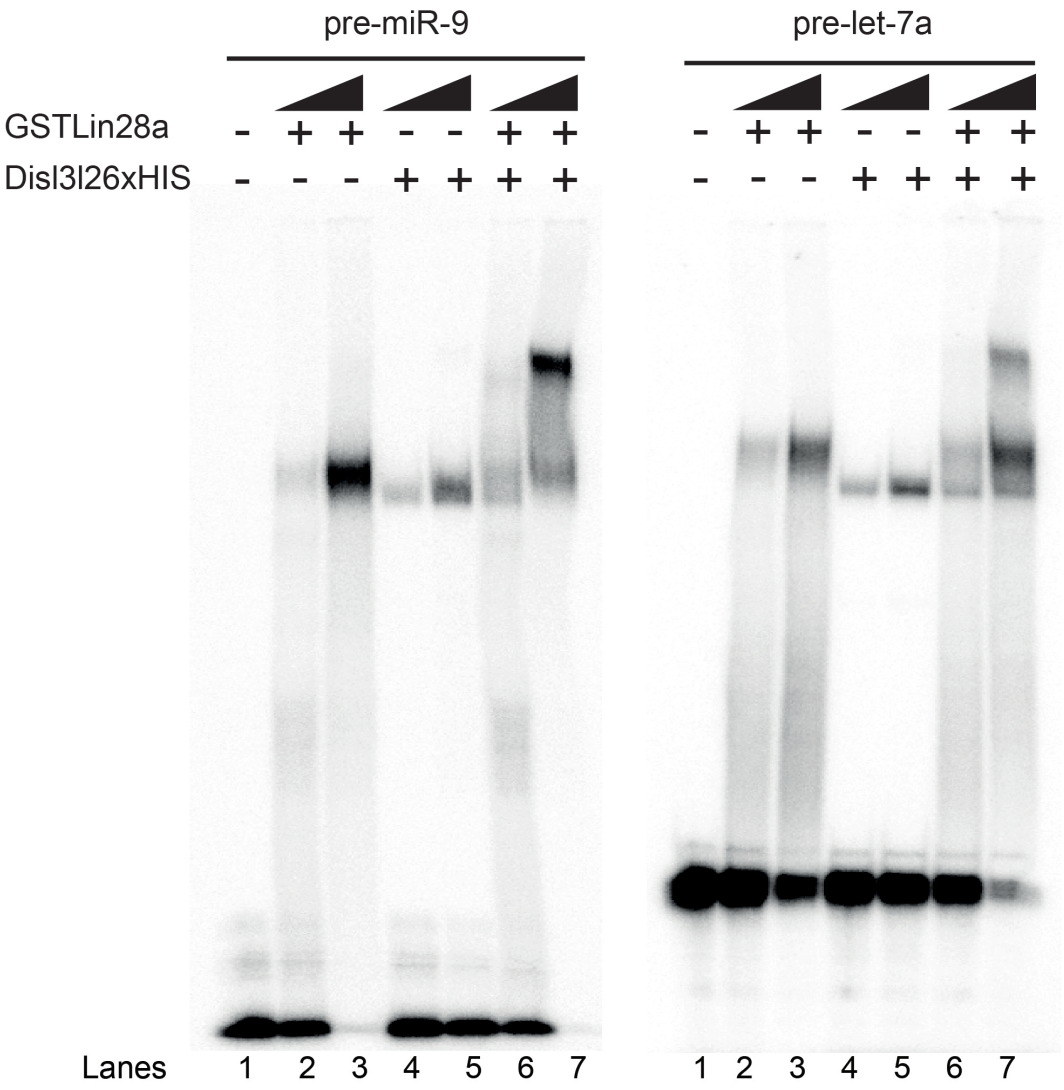

Figure 4-20 EMSA with recLin28a and recDis3l2
Radiolabelled pre-miR-9 and pre-let-7a were incubated with recombinant Lin28a and Dis3l2 (Lin28a and Dis3l2 individually – lanes 2 to 5, Lin28a and Dis3l2 together – lanes 6 and 7). Following the incubation, protein ribonucleoprotein complexes were resolved on 10% PAGE and visualised with phosphoimager.

To prove that this tertiary complex is achieved via direct interaction of Dis3l2 with Lin28a and not by two independent binding sites of proteins to the RNA, I performed competition-binding assay where Lin28a specific antibody (Lin28a ab) was added to the reaction setting (Figure 4-21). The addition of Lin28 ab resulted in a supershift or the disruption of an interaction between Lin28a as well as Dis3l2 and pre-miR-9. This unspecific effect on Dis3l2 antibody most likely accounts for its polyclonal nature. Lin28 ab was generated against His-tagged Lin28a and unfortunately the same tag was used to purify recombinant Dis3l2.

However, the addition of Lin28 ab in combination with recombinant Lin28a and Dis3l2 resulted in a supershift of monomeric complexes, but did not affect formation of tertiary complex Dis3l2/Lin28/pre-miR-9. This suggested that in the case of tertiary complex epitope for the antibody, the interaction is buried inside the assembly. To demonstrate that the observed result is specific to Lin28 ab, I used non-specific anti-IgG antibody (IgG ab) that did not result in the shift or disruption of complex formation when used with recombinant proteins in combination or individually (Figure 4-21).

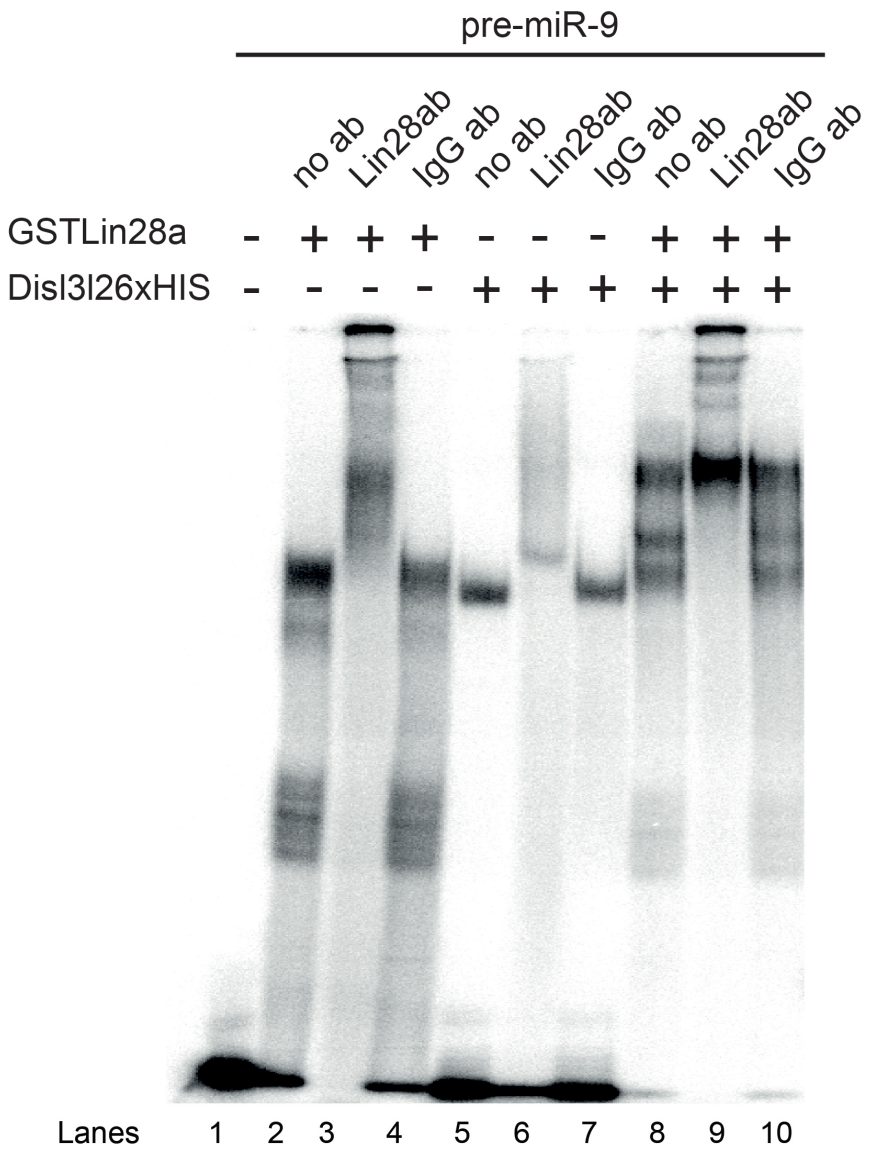

Figure 4-21 EMSA - recombinant proteins and antibody competitors
Radiolabelled pre-miRNA were incubated with recombinant Lin28a and Dis3l2 (lanes 2, 5 and 8). Lin28a (lanes 3, 6 and 9) and non-specific mouse IgG (lanes 4, 7 and 10) antibodies were added to compete for protein binding.

To further strengthen the specificity of Lin28 ab action, I showed that the addition of an antibody against another RNA-binding protein, Msi-2, similarly to IgG ab did not result in the supershift or complex disruption (Figure 4-22). These results prove that Dis3l2 via direct interaction with Lin28a bound to pre-miR-9 and this interaction is essential for the formation of tertiary complexes when both proteins are in contact with pre-miR-9.

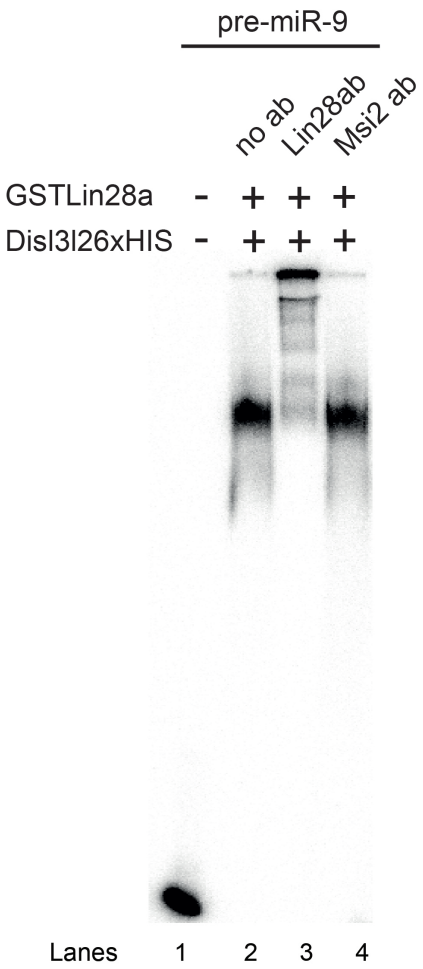

Figure 4-22 EMSA - recLin28a and recDis3l2 - Lin28a and Msi2 ab competition
Radiolabelled pre-miR-9 was incubated with recombinant Lin28a and Dis3l2 (lane 2). Lin28a and Msi2 antibodies were added to compete for protein binding (lanes 3 and 4, respectively).

4.5.4 Depletion of Dis3l2 leads to stabilisation of pre-miR-9

I showed that Lin28a and Dis3l2 form a tertiary complex with pre-miR-9. Previously, I also showed that pre-miR-9 is destabilised during the early stages of P19 neuronal differentiation (Nowak et al., 2014). To determine whether the formation of the Lin28-Dis3l2 complex would result in the degradation of pre-miR-9, I performed *in vitro* processing assays using P19 day 0 extracts with RNAi depleted Dis3l2. To strengthen the evidence that the observed effect is directly associated with the absence of the knocked-

down protein, I rescued RNAi condition by adding either active Dis3l2 or enzymatically inactive Dis3l2 mutant with the mutation in the RNB domain, in which a conserved aspartic acid residue predicted to coordinate a divalent cation was replaced by asparagine (D391N). Importantly, the depletion of Dis3l2 resulted in stabilisation of pre-let-7a uridylated form – the observation that remained in agreement with previous findings (Figure 4-23a,c) (Chang et al., 2013). This effect was rescued by the addition of recombinant Dis3l2. Reinstating with enzymatically active Dis3l2 resulted in complete degradation of the uridylated form of pre-let-7a. On the other hand, functionally inactive recombinant Dis3l2 was not able to restore the degradation of uridylated precursor.

Interestingly, the depletion of Dis3l2 also resulted in a stabilisation of pre-miR-9 despite its non-uridylated form (Figure 4-23b,c). The degradation of the pre-miR-9 precursor observed during the early stages was again detected when functionally active recombinant Dis32 was added. Functionally inactive Dis3l2 had a moderate effect on destabilisation of the precursor.

These and my previous results suggested that Dis3l2 is directly involved in uridylation-independent degradation of pre-miR-9. This direct mechanism of degradation mediated by Dis3l2 is achieved by its interaction with Lin28.

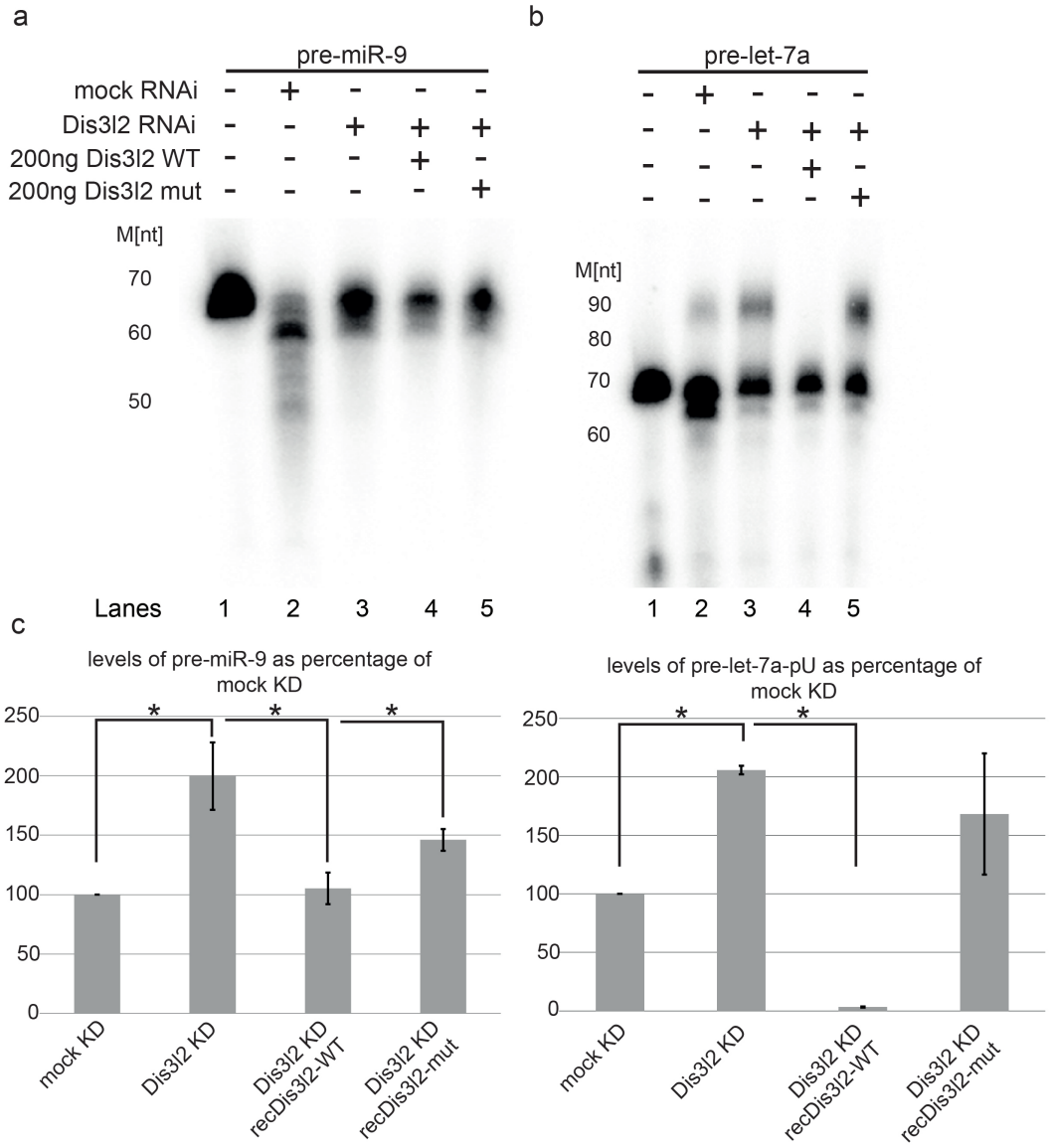

Figure 4-23 P19 day 0 Dis3l2 RNAi *in vitro* processing
Radiolabelled pre-miR-9 and pre-let-7a probes were incubated with P19 day 0 extracts treated with mock or Dis3l2 siRNA (lanes 2 and 3). Recombinant active Dis3l2 or its inactive mutant was added to reconstitute wild type conditions (lanes 4 and 5 respectively).

a) Processing results for pre-miR-9
b) Processing results for pre-let-7a
c) For pre-miR-9 processing in individual conditions (lanes 2-5) were quantified and normalised against processing of the control (lane 1). For pre-let-7a uridylated form was quantified in individual conditions (lane 2-5) and normalised against uridylation efficiency of mock siRNA-treated extract (lane 2).

Chapter 5

5 Genome-wide analysis of Lin28a effects on miRNA biogenesis during neuronal differentiation

5.1 Analysis of miRNA changes during neuronal differentiation

My results so far have indicated that pre-let-7a and pre-miR-9 are regulated via two distinct mechanisms involving Lin28a and Dis3l2. Therefore, it would be interesting to see how these two mechanisms affect biogenesis of other miRNAs in genome-wide context. To test this, I decided to employ a small-RNA sequencing technique on samples derived from day 0 and day 9 of P19:Lin28a as well as P19:Lin28aGFP stable cell lines. As a reference for P19:Lin28a and P19:Lin28aGFP, I also sequenced small RNAs derived from P19:FRT and P19:GFP stable cell lines, respectively.

Following RNA-sequencing, normalised reads were subsequently mapped to known miRNA according to miRBase using SOAPaligner. Subsequently, differential expression profiles of miRNAs between day 9 and day 0 of above stable cell lines were generated. I used scatterplots to visualise day 9/day 0 fold change between P19:Lin28a: and P19:FRT (group 1) or P19:Lin28aGFP and P19:GFP (group 2) (Figure 5-1). Interestingly, analysis of overall miRNA change between differentiated and undifferentiated stable cell lines revealed that constitutive expression of untagged Lin28a regulated a larger number of miRNAs when compared to its Lin28aGFP counterpart.

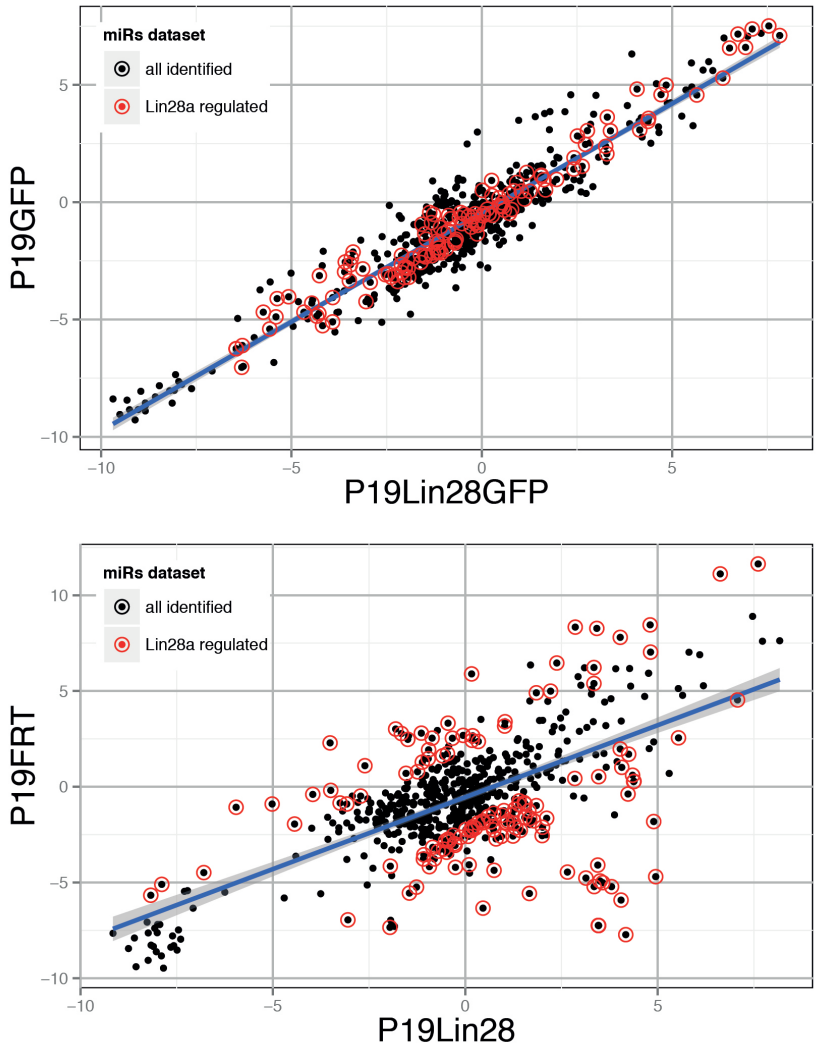

Figure 5-1 Comparison of miRNA levels in P19 stable cell lines - small RNA-seq.
miRNAs ratio day 9/day 0 ratio of expression levels were compared between P19:GFP and P19:Lin28aGFP (top panel) as well as P19:FRT and P19:Lin28a (bottom panel). Subsequently, Lin28a:GFP/P19:GFP and P19:Lin28a/P19:FRT ratios for related miRNAs were calculated and miRNAs with less than 2-fold change in P19:Lin28aGFP/P19:GFP group were marked with red circles for both of the groups.

I performed validation of small RNA-sequencing data using qRT-PCR and analysing changes of mature miRNA in day 0 and day 9 of the stable cell lines (Figure 5-2). Based on the analysis of several miRNAs I was able to show a similar dynamic pattern of miRNA levels using qRT-PCR analysis and a small RNA-sequencing technique, which validates the results obtained with the latter technique.

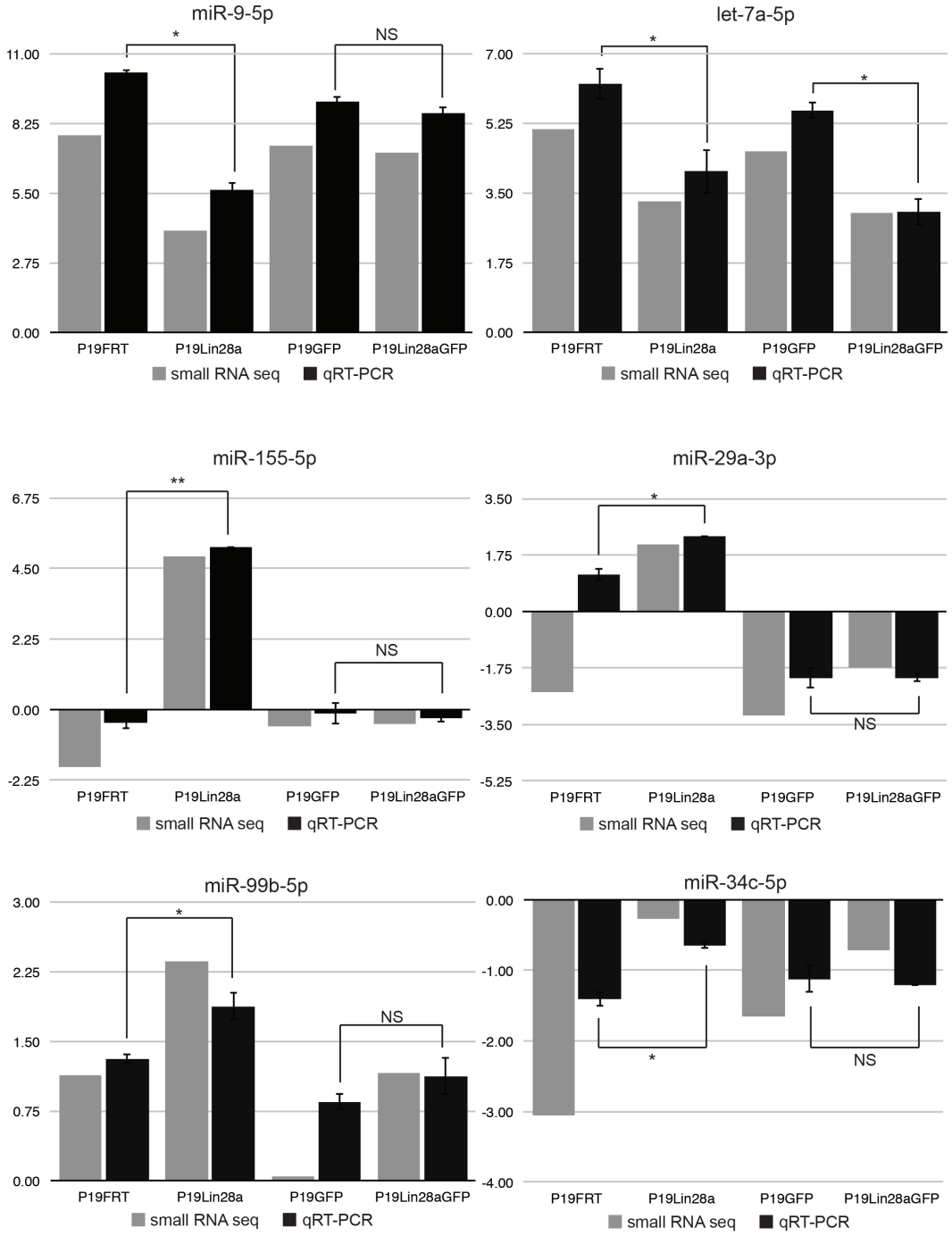

Figure 5-2 validation of small RNA-sequencing
Selected mature miRNA were analysed with qRT-PCR on day 0 and day 9 of the differentiation of P19 cells. Results were represented as ratio day 9/day 0 for each of the stable cell lines. As a reference, similar calculations were performed for the related miRNAs changes that were obtained from small RNA sequencing. Statistical analysis was performed on qRT-PCR data using t-test on sample size n=3.

5.2 Dual role of Lin28a during P19 neuronal differentiation

To further characterise genome-wide miRNA changes caused by constitutive expression of untagged Lin28a, I used day 9/day 0 fold-changes to generate comparative ratios of changes between groups 1 and 2. Subsequently, I selected those miRNAs that were relatively unchanged between P19:Lin28aGFP and P19:GFP (Figure 5-1 – red circles) and visualised their fold-change between P19:Lin28a and P19:FRT using heatmap (Figure 5-3).

I was able to verify miR-9-3p and miR-9-5p levels to be strongly downregulated during neuronal differentiation of P19:Lin28a stable cell line. Moreover I observed downregulation of miR-124-5p, miR-124-3p and miR-134; miRNAs that were previously described to play a role in neuronal development. Interestingly, large groups of miRNAs were shown to be upregulated upon neuronal differentiation of the Lin28a stable cell line including miR-212, a miRNA involved in the maturation of dendrites.

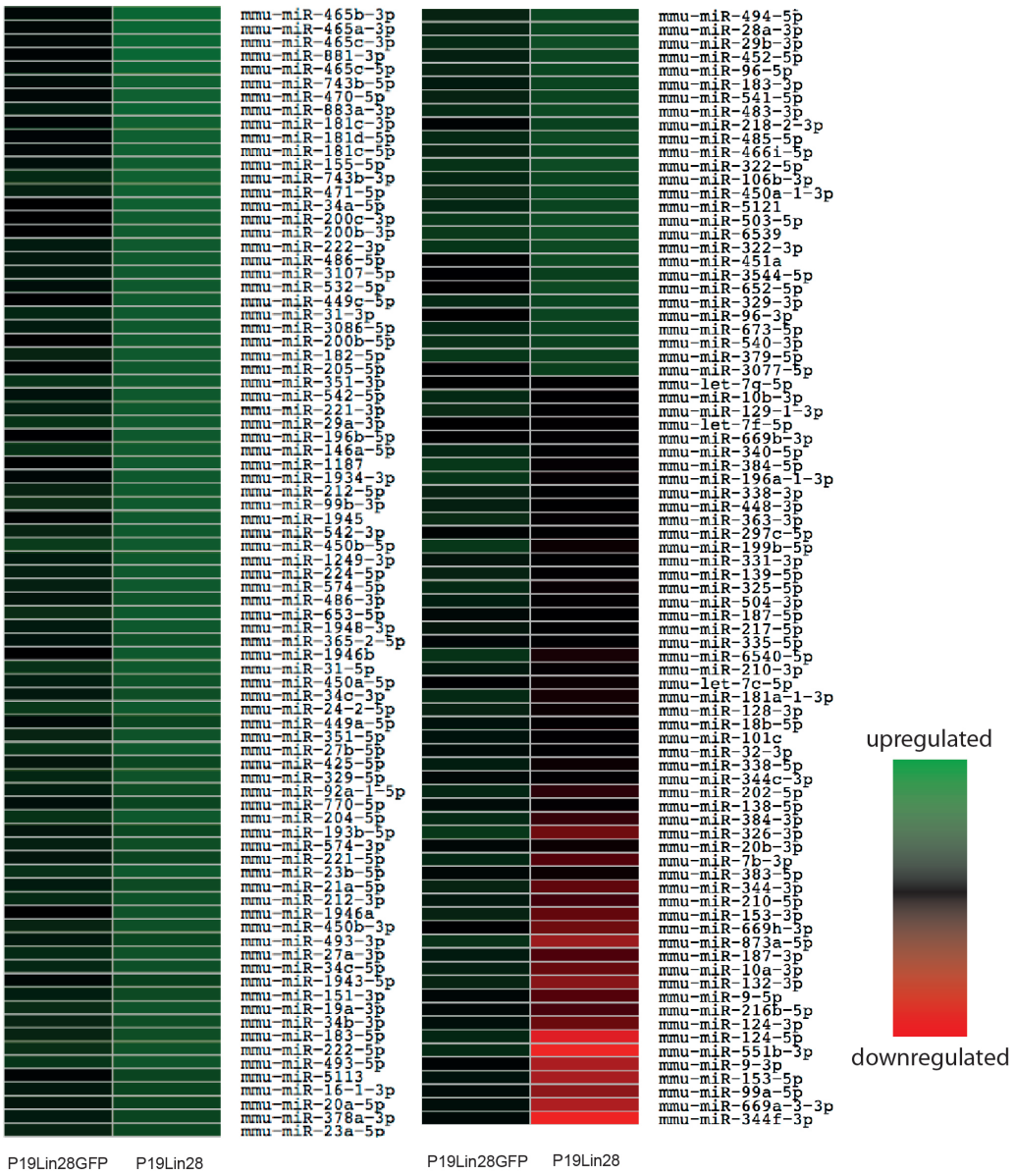

Figure 5-3 small RNA-sequencing - heatmap expression analysis
miRNAs with stable day 9/day 0 ratio in P19:Lin28a:GFP and P19:GFP (less than 2-fold change) were selected and their change between P19:Lin28a and P19:FRT were calculated, represented as a ratio and visualised with the heatmap. MiRNAs with positive P19:Lin28a/P19:FRT ratio are represented by a green colour whereas miRNAs with negative P19:Lin28a/P19:FRT ratio are represented by a red colour.

5.3 Sequence analysis of pri-miRNA proximal genomic regions

My genome-wide data suggest that Lin28a could potentially stabilise a range of precursor miRNAs. Therefore, it was interesting to determine

whether they have the potential to associate with Lin28a via previously characterised binding sites (Cho et al., 2012; Wilbert et al., 2012). To test that, I decided to map identified Lin28a binding motifs to regions flanking each direction 500bp of pre-miRNA genomic coordinates of previously selected miRNAs. This approach should allow me to include potential regulatory site within pre-miRNAs and their immediate vicinity as well. I was able to show that the motifs "CCGGCC", "GAGCAC", "GAGGGC", "AAGAAA", "CAGAGG", "GAGGAG" are overrepresented in genomic regions proximal to selected miRNAs as related to overall miRNA population (excluding selected miRNAs) (Figure 5-4).

Moreover, the majority of these motifs reside outside the mapped pre-miRNA sequence within pri-miRNA or its genomic proximity, as shown for group of representative miRNAs (Figure 5-4).

These could potentially suggest the direct involvement of Lin28a in the stabilisation of their precursor RNA molecules.

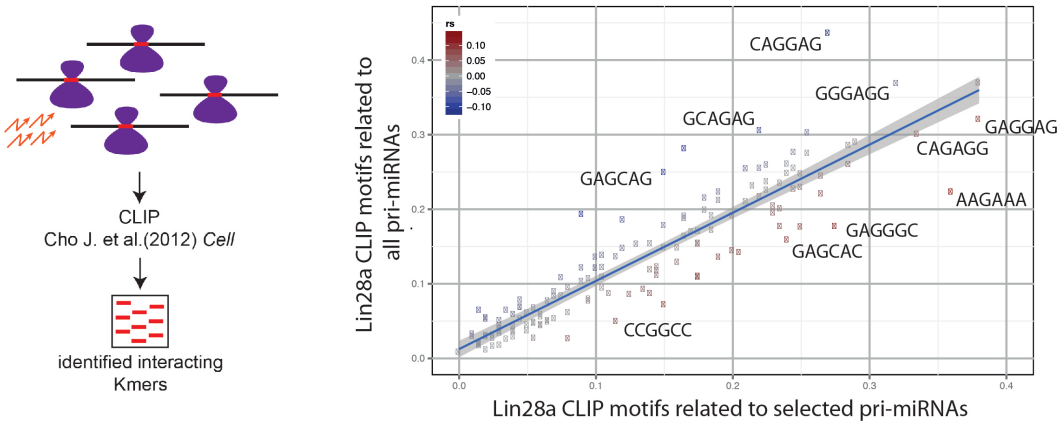

Figure 5-4 Characterisation of Lin28a binding motifs based on CLIP-data.

Hexamers identified previously with CLIP sequencing (left panel) were mapped within the genomic proximity (500bp upstream and downstream) of the selected group of pri-miRNAs and their overall enrichment within pri-miRNAs loci was represented between selected miRNAs group and all remaining known miRNAs (right panel).

5.4 Stimulatory effect of Lin28a is likely indirect or transcriptionally-dependent

In order to determine whether Lin28a is involved in the stabilisation of precursor miRNA at early stages of neuronal differentiation I decided to perform *in vitro* processing reaction. I used P19 day 0 extracts with RNAi-depleted Lin28a and compared the *in vitro* processing to mock P19 day 0 reactions. The assays were performed with representative group of internally radiolabelled *in vitro*-transcribed pri-miRNAs and pre-miRNAs (Figure 5-5). Unfortunately, I was not able to find a strong candidate that would confirm that the depletion of Li28a would lead to its destabilisation.

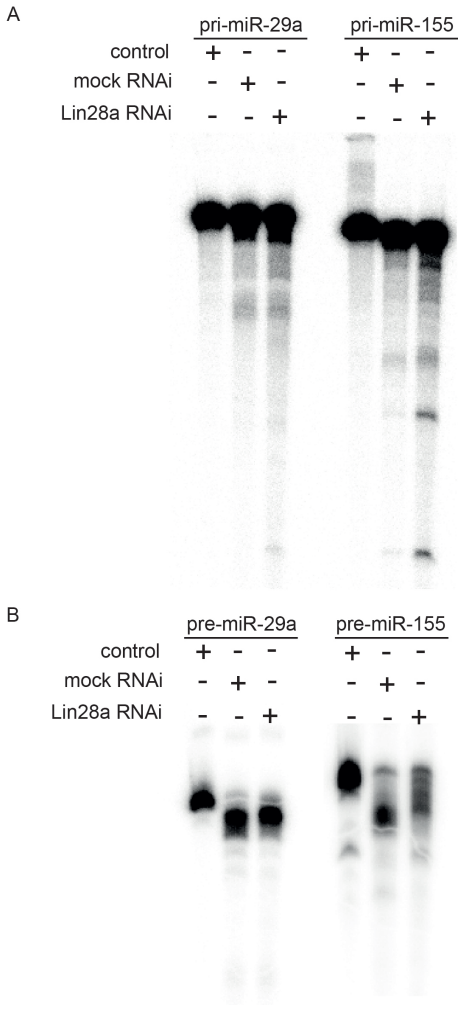

Figure 5-5 P19 day0 - *in vitro* processing of pri-miRNAs and pre-miRNAs

Radiolabelled pri- and pre-miRNA probes were synthesised for miR-29a and miR-155 and subsequently incubated with P19 day 0 extracts from cells treated with mock or Lin28a siRNA.

a) *In-vitro* processing results of pri-miR-29a and pri-miR-155
b) *In-vitro* processing results of pre-miR-29a and pre-miR-155

This observation could mean that the stabilisation is due to another post-transcriptional event indirectly regulated by Lin28a. Alternatively, it could be an effect of steady-state level control regulated in some way by Lin28a. To test whether the steady-state levels of selected miRNA groups is affected by the constitutive expression of Lin28a, I performed qRT-PCR analysis of their pri-miRNAs on day 0 and day 9. Importantly, I found that the steady-state levels of pri-miR-155 was upregulated in the presence of Lin28a (Figure 5-6). This potentially suggests that at least in a subset of instances, the observed upregulation of mature miRNA could be partially accounted for the control of miRNAs steady-state levels.

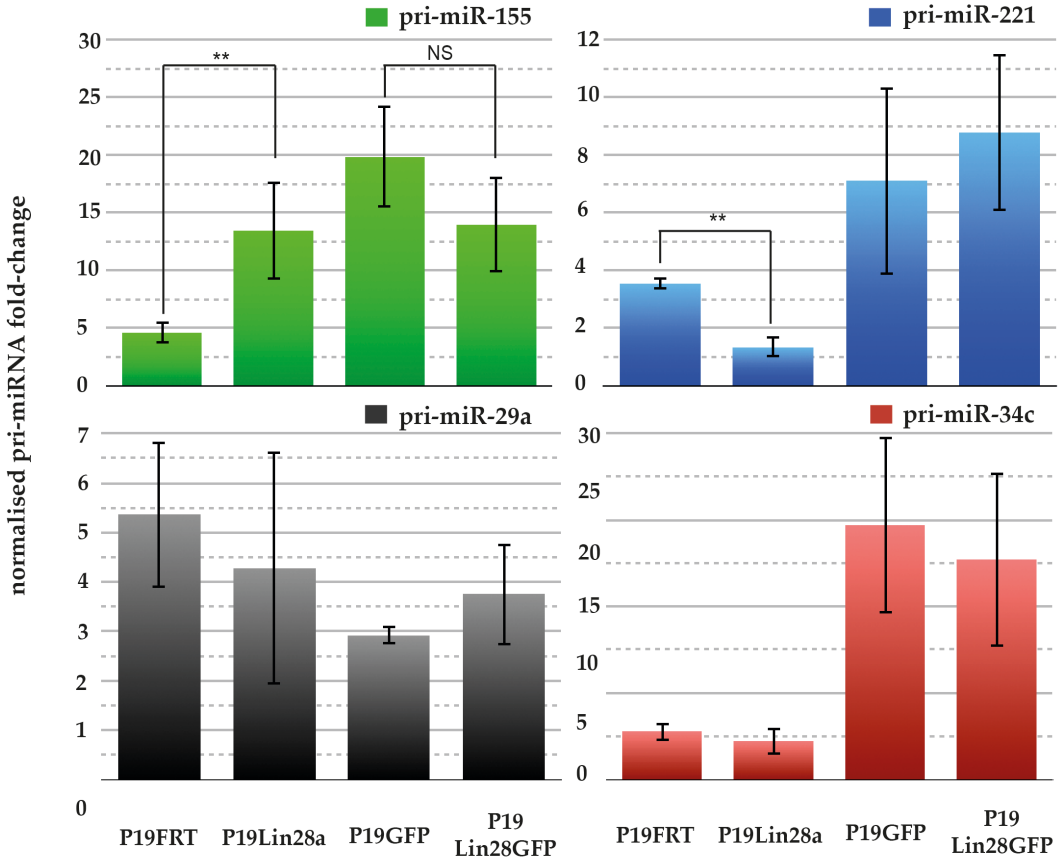

Figure 5-6 qRT-PCR - pri-miRNAs change during neuronal differentiation
Selected pri-miRNAs levels were analysed on day 0 and day 9 and subsequently day 9/day 0 ratios were calculated and visualised for each P19 stable cell line.

5.5 Characterisation of pre-miRNA secondary-structure arrangements between different functional groups

My current findings suggest that Lin28a regulates pre-let-7a and pre-miR-9 post-transcriptionally via distinct but to some extent similar mechanisms. Interestingly, genome-wide analysis showed a large group of miRNAs affected with the constitutive expression of untagged Lin28a. I decided to determine whether certain secondary arrangements, like an abundance of double-stranded regions, are overrepresented in this group. To test that, I obtained information in "miRBase", which is a miRNA database about paired-bases with pre-miRNAs regions. Subsequently, I developed python script to count the number of paired-bases across a selected pre-miRNA group. Analysis was performed counting positions up and down the centre of individual pre-miRNA – representing the terminal. As a benchmark, I used analysis of randomly selected pre-miRNA sequences from "miRBase" that were primed in ten independent drawing rounds (Figure 5-7).

Interestingly, using this approach I was able to demonstrate that groups affected by untagged Lin28a have fewer base-paired nucleotides within their pre-miRNA sequence when compared to the overall population of pre-miRNAs.

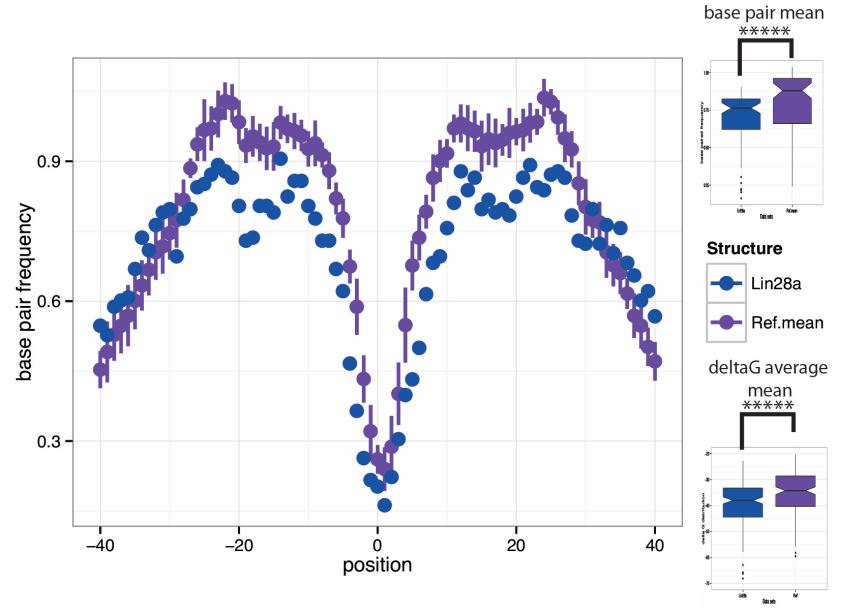

Figure 5-7 Analysis of secondary structures features of selected pre-miRNAs.

Centre of the terminal loop was marked as position 0 and subsequently the number of paired nucleotides along the pre-miRNA sequence (upstream and downstream from position 0) was summed up and represented as a frequency per total pre-miRNA size. Calculations were performed on the selected group of the pre-miRNAs as well as on pre-miRNAs obtained from ten independent and random drawing rounds. Additionally, average free energy and base pair number were plotted as whisker plots (right panel)

Chapter 6

6 Discussion

In recent years, miRNAs have drawn a great amount of interest across various life science disciplines, supporting their extensive role in all aspects of cell biology in higher eukaryotes. For instance, the genome-wide approach has shown that miR-221 induces sprouting in zebrafish endothelial cells (Nicoli et al., 2012). Moreover, zebrafish knockdown of miR-221 inhibits the proliferation and migration of tip cells, whereas the overexpression of miR-221 in endothelial cells promotes vessel sprouting. Another example involves the role of miRNAs in the regulation of β-cell activity and subsequent management of glucose metabolism (Walker, 2008). Overexpression of miR-375 suppresses glucose-induced insulin secretion, whereas its inhibition enhances insulin production. Moreover El Quaamari and colleagues showed that in rat, miR-375 levels are regulated by glucose. In liver hepatocytes, the cell cycle is affected by miR-21, which was shown to control levels of several cell cycle regulators (Song et al., 2010). As mentioned in the Introduction, there are many more examples of miRNAs playing essential roles in the development and maintenance of the nervous system (Meza-Sosa et al., 2012). Therefore, miRNAs appear to be very important mediators of various diseases and targets for developing novel therapeutics (Broderick and Zamore, 2011). Not surprisingly, the multi-step miRNA maturation pathway has also been proposed as a target for developing miRNA-based therapeutics (Roberts, 2014).

6.1 Dis3l2 degrades pre-let-7a in a uridylation-dependent fashion

A large amount of attention has been dedicated in recent years to Lin28 regulation of the let-7 family, partially because it was one of the first identified miRNAs (Bracht et al., 2004). Moreover, it has been shown that let-7 and Lin28 are very important for embryonic development (Moss and Tang, 2003; Van Wynsberghe et al., 2011). In general, during development, let-7 levels are controlled by post-transcriptional regulatory mechanisms. Several studies have proposed that in a canonical way, Lin28 associates with pre-let-7 and serves as a platform for the Zcchc family, also known as TuTase – an enzyme catalysing the addition of uracil to the 3′-end (Hagan et al., 2009; Heo et al., 2008). Subsequently pre-let-7a-p(U) acts as a substrate for Dis3l2, an RNA 3′-5′-exonuclease (Chang et al., 2013; Ustianenko et al., 2013). Non-canonical mechanisms post-transcriptionally regulating let-7 levels were also described. Lightfoot and colleagues first proposed an alternative pathway; they showed that Lin28a association with the pre-let-7a terminal loop also interferes with Dicer processing by melting a stem of the terminal. Another mechanism is based on the fact that the Lin28 family includes two paralogues - Lin28a and Lin28b. The latter protein contains nuclear localisation signal (NLS) and nucleolar localisation signal (NLoS), which is important for its nucleoli localisation (Piskounova et al., 2011). Piskounova and colleagues suggested that Lin28b sequesters its target from the microprocessor by transferring them to nucleoli, which impede their processing inside the nucleus.

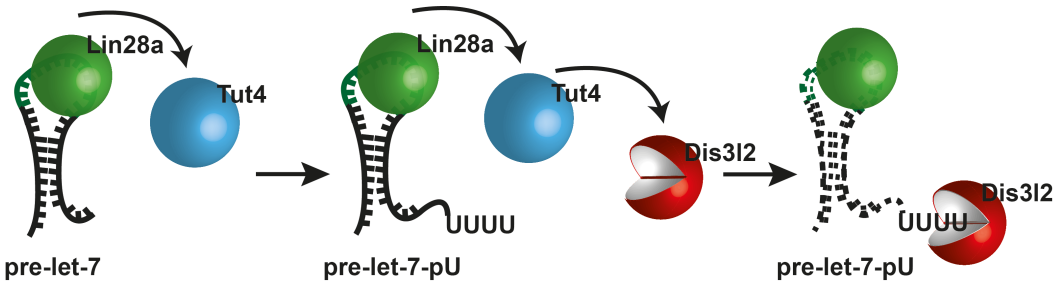

Figure 6-1 Model of Lin28a mechanism regulating pre-let-7a post-transcriptional degradation.
Lin28a associates with pre-let-7a terminal loop and engages Tut4 to generate 3′-poly(U) tail. Subsequently the pre-let-7a uridylation leads to degradation driven by 3′-5′ exonuclease Dis3l2.

Results of my PhD work support the finding that pre-let-7a is uridylated and subsequently degraded by a 3′-5′ exonuclease Dis3l2. P19 *in vivo* data reinforced the hypothesis that Lin28a and Lin28b levels are high in undifferentiated cells and as the cell progress through differentiation, their levels gradually decrease with no detectable expression beyond day 6. As expected, this change of Lin28a expression coincides with an increase in mature let-7 levels.

I also confirmed previous findings regarding the molecular mechanism of Lin28a action. My *in vitro* processing indicated that pre-let-7a is highly uridylated in undifferentiated cells and this uridylation gradually decreased as cells were progressing through differentiation. This gradual decrease in uridylation overlaps with a decrease in Lin28 levels. Interestingly, loss of uridylation very modestly affected the stability of pre-let-7a during neuronal differentiation. This could be caused by the presence of Lin28b, which might affect the stability of pre-let-7a or alternatively might be a result of destabilisation via various RNA nucleases during the *in vitro* reaction itself. *In vivo*, pre-let-7a might be shielded from the non-specific degradation. Alternatively, cells express a large amount of RNA molecules that could compete for interaction with the RNA nucleases that could favour them based on affinity. Poor agreement between loss of uridylation and stabilisation of the pre-let-7a form was particularly visible upon depletion of Lin28a. Knockdown of Lin28a resulted in a clear decrease in the pre-let-7a-p(U) form and did not

increase the stability of pre-let-7a. Having said that, the maintained expression of Lin28a in differentiated P19 cells not only led to the formation of poly-uridylated pre-let-7a but also strongly supported its destabilisation. These opposing states clearly indicate that uridylation of pre-let-7a is sufficient to trigger its destabilisation and that pre-let-7a could also be degraded non-specifically *in vitro* with other RNA nucleases. Analysis of mature let-7a levels in Lin28a's loss-of-function and gain-of-function in P19 cells supported the possibility of pre-let-7a non-specific degradation *in vitro.* The knockdown of Lin28a ultimately resulted in increased let-7a levels. On the other hand, constitutive expression of Lin28a or induction followed differentiation greatly supress the expression of mature let-7a. These findings recapitulated previous observations regarding the effect of Lin28a on mature let-7. At least two groups previously reported that Lin28a knock down ultimately leads to increase let-7 levels (Heo et al., 2008; Piskounova et al., 2011). Moreover, Balzer and colleagues also showed that constitutive expression of Lin28a:GFP fusion protein in P19 cells resulted in strong inhibition of let-7 production during neuronal differentiation *in vitro* (Balzer et al., 2010).

Lin28a belongs to small set of proteins that when combined efficiently can promote pluripotency (Yu et al., 2007). Interestingly, it is the only protein which is not a transcription factor from the group of pluripotency factors. However, because Lin28 is expressed in broad range of tissues, it could potentially play a role beyond pluripotency maintenance (Yang and Moss, 2003; Yokoyama et al., 2008). Balzer and colleagues suggested that Lin28 could act as a fate-promoting factor (Balzer et al., 2010). They showed that prolonged expression of Lin28a during neurogliogenesis primed cells to favour earlier occurring neurogenesis over late occurring gliogenesis. They suggested that Lin28 arbitrated the switch between neuro-glia fates could account for the two independent modes of Lin28 action that depend on the activity of CSD and ZnFD (RNA binding domains). (Balzer et al., 2010). Furthermore, they showed that the repression of let-7 correlated with the inhibition of gliogenesis. However, its low mature levels did not inhibit neurogenesis, as observed during the differentiation of the

Lin28a:GFP and Lin28b:GFP stable cell lines (Balzer et al., 2010). My results with P19 stable cell lines further supported Balzer and colleagues findings. I observed the occurrence of neurogenesis despite constitutive expression of Lin28a:GFP fusion protein. The cells differentiated normally presenting embryonic bodies of a size similar to P19:GFP embryonic bodies. Importantly, Lin28a:GFP stable cells favoured neuronal differentiation events but did not allow for the accumulation of high let-7a levels. This is a striking finding, as during development, low let-7 levels are generally associated with less efficient differentiation and large quantities of let-7 were shown to promote differentiation (Roush and Slack, 2008). What is more, several groups reported a link between high let-7 levels and neuronal differentiation (Rybak et al., 2008; Wulczyn et al., 2007). These dissonant findings might suggest that low let-7 levels permit neuronal differentiation in certain cellular systems. One potential explanation is the lack of lineage specificity observed during the global differentiation of P19 cells. The nervous system of higher vertebrates is extremely complex and contains various groups of neurons that can be differentially grouped based on their anatomical characteristics or functional output (Peters, 1984; Ramón y Cajal, 1995). Therefore, it would be interesting to test the role of Lin28 and let-7 in the differentiation of specific neuronal lineages. Fast development of stem cell research nowadays allows for their very specific differentiation. There have been methods describing the differentiation of induced pluripotent stem cells into dopaminergic neurons, ventral motoneurons, retinal neurons, etc. (Schwartz et al., 2008). Alternatively, the development of an animal model with knock-in expression of Lin28a in the brain would allow these lineages to be tracked within their native environment and the role of let-7 in their development to be assessed.

The major finding of my thesis is that unlike constitutive expression of Lin28a:GFP, constitutive expression of untagged Lin28a blocked neuronal differential progression. This finding further supported the hypothesis suggested by Balzer and colleagues that two distinctive pathways control gliogenesis and neurogenesis. Not surprisingly, untagged protein also supported the repression of let-7 observed in the Lin28a:GFP cell line. This

strongly suggests the existence of additional factors affected by untagged Lin28a that regulate neuronal differentiation. Moreover, phenotypic differences between Lin28a:GFP and untagged Lin28a observed during differentiation of P19 stable cells also suggest that neurogliogenesis is controlled by two genetically distinctive pathways and that Lin28a regulates these fate-outcomes employing two distinctive molecular mechanisms.

6.2 miR-9 levels are regulated both transcriptionally and post-transcriptionally

miR-9 is a very ancient miRNA that dates back to the transition toward triploblast with functions and set of targets that encountered substantial changes during the evolution of bilatera (Wheeler et al., 2009). Throughout the evolution of various species, miR-9 proved to be involved in processes related to neuronal development by employing mechanisms based on opposing strategies. For instance, in *Drosophila*, miR-9 sensory precursors (SOP) are specified in two-step process (Skeath and Carroll, 1994). In the first step, groups of cells acquire pre-neuronal competence. In the second step, one of these cells become SOP as a consequence of lateral inhibition mediated by non-SOP neighbours. Interestingly, miR-9 plays an indirect role in specifying SOP cell by being restricted to non-SOP and arbitrating lateral inhibition processes (Li et al., 2006). However, in higher vertebrates miR-9 has been directly linked with neuronal development. At first, the genome-wide profiling of miRNA classifies miR-9 as a brain-enriched miRNA (Krichevsky et al., 2003; Lagos-Quintana et al., 2002). Furthermore, its expression profiling suggests that miR-9 is dynamically regulated throughout neuronal differentiation (Miska et al., 2004; Sempere et al., 2004). It has been shown that the expression of miR-9 is switched on during mid-embryogenesis after the development of the neuronal scaffold and is associated with active neurogenic areas (Coolen et al., 2012; Darnell et al., 2006; Walker and Harland, 2008). MiR-9 is generally excluded from brain regions containing undifferentiated neuronal progenitors or from areas with late differentiation onset, midbrain-hindbrain region or retina, respectively (La Torre et al., 2013; Leucht et al., 2008).

For these reasons, miR-9 is a perfect candidate to play an essential role in the neuronal differentiation of P19 cells. My experiments showed that the expression of both primary and mature miR-9 does not occur in undifferentiated P19 cells, but only in differentiating neurones. This observation of the delayed expression of miR-9 is consistent with the differentiation of hESC and rat neuronal progenitors (Delaloy et al., 2010). Transcription of the miR-9 precursor has been previously studied in

human neuroblastoma derived SK-N-BE cell line (Laneve et al., 2010). Laneve and colleagues showed that pri-miR-9-2 transcription does not depend on its host gene and is linked to the regulatory elements REST and CREB. REST, as a chromatin remodelling factor, regulates several neuronal genes, whereas CREB was shown to be involved in several neuronal functions, including neuronal proliferation and differentiation and synaptic plasticity (Impey et al., 1996). In undifferentiated cells, the association of unphosphorylated CREB and REST directly blocks transcription of miR-9 primary transcripts. During the differentiation, REST expression levels drop and CREB undergoes phosphorylation, which causes its activation, subsequently leading to the removal of pri-miR-9 transcription blockage (Laneve et al., 2010). It would be interesting to determine whether the REST/CREB mechanism operates in the same manner in P19 cells as in the SK-N-BE model. It could be performed using ChIP and luciferase reporter assays.

Importantly, I found a substantial delay between the expression of mature miR-9 and pri-miR-9 during the differentiation of P19 cells. In particular, I observed that early after the start of differentiation, only 10% of pri-miR-9 was processed into mature miRNA. This observation indicated additional layers of post-transcriptional control of miR-9 production. In fact, I was able to uncouple transcriptional and post-transcriptional events with *in vitro* processing assays, which showed that pri-miR-9 is more efficiently processed in differentiated than in undifferentiated cells. Moreover, I showed that this post-transcriptional regulation is linked to the terminal loop of pri-miR-9. Indeed, terminal loops have been shown in the past to play an important role in the processing of at least pri-let-7, pri-miR-7 or pri-miR-18a. It has been discovered that terminal loops are platforms for binding auxiliary factors such as Lin28a/KSRP, HuR/Msi2 or hnRNPA1 (Michlewski and Caceres, 2010; Michlewski et al., 2008; Piskounova et al., 2008). Following these examples, I used RNA pull-down assays coupled with quantitative mass spectrometry to identify factors that had the potential to specifically interact with pre-miR-9 CTL (Conserved Terminal Loop) in undifferentiated cells. Surprisingly, one of the most potent

protein interactors turned out to be Lin28a. Using the same strategy, I identified Lin28a to interact with pre-let-7a, but I could not validate its interaction with TuT4 protein (Piskounova et al., 2011). Potentially, this was an effect of its transient interaction with pre-let-7 and therefore further optimisation of capture conditions could help to eliminate this issue.

To date, several studies have used UV crosslinking and immunoprecipitation coupled with high-throughput sequencing (CLIP-seq) to identify targets for Lin28a binding (Cho et al., 2012; Wilbert et al., 2012). However, these studies focused on undifferentiated embryonic stem cells and somatic cells, which could possibly result in an incomplete identification of Lin28a targets. Especially when these targets display a spatio-temporal expression pattern depending on the cell type or developmental timing. In my studies, using retinoic acid-induced P19 cells, I managed to capture physiologically relevant roles of Lin28a in the context of neuronal differentiation. I validated high-throughput pull-down and mass spectrometry findings and proved that pri-miR-9-CTL interacts specifically with Lin28a in undifferentiated cells. I also proved that Lin28a has a role in restricting miR-9 production to the later stages of neuronal differentiation. In the past, it has been shown that the depletion of Lin28a de-repressed let-7 levels in embryonic stem cells (Viswanathan et al., 2008). I applied a similar strategy and succeeded in showing that the knockdown of Lin28a resulted in increased miR-9 levels in differentiating P19 cells. However, an increase in miR-9 was approximately less than 3-fold when compared to let-7. This could be explained by the difference in the levels of primary transcripts between the two miRNAs. As mentioned above, pri-miR-9, in contrast to pri-let-7a, is not transcribed due to REST/CREB blockage in undifferentiated cells (Laneve et al., 2010). Therefore, this delay in pri-miR-9 production when compared with pri-let-7 could have directly translated to the differences in de-repression of miR-9 and let-7. It would be interesting to test whether this discrepancy could be erased by providing equal levels of primary transcripts of let-7 and miR-9. One way of achieving that could involve providing higher levels of

pri-miR-9 in undifferentiated P19 to match levels of pri-let-7 by transient transfection or the generation of stable cell lines expressing pri-miR-9 independently from REST/CREB repressors.

In addition, the poor match between let-7 and miR-9 induction could be a result of the presence of Lin28b. It is possible that their precursors respond differentially to Lin28a and Lin28b. Therefore, the depletion of Lin28a is sufficient to increase of let-7 levels but is not sufficient to provide enough background for miR-9 induction. In the future, it would be interesting to compare the increase in miR-9 levels upon double Lin28a and Lin28b knockdown.

The most interesting result of my thesis came from the analysis of Lin28a gain-of-function experiments. As described above, let-7 levels were repressed in differentiated cells carrying constitutively expressed Lin28a:GFP or untagged Lin28a. However mature miR-9 levels were only down-regulated in P19 lines expressing untagged Lin28a and were not affected by the constant expression of Lin28a:GFP fusion protein. This is of particular interest as the repression of let-7 was not sufficient for the inhibition of neurogenesis. Moreover, I observed that down-regulation of mature miR-9 level by constitutive expression of Lin28 was associated with a morphological phenotype. Developing embryonic bodies presented significantly smaller size than their counterparts obtained from control P19 cell lines as well as the Lin28a:GFP cell line. This finding is in agreement with a previous study of Delaloy and colleagues. They found that direct blocking of miR-9 activity using locked-nucleic acid strategy resulted in the formation of much smaller neurospheres upon differentiation of human embryonic stem cells and rat primary cortical progenitors (Delaloy et al., 2010). Furthermore, they suggested that miR-9 is important at early stages of neurosphere formation for the maintenance of a pool of neuronal progenitor cells by limiting their migration and promoting proliferation. This action of miR-9 was linked to stathmin – its molecular target, which was shown to affect these cellular processes (Delaloy et al., 2010). That said, the exact role of miR-9 in the early stages

of neuronal differentiation is still not fully understood, especially as a reduction in the differentiation rate and an increase in proliferation have been observed upon miR-9 loss-of-function studies in embryonic neuronal progenitors or adult neural stem cells (Bonev et al., 2011; Coolen et al., 2012; Shibata et al., 2011).

These discrepancies could suggest that the execution of miR-9 functions depends on the developmental stage of cells, and that this could be accounted for miR-9 distinctive spatio-temporal regulation of its mRNA targets. Therefore, stage-specific analysis of miR-9 targets would help to build a more accurate model of miR-9 function during neuronal differentiation. Equally important to miR-9 loss-of-function study is analysis of the mature miR-9 overexpression phenotype. It was shown that miR-9 gain-of-function leads to reduced proliferation in zebrafish embryo or mouse embryonic cortex and promotes differentiation of neuronal progenitors (Leucht et al., 2008; Zhao et al., 2009). In the future, it would be interesting to determine whether an increase in mature miR-9 levels in P19 cells would result in an increase in their differentiation upon retinoic acid priming. This could be determined by delivering miR-9-5p/-3p duplexes into differentiating P19 cells or expressing a pri-miR-9 mutant with the ability to escape transcriptional and post-transcriptional regulatory mechanisms.

My results demonstrated that the terminal loop of pri-miR-9 is an important element for association with factors involved in post-transcriptional regulation of its biogenesis. Therefore, I attempted to test this role of the terminal loop by overexpressing pri-miR-9 and pri-let-7a mutants that could be transcribed independently of the differentiation state and escape post-transcriptional blockage. Overexpression of pri-let-7a/miR-16-CTL mutant in undifferentiated P19 cells resulted in strong de-repression of let-7a levels. Unfortunately levels of mature miR-9 did not change upon transfection with the pri-miR-9/miR-16-CTL mutant suggesting additional layers of miR-9 regulation, possibly affecting the stability of mature miR-9. Potential regulation via the stability of miR-9

will not be a great surprise as several examples describing the molecular mechanisms affecting the stability of mature miRNAs have been reported. For example, in *C. elegans* 5'-3' exonucleases XRN1 and XRN2 were shown to degrade a variety of miRNAs (Chatterjee et al., 2011; Chatterjee and Grosshans, 2009). In mammals, an unknown exonuclease is involved in the degradation of miR-183, miR-96, miR-192, miR-204 and miR-211 (Krol et al., 2010a). Degradation of mature miRNA was also reported in pathological conditions. In melanomas, interferon-inducible 3'-5' exonuclease PNPase-old-35 (PNPT1) is involved in the degradation of miR-221, miR-222 and miR-106 (Das et al., 2010).

I further proved that this potentially additional mechanism was specific to P19 undifferentiated cells, as overexpression of similar mutants in HeLa cells resulted in de-repression of the processing of both pre-let-7a/miR-16 and pre-miR-9/miR16 terminal loop mutants. HeLa cells are not primed to undergo neuronal differentiation and do not express endogenous Lin28a. Thus, the above observation is important for two reasons. First, it shows that additional mechanisms controlling levels of miR-9 are operating in P19 undifferentiated cells. Second, it also indicates that Lin28a-mediated post-transcriptional mechanism controlling miR-9 production is independent from a differentiation state of the cell. However, it would be interesting in the future to establish P19 stable cell line expressing pri-miR-9/miR-16-CTL mutant and determine whether this additional putative post-transcriptional blockage is associated with certain stages of P19 cells and can be removed upon priming neuronal differentiation with retinoic acid.

6.3 Lin28a regulates pre-miR-9 stability in a uridylation-independent manner

The current understanding of transcription events occurring in humans and yeast suggest that their entire genome operates as a huge RNA factory (Amaral et al., 2008). Therefore, proper surveillance machinery allows for the rapid and precise selection of functional RNA molecules (Houseley and Tollervey, 2009). These processes are especially prevalent and important for the biology of non-coding RNA. For example, transcribed miRNA precursor has to undergo two steps of maturation before stable mature miRNA is generated. Within the time of maturation, both pri-miRNA and pre-miRNA could be rapidly degraded as a result of mechanisms that monitor subcellular miRNA levels. In fact one of the oldest and most well-studied human miRNAs, let-7, employs this surveillance machinery to control its levels in cells (Viswanathan et al., 2008).

In my PhD work, I suggested that the production of miR-9 relies on post-transcriptional control of pre-miR-9 stability. Using the P19 differentiation model, I showed that pre-miR-9 is highly unstable in cell extracts derived from undifferentiated cells and gradually becomes stabilised during the time course of neuronal the differentiation. Interestingly, I observed that this effect is independent of uridylation as no higher molecular weight intermediate was detected. This finding is particularly interesting in light of the recent work by Lim and colleagues. Using a genome-wide approach, they were able to show that mammalian mRNA molecules are consistently oligo-uridylated and that this process promotes their decay (Lim et al., 2014). This was also observed for pre-let-7, which in embryonic stem cells is uridylated by the Lin28/TuT4-mediated mechanism, followed by Dis3l2-mediated degradation (Heo et al., 2008; Heo et al., 2009; Piskounova et al., 2011). However, Suzuki and colleagues observed that in cells with low Lin28a/b levels. pre-let-7 is still degraded in spite of the lack of uridylation. They demonstrated that the mammalian immune

regulator MCPIP1 ribonuclease also known as Zc3h12a mediates uridylation-independent degradation of pre-let-7 (Suzuki et al., 2015).
These observations were particularly relevant to my findings. I also showed that Lin28a mediates the uridylation-independent degradation of pre-miR-9. I reported that the knockdown of Lin28a abolished the destabilisation of pre-miR-9 in extracts derived from undifferentiated cells. Furthermore, reconstitution with recombinant Lin28a is sufficient for restoring the degradation process. Interestingly, Lin28a:GFP fusion protein was not able to destabilise pre-miR-9 in differentiated cells, whereas untagged Lin28a was sufficient to induce the destabilisation of pre-miR-9, similar to that which was observed in the early stages of differentiation. This finding was in contrast to the *in vitro* processing of pre-let-7a, which was strongly destabilised by both Lin28a:GFP and untagged Lin28a. The difference observed between the *in vitro* processing of pre-miR-9 and pre-let-7a is important as its provides more support for previously suggested hypothesis regarding the different molecular mechanisms affecting neurogenesis and gliogenesis observed during differentiation of the P19 stable lines. These findings implied that the positioning of GFP at C-terminal of Lin28a interfered with its activity on pre-miR-9 destabilisation. Interestingly, recombinant, N-terminally tagged GST-Lin28a was able to destabilise pre-miR-9 after reconstitution in Lin28a-depleted extracts. Even though GST and GFP are different biological molecules, they both share a similar size. Therefore, distinct positioning of tags, C-terminal and N-terminal for GFP and GST respectively, would suggest that the mechanism of action could depend on Lin28a activity at its C-terminus.

Lin28a was shown previously using genome-wide techniques to interact with a large number of RNAs, including mRNA and ncRNA (Cho et al., 2012; Wilbert et al., 2012). Importantly, Lin28a, as opposed to DHX9, a non-specific RNA-binding protein, did not bind to pre-miR-16. Furthermore, interaction between Lin28a and pre-miR-9 was abolished after its conserved terminal loop was changed to the terminal loop of pre-miR-16. Significantly, the pre-miR-9/miR-16-TL mutant was not

destabilised by Lin28a in undifferentiated cells. These results prove that Lin28 interacted in a specific manner with pre-miR-9-CTL.

RNA molecules are known to form large multimeric complexes with various proteins, for instance Drosha/DGCR8 or RISC complexes. Therefore, it was important to establish whether the interaction between Lin28a and pre-miR-9 is direct. Using whole cell extract and recombinant protein, I showed that Lin28a was able to shift pre-miR-9, which demonstrated its capacity to directly interact with pre-miR-9. Interestingly, I observed that two prominent protein complexes are formed with pre-miR-9 as opposed to one discrete complex with pre-let-7a. Interestingly, previous structural studies of pre-let-7a and Lin28a suggested that Lin28a interacts with two or even possibly three distinct sequence motifs within the terminal loop of pre-let-7 (Desjardins et al., 2014; Loughlin et al., 2012; Nam et al., 2011). Moreover, recent findings suggested also that Lin28a likely undergoes stepwise assembly on pre-let-7-CTL, as 1:1, 1:2 and 1:3 complexes were observed (Desjardins et al., 2014). Furthermore, the association of one or more Lin28a molecules could modulate its activity. Desjardins and colleagues demonstrated that a 1:1 complex of pre-let-7g/Lin28a is sufficient for maximum dicer inhibition, whereas for pre-let-7a, maximum inhibition was observed in the case of a 1:3 complex (Desjardins et al., 2014). Surprisingly, in my EMSA assay with recombinant Lin28a:GST, I did not observe the efficient assembly of multimeric Lin28a molecules on pre-let-7a terminal loop. This was potentially a consequence of either protein concentration below saturation levels suggested in Desjardins and colleagues' work or the presence of GST at the N-terminus of Lin28a, which could interfere with step-wise assembly.

Therefore, these findings could mean that pre-miR-9 can also associate with more than a single molecule of Lin28a. However, I showed that in the case of two complexes formed upon pre-miR-9 incubation with whole cell extracts, only the one with the lower molecular weight was displaced with Lin28a-specific antibody. This observation is important for two reasons. Firstly, the complete disappearance of a lower MW band reinforced the fact that Lin28a directly interacted with pre-miR-9. A potential

explanation for the observed phenomena could be that the antibody sequestered Lin28a and buried the pre-miR-9 interaction site, which subsequently prevented the formation of the pre-miR-9/Lin28a complex. Nevertheless, if pre-miR-9/Lin28a interaction is mediated by an additional protein, then the displacement of Lin28a would result in a moderate shift of one of the observed discrete bands rather than its complete disappearance. The second important reason is that the higher MW band was not displaced in the presence of the Lin28a-specific antibody. The model of step-wise assembly of Lin28a suggested by Desjardins and colleagues indicates that each molecule of Lin28a interacts with pre-let-7 independently (Desjardins et al., 2014). For that reason, every additional molecule of Lin28a present on pre-miR-9 should be displaced by Lin28a antibody in similar manner. Therefore, the observed higher MW should be counted as the assembly of pre-miR-9 in some other tertiary complex that potentially contain Lin28a together with other proteins.

My findings also suggest that Lin28a associates with pre-miR-9 engaging only one of its two RBDs. I showed computationally that pre-miR-9 folds into the hairpin structure containing a much smaller terminal loop in comparison to its counterpart on pre-let-7a, which is capable of interacting with both of Lin28a domains at the same time (Loughlin et al., 2012; Nam et al., 2011). Two motifs within pre-miR-9-CTL that could potentially bind Lin28a are in close proximity to each other. Such presentation of the motifs would require the RBDs in close proximity if Lin28a:pre-miR-9 interaction was mediated by both of the domains at the same time. This type of arrangement would very likely force great tension inside the Lin28a backbone which is why it is unlikely that pre-miR-9-CTL interacts with both RBDs at any given moment. In fact, using footprinting cleavage assay I showed that Lin28a associates pre-let-7a with both characterised previously motifs within its terminal loop (Desjardins et al., 2014; Loughlin et al., 2012; Nam et al., 2011). However, footprinting with Lin28a and pre-miR-9 showed that protected nucleotides were located upstream from its consensus “GGAG” motif. Moreover, I showed that “GGAG”

mutants of pre-miR-9-CTL escaped Lin28a-mediated regulation suggesting that this region of the loop is functionally redundant regarding the interaction with Lin28a. I also showed using Lin28a truncations that both domains were capable of interacting with their characterised motifs within the loops of pre-miR-9 and pre-let-7a. However, I observed substantial differences between their binding efficiency when presented independently from each other. Lin28a-ZNF(123-209) mutants interacted substantially stronger with pre-let-7a than with pre-miR-9 when compared to full length Lin28a interaction with the corresponding pre-miRNAs. The observed increase in binding efficiency in the case of pre-let-7a could potentially be explained by the step-wise assembly model (Desjardins et al., 2014). It is quite possible that the ZNF domain when presented independently could assemble the multimeric pre-let-7a/Lin28a complex more efficiently than in context together with CSD. However, more detailed biophysical characterisation of Lin28a-ZNF(123-209) in complex with pre-let-7a should follow to allow the more accurate interpretation of this finding. Interestingly, both zinc-knuckles are required for efficient binding to both pre-let-7a and pre-miR-9-1. Lin28a-ZNF(156-209) mutant failed to bind pre-let-7a and associated very weakly with pre-miR-9. It is likely that zinc-fingers within Lin28a are presented in a structural context that allows the efficient interaction with specific sequence motifs. Disruption of this structural arrangement likely results in a loss of activity of the ZNF domain of Lin28a. In fact, there are few examples of domains where individual elements have to be presented in certain structural arrangements to retain functional activity. One of these examples is the arrangement of WD40 domains. In the normal situation, they are presented in proteins as a run of 7-8 repeats that form well defined β-propellers. The removal of individual WD40 domains breaks the arrangement and results in a loss of functional activity of WD40 domains (Smith et al., 1999).

Nevertheless, the most striking observation was in the case of Lin28a-CSD(1-74) and Lin28a-CSD(1-123) mutants. I showed that both mutants had very low binding efficiency with pre-let-7a. However, their binding

efficiency to pre-miR-9 was 2-3-fold higher than to pre-let-7a. These observations suggest that in the case of pre-miR-9, a cold shock domain might be sufficient to mediate the formation of a pre-miR-9/Lin28a complex. Importantly, this possibility remains in agreement with footprinting and mutational analysis. Both showed that ZNF domain consensus motif, "GGAG", is not relevant in the case of pre-miR-9 for Lin28a function and binding. Together, these findings allow speculation that the ZNF domain remains unoccupied following binding to the pre-miR-9 terminal loop and could be important for interactions with putative downstream effectors that lead to destabilisation of pre-miR-9 observed in undifferentiated P19 cell extracts.

To date, many different pathways for RNA degradation have been proposed (Houseley and Tollervey, 2009). RNA nucleases are especially relevant for the biology of miRNAs as they control various stages of their biogenesis (Ha and Kim, 2014). In particular, certain pre-miRNAs could be degraded by MCPIP1 and IRE1α endonucleases, whereas mature miRNAs stability is controlled by the activity of XRN1 and XRN2 exonucleases (Chatterjee et al., 2011; Ramachandran and Chen, 2008; Suzuki et al., 2011; Upton et al., 2012). I showed that pre-miR-9 is actively destabilised in undifferentiated P19 cells in the process dependent on Lin28a association with its conserved terminal loop (Nowak et al., 2014). Importantly, Lin28a can only play a role of an adaptor protein as it lacks nuclease activity. Following RNAi experiments with selected RNA nucleases, I found that Dis3l2 knockdown resulted in a modest but significant 1.5-fold increase in miR-9 levels. This increase resembled the change of miR-9 levels observed upon knockdown of Lin28a. Modest change observed in Dis3l2 and Lin28a knockdowns can be explained with low pri-miR-9 levels during early stages of neuronal differentiation.

The involvement of Dis3l2 in the degradation of pre-miR-9 is particularly interesting because I showed that its destabilisation is independent from uridylation, whereas the uridylation process was shown previously to be a prerequisite for Dis3l2 activity in context of pre-let-7 degradation (Chang

et al., 2013; Ustianenko et al., 2013). However, in spite of the lack of uridylation, I showed that Dis3l2 associates with pre-miR-9 in undifferentiated cells but was not able interact with non-uridylated pre-let-7a. Moreover, I showed that this interaction is most likely mediated by the direct interaction of Lin28a and Dis3l2 but this remains to be further validated in detail. By co-immunoprecipitating recombinant Lin28a and Dis3l2, I showed that these proteins interact but the confidence level remained low in this experiment due to potential inference from a similar tag presented on both proteins. However, using EMSA, I showed that both recombinant Lin28a and Dis3l2 formed a tertiary complex with pre-miR-9. Furthermore, this complex was not displaced using a Lin28a-specific antibody, which corroborated EMSA assays performed with pre-miR-9 and total cell extract derived from undifferentiated P19 cells.

Furthermore, I showed *in vitro* that pre-miR-9 was stabilised upon RNAi-mediated depletion of Dis3l2 and its degradation was restored in a uridylation-independent manner with the addition of enzymatically active recombinant Dis3l2. Interestingly, the addition of enzymatically inactive Dis3l2 also resulted in low-level pre-miR-9 degradation. This was in contrast to pre-let-7a, where the depletion of Dis3l2 resulted in stabilisation of the uridylated form and only the addition of enzymatically active recombinant Dis3l2 affected its stability. These experiments were performed in total cell extracts with the depletion of only endogenous Dis3l2.

Therefore, this discrepancy in functionality of enzymatically inactive Dis3l2 between pre-miR-9 and pre-let-7a could potentially be accounted for the increased activity of some other unknown nuclease. Furthermore, using 5′-end labelling *in vitro* processing, I showed that 5′-end of pre-miR-9 is unstable compared to pre-let-7a. Therefore, formation of the tertiary complex could cause structural rearrangements of pre-miR-9 that would potentially favour its 5′-3′ degradation by other exonucleases. However, this issue still remains to be fully understood with more detail biochemical characterisation.

6.4 Lin28a regulates a wide range of miRNAs during neuronal differentiation

At least three independent studies have shown a broad scope of Lin28a targets genome-wide (Cho et al., 2012; Hafner et al., 2013; Wilbert et al., 2012). Interestingly, in the majority of cases, Lin28a was shown to interact with mRNA, whereas snoRNA and miRNA were in the minority of the targets (Hafner et al., 2013). However, these studies concentrated either on undifferentiated embryonic stem cells or differentiated well-established cell models like HEK293 (Cho et al., 2012; Wilbert et al., 2012). None of the studies so far have attempted to capture the dynamic role of Lin28a throughout the differentiation in genome-wide context.

Encouraged by the fact that large group of miRNAs display neurospecific or neuroenriched expression pattern, I performed small RNA sequencing analysis of RNA samples derived from P19 cells with constitutive expression of untagged Lin28a and Lin28a:GFP fusion protein at two stages of the differentiation. This strategy allowed capturing the dynamic role of Lin28a and Lin28a:GFP on global miRNA production. Interestingly, I observed that the constitutive expression of Lin28a:GFP – a uridylation permissive mutant, affected only a small group of miRNAs, including some of let-7 members. However, the constitutive expression of untagged Lin28a resulted in extensive changes in the miRNA profile across two stages of differentiation. Importantly, the levels of corresponding proteins were similar. I observed that levels of the large group of miRNAs that were predominantly unchanged by the expression of Lin28a:GFP were upregulated in the presence of untagged Lin28a during differentiation. Furthermore, I used published information about motifs that were previously identified in a genome-wide context to interact with Lin28a (Wilbert et al., 2012). Mapping these motifs to the genomic proximity of pre-miRNAs of the selected group of miRNAs displayed their large potential to interact with Lin28a. In the majority of cases, these motifs occupied regions were outside pre-miRNA, presumably within pri-miRNA sequence.

There are examples of RNA proteins that regulate their target mRNA by binding sequences upstream or downstream of the transcription unit. For example, Roquin is known to regulate the deadenylation of mRNAs by interacting with constitutive decay-elements with stem-loop motifs usually located outside core coding sequence of the targeted mRNAs (Schuetz et al., 2014). Thus, it seems feasible for Lin28a to utilise motifs that were mapped in the proximity of pre-miRNAs sequence to stabilise the precursor molecule. Unfortunately, I was not able to demonstrate the direct involvement of Lin28a in the stabilisation of a selected group of pre-miRNAs that were upregulated in the Lin28a-differentiated state. This potentially could mean that constitutive expression of Lin28a during differentiation indirectly leads to upregulation of these miRNAs, possibly by affecting other uncharacterised protein factors. Additionally, Lin28a might have an impact on the transcription of pri-miRNAs. In fact, I showed that pri-miR-155 was upregulated upon differentiation of P19:Lin28a line when compared to control cell lines.

Alternatively, the negative results, observed *in vitro*, might be a result of Lin28b activity in the extracts. Lin28b is thought to localise inside the nucleolus of cells. Therefore, it is potentially sequestered from these pri-miRNAs, where levels were upregulated and play a marginal role in their regulation. However, in extracts, Lin28b is no longer stored in the nucleolus and due to its sequence similarity to Lin28a, might play a redundant role in the regulation of pri- or pre-miRNA stability. Therefore, in the future it will be beneficial to perform similar analysis in context of Lin28a/b double knockdown. In fact, it has been shown in the case of pri-miR-155 that the endonuclease MCPIP1 interacts and cleaves the terminal loop of the precursor miRNA (Suzuki et al., 2011). Therefore, binding of Lin28a or Lin28b to the pri-miR-155 terminal loop could have an opposing effect on the regulation of RNA destabilisation.

I also performed analysis of double-stranded regions in subset of miRNAs precursors, levels of which were upregulated by the constitutive expression of Lin28a during the neuronal differentiation. Interestingly, I

found that their pre-miRNAs contained fewer paired nucleotides across the stem when compared to the global population of pre-miRNAs. This observation could pave the way to understand in detail the events leading to destabilisation of pre-miR-9 executed by Lin28a/Dis3l2. It has been shown that the Dis3l2 RNA entry point forms a wide funnel, allowing the entrance of structured RNAs (Chang et al., 2013). In the case of pre-let-7, the poly(U) tail was indicated to play important role in the initiation of pre-let-7 degradation. However, it is possible that unstructured, single stranded RNA might have more space inside the wide funnel and could potentially reach the active site of Dis3l2 utilising non-specific interactions and hydrolysis events, shown previously to be crucial for later stages of pre-let-7 degradation (Chang et al., 2013).

Lin28a association with the terminal loop of pre-let-7g leads to the subsequent dissociation of the double-stranded region in the proximity of its binding (Lightfoot et al., 2011). Using computational modelling and structure probing, I revealed that pre-miR-9 is less structured. Therefore, the association of Lin28a might lead to the dissociation of not only a small double-stranded region around its binding site, but could be propagated across the entire pre-miRNA hairpin, leading to relaxed RNA conformation. Association of Dis3l2 could further propagate this effect and subsequently this unstructured pre-miR-9 could be in the final step targeted for uridylation-independent degradation. Further structural and biophysical characterisation of the pre-miR-9/Lin28a/Dis3l2 complex should allow to its molecular mode of action to be unravelled.

6.5 Biological implications of Lin28a regulation of miR-9 production

6.5.1 Role in neuronal development

Highly evolutionarily conserved miR-9 was shown to be involved in various biological processes associated with the central nervous system (CNS). For example, it was shown to control microglia inflammatory response in CNS by down-regulating monocyte chemotactic protein-induced protein 1 (MCPIP1), a crucial component of an activation pathway (Yao et al., 2014). Simultaneously, miR-9 is known to play an important role in shaping the development of the nervous system. It was previously shown to control cellular pathways defining sensory organs in Drosophila (Li et al., 2006) or structuring the midbrain-hindbrain barrier in zebrafish (Leucht et al., 2008). The role of miR-9 in mammals was directly linked to the regulation of progenitor fate. In particular, its expression was shown to be associated with active neurogenic areas and excluded from regions destined to contain undifferentiated progenitors for an extensive amount of time, like the midbrain-hindbrain boundary or ciliary marginal zone (Coolen et al., 2012; Kapsimali et al., 2007; Leucht et al., 2008). Also, gain-of-function studies showed that the expression of miR-9 and miR-124 led to reprogramming of adult fibroblasts into neurons (Yoo et al., 2011). Interestingly, miR-9 downregulation increased the proliferation of progenitor cells, but only temporarily as the cell differentiation was reversed after a certain amount of cell cycles (Coolen et al., 2012; Shibata et al., 2011). Altogether, these observations suggest that miR-9 is not a master regulator of differentiation fate, but acts as switch promoter favouring the transition of progenitors from a proliferative to neurogenic mode. Therefore, all major findings of my thesis corroborate with previously suggested functions of miR-9. During neuronal differentiation, miR-9 levels are controlled by a two-step mechanism. In the first step, chromatin co-repressor factors alter the epigenetic landscape of the genome, promoting the expression of many neurogenic genes. These events include REST/CREB orchestrated regulation of pri-miR-9 transcription (Laneve et al., 2010). In the second step, Lin28a acts as a

surveillance mechanism, allowing the production of miR-9 only at the eligible developmental timing, ensuring proper progression of the neuronal differentiation steps.

6.5.2 Role of Lin28a and miR-9 in neuropathies

Evolution placed miR-9 in the central point of the switch controlling the proliferation and differentiation modes of progenitor cells. This is not surprising as its role is associated with development of brain cancers, including meduloblastomas (MB), the most frequent paediatric brain cancers originating from cerebellar progenitors, and glioblastomas (GB), the most common and aggressive form of adult brain cancer. In MB, levels of miR-9 were shown to be reduced compared to the surrounding samples. Furthermore, in cell lines originating from MB, the down-regulation of miR-9 resulted in an increased proliferation rate of the cells (Ferretti et al., 2009). In contrast, in samples extracted from GB, elevated levels of miR-9 were observed (Schraivogel et al., 2011). Interestingly, a reduction of miR-9 in primary cell cultures derived from GB resulted in the inhibition of their self-renewal potential (Schraivogel et al., 2011). Abnormal miR-9 levels were also found in neurodegenerative disorders. In particular, its levels were down-regulated in the brain of Alzheimer patients and up-regulated in the cortex of patients with Parkinson disease (Cogswell et al., 2008; Hebert et al., 2008; Kim et al., 2007). In addition, miR-9 was also associated with the progression of amyotrophic lateral sclerosis (ALS), a disorder of the motor neurons. In particular, miR-9 levels were down-regulated in a mouse model of motoneuron disorder and ectopic expression of miR-9 can reduce levels of neurofilament heavy subunit, a major cause of neurodegenerative symptoms (Haramati et al., 2010).

For these reasons, understanding the molecular mechanism regulating production of miR-9 is very important and can lead towards designing novel therapeutic strategies. For instance, in the case of ALS and MB, it

would be interesting to determine using mouse models whether Lin28a activation is accompanied by miR-9 down-regulation. If so, delivering pre-miR-9/miR-16-TL mutants could result in increased levels of mature miR-9 and subsequently ameliorate disease symptoms. On the other hand, the information obtained from molecular analysis of Lin28a and pre-miR-9-CTL could help to design a CRISPR-based tethering assay to bring Dis3l2 to pre-miR-9 and subsequently prime it for degradation. This tethering approach could be used to reduce the growth of GB and the addition of an expression cassette specific for GB hotspots could further optimise this strategy.

6.6 Closing remarks

In my PhD project, I determined that the biogenesis of brain-specific miR-9 is controlled both transcriptionally and post-transcriptionally. I showed that its post-transcriptional regulation is based on a mechanism that relies on pre-miR-9 destabilisation in the early stages of neuronal differentiation. Furthermore, I showed that Lin28a protein associates with the terminal loop of pre-miR-9 and in uridylation-independent mode leads to the association of Dis3l2, which targets pre-miR-9 for degradation (Figure 6-2). Importantly, I showed that lower miR-9 but not let-7 levels are associated with abnormal neuronal differentiation. Furthermore, using a genome-wide approach, I demonstrated that Lin28a dynamically regulates numerous miRNA during neuronal differentiation. Interestingly, mature levels of a subset of regulated miRNAs are upregulated during differentiation in the presence of Lin28a.

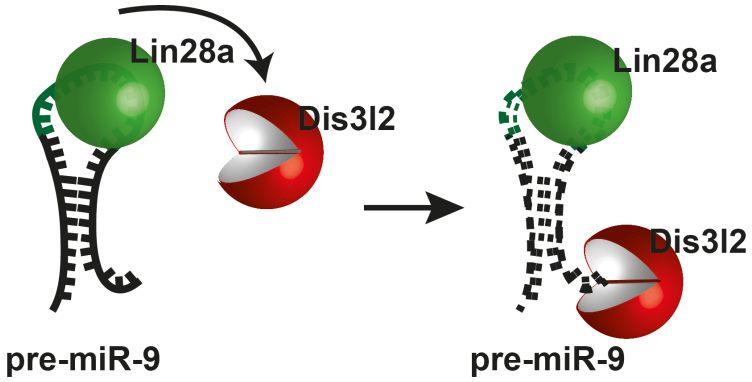

Figure 6-2 Model of Lin28a mechanism destabilising pre-miR-9 in early stages of neuronal differentiation
Lin28a associates with the pre-miR-9 terminal loop and in the uridylation-independent mode leads to association of 3′-5′ Dis3l2 exonuclease that subsequently mediates pre-miR-9 degradation.

Several questions remain unanswered and require detailed analysis to obtain better picture of Lin28a function in the regulation of miR-9 and other miRNAs. Firstly, co-crystal or NMR structural analysis should be performed to determine in detail the molecular architecture that supports the formation of a Lin28a/Dis3l2 tertiary complex and the degradation of pre-miR-9. Furthermore, precise analysis upon clear Lin28a/b knockdown or knockout should be performed to determine whether the role of Lin28

in the upregulation of mature miRNA levels is orchestrated by direct or indirect mechanisms.

7 Bibliography

Aggarwal, M., Gobius, I., Richards, L.J., and Mori, S. (2015). Diffusion MR Microscopy of Cortical Development in the Mouse Embryo. Cereb Cortex *25*, 1970-1980.

Amaral, P.P., Dinger, M.E., Mercer, T.R., and Mattick, J.S. (2008). The eukaryotic genome as an RNA machine. Science *319*, 1787-1789.

Ameres, S.L., and Zamore, P.D. (2013). Diversifying microRNA sequence and function. Nature reviews Molecular cell biology *14*, 475-488.

Amir, R.E., Van den Veyver, I.B., Wan, M., Tran, C.Q., Francke, U., and Zoghbi, H.Y. (1999). Rett syndrome is caused by mutations in X-linked MECP2, encoding methyl-CpG-binding protein 2. Nature genetics *23*, 185-188.

Anko, M.L., and Neugebauer, K.M. (2010). Long noncoding RNAs add another layer to pre-mRNA splicing regulation. Molecular cell *39*, 833-834.

Babiarz, J.E., Ruby, J.G., Wang, Y., Bartel, D.P., and Blelloch, R. (2008). Mouse ES cells express endogenous shRNAs, siRNAs, and other Microprocessor-independent, Dicer-dependent small RNAs. Genes & development *22*, 2773-2785.

Backes, S., Shapiro, J.S., Sabin, L.R., Pham, A.M., Reyes, I., Moss, B., Cherry, S., and tenOever, B.R. (2012). Degradation of host microRNAs by poxvirus poly(A) polymerase reveals terminal RNA methylation as a protective antiviral mechanism. Cell Host Microbe *12*, 200-210.

Baek, D., Villen, J., Shin, C., Camargo, F.D., Gygi, S.P., and Bartel, D.P. (2008). The impact of microRNAs on protein output. Nature *455*, 64-71.

Bagga, S., Bracht, J., Hunter, S., Massirer, K., Holtz, J., Eachus, R., and Pasquinelli, A.E. (2005). Regulation by let-7 and lin-4 miRNAs results in target mRNA degradation. Cell *122*, 553-563.

Balzer, E., Heine, C., Jiang, Q., Lee, V.M., and Moss, E.G. (2010). LIN28 alters cell fate succession and acts independently of the let-7 microRNA during neurogliogenesis in vitro. Development *137*, 891-900.

Bartel, D.P. (2004). MicroRNAs: genomics, biogenesis, mechanism, and function. Cell *116*, 281-297.

Bartel, D.P. (2009). MicroRNAs: target recognition and regulatory functions. Cell *136*, 215-233.

Behm-Ansmant, I., Rehwinkel, J., Doerks, T., Stark, A., Bork, P., and Izaurralde, E. (2006). mRNA degradation by miRNAs and GW182 requires both CCR4:NOT deadenylase and DCP1:DCP2 decapping complexes. Genes & development *20*, 1885-1898.

Berezikov, E. (2011). Evolution of microRNA diversity and regulation in animals. Nature reviews Genetics *12*, 846-860.

Bernard, D., Prasanth, K.V., Tripathi, V., Colasse, S., Nakamura, T., Xuan, Z., Zhang, M.Q., Sedel, F., Jourdren, L., Coulpier, F., *et al.* (2010). A long nuclear-retained non-coding RNA regulates synaptogenesis by modulating gene expression. The EMBO journal *29*, 3082-3093.

Beveridge, N.J., Tooney, P.A., Carroll, A.P., Gardiner, E., Bowden, N., Scott, R.J., Tran, N., Dedova, I., and Cairns, M.J. (2008). Dysregulation of miRNA 181b in the temporal cortex in schizophrenia. Hum Mol Genet *17*, 1156-1168.

Blaszczyk, J., Tropea, J.E., Bubunenko, M., Routzahn, K.M., Waugh, D.S., Court, D.L., and Ji, X. (2001). Crystallographic and modeling studies of RNase III suggest a mechanism for double-stranded RNA cleavage. Structure *9*, 1225-1236.

Bleichert, F., and Baserga, S.J. (2007). The long unwinding road of RNA helicases. Molecular cell *27*, 339-352.

Bonev, B., Pisco, A., and Papalopulu, N. (2011). MicroRNA-9 reveals regional diversity of neural progenitors along the anterior-posterior axis. Developmental cell *20*, 19-32.

Bracht, J., Hunter, S., Eachus, R., Weeks, P., and Pasquinelli, A.E. (2004). Trans-splicing and polyadenylation of let-7 microRNA primary transcripts. Rna *10*, 1586-1594.

Broderick, J.A., and Zamore, P.D. (2011). MicroRNA therapeutics. Gene Ther *18*, 1104-1110.

Cai, X., Hagedorn, C.H., and Cullen, B.R. (2004). Human microRNAs are processed from capped, polyadenylated transcripts that can also function as mRNAs. Rna *10*, 1957-1966.

Cao, X., Yeo, G., Muotri, A.R., Kuwabara, T., and Gage, F.H. (2006). Noncoding RNAs in the mammalian central nervous system. Annu Rev Neurosci *29*, 77-103.

Carthew, R.W., and Sontheimer, E.J. (2009). Origins and Mechanisms of miRNAs and siRNAs. Cell *136*, 642-655.

Chan, M.C., Hilyard, A.C., Wu, C., Davis, B.N., Hill, N.S., Lal, A., Lieberman, J., Lagna, G., and Hata, A. (2010). Molecular basis for antagonism between PDGF and the TGFbeta family of signalling pathways by control of miR-24 expression. The EMBO journal *29*, 559-573.

Chang, H.M., Triboulet, R., Thornton, J.E., and Gregory, R.I. (2013). A role for the Perlman syndrome exonuclease Dis3l2 in the Lin28-let-7 pathway. Nature *497*, 244-248.

Chang, S., Wen, S., Chen, D., and Jin, P. (2009a). Small regulatory RNAs in neurodevelopmental disorders. Hum Mol Genet *18*, R18-26.

Chang, T.C., Zeitels, L.R., Hwang, H.W., Chivukula, R.R., Wentzel, E.A., Dews, M., Jung, J., Gao, P., Dang, C.V., Beer, M.A., *et al.* (2009b). Lin-28B transactivation is necessary for Myc-mediated let-7 repression and proliferation. Proceedings of the National Academy of Sciences of the United States of America *106*, 3384-3389.

Chatterjee, S., Fasler, M., Bussing, I., and Grosshans, H. (2011). Target-mediated protection of endogenous microRNAs in C. elegans. Developmental cell *20*, 388-396.

Chatterjee, S., and Grosshans, H. (2009). Active turnover modulates mature microRNA activity in Caenorhabditis elegans. Nature *461*, 546-549.

Chendrimada, T.P., Gregory, R.I., Kumaraswamy, E., Norman, J., Cooch, N., Nishikura, K., and Shiekhattar, R. (2005). TRBP recruits the Dicer complex to Ago2 for microRNA processing and gene silencing. Nature *436*, 740-744.

Cheng, T.L., Wang, Z., Liao, Q., Zhu, Y., Zhou, W.H., Xu, W., and Qiu, Z. (2014). MeCP2 suppresses nuclear microRNA processing and dendritic growth by regulating the DGCR8/Drosha complex. Developmental cell *28*, 547-560.

Cho, J., Chang, H., Kwon, S.C., Kim, B., Kim, Y., Choe, J., Ha, M., Kim, Y.K., and Kim, V.N. (2012). LIN28A is a suppressor of ER-associated translation in embryonic stem cells. Cell *151*, 765-777.

Chomczynski, P., and Sacchi, N. (1987). Single-step method of RNA isolation by acid guanidinium thiocyanate-phenol-chloroform extraction. Anal Biochem *162*, 156-159.

Choudhury, N.R., de Lima Alves, F., de Andres-Aguayo, L., Graf, T., Caceres, J.F., Rappsilber, J., and Michlewski, G. (2013). Tissue-specific control of brain-enriched miR-7 biogenesis. Genes & development *27*, 24-38.

Choudhury, N.R., Nowak, J.S., Zuo, J., Rappsilber, J., Spoel, S.H., and Michlewski, G. (2014). Trim25 Is an RNA-Specific Activator of Lin28a/TuT4-Mediated Uridylation. Cell reports *9*, 1265-1272.

Cochran, B.M., and Michael, F.E. (2008). Synthesis of 2,6-disubstituted piperazines by a diastereoselective palladium-catalyzed hydroamination reaction. Organic letters *10*, 329-332.

Cogswell, J.P., Ward, J., Taylor, I.A., Waters, M., Shi, Y., Cannon, B., Kelnar, K., Kemppainen, J., Brown, D., Chen, C., *et al.* (2008). Identification of miRNA changes in Alzheimer's disease brain and CSF yields putative biomarkers and insights into disease pathways. J Alzheimers Dis *14*, 27-41.

Conaco, C., Otto, S., Han, J.J., and Mandel, G. (2006). Reciprocal actions of REST and a microRNA promote neuronal identity. Proceedings of the National Academy of Sciences of the United States of America *103*, 2422-2427.

Coolen, M., Thieffry, D., Drivenes, O., Becker, T.S., and Bally-Cuif, L. (2012). miR-9 controls the timing of neurogenesis through the direct inhibition of antagonistic factors. Developmental cell *22*, 1052-1064.

Corcoran, D.L., Pandit, K.V., Gordon, B., Bhattacharjee, A., Kaminski, N., and Benos, P.V. (2009). Features of mammalian microRNA promoters emerge from polymerase II chromatin immunoprecipitation data. PloS one *4*, e5279.

Cull-Candy, S., Brickley, S., and Farrant, M. (2001). NMDA receptor subunits: diversity, development and disease. Curr Opin Neurobiol *11*, 327-335.

Czech, B., Zhou, R., Erlich, Y., Brennecke, J., Binari, R., Villalta, C., Gordon, A., Perrimon, N., and Hannon, G.J. (2009). Hierarchical rules for Argonaute loading in Drosophila. Molecular cell *36*, 445-456.

Darnell, D.K., Kaur, S., Stanislaw, S., Konieczka, J.H., Yatskievych, T.A., and Antin, P.B. (2006). MicroRNA expression during chick embryo development. Dev Dyn *235*, 3156-3165.

Darr, H., and Benvenisty, N. (2009). Genetic analysis of the role of the reprogramming gene LIN-28 in human embryonic stem cells. Stem cells *27*, 352-362.

Das, S.K., Sokhi, U.K., Bhutia, S.K., Azab, B., Su, Z.Z., Sarkar, D., and Fisher, P.B. (2010). Human polynucleotide phosphorylase selectively and preferentially degrades microRNA-221 in human melanoma cells. Proceedings of the National Academy of Sciences of the United States of America *107*, 11948-11953.

Davis, B.N., Hilyard, A.C., Lagna, G., and Hata, A. (2008). SMAD proteins control DROSHA-mediated microRNA maturation. Nature *454*, 56-61.

Davis, B.N., Hilyard, A.C., Nguyen, P.H., Lagna, G., and Hata, A. (2009). Induction of microRNA-221 by platelet-derived growth factor signaling is critical for modulation of vascular smooth muscle phenotype. The Journal of biological chemistry *284*, 3728-3738.

Davis, B.N., Hilyard, A.C., Nguyen, P.H., Lagna, G., and Hata, A. (2010). Smad proteins bind a conserved RNA sequence to promote microRNA maturation by Drosha. Molecular cell *39*, 373-384.

Davis-Dusenbery, B.N., and Hata, A. (2010). Mechanisms of control of microRNA biogenesis. Journal of biochemistry *148*, 381-392.

Delaloy, C., and Gao, F.B. (2010). A new role for microRNA-9 in human neural progenitor cells. Cell Cycle *9*, 2913-2914.

Delaloy, C., Liu, L., Lee, J.A., Su, H., Shen, F., Yang, G.Y., Young, W.L., Ivey, K.N., and Gao, F.B. (2010). MicroRNA-9 coordinates proliferation and migration of human embryonic stem cell-derived neural progenitors. Cell Stem Cell *6*, 323-335.

Denli, A.M., Tops, B.B., Plasterk, R.H., Ketting, R.F., and Hannon, G.J. (2004). Processing of primary microRNAs by the Microprocessor complex. Nature *432*, 231-235.

Derrien, T., Johnson, R., Bussotti, G., Tanzer, A., Djebali, S., Tilgner, H., Guernec, G., Martin, D., Merkel, A., Knowles, D.G., *et al.* (2012). The GENCODE v7 catalog of human long noncoding RNAs: analysis of their gene structure, evolution, and expression. Genome research *22*, 1775-1789.

Derry, M.C., Yanagiya, A., Martineau, Y., and Sonenberg, N. (2006). Regulation of poly(A)-binding protein through PABP-interacting proteins. Cold Spring Harbor symposia on quantitative biology *71*, 537-543.

Desjardins, A., Bouvette, J., and Legault, P. (2014). Stepwise assembly of multiple Lin28 proteins on the terminal loop of let-7 miRNA precursors. Nucleic acids research *42*, 4615-4628.

Diederichs, S., and Haber, D.A. (2007). Dual role for argonautes in microRNA processing and posttranscriptional regulation of microRNA expression. Cell *131*, 1097-1108.

Ding, X.C., and Grosshans, H. (2009). Repression of C. elegans microRNA targets at the initiation level of translation requires GW182 proteins. The EMBO journal *28*, 213-222.

Dreyfuss, G., Kim, V.N., and Kataoka, N. (2002). Messenger-RNA-binding proteins and the messages they carry. Nature reviews Molecular cell biology *3*, 195-205.

Dunham, I., Kundaje, A., Aldred, S.F., Collins, P.J., Davis, C., Doyle, F., Epstein, C.B., Frietze, S., Harrow, J., Kaul, R., *et al.* (2012). An integrated encyclopedia of DNA elements in the human genome. Nature *489*, 57-74.

Edbauer, D., Neilson, J.R., Foster, K.A., Wang, C.F., Seeburg, D.P., Batterton, M.N., Tada, T., Dolan, B.M., Sharp, P.A., and Sheng, M. (2010). Regulation of synaptic structure and function by FMRP-associated microRNAs miR-125b and miR-132. Neuron *65*, 373-384.

Edgar, R.C. (2004). MUSCLE: multiple sequence alignment with high accuracy and high throughput. Nucleic acids research *32*, 1792-1797.

Elkayam, E., Kuhn, C.D., Tocilj, A., Haase, A.D., Greene, E.M., Hannon, G.J., and Joshua-Tor, L. (2012). The structure of human argonaute-2 in complex with miR-20a. Cell *150*, 100-110.

Eulalio, A., Huntzinger, E., Nishihara, T., Rehwinkel, J., Fauser, M., and Izaurralde, E. (2009). Deadenylation is a widespread effect of miRNA regulation. Rna *15*, 21-32.

Eulalio, A., Rehwinkel, J., Stricker, M., Huntzinger, E., Yang, S.F., Doerks, T., Dorner, S., Bork, P., Boutros, M., and Izaurralde, E. (2007). Target-specific requirements for enhancers of decapping in miRNA-mediated gene silencing. Genes & development *21*, 2558-2570.

Faehnle, C.R., Walleshauser, J., and Joshua-Tor, L. (2014). Mechanism of Dis3l2 substrate recognition in the Lin28-let-7 pathway. Nature *514*, 252-256.

Ferretti, E., De Smaele, E., Po, A., Di Marcotullio, L., Tosi, E., Espinola, M.S., Di Rocco, C., Riccardi, R., Giangaspero, F., Farcomeni, A., *et al.* (2009). MicroRNA profiling in human medulloblastoma. Int J Cancer *124*, 568-577.

Forstemann, K., Horwich, M.D., Wee, L., Tomari, Y., and Zamore, P.D. (2007). Drosophila microRNAs are sorted into functionally distinct argonaute complexes after production by dicer-1. Cell *130*, 287-297.

Fowler, A., Thomson, D., Giles, K., Maleki, S., Mreich, E., Wheeler, H., Leedman, P., Biggs, M., Cook, R., Little, N., *et al.* (2011). miR-124a is frequently down-regulated in glioblastoma and is involved in migration and invasion. Eur J Cancer *47*, 953-963.

Frank, F., Sonenberg, N., and Nagar, B. (2010). Structural basis for 5'-nucleotide base-specific recognition of guide RNA by human AGO2. Nature *465*, 818-822.

Ghildiyal, M., Xu, J., Seitz, H., Weng, Z., and Zamore, P.D. (2010). Sorting of Drosophila small silencing RNAs partitions microRNA* strands into the RNA interference pathway. Rna *16*, 43-56.

Giraldez, A.J., Mishima, Y., Rihel, J., Grocock, R.J., Van Dongen, S., Inoue, K., Enright, A.J., and Schier, A.F. (2006). Zebrafish MiR-430 promotes deadenylation and clearance of maternal mRNAs. Science *312*, 75-79.

Graf, R., Munschauer, M., Mastrobuoni, G., Mayr, F., Heinemann, U., Kempa, S., Rajewsky, N., and Landthaler, M. (2013). Identification of LIN28B-bound mRNAs reveals features of target recognition and regulation. RNA Biol *10*, 1146-1159.

Gregory, R.I., Yan, K.P., Amuthan, G., Chendrimada, T., Doratotaj, B., Cooch, N., and Shiekhattar, R. (2004). The Microprocessor complex mediates the genesis of microRNAs. Nature *432*, 235-240.

Griffiths-Jones, S., Saini, H.K., van Dongen, S., and Enright, A.J. (2008). miRBase: tools for microRNA genomics. Nucleic acids research *36*, D154-158.

Gu, S., Jin, L., Zhang, Y., Huang, Y., Zhang, F., Valdmanis, P.N., and Kay, M.A. (2012). The loop position of shRNAs and pre-miRNAs is critical for the accuracy of dicer processing in vivo. Cell *151*, 900-911.

Gu, Y., Liu, Y., Zhang, J., Liu, H., Hu, Y., Du, H., Li, Y., Chen, J., Wei, B., and Huang, Y. (2013). Identification and characterization of microRNAs in the developing maize endosperm. Genomics *102*, 472-478.

Guil, S., and Caceres, J.F. (2007). The multifunctional RNA-binding protein hnRNP A1 is required for processing of miR-18a. Nature structural & molecular biology *14*, 591-596.

Guo, H., Ingolia, N.T., Weissman, J.S., and Bartel, D.P. (2010). Mammalian microRNAs predominantly act to decrease target mRNA levels. Nature *466*, 835-840.

Gwizdek, C., Ossareh-Nazari, B., Brownawell, A.M., Doglio, A., Bertrand, E., Macara, I.G., and Dargemont, C. (2003). Exportin-5 mediates nuclear export of minihelix-containing RNAs. The Journal of biological chemistry *278*, 5505-5508.

Ha, M., and Kim, V.N. (2014). Regulation of microRNA biogenesis. Nature reviews Molecular cell biology *15*, 509-524.

Haase, A.D., Jaskiewicz, L., Zhang, H., Laine, S., Sack, R., Gatignol, A., and Filipowicz, W. (2005). TRBP, a regulator of cellular PKR and HIV-1 virus expression, interacts with Dicer and functions in RNA silencing. EMBO reports *6*, 961-967.

Hafner, M., Max, K.E., Bandaru, P., Morozov, P., Gerstberger, S., Brown, M., Molina, H., and Tuschl, T. (2013). Identification of mRNAs bound and regulated by human LIN28 proteins and molecular requirements for RNA recognition. Rna *19*, 613-626.

Hagan, J.P., Piskounova, E., and Gregory, R.I. (2009). Lin28 recruits the TUTase Zcchc11 to inhibit let-7 maturation in mouse embryonic stem cells. Nature structural & molecular biology *16*, 1021-1025.

Hammond, S.M., Boettcher, S., Caudy, A.A., Kobayashi, R., and Hannon, G.J. (2001). Argonaute2, a link between genetic and biochemical analyses of RNAi. Science *293*, 1146-1150.

Han, J., Lee, Y., Yeom, K.H., Kim, Y.K., Jin, H., and Kim, V.N. (2004). The Drosha-DGCR8 complex in primary microRNA processing. Genes & development *18*, 3016-3027.

Han, J., Lee, Y., Yeom, K.H., Nam, J.W., Heo, I., Rhee, J.K., Sohn, S.Y., Cho, Y., Zhang, B.T., and Kim, V.N. (2006). Molecular basis for the recognition of primary microRNAs by the Drosha-DGCR8 complex. Cell *125*, 887-901.

Haramati, S., Chapnik, E., Sztainberg, Y., Eilam, R., Zwang, R., Gershoni, N., McGlinn, E., Heiser, P.W., Wills, A.M., Wirguin, I., *et al.* (2010). miRNA malfunction causes spinal motor neuron disease. Proceedings of the National Academy of Sciences of the United States of America *107*, 13111-13116.

He, X., Zhang, Q., Liu, Y., and Pan, X. (2007). Cloning and identification of novel microRNAs from rat hippocampus. Acta Biochim Biophys Sin (Shanghai) *39*, 708-714.

Hebert, S.S., Horre, K., Nicolai, L., Papadopoulou, A.S., Mandemakers, W., Silahtaroglu, A.N., Kauppinen, S., Delacourte, A., and De Strooper, B. (2008). Loss of microRNA cluster miR-29a/b-1 in sporadic Alzheimer's disease correlates with increased BACE1/beta-secretase expression. Proceedings of the National Academy of Sciences of the United States of America *105*, 6415-6420.

Hendrickson, D.G., Hogan, D.J., McCullough, H.L., Myers, J.W., Herschlag, D., Ferrell, J.E., and Brown, P.O. (2009). Concordant regulation of translation and mRNA abundance for hundreds of targets of a human microRNA. PLoS Biol *7*, e1000238.

Heo, I., Ha, M., Lim, J., Yoon, M.J., Park, J.E., Kwon, S.C., Chang, H., and Kim, V.N. (2012). Mono-uridylation of pre-microRNA as a key step in the biogenesis of group II let-7 microRNAs. Cell *151*, 521-532.

Heo, I., Joo, C., Cho, J., Ha, M., Han, J., and Kim, V.N. (2008). Lin28 mediates the terminal uridylation of let-7 precursor MicroRNA. Molecular cell *32*, 276-284.

Heo, I., Joo, C., Kim, Y.K., Ha, M., Yoon, M.J., Cho, J., Yeom, K.H., Han, J., and Kim, V.N. (2009). TUT4 in concert with Lin28 suppresses microRNA biogenesis through pre-microRNA uridylation. Cell *138*, 696-708.

Herbert, K.M., Pimienta, G., DeGregorio, S.J., Alexandrov, A., and Steitz, J.A. (2013). Phosphorylation of DGCR8 increases its intracellular stability and induces a progrowth miRNA profile. Cell reports *5*, 1070-1081.

Hertel, J., Lindemeyer, M., Missal, K., Fried, C., Tanzer, A., Flamm, C., Hofacker, I.L., Stadler, P.F., and Students of Bioinformatics Computer Labs, a. (2006). The expansion of the metazoan microRNA repertoire. BMC genomics *7*, 25.

Ho, L., and Crabtree, G.R. (2010). Chromatin remodelling during development. Nature *463*, 474-484.

Horman, S.R., Janas, M.M., Litterst, C., Wang, B., MacRae, I.J., Sever, M.J., Morrissey, D.V., Graves, P., Luo, B., Umesalma, S., *et al.* (2013). Akt-mediated phosphorylation of argonaute 2 downregulates cleavage and upregulates translational repression of MicroRNA targets. Molecular cell *50*, 356-367.

Houseley, J., and Tollervey, D. (2009). The many pathways of RNA degradation. Cell *136*, 763-776.

Hu, H.Y., Yan, Z., Xu, Y., Hu, H., Menzel, C., Zhou, Y.H., Chen, W., and Khaitovich, P. (2009). Sequence features associated with microRNA strand selection in humans and flies. BMC genomics *10*, 413.

Huang, Y., Myers, S.J., and Dingledine, R. (1999). Transcriptional repression by REST: recruitment of Sin3A and histone deacetylase to neuronal genes. Nat Neurosci *2*, 867-872.

Humphreys, D.T., Westman, B.J., Martin, D.I., and Preiss, T. (2005). MicroRNAs control translation initiation by inhibiting eukaryotic initiation factor 4E/cap and poly(A) tail function. Proceedings of the National Academy of Sciences of the United States of America *102*, 16961-16966.

Huntzinger, E., and Izaurralde, E. (2011). Gene silencing by microRNAs: contributions of translational repression and mRNA decay. Nature reviews Genetics *12*, 99-110.

Hutvagner, G., McLachlan, J., Pasquinelli, A.E., Balint, E., Tuschl, T., and Zamore, P.D. (2001). A cellular function for the RNA-interference enzyme Dicer in the maturation of the let-7 small temporal RNA. Science *293*, 834-838.

Iliopoulos, D., Hirsch, H.A., and Struhl, K. (2009). An epigenetic switch involving NF-kappaB, Lin28, Let-7 MicroRNA, and IL6 links inflammation to cell transformation. Cell *139*, 693-706.

Impey, S., Mark, M., Villacres, E.C., Poser, S., Chavkin, C., and Storm, D.R. (1996). Induction of CRE-mediated gene expression by stimuli that generate long-lasting LTP in area CA1 of the hippocampus. Neuron *16*, 973-982.

Jacob, F., and Monod, J. (1961). Genetic regulatory mechanisms in the synthesis of proteins. Journal of molecular biology *3*, 318-356.

Jin, P., Alisch, R.S., and Warren, S.T. (2004). RNA and microRNAs in fragile X mental retardation. Nature cell biology *6*, 1048-1053.

Johnston, R.J., Jr., Chang, S., Etchberger, J.F., Ortiz, C.O., and Hobert, O. (2005). MicroRNAs acting in a double-negative feedback loop to control a neuronal cell fate decision. Proceedings of the National Academy of Sciences of the United States of America *102*, 12449-12454.

Kapsimali, M., Kloosterman, W.P., de Bruijn, E., Rosa, F., Plasterk, R.H., and Wilson, S.W. (2007). MicroRNAs show a wide diversity of expression profiles in the developing and mature central nervous system. Genome Biol *8*, R173.

Katoh, T., Sakaguchi, Y., Miyauchi, K., Suzuki, T., Kashiwabara, S., Baba, T., and Suzuki, T. (2009). Selective stabilization of mammalian microRNAs by 3' adenylation mediated by the cytoplasmic poly(A) polymerase GLD-2. Genes & development *23*, 433-438.

Kawamata, T., Seitz, H., and Tomari, Y. (2009). Structural determinants of miRNAs for RISC loading and slicer-independent unwinding. Nature structural & molecular biology *16*, 953-960.

Kawamata, T., and Tomari, Y. (2010). Making RISC. Trends in biochemical sciences *35*, 368-376.

Ketting, R.F., Fischer, S.E., Bernstein, E., Sijen, T., Hannon, G.J., and Plasterk, R.H. (2001). Dicer functions in RNA interference and in synthesis

of small RNA involved in developmental timing in C. elegans. Genes & development *15*, 2654-2659.
Khvorova, A., Reynolds, A., and Jayasena, S.D. (2003). Functional siRNAs and miRNAs exhibit strand bias. Cell *115*, 209-216.
Kim, J., Inoue, K., Ishii, J., Vanti, W.B., Voronov, S.V., Murchison, E., Hannon, G., and Abeliovich, A. (2007). A MicroRNA feedback circuit in midbrain dopamine neurons. Science *317*, 1220-1224.
Kim, J.B., Sebastiano, V., Wu, G., Arauzo-Bravo, M.J., Sasse, P., Gentile, L., Ko, K., Ruau, D., Ehrich, M., van den Boom, D., *et al.* (2009). Oct4-induced pluripotency in adult neural stem cells. Cell *136*, 411-419.
Klein, M.E., Lioy, D.T., Ma, L., Impey, S., Mandel, G., and Goodman, R.H. (2007). Homeostatic regulation of MeCP2 expression by a CREB-induced microRNA. Nat Neurosci *10*, 1513-1514.
Kozomara, A., and Griffiths-Jones, S. (2014). miRBase: annotating high confidence microRNAs using deep sequencing data. Nucleic acids research *42*, D68-73.
Krichevsky, A.M., King, K.S., Donahue, C.P., Khrapko, K., and Kosik, K.S. (2003). A microRNA array reveals extensive regulation of microRNAs during brain development. Rna *9*, 1274-1281.
Krichevsky, A.M., Sonntag, K.C., Isacson, O., and Kosik, K.S. (2006). Specific microRNAs modulate embryonic stem cell-derived neurogenesis. Stem cells *24*, 857-864.
Krol, J., Busskamp, V., Markiewicz, I., Stadler, M.B., Ribi, S., Richter, J., Duebel, J., Bicker, S., Fehling, H.J., Schubeler, D., *et al.* (2010a). Characterizing light-regulated retinal microRNAs reveals rapid turnover as a common property of neuronal microRNAs. Cell *141*, 618-631.
Krol, J., Loedige, I., and Filipowicz, W. (2010b). The widespread regulation of microRNA biogenesis, function and decay. Nature reviews Genetics *11*, 597-610.
Krutzfeldt, J., Rajewsky, N., Braich, R., Rajeev, K.G., Tuschl, T., Manoharan, M., and Stoffel, M. (2005). Silencing of microRNAs in vivo with 'antagomirs'. Nature *438*, 685-689.
La Torre, A., Georgi, S., and Reh, T.A. (2013). Conserved microRNA pathway regulates developmental timing of retinal neurogenesis.

Proceedings of the National Academy of Sciences of the United States of America *110*, E2362-2370.

Lagos-Quintana, M., Rauhut, R., Yalcin, A., Meyer, J., Lendeckel, W., and Tuschl, T. (2002). Identification of tissue-specific microRNAs from mouse. Curr Biol *12*, 735-739.

Landgraf, P., Rusu, M., Sheridan, R., Sewer, A., Iovino, N., Aravin, A., Pfeffer, S., Rice, A., Kamphorst, A.O., Landthaler, M., *et al.* (2007). A mammalian microRNA expression atlas based on small RNA library sequencing. Cell *129*, 1401-1414.

Laneve, P., Gioia, U., Andriotto, A., Moretti, F., Bozzoni, I., and Caffarelli, E. (2010). A minicircuitry involving REST and CREB controls miR-9-2 expression during human neuronal differentiation. Nucleic acids research *38*, 6895-6905.

Lee, R. C., Feinbaum, R. L., Ambros, V. (1993) The C. elegans heterochronic gene lin-4 encodes small RNAs with antisense complementarity to lin-14. Cell *75*, 843-854.

Lee, Y., Ahn, C., Han, J., Choi, H., Kim, J., Yim, J., Lee, J., Provost, P., Radmark, O., Kim, S., *et al.* (2003). The nuclear RNase III Drosha initiates microRNA processing. Nature *425*, 415-419.

Lee, Y., Jeon, K., Lee, J.T., Kim, S., and Kim, V.N. (2002). MicroRNA maturation: stepwise processing and subcellular localization. The EMBO journal *21*, 4663-4670.

Leucht, C., Stigloher, C., Wizenmann, A., Klafke, R., Folchert, A., and Bally-Cuif, L. (2008). MicroRNA-9 directs late organizer activity of the midbrain-hindbrain boundary. Nat Neurosci *11*, 641-648.

Leuschner, P.J., Ameres, S.L., Kueng, S., and Martinez, J. (2006). Cleavage of the siRNA passenger strand during RISC assembly in human cells. EMBO reports *7*, 314-320.

Li, R., Li, Y., Kristiansen, K., and Wang, J. (2008). SOAP: short oligonucleotide alignment program. Bioinformatics *24*, 713-714.

Li, Y., Wang, F., Lee, J.A., and Gao, F.B. (2006). MicroRNA-9a ensures the precise specification of sensory organ precursors in Drosophila. Genes & development *20*, 2793-2805.

Lightfoot, H.L., Bugaut, A., Armisen, J., Lehrbach, N.J., Miska, E.A., and Balasubramanian, S. (2011). A LIN28-dependent structural change in pre-let-7g directly inhibits dicer processing. Biochemistry *50*, 7514-7521.

Lim, J., Ha, M., Chang, H., Kwon, S.C., Simanshu, D.K., Patel, D.J., and Kim, V.N. (2014). Uridylation by TUT4 and TUT7 marks mRNA for degradation. Cell *159*, 1365-1376.

Lim, L.P., Lau, N.C., Garrett-Engele, P., Grimson, A., Schelter, J.M., Castle, J., Bartel, D.P., Linsley, P.S., and Johnson, J.M. (2005). Microarray analysis shows that some microRNAs downregulate large numbers of target mRNAs. Nature *433*, 769-773.

Lipchina, I., Elkabetz, Y., Hafner, M., Sheridan, R., Mihailovic, A., Tuschl, T., Sander, C., Studer, L., and Betel, D. (2011). Genome-wide identification of microRNA targets in human ES cells reveals a role for miR-302 in modulating BMP response. Genes & development *25*, 2173-2186.

Liu, G.Q., Mattick, J.S., and Taft, R.J. (2013). A meta-analysis of the genomic and transcriptomic composition of complex life. Cell Cycle *12*, 2061-2072.

Liu, J., Carmell, M.A., Rivas, F.V., Marsden, C.G., Thomson, J.M., Song, J.J., Hammond, S.M., Joshua-Tor, L., and Hannon, G.J. (2004). Argonaute2 is the catalytic engine of mammalian RNAi. Science *305*, 1437-1441.

Liu, Y., Ye, X., Jiang, F., Liang, C., Chen, D., Peng, J., Kinch, L.N., Grishin, N.V., and Liu, Q. (2009). C3PO, an endoribonuclease that promotes RNAi by facilitating RISC activation. Science *325*, 750-753.

Loughlin, F.E., Gebert, L.F., Towbin, H., Brunschweiger, A., Hall, J., and Allain, F.H. (2012). Structural basis of pre-let-7 miRNA recognition by the zinc knuckles of pluripotency factor Lin28. Nature structural & molecular biology *19*, 84-89.

Macrae, I.J., Zhou, K., Li, F., Repic, A., Brooks, A.N., Cande, W.Z., Adams, P.D., and Doudna, J.A. (2006). Structural basis for double-stranded RNA processing by Dicer. Science *311*, 195-198.

Maes, O.C., Chertkow, H.M., Wang, E., and Schipper, H.M. (2009). MicroRNA: Implications for Alzheimer Disease and other Human CNS Disorders. Curr Genomics *10*, 154-168.

Magill, S.T., Cambronne, X.A., Luikart, B.W., Lioy, D.T., Leighton, B.H., Westbrook, G.L., Mandel, G., and Goodman, R.H. (2010). microRNA-132 regulates dendritic growth and arborization of newborn neurons in the adult hippocampus. Proceedings of the National Academy of Sciences of the United States of America *107*, 20382-20387.

Makeyev, E.V., Zhang, J., Carrasco, M.A., and Maniatis, T. (2007). The MicroRNA miR-124 promotes neuronal differentiation by triggering brain-specific alternative pre-mRNA splicing. Molecular cell *27*, 435-448.

Maroney, P.A., Yu, Y., Fisher, J., and Nilsen, T.W. (2006). Evidence that microRNAs are associated with translating messenger RNAs in human cells. Nature structural & molecular biology *13*, 1102-1107.

Matera, A.G., Terns, R.M., and Terns, M.P. (2007). Non-coding RNAs: lessons from the small nuclear and small nucleolar RNAs. Nature reviews Molecular cell biology *8*, 209-220.

Mathonnet, G., Fabian, M.R., Svitkin, Y.V., Parsyan, A., Huck, L., Murata, T., Biffo, S., Merrick, W.C., Darzynkiewicz, E., Pillai, R.S., *et al.* (2007). MicroRNA inhibition of translation initiation in vitro by targeting the cap-binding complex eIF4F. Science *317*, 1764-1767.

Matranga, C., Tomari, Y., Shin, C., Bartel, D.P., and Zamore, P.D. (2005). Passenger-strand cleavage facilitates assembly of siRNA into Ago2-containing RNAi enzyme complexes. Cell *123*, 607-620.

Mayr, F., and Heinemann, U. (2013). Mechanisms of Lin28-mediated miRNA and mRNA regulation--a structural and functional perspective. International journal of molecular sciences *14*, 16532-16553.

Mayr, F., Schutz, A., Doge, N., and Heinemann, U. (2012). The Lin28 cold-shock domain remodels pre-let-7 microRNA. Nucleic acids research *40*, 7492-7506.

McBurney, M.W. (1993). P19 embryonal carcinoma cells. Int J Dev Biol *37*, 135-140.

Meister, G., Landthaler, M., Patkaniowska, A., Dorsett, Y., Teng, G., and Tuschl, T. (2004). Human Argonaute2 mediates RNA cleavage targeted by miRNAs and siRNAs. Molecular cell *15*, 185-197.

Melo, S.A., Ropero, S., Moutinho, C., Aaltonen, L.A., Yamamoto, H., Calin, G.A., Rossi, S., Fernandez, A.F., Carneiro, F., Oliveira, C., *et al.* (2009). A

TARBP2 mutation in human cancer impairs microRNA processing and DICER1 function. Nature genetics *41*, 365-370.

Meza-Sosa, K.F., Valle-Garcia, D., Pedraza-Alva, G., and Perez-Martinez, L. (2012). Role of microRNAs in central nervous system development and pathology. J Neurosci Res *90*, 1-12.

Michlewski, G., and Caceres, J.F. (2010). Antagonistic role of hnRNP A1 and KSRP in the regulation of let-7a biogenesis. Nature structural & molecular biology *17*, 1011-1018.

Michlewski, G., Guil, S., Semple, C.A., and Caceres, J.F. (2008). Posttranscriptional regulation of miRNAs harboring conserved terminal loops. Molecular cell *32*, 383-393.

Mihailovich, M., Militti, C., Gabaldon, T., and Gebauer, F. (2010). Eukaryotic cold shock domain proteins: highly versatile regulators of gene expression. Bioessays *32*, 109-118.

Miska, E.A., Alvarez-Saavedra, E., Townsend, M., Yoshii, A., Sestan, N., Rakic, P., Constantine-Paton, M., and Horvitz, H.R. (2004). Microarray analysis of microRNA expression in the developing mammalian brain. Genome Biol *5*, R68.

Miyoshi, K., Tsukumo, H., Nagami, T., Siomi, H., and Siomi, M.C. (2005). Slicer function of Drosophila Argonautes and its involvement in RISC formation. Genes & development *19*, 2837-2848.

Monod, J., and Jacob, F. (1961). Teleonomic mechanisms in cellular metabolism, growth, and differentiation. Cold Spring Harbor symposia on quantitative biology *26*, 389-401.

Monteys, A.M., Spengler, R.M., Wan, J., Tecedor, L., Lennox, K.A., Xing, Y., and Davidson, B.L. (2010). Structure and activity of putative intronic miRNA promoters. Rna *16*, 495-505.

Moss, E.G., Lee, R.C., and Ambros, V. (1997). The cold shock domain protein LIN-28 controls developmental timing in C. elegans and is regulated by the lin-4 RNA. Cell *88*, 637-646.

Moss, E.G., and Tang, L. (2003). Conservation of the heterochronic regulator Lin-28, its developmental expression and microRNA complementary sites. Developmental biology *258*, 432-442.

Nakanishi, K., Weinberg, D.E., Bartel, D.P., and Patel, D.J. (2012). Structure of yeast Argonaute with guide RNA. Nature *486*, 368-374.
Nam, Y., Chen, C., Gregory, R.I., Chou, J.J., and Sliz, P. (2011). Molecular basis for interaction of let-7 microRNAs with Lin28. Cell *147*, 1080-1091.
Newman, M.A., Thomson, J.M., and Hammond, S.M. (2008). Lin-28 interaction with the Let-7 precursor loop mediates regulated microRNA processing. Rna *14*, 1539-1549.
Nicoli, S., Knyphausen, C.P., Zhu, L.J., Lakshmanan, A., and Lawson, N.D. (2012). miR-221 is required for endothelial tip cell behaviors during vascular development. Developmental cell *22*, 418-429.
Nishino, J., Kim, I., Chada, K., and Morrison, S.J. (2008). Hmga2 promotes neural stem cell self-renewal in young but not old mice by reducing p16Ink4a and p19Arf Expression. Cell *135*, 227-239.
Niwa, H., Miyazaki, J., and Smith, A.G. (2000). Quantitative expression of Oct-3/4 defines differentiation, dedifferentiation or self-renewal of ES cells. Nature genetics *24*, 372-376.
Nottrott, S., Simard, M.J., and Richter, J.D. (2006). Human let-7a miRNA blocks protein production on actively translating polyribosomes. Nature structural & molecular biology *13*, 1108-1114.
Nowak, J.S., Choudhury, N.R., de Lima Alves, F., Rappsilber, J., and Michlewski, G. (2014). Lin28a regulates neuronal differentiation and controls miR-9 production. Nat Commun *5*, 3687.
Okada, C., Yamashita, E., Lee, S.J., Shibata, S., Katahira, J., Nakagawa, A., Yoneda, Y., and Tsukihara, T. (2009). A high-resolution structure of the pre-microRNA nuclear export machinery. Science *326*, 1275-1279.
Okamura, K., Liu, N., and Lai, E.C. (2009). Distinct mechanisms for microRNA strand selection by Drosophila Argonautes. Molecular cell *36*, 431-444.
Olde Loohuis, N.F., Kos, A., Martens, G.J., Van Bokhoven, H., Nadif Kasri, N., and Aschrafi, A. (2012). MicroRNA networks direct neuronal development and plasticity. Cell Mol Life Sci *69*, 89-102.
Olsen, P.H., and Ambros, V. (1999). The lin-4 regulatory RNA controls developmental timing in Caenorhabditis elegans by blocking LIN-14

protein synthesis after the initiation of translation. Developmental biology *216*, 671-680.
Ozsolak, F., Poling, L.L., Wang, Z., Liu, H., Liu, X.S., Roeder, R.G., Zhang, X., Song, J.S., and Fisher, D.E. (2008). Chromatin structure analyses identify miRNA promoters. Genes & development *22*, 3172-3183.
Packer, A.N., Xing, Y., Harper, S.Q., Jones, L., and Davidson, B.L. (2008). The bifunctional microRNA miR-9/miR-9* regulates REST and CoREST and is downregulated in Huntington's disease. J Neurosci *28*, 14341-14346.
Parchem, R.J., Moore, N., Fish, J.L., Parchem, J.G., Braga, T.T., Shenoy, A., Oldham, M.C., Rubenstein, J.L., Schneider, R.A., and Blelloch, R. (2015). miR-302 Is Required for Timing of Neural Differentiation, Neural Tube Closure, and Embryonic Viability. Cell reports *12*, 760-773.
Park, C.S., and Tang, S.J. (2009). Regulation of microRNA expression by induction of bidirectional synaptic plasticity. J Mol Neurosci *38*, 50-56.
Park, J.E., Heo, I., Tian, Y., Simanshu, D.K., Chang, H., Jee, D., Patel, D.J., and Kim, V.N. (2011). Dicer recognizes the 5' end of RNA for efficient and accurate processing. Nature *475*, 201-205.
Paroo, Z., Ye, X., Chen, S., and Liu, Q. (2009). Phosphorylation of the human microRNA-generating complex mediates MAPK/Erk signaling. Cell *139*, 112-122.
Pasquinelli, A. E., et al. (2000) Conservation of the sequence and temporal expression of let-7 heterochronic regulatory RNA. Nature *408*, 86-89.
Pauli, A., Valen, E., Lin, M.F., Garber, M., Vastenhouw, N.L., Levin, J.Z., Fan, L., Sandelin, A., Rinn, J.L., Regev, A., *et al.* (2012). Systematic identification of long noncoding RNAs expressed during zebrafish embryogenesis. Genome research *22*, 577-591.
Pei, D. (2009). Regulation of pluripotency and reprogramming by transcription factors. The Journal of biological chemistry *284*, 3365-3369.
Peters, A., Jones, E.G. (1984). Cellular Components of the Cerebral Cortex In (Plennum New York).
Petersen, C.P., Bordeleau, M.E., Pelletier, J., and Sharp, P.A. (2006). Short RNAs repress translation after initiation in mammalian cells. Molecular cell *21*, 533-542.

Pfeffer, S., Sewer, A., Lagos-Quintana, M., Sheridan, R., Sander, C., Grasser, F.A., van Dyk, L.F., Ho, C.K., Shuman, S., Chien, M., *et al.* (2005). Identification of microRNAs of the herpesvirus family. Nature methods *2*, 269-276.

Piao, X., Zhang, X., Wu, L., and Belasco, J.G. (2010). CCR4-NOT deadenylates mRNA associated with RNA-induced silencing complexes in human cells. Molecular and cellular biology *30*, 1486-1494.

Pillai, R.S., Bhattacharyya, S.N., Artus, C.G., Zoller, T., Cougot, N., Basyuk, E., Bertrand, E., and Filipowicz, W. (2005). Inhibition of translational initiation by Let-7 MicroRNA in human cells. Science *309*, 1573-1576.

Piskounova, E., Polytarchou, C., Thornton, J.E., LaPierre, R.J., Pothoulakis, C., Hagan, J.P., Iliopoulos, D., and Gregory, R.I. (2011). Lin28A and Lin28B inhibit let-7 microRNA biogenesis by distinct mechanisms. Cell *147*, 1066-1079.

Piskounova, E., Viswanathan, S.R., Janas, M., LaPierre, R.J., Daley, G.Q., Sliz, P., and Gregory, R.I. (2008). Determinants of microRNA processing inhibition by the developmentally regulated RNA-binding protein Lin28. The Journal of biological chemistry *283*, 21310-21314.

Polesskaya, A., Cuvellier, S., Naguibneva, I., Duquet, A., Moss, E.G., and Harel-Bellan, A. (2007). Lin-28 binds IGF-2 mRNA and participates in skeletal myogenesis by increasing translation efficiency. Genes & development *21*, 1125-1138.

Qi, H.H., Ongusaha, P.P., Myllyharju, J., Cheng, D., Pakkanen, O., Shi, Y., Lee, S.W., Peng, J., and Shi, Y. (2008). Prolyl 4-hydroxylation regulates Argonaute 2 stability. Nature *455*, 421-424.

Qiu, C., Ma, Y., Wang, J., Peng, S., and Huang, Y. (2010). Lin28-mediated post-transcriptional regulation of Oct4 expression in human embryonic stem cells. Nucleic acids research *38*, 1240-1248.

Ramachandran, V., and Chen, X. (2008). Degradation of microRNAs by a family of exoribonucleases in Arabidopsis. Science *321*, 1490-1492.

Ramón y Cajal, S. (1995). Histology of the nervous system of man and vertebrates (New York: Oxford University Press).

Rand, T.A., Petersen, S., Du, F., and Wang, X. (2005). Argonaute2 cleaves the anti-guide strand of siRNA during RISC activation. Cell *123*, 621-629.
Rehwinkel, J., Behm-Ansmant, I., Gatfield, D., and Izaurralde, E. (2005). A crucial role for GW182 and the DCP1:DCP2 decapping complex in miRNA-mediated gene silencing. Rna *11*, 1640-1647.
Rehwinkel, J., Natalin, P., Stark, A., Brennecke, J., Cohen, S.M., and Izaurralde, E. (2006). Genome-wide analysis of mRNAs regulated by Drosha and Argonaute proteins in Drosophila melanogaster. Molecular and cellular biology *26*, 2965-2975.
Rice, P., Longden, I., and Bleasby, A. (2000). EMBOSS: the European Molecular Biology Open Software Suite. Trends in genetics : TIG *16*, 276-277.
Roberts, T.C. (2014). The MicroRNA Biology of the Mammalian Nucleus. Mol Ther Nucleic Acids *3*, e188.
Romanelli, M.G., Lorenzi, P., and Morandi, C. (2000). Organization of the human gene encoding heterogeneous nuclear ribonucleoprotein type I (hnRNP I) and characterization of hnRNP I related pseudogene. Gene *255*, 267-272.
Roush, S., and Slack, F.J. (2008). The let-7 family of microRNAs. Trends Cell Biol *18*, 505-516.
Rudel, S., and Meister, G. (2008). Phosphorylation of Argonaute proteins: regulating gene regulators. The Biochemical journal *413*, e7-9.
Rudel, S., Wang, Y., Lenobel, R., Korner, R., Hsiao, H.H., Urlaub, H., Patel, D., and Meister, G. (2011). Phosphorylation of human Argonaute proteins affects small RNA binding. Nucleic acids research *39*, 2330-2343.
Rybak, A., Fuchs, H., Smirnova, L., Brandt, C., Pohl, E.E., Nitsch, R., and Wulczyn, F.G. (2008). A feedback loop comprising lin-28 and let-7 controls pre-let-7 maturation during neural stem-cell commitment. Nature cell biology *10*, 987-993.
Saito, Y., Liang, G., Egger, G., Friedman, J.M., Chuang, J.C., Coetzee, G.A., and Jones, P.A. (2006). Specific activation of microRNA-127 with downregulation of the proto-oncogene BCL6 by chromatin-modifying drugs in human cancer cells. Cancer cell *9*, 435-443.

Sakamoto, K., Karelina, K., and Obrietan, K. (2011). CREB: a multifaceted regulator of neuronal plasticity and protection. J Neurochem *116*, 1-9.

Schmitter, D., Filkowski, J., Sewer, A., Pillai, R.S., Oakeley, E.J., Zavolan, M., Svoboda, P., and Filipowicz, W. (2006). Effects of Dicer and Argonaute down-regulation on mRNA levels in human HEK293 cells. Nucleic acids research *34*, 4801-4815.

Schraivogel, D., Weinmann, L., Beier, D., Tabatabai, G., Eichner, A., Zhu, J.Y., Anton, M., Sixt, M., Weller, M., Beier, C.P., *et al.* (2011). CAMTA1 is a novel tumour suppressor regulated by miR-9/9* in glioblastoma stem cells. The EMBO journal *30*, 4309-4322.

Schratt, G.M., Tuebing, F., Nigh, E.A., Kane, C.G., Sabatini, M.E., Kiebler, M., and Greenberg, M.E. (2006). A brain-specific microRNA regulates dendritic spine development. Nature *439*, 283-289.

Schuetz, A., Murakawa, Y., Rosenbaum, E., Landthaler, M., and Heinemann, U. (2014). Roquin binding to target mRNAs involves a winged helix-turn-helix motif. Nat Commun *5*, 5701.

Schwamborn, J.C., Berezikov, E., and Knoblich, J.A. (2009). The TRIM-NHL protein TRIM32 activates microRNAs and prevents self-renewal in mouse neural progenitors. Cell *136*, 913-925.

Schwartz, P.H., Brick, D.J., Stover, A.E., Loring, J.F., and Muller, F.J. (2008). Differentiation of neural lineage cells from human pluripotent stem cells. Methods *45*, 142-158.

Schwarz, D.S., Hutvagner, G., Du, T., Xu, Z., Aronin, N., and Zamore, P.D. (2003). Asymmetry in the assembly of the RNAi enzyme complex. Cell *115*, 199-208.

Scott, G.K., Mattie, M.D., Berger, C.E., Benz, S.C., and Benz, C.C. (2006). Rapid alteration of microRNA levels by histone deacetylase inhibition. Cancer research *66*, 1277-1281.

Seggerson, K., Tang, L., and Moss, E.G. (2002). Two genetic circuits repress the Caenorhabditis elegans heterochronic gene lin-28 after translation initiation. Developmental biology *243*, 215-225.

Selbach, M., Schwanhausser, B., Thierfelder, N., Fang, Z., Khanin, R., and Rajewsky, N. (2008). Widespread changes in protein synthesis induced by microRNAs. Nature *455*, 58-63.

Sempere, L.F., Freemantle, S., Pitha-Rowe, I., Moss, E., Dmitrovsky, E., and Ambros, V. (2004). Expression profiling of mammalian microRNAs uncovers a subset of brain-expressed microRNAs with possible roles in murine and human neuronal differentiation. Genome Biol *5*, R13.

Shabalina, S.A., and Koonin, E.V. (2008). Origins and evolution of eukaryotic RNA interference. Trends in ecology & evolution *23*, 578-587.

Shen, J., Xia, W., Khotskaya, Y.B., Huo, L., Nakanishi, K., Lim, S.O., Du, Y., Wang, Y., Chang, W.C., Chen, C.H., *et al.* (2013). EGFR modulates microRNA maturation in response to hypoxia through phosphorylation of AGO2. Nature *497*, 383-387.

Shi, Y., Lan, F., Matson, C., Mulligan, P., Whetstine, J.R., Cole, P.A., Casero, R.A., and Shi, Y. (2004). Histone demethylation mediated by the nuclear amine oxidase homolog LSD1. Cell *119*, 941-953.

Shi, Y., Zhao, X., Hsieh, J., Wichterle, H., Impey, S., Banerjee, S., Neveu, P., and Kosik, K.S. (2010). MicroRNA regulation of neural stem cells and neurogenesis. J Neurosci *30*, 14931-14936.

Shibata, M., Kurokawa, D., Nakao, H., Ohmura, T., and Aizawa, S. (2008). MicroRNA-9 modulates Cajal-Retzius cell differentiation by suppressing Foxg1 expression in mouse medial pallium. J Neurosci *28*, 10415-10421.

Shibata, M., Nakao, H., Kiyonari, H., Abe, T., and Aizawa, S. (2011). MicroRNA-9 regulates neurogenesis in mouse telencephalon by targeting multiple transcription factors. J Neurosci *31*, 3407-3422.

Shiohama, A., Sasaki, T., Noda, S., Minoshima, S., and Shimizu, N. (2007). Nucleolar localization of DGCR8 and identification of eleven DGCR8-associated proteins. Experimental cell research *313*, 4196-4207.

Siegel, G., Obernosterer, G., Fiore, R., Oehmen, M., Bicker, S., Christensen, M., Khudayberdiev, S., Leuschner, P.F., Busch, C.J., Kane, C., *et al.* (2009). A functional screen implicates microRNA-138-dependent regulation of the depalmitoylation enzyme APT1 in dendritic spine morphogenesis. Nature cell biology *11*, 705-716.

Skeath, J.B., and Carroll, S.B. (1994). The achaete-scute complex: generation of cellular pattern and fate within the Drosophila nervous system. FASEB journal : official publication of the Federation of American Societies for Experimental Biology *8*, 714-721.

Smith, T.F., Gaitatzes, C., Saxena, K., and Neer, E.J. (1999). The WD repeat: a common architecture for diverse functions. Trends in biochemical sciences *24*, 181-185.

Song, G., Sharma, A.D., Roll, G.R., Ng, R., Lee, A.Y., Blelloch, R.H., Frandsen, N.M., and Willenbring, H. (2010). MicroRNAs control hepatocyte proliferation during liver regeneration. Hepatology *51*, 1735-1743.

Song, J.J., Smith, S.K., Hannon, G.J., and Joshua-Tor, L. (2004). Crystal structure of Argonaute and its implications for RISC slicer activity. Science *305*, 1434-1437.

Stark, K.L., Xu, B., Bagchi, A., Lai, W.S., Liu, H., Hsu, R., Wan, X., Pavlidis, P., Mills, A.A., Karayiorgou, M., *et al.* (2008). Altered brain microRNA biogenesis contributes to phenotypic deficits in a 22q11-deletion mouse model. Nature genetics *40*, 751-760.

Suzuki, H.I., Arase, M., Matsuyama, H., Choi, Y.L., Ueno, T., Mano, H., Sugimoto, K., and Miyazono, K. (2011). MCPIP1 ribonuclease antagonizes dicer and terminates microRNA biogenesis through precursor microRNA degradation. Molecular cell *44*, 424-436.

Suzuki, H.I., Katsura, A., and Miyazono, K. (2015). A role of uridylation pathway for blockade of let-7 microRNA biogenesis by Lin28B. Cancer Sci.

Tang, X., Li, M., Tucker, L., and Ramratnam, B. (2011). Glycogen synthase kinase 3 beta (GSK3beta) phosphorylates the RNAase III enzyme Drosha at S300 and S302. PloS one *6*, e20391.

Tang, X., Wen, S., Zheng, D., Tucker, L., Cao, L., Pantazatos, D., Moss, S.F., and Ramratnam, B. (2013). Acetylation of drosha on the N-terminus inhibits its degradation by ubiquitination. PloS one *8*, e72503.

Tang, X., Zhang, Y., Tucker, L., and Ramratnam, B. (2010). Phosphorylation of the RNase III enzyme Drosha at Serine300 or Serine302 is required for its nuclear localization. Nucleic acids research *38*, 6610-6619.

Thermann, R., and Hentze, M.W. (2007). Drosophila miR2 induces pseudo-polysomes and inhibits translation initiation. Nature *447*, 875-878.

Thomas, M.F., Abdul-Wajid, S., Panduro, M., Babiarz, J.E., Rajaram, M., Woodruff, P., Lanier, L.L., Heissmeyer, V., and Ansel, K.M. (2012). Eri1

regulates microRNA homeostasis and mouse lymphocyte development and antiviral function. Blood *120*, 130-142.

Tian, Y., Simanshu, D.K., Ma, J.B., Park, J.E., Heo, I., Kim, V.N., and Patel, D.J. (2014). A phosphate-binding pocket within the platform-PAZ-connector helix cassette of human Dicer. Molecular cell *53*, 606-616.

Trabucchi, M., Briata, P., Garcia-Mayoral, M., Haase, A.D., Filipowicz, W., Ramos, A., Gherzi, R., and Rosenfeld, M.G. (2009). The RNA-binding protein KSRP promotes the biogenesis of a subset of microRNAs. Nature *459*, 1010-1014.

Tsutsumi, A., Kawamata, T., Izumi, N., Seitz, H., and Tomari, Y. (2011). Recognition of the pre-miRNA structure by Drosophila Dicer-1. Nature structural & molecular biology *18*, 1153-1158.

Upton, J.P., Wang, L., Han, D., Wang, E.S., Huskey, N.E., Lim, L., Truitt, M., McManus, M.T., Ruggero, D., Goga, A., *et al.* (2012). IRE1alpha cleaves select microRNAs during ER stress to derepress translation of proapoptotic Caspase-2. Science *338*, 818-822.

Ustianenko, D., Hrossova, D., Potesil, D., Chalupnikova, K., Hrazdilova, K., Pachernik, J., Cetkovska, K., Uldrijan, S., Zdrahal, Z., and Vanacova, S. (2013). Mammalian DIS3L2 exoribonuclease targets the uridylated precursors of let-7 miRNAs. Rna *19*, 1632-1638.

Van Wynsberghe, P.M., Kai, Z.S., Massirer, K.B., Burton, V.H., Yeo, G.W., and Pasquinelli, A.E. (2011). LIN-28 co-transcriptionally binds primary let-7 to regulate miRNA maturation in Caenorhabditis elegans. Nature structural & molecular biology *18*, 302-308.

Visvanathan, J., Lee, S., Lee, B., Lee, J.W., and Lee, S.K. (2007). The microRNA miR-124 antagonizes the anti-neural REST/SCP1 pathway during embryonic CNS development. Genes & development *21*, 744-749.

Viswanathan, S.R., and Daley, G.Q. (2010). Lin28: A microRNA regulator with a macro role. Cell *140*, 445-449.

Viswanathan, S.R., Daley, G.Q., and Gregory, R.I. (2008). Selective blockade of microRNA processing by Lin28. Science *320*, 97-100.

Viswanathan, S.R., Powers, J.T., Einhorn, W., Hoshida, Y., Ng, T.L., Toffanin, S., O'Sullivan, M., Lu, J., Phillips, L.A., Lockhart, V.L., *et al.*

(2009). Lin28 promotes transformation and is associated with advanced human malignancies. Nature genetics *41*, 843-848.
Vogt, E.J., Meglicki, M., Hartung, K.I., Borsuk, E., and Behr, R. (2012). Importance of the pluripotency factor LIN28 in the mammalian nucleolus during early embryonic development. Development *139*, 4514-4523.
Wada, T., Kikuchi, J., and Furukawa, Y. (2012). Histone deacetylase 1 enhances microRNA processing via deacetylation of DGCR8. EMBO reports *13*, 142-149.
Wakiyama, M., Takimoto, K., Ohara, O., and Yokoyama, S. (2007). Let-7 microRNA-mediated mRNA deadenylation and translational repression in a mammalian cell-free system. Genes & development *21*, 1857-1862.
Walker, J.C., and Harland, R.M. (2008). Expression of microRNAs during embryonic development of Xenopus tropicalis. Gene Expr Patterns *8*, 452-456.
Walker, M.D. (2008). Role of MicroRNA in pancreatic beta-cells: where more is less. Diabetes *57*, 2567-2568.
Wan, M., Lee, S.S., Zhang, X., Houwink-Manville, I., Song, H.R., Amir, R.E., Budden, S., Naidu, S., Pereira, J.L., Lo, I.F., *et al.* (1999). Rett syndrome and beyond: recurrent spontaneous and familial MECP2 mutations at CpG hotspots. Am J Hum Genet *65*, 1520-1529.
Wang, J., Park, J.W., Drissi, H., Wang, X., and Xu, R.H. (2014). Epigenetic regulation of miR-302 by JMJD1C inhibits neural differentiation of human embryonic stem cells. The Journal of biological chemistry *289*, 2384-2395.
Wang, Y., Juranek, S., Li, H., Sheng, G., Tuschl, T., and Patel, D.J. (2008a). Structure of an argonaute silencing complex with a seed-containing guide DNA and target RNA duplex. Nature *456*, 921-926.
Wang, Y., Sheng, G., Juranek, S., Tuschl, T., and Patel, D.J. (2008b). Structure of the guide-strand-containing argonaute silencing complex. Nature *456*, 209-213.
Wheeler, B.M., Heimberg, A.M., Moy, V.N., Sperling, E.A., Holstein, T.W., Heber, S., and Peterson, K.J. (2009). The deep evolution of metazoan microRNAs. Evolution & development *11*, 50-68.
Wibrand, K., Panja, D., Tiron, A., Ofte, M.L., Skaftnesmo, K.O., Lee, C.S., Pena, J.T., Tuschl, T., and Bramham, C.R. (2010). Differential regulation of

mature and precursor microRNA expression by NMDA and metabotropic glutamate receptor activation during LTP in the adult dentate gyrus in vivo. Eur J Neurosci *31*, 636-645.

Wilbert, M.L., Huelga, S.C., Kapeli, K., Stark, T.J., Liang, T.Y., Chen, S.X., Yan, B.Y., Nathanson, J.L., Hutt, K.R., Lovci, M.T., *et al.* (2012). LIN28 binds messenger RNAs at GGAGA motifs and regulates splicing factor abundance. Molecular cell *48*, 195-206.

Wu, C., So, J., Davis-Dusenbery, B.N., Qi, H.H., Bloch, D.B., Shi, Y., Lagna, G., and Hata, A. (2011). Hypoxia potentiates microRNA-mediated gene silencing through posttranslational modification of Argonaute2. Molecular and cellular biology *31*, 4760-4774.

Wu, L., and Belasco, J.G. (2005). Micro-RNA regulation of the mammalian lin-28 gene during neuronal differentiation of embryonal carcinoma cells. Molecular and cellular biology *25*, 9198-9208.

Wulczyn, F.G., Smirnova, L., Rybak, A., Brandt, C., Kwidzinski, E., Ninnemann, O., Strehle, M., Seiler, A., Schumacher, S., and Nitsch, R. (2007). Post-transcriptional regulation of the let-7 microRNA during neural cell specification. FASEB journal : official publication of the Federation of American Societies for Experimental Biology *21*, 415-426.

Wurst, W., and Bally-Cuif, L. (2001). Neural plate patterning: upstream and downstream of the isthmic organizer. Nat Rev Neurosci *2*, 99-108.

Xhemalce, B., Robson, S.C., and Kouzarides, T. (2012). Human RNA methyltransferase BCDIN3D regulates microRNA processing. Cell *151*, 278-288.

Xu, B., and Huang, Y. (2009). Histone H2a mRNA interacts with Lin28 and contains a Lin28-dependent posttranscriptional regulatory element. Nucleic acids research *37*, 4256-4263.

Xu, B., Zhang, K., and Huang, Y. (2009). Lin28 modulates cell growth and associates with a subset of cell cycle regulator mRNAs in mouse embryonic stem cells. Rna *15*, 357-361.

Yang, D.H., and Moss, E.G. (2003). Temporally regulated expression of Lin-28 in diverse tissues of the developing mouse. Gene Expr Patterns *3*, 719-726.

Yang, W., Chendrimada, T.P., Wang, Q., Higuchi, M., Seeburg, P.H., Shiekhattar, R., and Nishikura, K. (2006). Modulation of microRNA processing and expression through RNA editing by ADAR deaminases. Nature structural & molecular biology *13*, 13-21.

Yang, X., Lin, X., Zhong, X., Kaur, S., Li, N., Liang, S., Lassus, H., Wang, L., Katsaros, D., Montone, K., *et al.* (2010). Double-negative feedback loop between reprogramming factor LIN28 and microRNA let-7 regulates aldehyde dehydrogenase 1-positive cancer stem cells. Cancer research *70*, 9463-9472.

Yao, H., Ma, R., Yang, L., Hu, G., Chen, X., Duan, M., Kook, Y., Niu, F., Liao, K., Fu, M., *et al.* (2014). MiR-9 promotes microglial activation by targeting MCPIP1. Nat Commun *5*, 4386.

Ye, X., Huang, N., Liu, Y., Paroo, Z., Huerta, C., Li, P., Chen, S., Liu, Q., and Zhang, H. (2011). Structure of C3PO and mechanism of human RISC activation. Nature structural & molecular biology *18*, 650-657.

Yeom, K.H., Lee, Y., Han, J., Suh, M.R., and Kim, V.N. (2006). Characterization of DGCR8/Pasha, the essential cofactor for Drosha in primary miRNA processing. Nucleic acids research *34*, 4622-4629.

Yi, R., Qin, Y., Macara, I.G., and Cullen, B.R. (2003). Exportin-5 mediates the nuclear export of pre-microRNAs and short hairpin RNAs. Genes & development *17*, 3011-3016.

Yoda, M., Kawamata, T., Paroo, Z., Ye, X., Iwasaki, S., Liu, Q., and Tomari, Y. (2010). ATP-dependent human RISC assembly pathways. Nature structural & molecular biology *17*, 17-23.

Yokoyama, S., Hashimoto, M., Shimizu, H., Ueno-Kudoh, H., Uchibe, K., Kimura, I., and Asahara, H. (2008). Dynamic gene expression of Lin-28 during embryonic development in mouse and chicken. Gene Expr Patterns *8*, 155-160.

Yoo, A.S., Sun, A.X., Li, L., Shcheglovitov, A., Portmann, T., Li, Y., Lee-Messer, C., Dolmetsch, R.E., Tsien, R.W., and Crabtree, G.R. (2011). MicroRNA-mediated conversion of human fibroblasts to neurons. Nature *476*, 228-231.

Young, R.S., Marques, A.C., Tibbit, C., Haerty, W., Bassett, A.R., Liu, J.L., and Ponting, C.P. (2012). Identification and properties of 1,119 candidate

lincRNA loci in the Drosophila melanogaster genome. Genome biology and evolution *4*, 427-442.

Yu, J., Vodyanik, M.A., Smuga-Otto, K., Antosiewicz-Bourget, J., Frane, J.L., Tian, S., Nie, J., Jonsdottir, G.A., Ruotti, V., Stewart, R., *et al.* (2007). Induced pluripotent stem cell lines derived from human somatic cells. Science *318*, 1917-1920.

Zamore, P.D. (2001). Thirty-three years later, a glimpse at the ribonuclease III active site. Molecular cell *8*, 1158-1160.

Zdanowicz, A., Thermann, R., Kowalska, J., Jemielity, J., Duncan, K., Preiss, T., Darzynkiewicz, E., and Hentze, M.W. (2009). Drosophila miR2 primarily targets the m7GpppN cap structure for translational repression. Molecular cell *35*, 881-888.

Zeng, Y., Sankala, H., Zhang, X., and Graves, P.R. (2008). Phosphorylation of Argonaute 2 at serine-387 facilitates its localization to processing bodies. The Biochemical journal *413*, 429-436.

Zeng, Y., Yi, R., and Cullen, B.R. (2005). Recognition and cleavage of primary microRNA precursors by the nuclear processing enzyme Drosha. The EMBO journal *24*, 138-148.

Zhang, H., Kolb, F.A., Jaskiewicz, L., Westhof, E., and Filipowicz, W. (2004). Single processing center models for human Dicer and bacterial RNase III. Cell *118*, 57-68.

Zhang, Y.C., and Chen, Y.Q. (2013). Long noncoding RNAs: new regulators in plant development. Biochemical and biophysical research communications *436*, 111-114.

Zhao, C., Sun, G., Li, S., and Shi, Y. (2009). A feedback regulatory loop involving microRNA-9 and nuclear receptor TLX in neural stem cell fate determination. Nature structural & molecular biology *16*, 365-371.

Zhu, H., Shah, S., Shyh-Chang, N., Shinoda, G., Einhorn, W.S., Viswanathan, S.R., Takeuchi, A., Grasemann, C., Rinn, J.L., Lopez, M.F., *et al.* (2010). Lin28a transgenic mice manifest size and puberty phenotypes identified in human genetic association studies. Nature genetics *42*, 626-630.

Zhu, H., Shyh-Chang, N., Segre, A.V., Shinoda, G., Shah, S.P., Einhorn, W.S., Takeuchi, A., Engreitz, J.M., Hagan, J.P., Kharas, M.G., *et al.* (2011). The Lin28/let-7 axis regulates glucose metabolism. Cell *147*, 81-94.

Appendix A – List of primers and antibodies

Taq polymerase T7 template primers	
Pre-miR-9-Fw	TAATACGACTCACTATAGGTCTTTGGTTATCTAGCTGTA
Pre-miR-9-Rv	ACTTTCGGTTATCTAGCTTTA
Pre-miR-9 mutagenesis primers	
Pri-miR-9-GGAG/TTTT-Fw	TTTTTCTTCATAAAGCTAGATAACCGA
Pri-miR-9-GGAG/TTTT-Rv	ACACCACTCATACAGCTAGATAACCAA
Pri-miR-9-GGAG/TTAG-Fw	TTAGTCTTCATAAAGCTAGATAACCGA
Pri-miR-9-GGAG/TTAG-Rv	ACACCACTCATACAGCTAGATAACCAA
Pri-miR-9-GGAG/TTTG-Fw	TTTGTCTTCATAAAGCTAGATAACCGA
Pri-miR-9-GGAG/TTTG-Rv	ACACCACTCATACAGCTAGATAACCAA
Pri-miR-9-GGAG/GGTT-Fw	TTTCTTCATAAAGCTAGATAACCGAAA
Pri-miR-9-GGAG/GGTT-Rv	CCACACCACTCATACAGCTAGATAACC
qRT-PCR primers	
Mature let-7a F_qRT	TGACAGCACGTAAATATTGGCG
Mature miR-21 F_qRT	TAGCTTATCAGACTGATGTTGA
Mature miR-124 F_qRT	TAAGGCACGCGGTGAATGCC
Mature miR-9 F_qRT	TCTTTGGTTATCTAGCTGTATGA
Mature miR-302a F_qRT	TAAGTGCTTCCATGTTTTGGTGA
Mature miR-101	TACAGTACTGTGATAACTGAA
Pri-let-7a Fw	CAGGAAATGAAACCACAGCA
Pri-let-7a Rv	CCTCCTCGGTAATCCTGGTT
Pri-miR-16 Fw	TGGGGTTCGATCTTAACAGG
Pri-miR-16 Rv	TGTCACGATGGTAGGCAAAA
Pri-miR-124 Fw	TCCTCCTCCTAGTCCCCTTC
Pri-miR-124 Rv	CTGCAGCTCCAGACAATGAA
Pri-miR-9 Fw	TTCGGTCTCTGTCGTGTCTG
Pri-miR-9 Rv	AAGGGACACGAGTGGAGTTG
Pri-miR-302a Fw	TTCTGGAGGAGAACACGAATC
Pri-miR-302a Rv	TGAGGAGAAAGAAAACAAAATGG
Pri-miR-101 Fw	CTTCCTGCCCTGAGTTTCGT
Pri-miR-101 Rv	CACAGCTGCCTGAGAGTCAA
Pri-miR-9-1 Fw	GGAGCCTTTCCACTAGCA
Pri-miR-9-1 Rv	AGGTCGGAATCTAGGCTGAAACCAAGC
Pri-miR-9-2 Fw	AGCTTGCTGCACCTTAGTCT

Pri-miR-9-2 Rv	TGTGTGCGGCTAGAACATCC
Pri-miR-9-3 Fw	CCATTGTAAGGCTGGGTGGT
Pri-miR-9-3 Rv	CTCCTCTCGCAGGCTAATCG
Pri-miR-124-1 Fw	GGAAACGAAAGGATGCGGGA
Pri-miR-124-1 Rv	GGGAACGCGATGAGCTAAGG
Pri-miR-124-2 Fv	TGGGTTTTAGGTGCGCTGTA
Pri-miR-124-2 Rv	ACTCCCACCTCAGCTTTCCT
Pri-miR-124-3 Fw	CTCTGCACCCGTCAGAAGAC
Pri-miR-124-3 Rv	CAACTCCGAGGAGCCAGTTT
Northern blot – primers for *miRVana* hybridization probe	
miR_124_mirVana	TAAGGCACGCGGTGAATGCCTTTCCTGTCTC
miR_9_mirVana	TCTTTGGTTATCTAGCTGTATGATTTCCTGTCTC
miR_302a_mirVana	TAAGTGCTTCCATGTTTTGGTGATTTCCTGTCTC
miR_let7a_mirVana	TGGAAGACTAGTGATTTTGTTGTCCTGTCTC
Terminal loop sequences – RNA chromatography	
miR-9_TL	UAUGAGUGGUGUGGAGUCUUCAU
miR-124_TL	CCUUGAUUUAAAUGUCCAUACAA
Lin28a truncations primers	
hLin28a_1_XbaI_Fw	TTTCTAGAATGGGCTCCGTGTCCAACCAGCGTTTG
hLin28a_190_BamHI_Rv	TTGGATCCTCAGTAGGTTGGCTTTCCCTGTGCACTAGGG
hLin28a_24_XbaI_Fw	TTTCTAGAGCGCCGGAGGACGCGGCC
hLin28a_209_BamHI_Rv	TTGGATCCTCAATTCTGTGCCTCCGGGAGCAGGGTAG
hLin28a_24_XbaI_Fw	TTTCTAGAGCGCCGGAGGACGCGGCC
hLin28a_123_BamHI_Rv	TTGGATCCTCACCGCCTCTCACTCCCAATACAGAATACTCC
hLin28a_123_XbaI_Fw	TTTCTAGACGGCCAAAAGGAAAGAGCATGCAGAAGCG
hLin28a_74_BamHI_Rv	TTGGATCCTCACACAAAGACATCCACTGGGGGGTCGAG
hLin28a_156_XbaI_Fw	TTTCTAGACCCCAGCCCAAGAAGTGCCACTTCTG

Antibody	Supplier	Dilution
Anti-Rabbit IgG HRP linked	Cell Signalling Technology	1:1000
Lin28 (A177)	Cell Signalling Technology	1:1000
Lin28a(Ab46020)	Abcam	1:2000
Msi1 (N3C3)	GeneTex	1:1000

hnRNP A1 (D21H11)	Cell Signalling Technology	1:1000
Exosc3	Abcam	1:2000
GFAP	Sigma Aldrich	1:500
β-tubulin III (Tuj1)	GeneTex	1:50000
α-tubulin	Sigma Aldrich	1:50000
Dis3l2	Custom Made	1:1000